Universitat de Girona

RATIONAL DESIGN OF BIOINSPIRED IRON AND MANGANESE CATALYSTS FOR THE EFFECTIVE AND SELECTIVE EPOXIDATION OF ALKENES AND OXIDATION OF ALKANES

Carlota Clarasó Petit

Universitat de Girona

Doctoral Thesis

Rational design of bioinspired iron and manganese catalysts for the effective and selective epoxidation of alkenes and oxidation of alkanes

Carlota Clarasó Petit

2018

Doctoral programme in Chemistry

Supervised by: Dr. Miquel Costas Salgueiro and Dr. Alfons Polo Ortiz

Tutor: Miquel Costas Salgueiro

Presented in partial fulfilment of the requirements for a doctoral degree from the University of Girona

Universitat de Girona

Dr. Miquel Costas Salgueiro and Dr. Alfons Polo Ortiz of Universitat de Girona,

WE DECLARE:

That the thesis “Rational design of bioinspired iron and manganese catalysts for the effective and selective epoxidation of alkenes and oxidation of alkanes”, presented by Carlota Clarasó Petit to obtain a doctoral degree, has been completed under our supervision.

For all intents and purposes, we hereby sign this document.

Dr. Miquel Costas Salgueiro

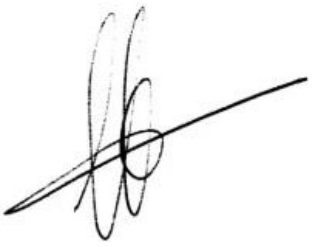

Dr. Alfons Polo Ortiz

Girona, 10th December 2018

There is nothing more wonderful than being a scientist,
nowhere I would rather be than in my lab,
staining up my clothes and getting paid to play

Marie Curie

A person who never made a mistake
never tried anything new

Albert Einstein

List of publications

Manuscripts in preparation derived from this thesis:

Chaptrer IV

- Synthesis, Characterization and Reactivity of Novel Bioinspired Aminopyridine Iron and Manganese Complexes for the Asymmetric Epoxidation of Olefins with H_2O_2.

Chaptrer V

- Highly Enantioselective Epoxidation of β,β-Disubstituted Enamides with a Manganese Catalyst and Aqueous Hydrogen Peroxide.
- Impact of the Chirality at the Metal on the Enantioselective Oxygen Atom Transfer.

List of abbreviations

[Ox]	Oxidant
2°	Secondary
2-eba	2-Ethylbutyric acid
2-eha	2-Ethylhexanoic acid
3°	Tertiary
3-AP	3-Aminopyridine
Aca	1-Adamantanecarboxylic acid
AcOEt	Ethyl acetate
AcOH	Acetic acid
AcOOH	Peracetic acid
Approx.	Approximately
aq.	Aqueous
Asp	Aspartate
ATR	Attenuated total reflection
biid	1,1'-Biisoindoline
bp	2,2'-Bipyrrolidine
BPhMeNH	N^1,N^2-Bis((*S*)-1-phenylethyl)ethane-1,2-diamine
bpmen	*N*,*N*'-dimethyl-*N*,*N*'-bis(2-pyridylmethyl)ethane-1,2-diamine
bpp	2,2'-Bipiperidine
BzIm	Benzimidazole
CA	Carboxylic acid
Cat	Catalyst
Conv.	Conversion
Chca	Cyclohexanecarboxilic acid
Cyp P450	Cytochrome P450
Cys	Cysteine
CV	Cyclic voltammetry
DCD	1,5-Diaza-*cis*-decalin
DMBA	2,2-Dimethylbutyric acid
DMCD	*N*,*N*'-dimethyl-*trans*-1,2-cyclohexanediamine

DMCH	Dimethylcyclohexane
DMF	Dimethyl formamide
dMM	Dimethylmethoxy
Ee	Enantiomeric excess
Equiv.	Equivalents
ESI	Electrospray ionization
FID	Flame ionization detector
FT-IR	Fourier transform infrared
GC	Gas chromatography
Glu	Glutamate
His	Histidine
HPLC	High pressure liquid chromatography
HRMS	High-resolution mass spectrometry
HS	High spin
IS	Internal standard
L	Ligand
LS	Low spin
M	Metal
mcp	*N,N'*-Dimethyl-*N,N'*-bis(2-pyridylmethyl)cyclohexane-*trans*-1,2-diamine
mCPBA	*meta*-Chloroperbenzoic acid
Me_2N	Dimethylamino
MLCT	Metal-to-ligand charge-transfer
MS	Mass spectrometry
NAD(P)H	Nicotinamide adenine dinucleotide(phosphate)
NDO	Naphthalene 1,2-dioxygenase
NMR	Nuclear magnetic resonance
Ohbiq	1,1',2,2',3,3',4,4'-Octahydro-1,1'-biisoquinoline
OTf	Trifluoromethanesulfonate anion
p.	Page
pdp	*N,N'*-bis(2-pyridylmethyl)-2,2'-bipyrrolidine
PTC	Phase-transfer catalyst
Pva	Pivalic acid

Q-TOF	Quadrupole time of flight
q	Quadruplet
RC	Retention of configuration
RO's	Rieske non-heme iron-dependent oxygenases
rt	Room temperature
s	Singlet
SOD	Superoxide dismutase
t	Triplet
T	Temperature
tacn	1,4,7-Triazacyclononane
TBAHP	Tetrabutylammonium hexafluorophosphate
THF	Tetrahydrofuran
Tips	Tris-(triisopropyl)silyl
TLC	Thin layer chromatography
TON	Turnover number
tpa	Tris(2-pyridylmethyl)amine
UV–vis	Ultraviolet-visible

Table of contents

Supplementary digital material

The material listed below can be found in the attached CD:

- PDF file of the PhD dissertation.
- PDF files containing IR of ligands and complexes; HRMS of ligands, complexes, synthesized substrates and epoxide products; ^{1}H-NMR and ^{13}C-NMR of synthesized substrates and epoxide products and HPLC spectra of the epoxide products. They can be found in the folder named *Characterization*.
- CIF files for each crystal structure presented in this thesis. They can be found in the folder named *CIF files* and they are named as **CX** for complexes or **P20** for the crystalized epoxide product.

List of figures

Acknowledgments

This work would not have been possible without the following collaborations:

- Serveis Tècnics de Recerca (STR) from Universitat de Girona for technical support, with special remark to Dr. Laura Gómez.
- Prof. Elena V. Rybak-Akimova from Tufts University of Boston for the (*R*,*R*)-2,2'-bipiperidine sample.
- Prof. Robertus J. M. Klein Gebbink from Utrecht University for the iron complexes based on the 1,1'-biisoindoline backbone.
- Financial support from:
    - the Ministerio de Economía, Industria y Competitividad for project CTQ2012-37420-C02-01/BQU to Miquel Costas and for a Pre-doctoral FPI grant Ref. BES-2013-066564.
    - The European Research Council for project ERC-009StG-239910 to Miquel Costas.
    - Generalitat de Catalunya for an ICREA Academia Award to Miquel Costas.

Graphical abstract

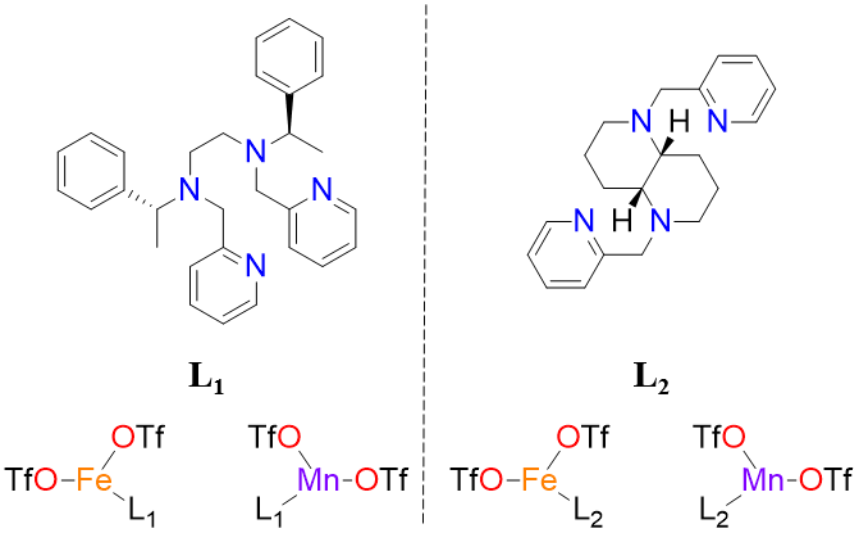

Chapter IV. Iron and manganese complexes based on the 1,1',2,2',3,3',4,4'-octahydro-1,1'-biisoquinoline backbone: synthesis, characterization and catalytic epoxidation activity (p. 65)

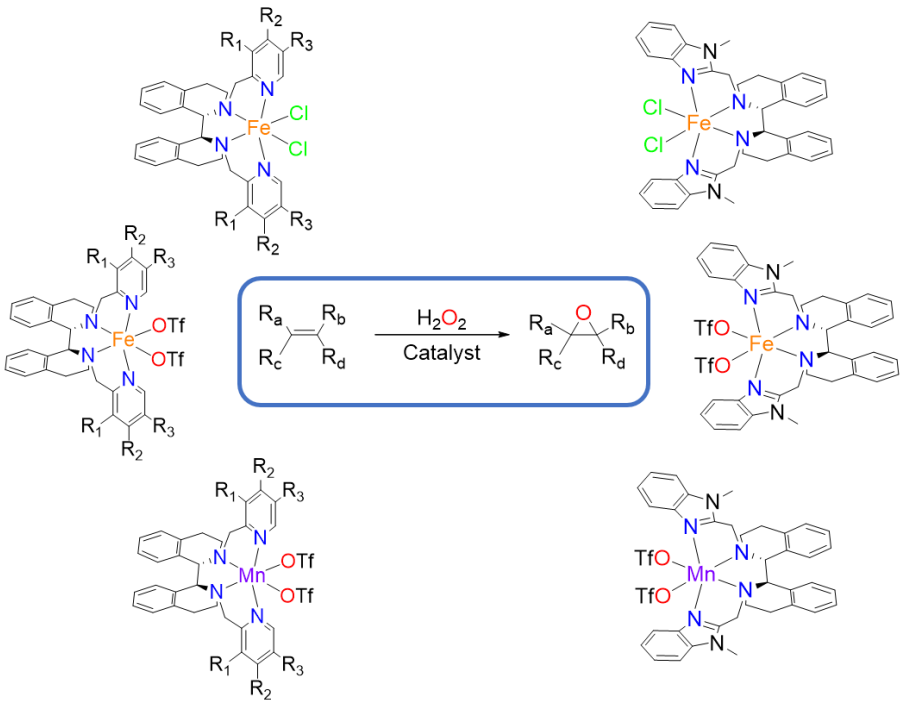

Chapter V. Manganese catalysed highly enantioselective epoxidation of β,β-disubstituted enamides with aqueous H_2O_2. Stereoselectivity reversal with catalysts having the same chirality at the metal (p. 113)

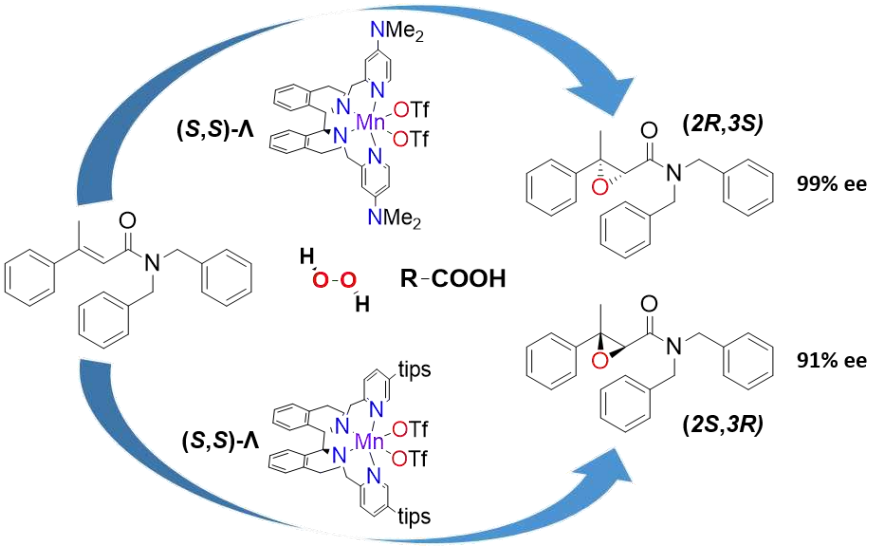

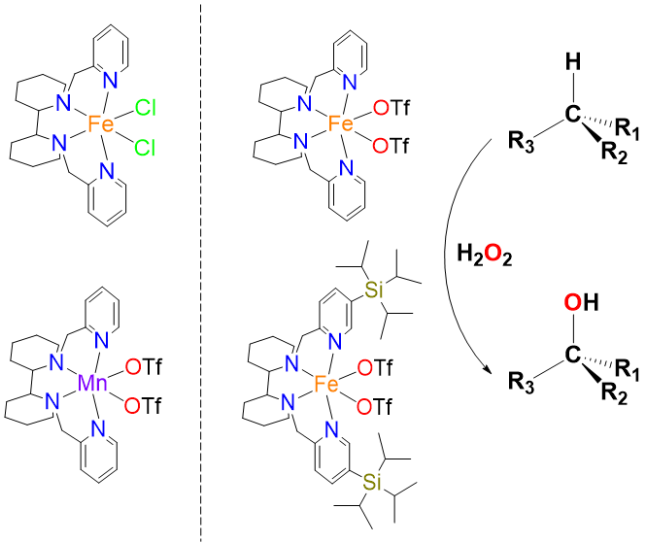

List of schemes

List of tables

Summary

Metalloenzymes are a fundamental source of inspiration for synthetic chemists. Oxidation metalloenzymes catalyze oxidation reactions with high efficiency under very mild experimental conditions exhibiting exquisite regio- and stereoselectivity. The present dissertation aims at designing efficient and selective bioinspired oxidation catalysts. Looking at the literature there's a very limited number of aliphatic diamines incorporated as ligand backbones in tetradentate aminopyridine based complexes, which have been revealed as one of the most successful catalysts for these transformations with peroxide type of oxidants. Thus, this thesis is focused on the synthesis of chiral iron and manganese complexes based on novel diamine backbones and employ them as catalysts in the stereoselective epoxidation of olefins and oxidation of C-H bonds by using hydrogen peroxide as oxidant.

In chapters III, IV and VI, different diamines backbones are used for the synthesis of new tetradentate N-donor ligands. In the former, the corresponding iron and manganese complexes exhibit very poor results in the catalytic epoxidation of alkenes, proving that catalyst activity is highly sensitive to the nature of the diamine.

On the other hand, complexes of chapter IV provide remarkable results in the epoxidation of some interesting substrates, being the electron-rich complexes the ones that display high yields and best enantioselectivities. Actually, in chapter V, a novel manganese complex accomplishes highly enantioselective epoxidation of β,β-disubstituted enamides (up to 99% ee), which are recognized substrates very difficult to epoxidize with high stereoselectivity. Moreover, an inversion in the enantiocontrol of this reaction by the use of sterically demanding groups in the ligand is discovered.

Finally, in chapter VI, we provide a comparison between iron complexes based on different backbones in C-H oxidation catalysis. The nature of the diamine again turns out to be a critical parameter in defining catalyst selectivity. The new catalysts presented in this chapter exhibit very promising results that, after some optimization, may let to a novel family of catalysts with outstanding activity.

Resum

Els metal·loenzims són una font fonamental d'inspiració per als químics sintètics. Els metal·loenzims oxidants catalitzen reaccions d'oxidació amb gran eficiència sota condicions experimentals molt suaus que presenten regio- i estereoselectivitats exquisides. L'objectiu d'aquesta tesi es basa en el disseny de catalitzadors d'oxidació bioinspirats eficients i selectius. Analitzant la literatura, es denota que hi ha una limitació important en el nombre i la naturalesa de la diamina incorporada als lligands en complexos basats en lligands tetradentats amb aminopiridines, que s'han demostrat com uns dels catalitzadors més exitosos per a aquestes transformacions amb oxidants de tipus peròxid. Així doncs, aquesta tesi se centra en la síntesi de complexos quirals de ferro i manganès basats en lligands tetradentats que incorporen noves diamines i el seu ús com a catalitzadors en l'epoxidació estereoselectiva d'olefines i l'oxidació dels enllaços C-H utilitzant el peròxid d'hidrogen com a oxidant.

En els capítols III, IV i VI, s'utilitzen diferents diamines per a la síntesi de nous lligands tetradentats basats en nitrogen. En el primer, els corresponents complexos de ferro i manganès presenten resultats molt pobres en l'epoxidació catalítica d'alquens, demostrant que l'activitat catalítica d'un complex és altament sensible a la naturalesa de la diamina utilitzada.

D'altra banda, els complexos del capítol IV proporcionen resultats remarcables en l'epoxidació de substrats interessants, essent els complexos rics en electrons els que mostren els rendiments més alts i les millors enantioselectivitats. En realitat, en el capítol V, el nou complex de manganès es capaç d'epoxidar enamides β,β-disubstituïdes, reconeguts com a substrats molt difícils d'epoxidar estereoselectivament, amb altíssimes enantioselectivitats (fins al 99% ee). A més, s'ha descobert una inversió de l'enantiocontrol d'aquesta reacció mitjançant l'ús de substituents voluminosos en el lligand.

Finalment, en el capítol VI, es facilita una comparació entre complexos de ferro basats en diferents diamines per a la catàlisi d'oxidació de C-H. Novament, la naturalesa de la diamina resulta un paràmetre crític per a la selectivitat de les reaccions. Els nous catalitzadors utilitzats en aquest capítol presenten uns resultats molt prometedors que, després d'una certa optimització, poden donar lloc a una nova família de catalitzadors amb una activitat excepcional.

Resumen

Las metaloenzimas son una fuente fundamental de inspiración para los químicos sintéticos. Las metaloenzimas oxidantes catalizan reacciones de oxidación con gran eficiencia en condiciones experimentales muy suaves que presentan regio- y estereoselectividades exquisitas. El objetivo de esta tesis se basa en el diseño de catalizadores de oxidación bioinspirados eficientes y selectivos. Analizando la literatura, se observa una limitación importante en el número y en la naturaleza de la diamina utilizada en complejos basados en ligandos tetradentados con aminopiridinas, que se han demostrado como unos de los catalizadores más exitosos para estas transformaciones con oxidantes de tipo peróxido. Así pues, esta tesis se centra en la síntesis de complejos quirales de hierro y manganeso basados en nuevas estructuras de diamina y su uso como catalizadores en la epoxidación estereoselectiva de olefinas y la oxidación de enlaces C-H utilizando el peróxido de hidrógeno como oxidante.

En los capítulos III, IV y VI, se utilizan diferentes diaminas para la síntesis de nuevos ligandos tetradentats basados en nitrógeno. En el primero, los correspondientes complejos de hierro y manganeso presentan resultados muy pobres en la epoxidación catalítica de alquenos, demostrando que la actividad catalítica de un complejo es altamente sensible a la naturaleza de la diamina utilizada.

Por otra parte, los complejos del capítulo IV proporcionan resultados remarcables en la epoxidación de sustratos interesantes, siendo los complejos ricos en electrones los que muestran los rendimientos más altos y las mejores enantioselectividades. En el capítulo V, se describe un nuevo complejo de manganeso que es capaz de epoxidar enamidas β,β-disubstituidas, reconocidos como sustratos muy difíciles de epoxidar estereoselectivamente, con muy altos niveles de enantioselectividad (hasta el 99% ee). Además, se ha descubierto una inversión del enantiocontrol de esta reacción mediante el uso de sustituyentes voluminosos en el ligando.

Finalmente, en el capítulo VI, se facilita una comparación entre complejos de hierro basados en diferentes diamina para la catálisis de oxidación de C-H. De nuevo, la naturaleza de la diamina resulta un parámetro crítico para la selectividad de las reacciones. Los nuevos catalizadores utilizados en este capítulo presentan unos resultados muy prometedores que, después de cierta optimización, pueden dar lugar a una nueva familia de catalizadores con una actividad excepcional.

CHAPTER I

General introduction

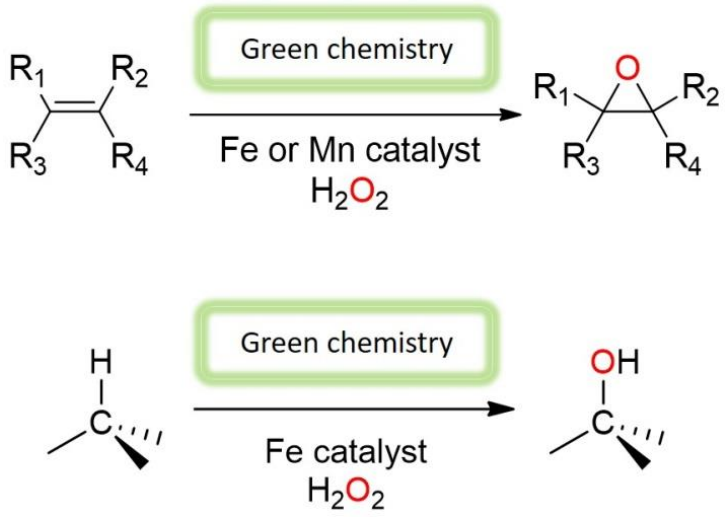

I.1 Importance of alkene and alkane oxidation

Oxidation of C-H and C=C bonds is an important transformation, essential in many biological and industrial processes.[1-4] Among them, epoxidation of alkenes and hydroxylation of alkanes are highly interesting reactions from a synthetic point of view (scheme I.1). To perform these reactions in a selective manner constitutes an important goal in modern synthetic chemistry, and is subject to intense research efforts.

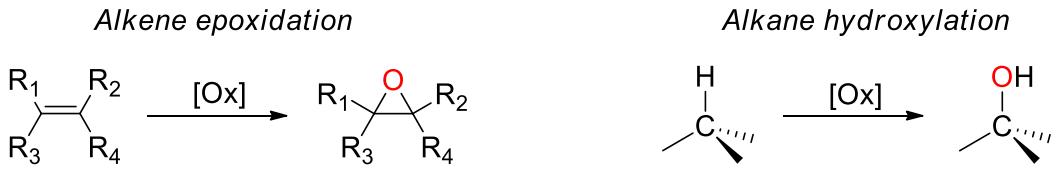

Scheme I.1. Challenging oxidation reactions

Taking on account the environmental and economic cost of those transformations with current methods, there is an increasing necessity to employ more environmentally benign reaction conditions. Important challenges that remain unsolved include substrate conversion with high selectivity, and the use of inexpensive and environmentally friendly metals. There is special interest on the use of "green" oxidants to minimize the amount of waste.[5] In particular, hydrogen peroxide is becoming increasingly fashionable as "green" oxidant since the only by-product after an oxidation reaction is water, it exhibits good atom efficiency and it is relatively cheap and easy to handle, when compared to dioxygen. Even though, it also presents some disadvantages: in high concentrations can be dangerous to handle and in the presence of metals, it easily generates highly reactive hydroxyl radicals (·OH) giving rise to non-selective oxidation reactions. Also, H_2O_2 often undergoes self-disproportionation reactions in the presence of transition metals.[6]

The bioinspired approach toward this problem appears to be the most suitable solution in all the aspects. It consists in the rational design of simpler complexes that should mimic key structural aspects of natural systems aiming at reproducing their activity. This translates in the preparation of mononuclear of iron and manganese complexes containing N and carboxylate based donors in their first coordination sphere. These complexes will activate H_2O_2, regarded as a $2e^-$ reduced source of O_2, to generate high valent metal-oxo species, as finally responsible for the oxidation reactions. This reaction mechanism reproduces then the basic features of O_2 activation at non-heme iron oxygenases.

I.1.1 Epoxidation of alkenes

Among the available feedstocks, alkenes are one of the most important starting materials for organic synthesis, due to their relatively rich reactivity. Their oxidation leads to a wide variety of value added compounds. Among them, epoxides are present in a large array of natural products and biologically active molecules,[7-9] and they constitute extremely useful building blocks and intermediates for the fine chemistry and pharmaceutical industries.[10-17] For this reason, the epoxidation is an important reaction that has attracted much research efforts during last decades.

Most remarkably and challenging constitutes the asymmetric epoxidation of olefins, as two stereogenic centers are formed. Moreover, these enantiomerically enriched epoxides can be further utilized as precursors for the synthesis of a broad diversity of important organic compounds that have industrial as well as medical applications, such as diols, alcohols, amino alcohols, chloride moieties, etc. (scheme I.2).

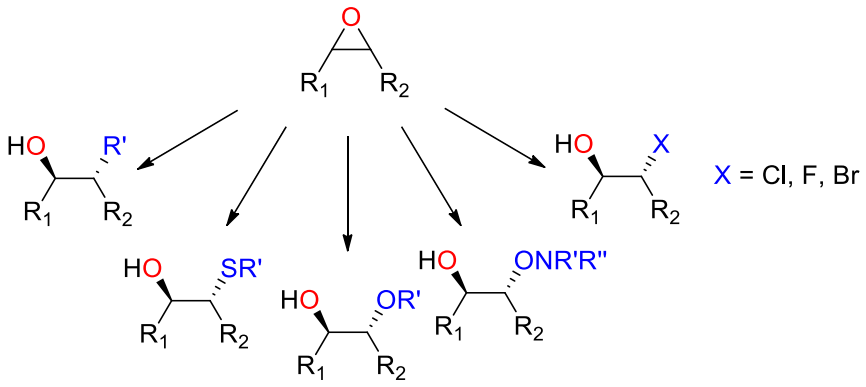

Scheme I.2. Schematic diagram of possible products from ring opening epoxides.

I.1.2 Alkane oxidation: an attractive but challenging synthetic tool

Alkanes are also convenient feedstocks because they are abundant, and the activation and functionalization of inert C–H bonds by transition metal complexes, are of general interest and significance.[2, 18-20] As non-activated alkyl C-H groups are ubiquitous in organic compounds, the control of site-selectivity is the main challenge of this reaction.[21]

A few methods are available, but many of these are unselective, yielding complicated mixture of products.[22] The four main problems are:

a) The high *reactivity* of the oxidizing species required prior to/during C-H functionalization.

b) The control of *chemoselectivity* to avoid undesired over-oxidized products.

c) The control of *regioselectivity* to discriminate among the various C-H groups present in a substrate with little electronic and structural differences.

d) The desirable *stereoselectivity* for the diastereoselective and/or enantioselective functionalization, which represents a very attractive method for the construction of enantiomerically enriched molecules.[23]

It is important to mention that C-H bonds present an innate relative reactivity against oxidizing agents,[24] and this reactivity is governed by bond strengths, sterics, electronics, stereoelectronics and torsional effects.[21, 25, 26] The intrinsic reactivity of such C-H bonds is the one that defines the site selectivity in the oxidation of molecules containing different C-H bonds.

The continuous development of new C-H functionalization methodologies offers to provide more efficient synthesis with minimal functional group manipulations, enabling the rapid build-up of complex molecules. Moreover, the site selective oxidation, overriding intrinsic reactivity patterns, by the use of catalysts makes these transformations particularly interesting.

I.2 Metalloenzymes as source of inspiration

In nature, enzymes catalyze most of the reactions in living organisms. The ones that contain metal ions as cofactor, are known as metalloenzymes. Metalloenzymes are involved in a number of diverse oxidative processes, which expand from biosynthesis of metabolites, to degradation of xenobiotics, DNA repair, and antibiotic biosynthesis, just to name a few.[27-33]

Typical oxidation reactions mediated by these enzymes include C-H hydroxylation and desaturation, olefin and arene epoxidation and *cis*-dihydroxylation, alcohol oxidation, C-C oxidative cleavage, sulfide and sulfoxide oxidation, and halogenations.[34-38] Most of these reactions exhibit exquisite substrate specificity as well as regio-, chemo- and enantioselectivity, and operate under mild conditions through inherently 'green' processes, as their reactions are remarkably efficient, producing minimum, if any, waste.

The active sites of these enzymes exhibit a rich structural diversity and are able to exist in multiple oxidation states. This high richness is crucial for the enzymes to carry out the biochemical transformations aforementioned. However,

common principles regarding the coordination architecture of the metal active sites can be identified. For instance, nitrogen, oxygen or sulfur donor molecules are the most frequently atoms bound to the active sites, and, in most of the cases, are part of amino acids residues present in the surrounding protein.

With all this aforementioned benefits, it is not surprising that synthetic chemists take metalloenzymes as source of inspiration for the design of functional models, trying to mimic the activity of the enzyme, and structural models, to gain insight into the biological systems. This strategy consists in designing and studying low weight synthetic complexes that could reproduce structural, spectroscopic and/or chemical properties of an enzyme (figure I.1).

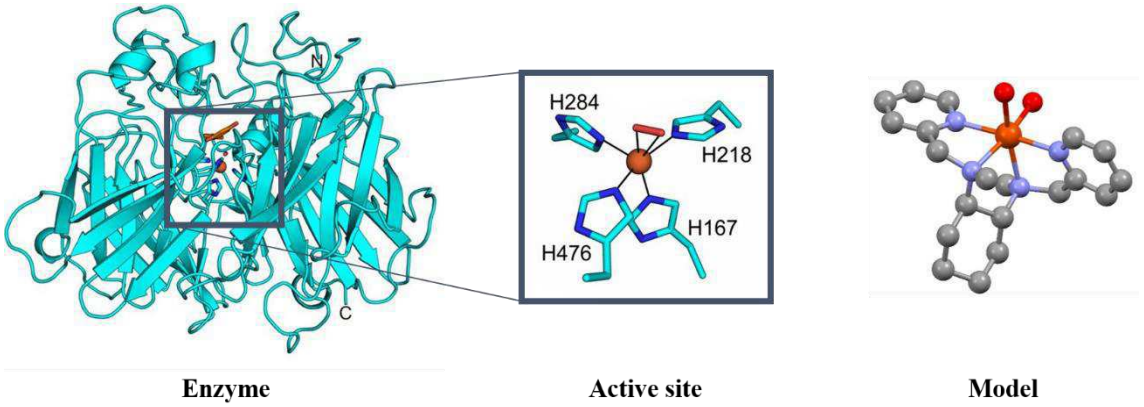

Figure I.1. Design of model compounds from the bioinspiration of metalloenzyme's metal active site.

In the particular case of oxidation reactions, biological inspiration can be taken to design metal catalysts, which often begins with the preparation of a suitable ligand, that will contain N, O or S donor ligands, that in combination with biologically relevant transition metals (basically iron, copper and manganese) should reproduce the catalytic reactivity of enzymes. Therefore, these catalysts must activate O_2 or peroxides to produce oxidizing species, finally responsible for substrate oxidation.

In this thesis, we take advantage of this biomimetic approach to develop some iron and manganese coordination complexes, inspired in structural aspects of the first coordination sphere of the active site of mononuclear iron or manganese enzymes, which then are further studied as catalyst for the selective oxidation of C-H and C=C bonds, with the aim to develop methodologies that could be suitable for preparative organic synthesis. Thus, some remarkable examples of oxidases relevant for the development of our catalysts are described in the following lines.

I.2.1 Iron in biological systems

Iron is the metal ion of choice for a number of crucial processes and it is necessary for many biological oxidations because of its rich coordination chemistry of its two main redox states, Fe^{2+} and Fe^{3+}, and because of its abundance in the Earth.[39] Iron-containing biological molecules play important roles in biologically essential transformations, such as biological oxidations and oxygen transport, and it is found in the active center of a variety of metalloenzymes such as oxidases, hydrogenases, reductases, dehydrogenases and dioxygenases. [40]

There are a lot of remarkable transition-metal-dependent oxidative enzymes capable of activating dioxygen and catalysing reactions of a wide range of substrate like alkanes, olefins, alcohols... Among them, cytochrome P450 and Rieske oxygenase families would be highlighted.

I.2.1.1 Cytochrome P450

The large superfamily of cytochrome P450 (Cyt P450) is one of the most widespread and diverse enzyme systems in nature, and has provided very detailed knowledge about how O_2 activation takes place in biological systems.[41-44] The most common oxidative reaction performed is the monooxygenation of an organic compound by the insertion of an oxygen atom from molecular oxygen.[32] This monooxygenation reactions include aliphatic and aromatic hydroxylation, N-hydroxylation, oxygenation of heteroatoms (N, S, P, I), alkene and arene epoxidation. Besides, the enzyme also catalyzes dehalogenation, deamination and N-, O- and S-dealkylation. Cyt P450 have long been known to mediate the oxidative processes involved in drug metabolism, biosynthesis of steroids and the detoxification of harmful substances.

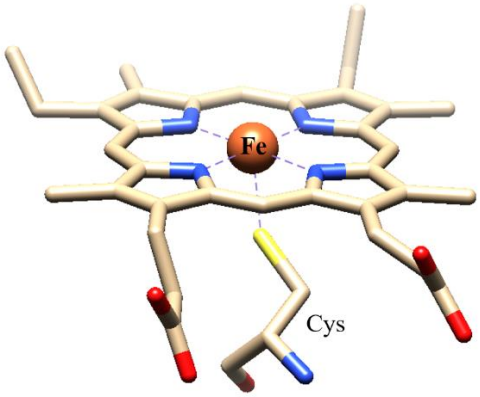

Figure I.2. The active site of cytochrome P450 enzymes adapted from ref. 17. The oxygen atoms are in red, the nitrogen atoms in blue, sulfur atom in yellow and the carbon atoms are in the same color as the bonds.

The active site of Cyt P450 enzymes is known in detail from several X-ray crystal structures.[45-50] It consists in a ferric iron atom ligated to four nitrogen atoms of a highly-conjugated and planar macrocycle (protoporphyrin),[51] the proximal ligand is a thiolate anion from a deprotonated cysteine residue located in the polypeptide chain[52] and the distal coordination site is occupied by an easily exchangeable water molecule or a hydroxide ligand that can be displaced by substrate binding to the active site (figure I.2).[53]

Extensive efforts have been dedicated to identify and to characterize the powerful oxidizing intermediates involved in the catalytic cycle of Cyt P450 to understand the underlying reaction mechanism of each enzymatic step. The principal features of the catalytic cycle are nowadays well-defined, and the mechanism of P450s in which the substrate RH is oxidized to R-OH in a series of steps is shown in scheme I.3.[54]

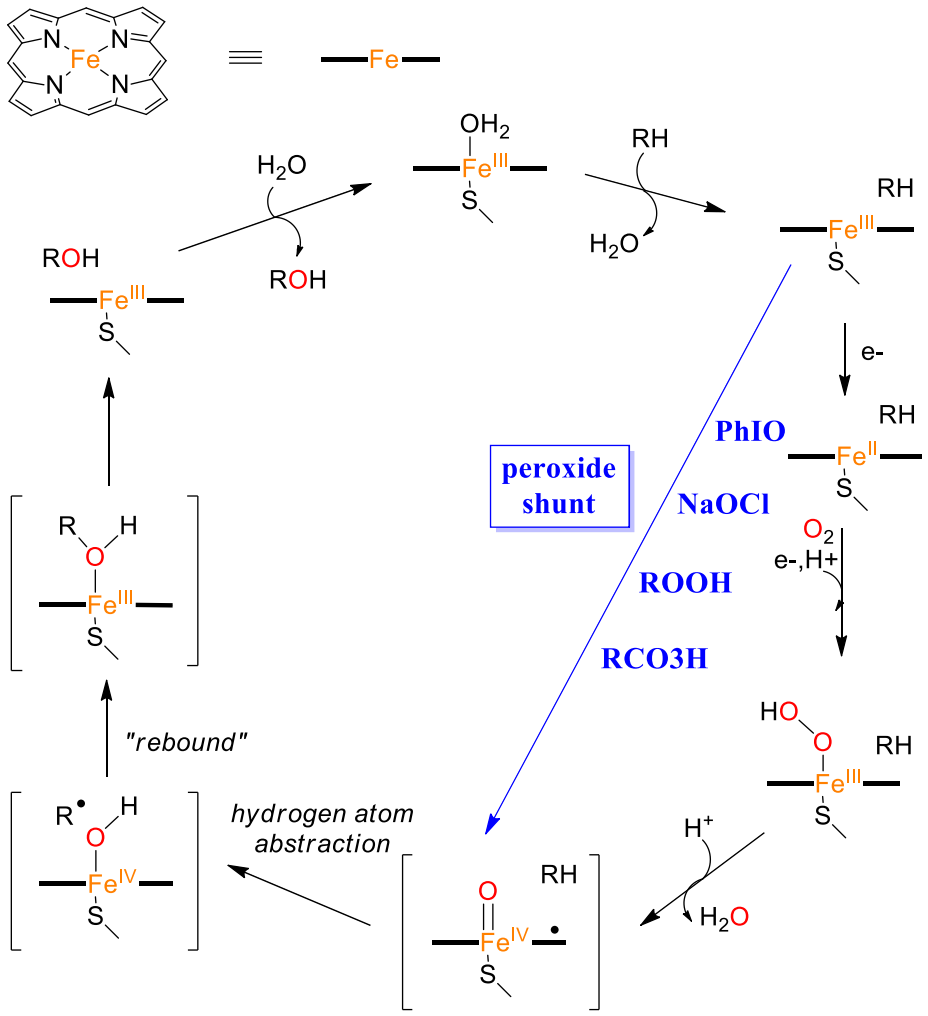

Scheme I.3. Established cytochrome P450 catalytic cycle.

In brief, substrate displaces the water ligand in a reversible manner with a subsequent one-electron reduction of Fe^{III}.[55-58] Oxygen binding to the ferrous state

leads to formation of the relatively stable ferric superoxo intermediate.[44] A second electron generates the ferric-peroxo intermediate, which corresponds to the rate-limiting step, due to the short life of the species formed. Protonation of this intermediate leads to the hydroperoxoiron(III) complex, which undergoes proton assisted heterolytic O-O bond cleavage and formation of a high valent oxoiron(IV) porphyrin π radical cation complex and a water molecule.[42, 59-62] This highly reactive species abstracts a H atom from the substrate resulting in a ferryl hydroxyl intermediate and a substrate radical, and then, hydroxyl moiety on the iron combines with the substrate radical. This two-step process is known as "oxygen rebound".[41, 63-65] The final release of the hydroxylated product regenerates the ferric resting state. Direct cycling between the resting state and the high-valent oxidant species can be performed by using oxidants such as hydro and alkylperoxides, NaOCl, PhIO or peracids. This shortcut is known as the "peroxide shunt" and it receives use in catalysis (scheme I.3).[51]

I.2.1.2 Rieske oxygenases

Rieske non-heme iron-dependent oxygenases (ROs) play an important role in bioremediation and are prominently found in soil bacteria.[66] Their reactions constitute the initial step for bacterial biodegradation of aromatic hydrocarbons.[28, 67-69] ROs are structurally more complex than other dioxygenases due to the need for an efficient electron transfer pathway to mediate the additional, simultaneous two-electron reduction of the aromatic substrate. In such pathways, they typically catalyse *cis*-1,2-dihydroxylation, introducing two hydroxy groups in only one enzymatic step.[70-72] However, they have also been shown to play important roles in natural product biosynthesis, such as monohydroxylations, dealkylations, desaturations, epoxidations and oxidative cyclizations, greatly expanding their catalytic repertoire.[68, 73-76] Such versatility has led to consider Rieske dioxygenases as the non-heme analogous of Cyt P450. Displaying a broad substrate scope, the conversion of unnatural substrates by ROs has started to receive a growing attention within recent years, as the regio- and stereospecific allylic hydroxylation of C-H bonds is of particular interest.

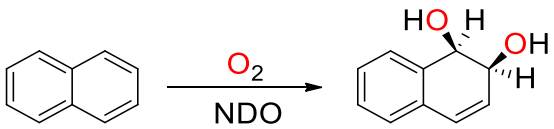

Scheme I.4. *cis*-Dihydroxylation reaction of naphthalene catalyzed by naphthalene 1,2-dioxygenase.

From all the enzyme's family, the best-characterized Rieske oxygenase is naphthalene 1,2-dioxygenase (NDO) from the bacteria *Pseudomonas putida*,[77-79] which catalyses the *cis*-dihydroxylation of naphthalene (scheme I.4) and it is

known that in the course of catalysis, both atoms of oxygen are incorporated into the *cis*-diol product. The active site of NDO shows the characteristic structure of ROs, formed by a reductase component (Rieske-type Fe_2S_2 cluster) which binds cysteine (Cys) and histidine (His) residues, and the oxygenase component where a His residues and an aspartate (Asp) residue in the C-terminal domain form a facial triad that coordinates the active site ferrous ion (figure I.3). A second Asp residue forms a bridge between the two components, and is believed to mediate the transfer of electrons (coming from NAD(P)H) from the reductase component to the oxygenase component, where O_2 activation and substrate dihydroxylation occur.[80, 81]

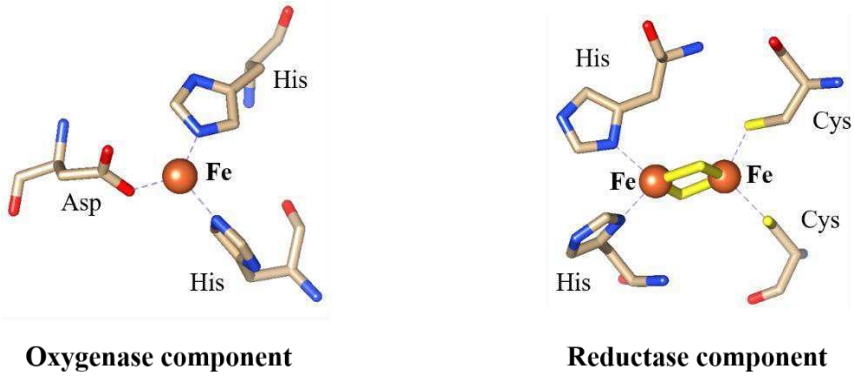

Figure I.3. Active center of Rieske dioxygenase showing the oxygenase and reductase components adapted from ref. 32. The oxygen atoms are in red, the nitrogen atoms in blue, sulfur atoms in yellow and the carbon atoms are in the same color as the bonds.

The iron–sulfur cluster from Rieske oxygenases marks them apart from other classes of non-heme iron-dependent oxygenases,[70] but crystallographic data on different iron oxygenases have established the occurrence of a common structural motif that binds the divalent iron center, the 2-His-1-carboxylate facial triad (figure I.4).[82] In ROs superfamily, this moiety is present in the oxygenase component and it consists in three protein residues (two His and a bidentate Asp or glutamate (Glu)) that leave three *cis* sites available for exogenous ligands binding (scheme 5). In the isolated enzymes, these sites are usually occupied by solvent molecules but they can accommodate both substrate (or co-substrate) and O_2, bringing them into close proximity for subsequent reaction.

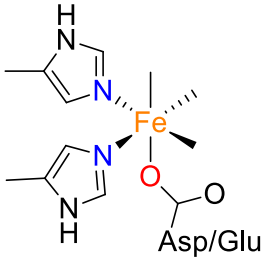

Figure I.4. Schematic representation of the 2-His-1-carboxylate facial triad found in some mononuclear non-heme iron enzymes.

The proposed catalytic cycle for NDO is shown in scheme I.5. Binding of naphthalene to the active site of the enzyme results in a change of the ferrous ion coordination geometry to a five-coordinate square pyramid. This modification together with the one electron reduction of the [Fe_2S_2] center promotes the oxygen binding to form a side-on peroxo (or hydroperoxo)-iron(III) species.[83, 84] Being the last detectable intermediate before the substrate oxidation.[82, 85] After that, O–O bond cleavage would generate presumably a Fe(V)(O)(OH) complex. This proposal is supported by labelling studies showing incorporation of ^{18}O from $H_2{}^{18}O$ in the *syn*-diol. Metal-oxo species rapidly exchange with water, and therefore, the incorporation of ^{18}O from $H_2{}^{18}O$ into products is an indirect evidence in favour of its formation in the reaction.[86] The high-valent species reacts with the substrate to form the ferric dihydroxynaphthalene complex, [30, 71, 87] which after protonation and a second electron transfer from the Rieske cluster, releases the product and regenerates the resting state of the enzyme. Nevertheless, the superoxoiron(III) (or hydroperoxoiron(III)) species have been also proposed to be the active oxidant for *cis*-diol formation.[88]

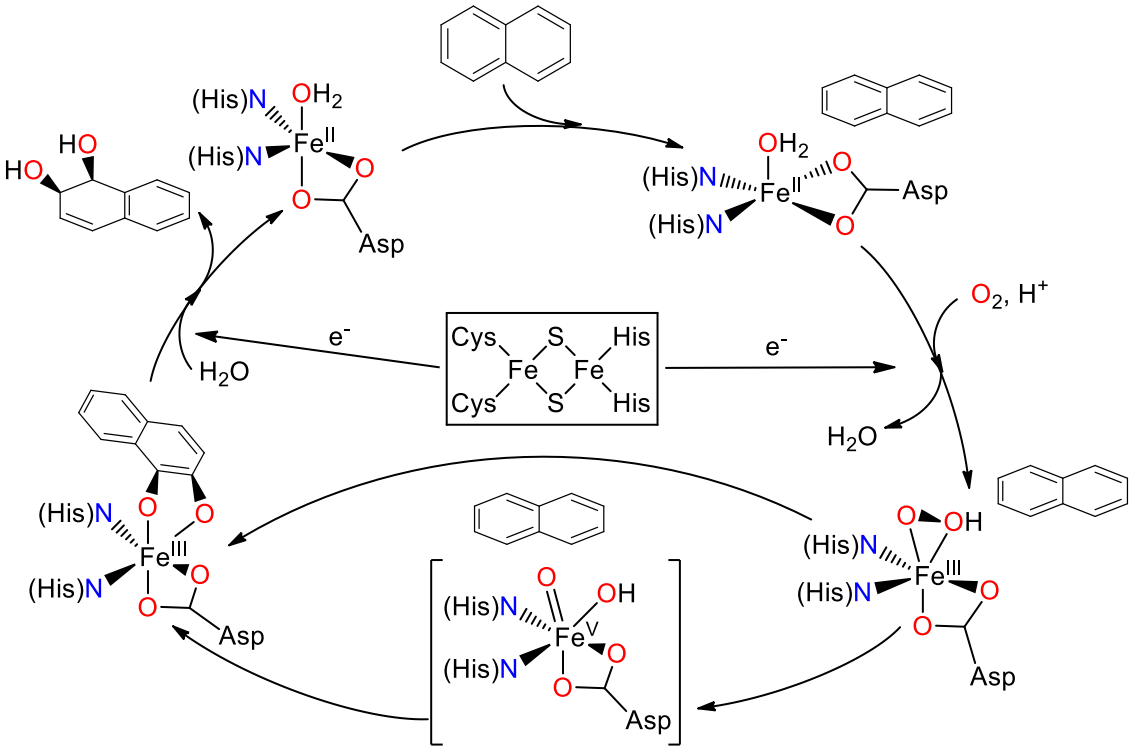

Scheme I.5. Catalytic cycle proposed for Rieske dioxygenases.

As in Cyt P450, NDO can carry out the oxidation reaction via a "peroxide shunt" by using hydrogen peroxide as oxidant. Overall, a number of evidences point towards a common mechanistic landscape operating in Cyt P450 and Rieske dioxygenases and suggesting that high-valent iron species are responsible for the catalysis.

I.2.2 Manganese in biological systems

Manganese is recognized as an absolutely required micro-nutrient in all forms of life, having a polyfunctional role in biological systems. It can act as a cofactor in a wide array of enzymes such as oxidoreductases, hydrolases, ligases, lectins, isomerases, oxygenases, transferases, lyases, etc. and the oxygen evolving center of photosystem II.[40] Its high abundance and ability to access different oxidation states (II-IV, VI and VII being the most commons) likely led to be recruited by biology to perform a remarkable range of catalytic functions. Its deficiency or uncontrolled excess provoke diseases, disorders or syndromes in living organisms.[89, 90]

The first functional role of Mn is as a Lewis acid, like the divalent ions Mg, Ca and Zn (M^{2+}), highly used in aqueous solution due to their stability in acid conditions.[91] A second practical function is their use as oxidation catalyst when it presents higher oxidation states (Mn^{+3} and Mn^{+4}).

In general, the relevant redox functions of manganese in enzymes come into play largely with oxygen as the substrate or product. The unique redox properties of Mn are essential to the generation of dioxygen from water in the oxygen-evolving complex. It has been proposed that $Mn^{V}(O)$ or a $Mn^{V}(O)$-organic radical is the active species able to oxidize H_2O_2 and form O_2.[92, 93] The water-splitting protein has four Mn atoms at its active center and these are thought to act as charge accumulators so that the four-electron oxidation of water can occur as one event.[94]

Another well-known enzyme which contains Mn and which also evolves O_2, is the superoxide dismutase (Mn-SOD). Superoxide is a normal by-product of aerobic metabolism and is produced in many of the key biological processes. Thus, superoxide dismutases catalyze the disproportionation of superoxide radical to oxygen and hydrogen peroxide, protecting the cell against toxic products of cellular respiration.[95] The mechanism involves the sequential reduction and oxidation of the metal center, with the concomitant oxidation and reduction of superoxide radicals.[96] The active site of Mn-SOD presents 3His and 1 Asp residues bound to the metal and a solvent molecule (water or hydroxide ion) forming a trigonal bipyramidal coordination (figure I.5, a).[97]

Another interesting group of enzymes that use O_2 as oxidant are catechol dioxygenases. They catalyze the cleavage of the carbon-carbon bond between the two hydroxyls of the catechol (intradiol) or the cleavage of the carbon-carbon bond adjacent to the enediol moiety (extradiol).[98] These enzymes also possess a mononuclear Mn(II) center, and the Mn(II) ion in the resting enzyme is

coordinated by the side chains of two histidine residues and a glutamate (figure I.5, b).

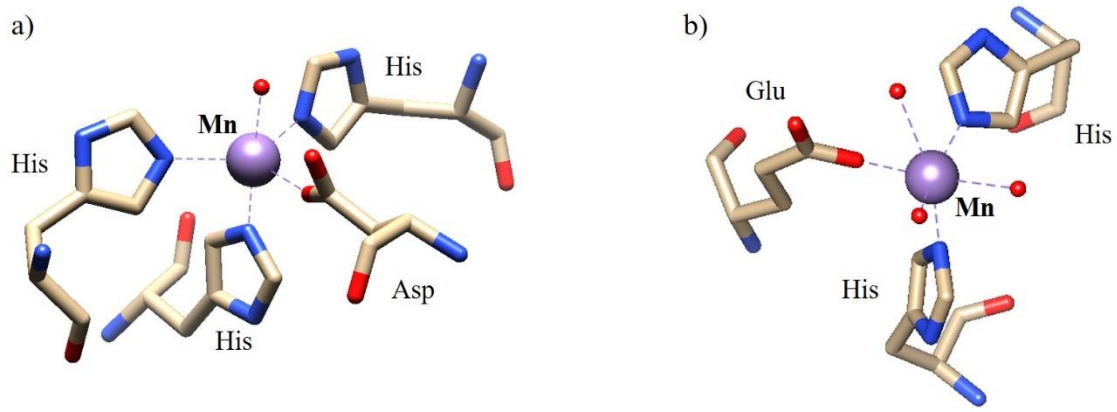

Figure I.5. Structure of the active center of a) manganese superoxide dismutase and b) manganese dependent extradiol-cleaving catechol dioxygenase adapted from refs. 45 and 47. The oxygen atoms are in red, the nitrogen atoms in blue and the carbon atoms are in the same color as the bonds.

More intriguing is that most of extradiol-cleaving enzymes typically use Fe(II), although few utilize Mn(II) in their active site.[98] They are able to catalyze the same reaction on the same substrate, but the protein requirements over the metal ion are distinct.[99] This homology between those metals also arises in Fe- and Mn-dependent superoxide dismutases. Suggesting that Mn and Fe oxidation chemistry is closely similar. Consequently, different authors have used and are using manganese as metal in "iron-like" oxidation catalysis.

I.3 Model compounds: bioinspired iron and manganese complexes

I.3.1 Relevance of synthetic model systems

For the efficient rational design of synthetic model systems, detailed knowledge of the metalloenzymes structure and function is crucial. Such 'bioinspired' or 'biomimetic' catalysts may have some advantages over metalloenzymes, like expanding the substrate scope, increasing the scale of productions and tuning the selectivity and/or the specificity of the processes.[100]

From an environmental and economic points of view, the requirement of using non-toxic and inexpensive reagents, oxidants, and abundant transition metals (such as Fe, Mn and Co) and avoiding energy-consuming processing steps and undesirable reaction media is gaining awareness.[101] There is special interest in the use of oxygen or hydrogen peroxide as environmentally friendly oxidants,

because water was obtained as the only by-product.[30] O_2 activation is very complex and often requires the use of sacrificial reducing agents, increasing the amount of waste. On the other hand, H_2O_2 presents few drawbacks, as it can disproportionate and its manipulation is dangerous at high concentrations.[102-104]

Therefore, the design of biologically inspired oxidation catalysts containing inexpensive and readily available metals can provide important insights into biological pathways and would led to understand and reproduce the catalytic functionality of metalloenzymes for practical applications. When compared to metalloenzymes, the synthesized complexes would be simpler, easier to handle, easier to purify and with easier ligand modulation, but at the same time, should be robust, efficient and selective.

I.3.1.1 Ligand design

The accurate design of the ligand for selective and efficient catalysts is essential, yet not obvious. The coordination substituents and the geometries from metal active sites in metalloenzymes offer an initial source of inspiration for small-molecule catalyst designs. But the continuous research and intensive effort of synthetic chemists in hunting the best catalyst is the major driving force for ligand design. Indeed, from the wide variety of ligands (and corresponding complexes) synthetized, only few example showed high efficiencies and selectivities when combined with H_2O_2. A common feature can be found in most of those scaffolds: they are tetradentate N-donor ligands (figure I.6).

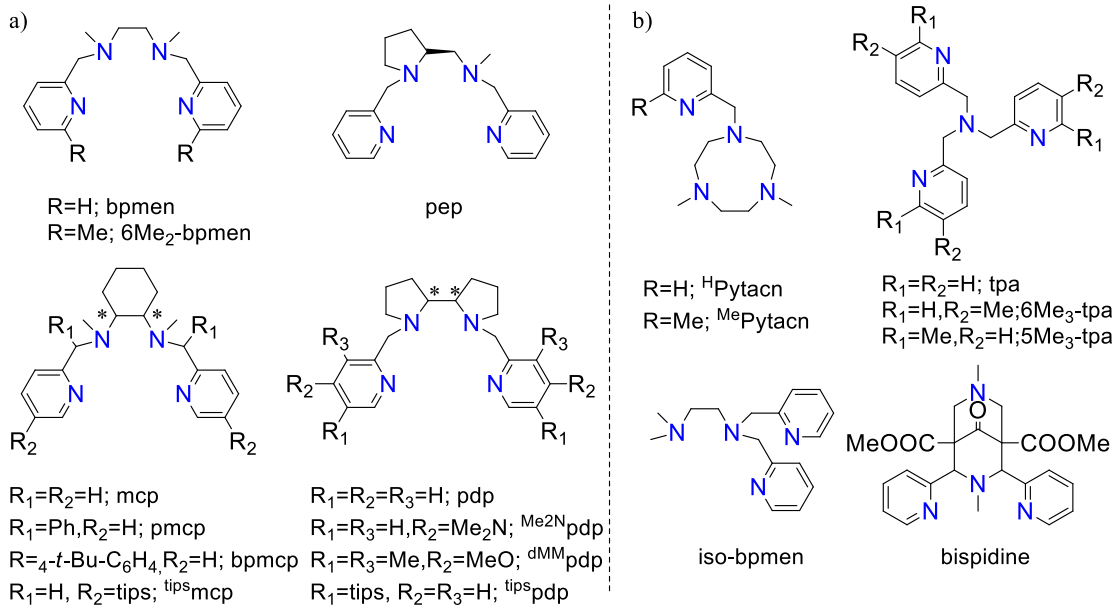

Figure I.6. Schematic representation of the most relevant tetradentate ligands used to prepare mononuclear iron(II) and manganese(II) complexes to perform oxidation catalysis of C-H bonds and epoxidation of C=C bonds.

It is known that linear tetradentate ligands (figure I.6, a) can form three isomerically related octahedral complexes depending on the way they wrap around the metal center: *cis*-α, *cis*-β and *trans* topologies (figure I.7, a).[105-110] Moreover, when *cis*-α topology was obtained, the chirality (*S*,*S*) or (*R*,*R*) of the corresponding diamine backbone used for the synthesis of the ligand, predetermines generation of complexes with Λ and Δ chirality at the metal, respectively (figure I.7, b).[106]

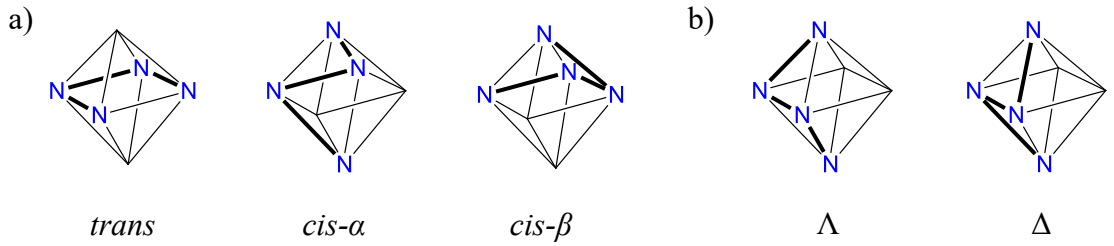

Figure I.7. a) Three different topologies that can be adopted by linear tetradentate ligands. b) The *cis*-α topologies that determines the Λ and Δ chirality at the metal.

Various studies have described the relationship between the geometry and the activity of the catalysts, being the *trans*- and *cis*-β topologies less active when compared to *cis*-α.[103, 107-109, 111-114] The importance of the presence of two *cis* labile sites mainly relies in the availability of those sites for the coordination of the oxidant and an additional ligand that facilitates O-O bond scission.[103, 115] Also, due to the intrinsic chirality at the metal defined by the backbone in the *cis*-α-topology, the chirality of the diamine can be transferred to the substrate, as during the catalysis the substrate moves closer to the metal.

I.3.2 Oxidation of alkanes (C-H bonds) by non-heme iron complexes

The first iron system that was able to hydroxylate alkanes with stereoretention by using H_2O_2 as oxidant was reported by Que and co-workers in 1997 using the corresponding iron(II) complex of the tpa ligand (figure I.6 and scheme I.6).[116] Tpa (tripodal) and its modifications together with bpmen (linear) family of ligands (figure I.6) have been also studied in the oxidation of alkanes by Que and co-workers.[117-119] The resulting mononuclear iron(II) complexes are quite efficient catalysts and exhibited a selectivity pattern that suggests a metal based oxidation.[118] However, they reported that the introduction of a methyl in the α position of the pyridine ring of the tpa ligand reduces the percentage of retention of configuration (RC) in the oxidation of *cis*-1,2-dimethylcyclohexane, due to formation of long lived free-radical intermediates. Electronic effects were also investigated by the introduction of substituents in the pyridine moiety. As mentioned before, the structural properties and the nature of the backbone appears to be an important factor in defining the catalytic performance.

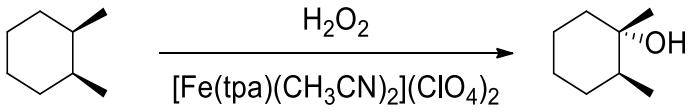

Scheme I.6. Stereospecific oxidation of *cis*-1,2-dimethylcyclohexane by tpa iron(II) complex reported by Que and co-workers.

After this milestone result, a system based on tryazacyclononane (tacn) ligands (figure I.6) was first reported by Costas and co-workers in 2007.[120, 121] The catalysts can efficiently oxidize alkanes using H_2O_2 with high selectivity and stereospecificity (scheme I.6). Moreover, the obtained alcohol products incorporate large amounts of water through a rebound-like mechanism. The substitution in the pyridine ring of the ligand was studied in order to analyze electronic and steric parameters,[122] and the 6-methyl substituted catalyst showed unprecedented efficiency in C-H hydroxylation with stereoretention of configuration. The high product yields obtained make this system amenable for synthetic purposes.[123] Besides its high activity, this catalyst exhibits enhanced selectivity toward methylene sites, while operating under mild experimental conditions.

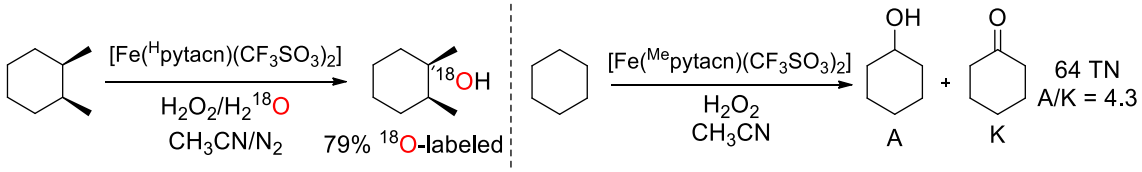

Scheme I.7. Oxidation of alkanes using pytacn based iron catalysts reported by Costas and co-workers.

A major breakthrough was introduced by White and co-workers, exhibiting for the first time the oxidation of aliphatic C-H under substrate-limiting conditions with high yields and selectivities.[124] The system consists on an iron catalyst based on the unsubstituted pdp ligand (figure I.6) that uses a combination of H_2O_2 and acetic acid (a key additive) as oxidant. The oxidation of a broad range of substrates was shown to proceed in moderate to good yield with a predictable selectivity. Although C-H are unactivated and presumed inert, the selective oxidation occurs on the basis of the electronic and steric properties of the C–H bonds, including complex molecules and obtaining synthetically useful yields (scheme I.8). Although the system needed 15% of catalyst loading, and very modest turnover numbers were obtained, the efficiency observed was noticeably better that the previous described. Indeed, in their report, they compare the activity of this new catalyst with the already mentioned bpmen based iron complex, being the former, more efficient under the same conditions.

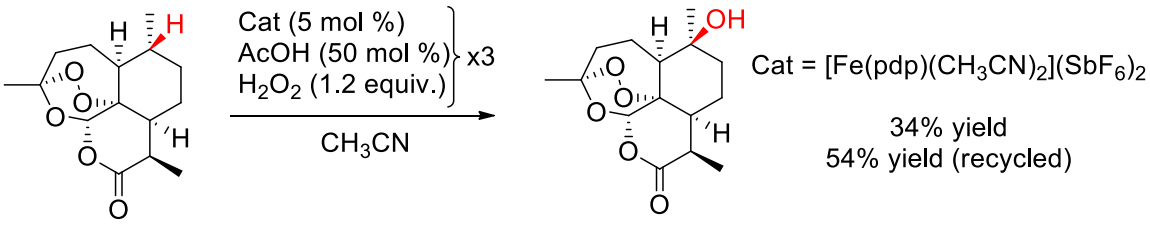

Scheme I.8. Selective hydroxylation of (+)-artemisinin by iron(II) pdp catalyst.

The selective oxidation of the natural molecule (+)-artemisinin took place at the most electron-rich and the least sterically hindered 3° C-H bond with moderate yield (34%), that could be increased to 54% by recycling the starting material twice. A second minor product was also formed from oxidation at a methylene site but was unnoticed. This was reported by the same authors three years later.[125] In the same publication, they study the impact of the combination of different effects on dictating selectivity in methylene oxidations. High chemo-, site-, and even diastereoselective methylene C–H oxidations can be accomplished, without the use of directing or activating groups, yet predictable using the fundamental concepts of electronics, sterics, and stereoelectronics.

Inspired by the well-established principles in oxidation catalysis with heme complexes, Costas and co-workers designed a new catalyst platform based on modifications at well-known bpmen, mcp and pdp ligands (figure I.6) by introducing pinene groups at the β and γ positions of the pyridine rings (figure I.8).[126] The bulky group generates a well-defined chiral cavity around the iron center that protects the iron site against catalyst deactivation and introduces site selectivity in the oxidation of complex molecules and a considerable enhancement in oxidative activity.[127] The chirality in these complexes arises from the stereochemistry of the backbone and from the topological chirality adopted by the ligand upon binding to the metal, giving rise to Λ and Δ complexes when using the (*S*,*S*) or (*R*,*R*) enantiopure diamine respectively. Using very low catalyst loadings (1 mol %) the new system was reported as more efficient than pdp iron based complexes for the oxidation of *cis*-1,2-dimethylcyclohexane, with yields and selectivities very similar to those previously reported by White and co-workers with 2,7-dimethyl-octane derivatives.[124]

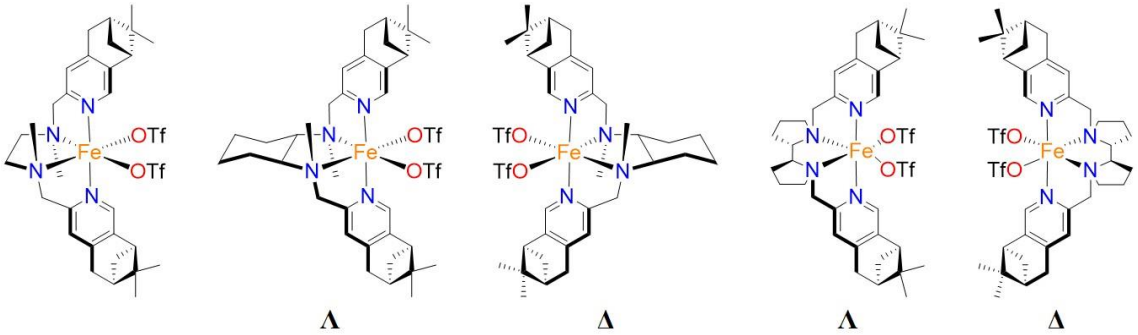

Figure I.8. Structure of pinene-based iron complexes reported by Costas and co-workers.[126]

This work demonstrated that the chirality of the catalysts, the nature of the ligand diamine backbone, and the presence of a cavity-like site surrounding the iron center are structural aspects that can translate into C–H site selectivity.

The same year, a similar strategy has been adopted by White by positioning electronically deactivated, rotationally blocked aryl rings on the β-pyridine position on the pdp ligand (scheme I.9).[128] The new catalyst narrows the cone of available trajectories for the approaching substrates enabling catalyst-controlled selectivity that enhances or overturns the substrate's inherent reactivity preference for oxidation. For example, as seen previously, the oxidation of (+)-artemisinin with $[Fe(pdp)(CH_3CN)_2](SbF_6)_2$ complex yields as major product (+)-10β-hydroxyartemisinin, corresponding to the oxidation at the most electron-rich and the least sterically hindered tertiary C-H bond (substrate control). Nevertheless, for the $[Fe(^{CF3}pdp)(CH_3CN)_2](SbF_6)_2$ catalyst, the major product consists on the oxidation at the methylenic carbon C9 (catalyst control), overriding a strong electronic substrate bias (scheme I.9). This performance can be observed over a range of topologically diverse substrates.

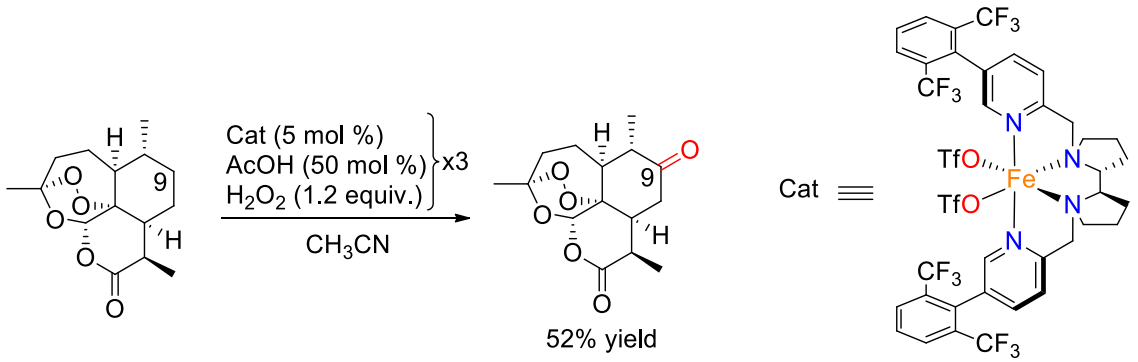

Scheme I.9. Selective oxidation of (+)-artemisinin by $[Fe(^{CF3}pdp)(CH_3CN)_2](SbF_6)_2$ catalyst reported by White and co-workers. The yield implies the recycling of the starting material 5 times.

Very recently, in our group, an alternative design introducing bulky substituents at the pyridine β position was reported.[129] The insertion of

triisopropylsilyl (tips) groups also create a cavity-like space around the metal site which leads to higher efficient catalysts with a preference oxidation of stronger but more accessible secondary C-H bonds over tertiary ones (scheme I.10). The discrimination among 3° and 2° alkyl C-H bonds is mainly due to steric effects, as the sterically bulky iron catalysts prefer secondary C-H bonds, which are less sterically crowded.

The enhanced selectivity toward the oxidation of methylenic sites was also observed in complex organic molecules such as terpenoids and steroidal compounds, achieving synthetically amenable yields and demonstrating a high potential for application in fine chemicals synthesis. Moreover, the major product obtained was dependent on the catalyst employed, and the chirality at the metal defined the oxidation regioselectivity between two distinct methylenic sites in steroidal molecules (scheme I.10).

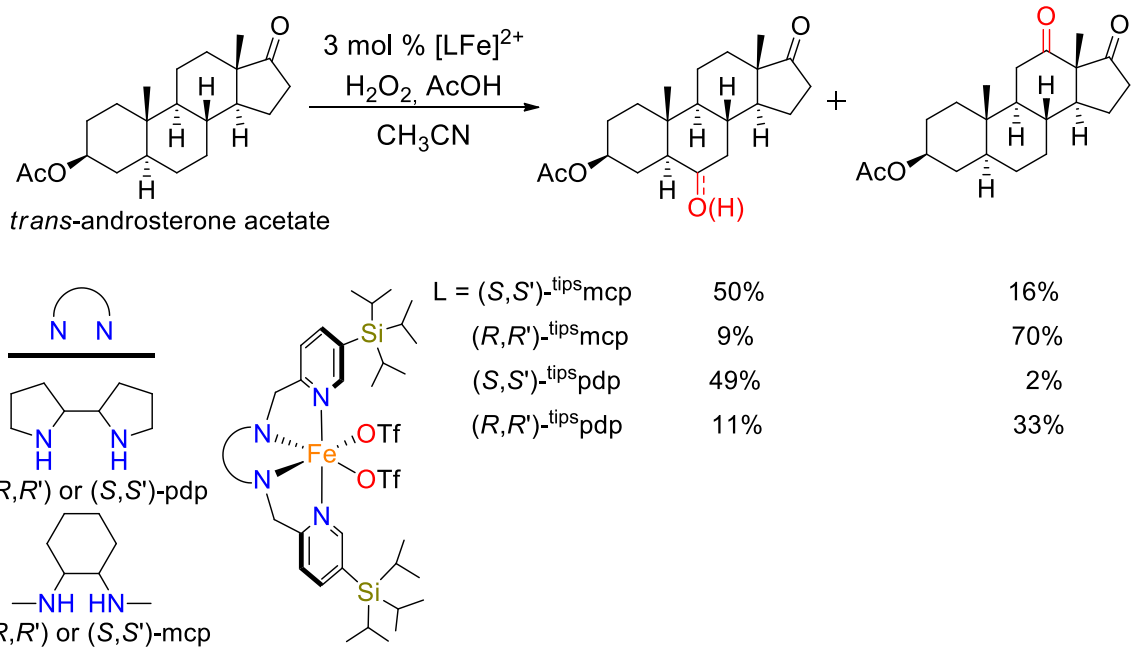

Scheme I.10. Oxidation of *trans*-androsterone acetate mediated by the opposite enantiomers of tips substituted iron complexes reported by Costas and co-workers.[129]

I.3.3 Epoxidation of alkenes (C=C double bonds) by non-heme iron complexes

Until the 2000s, the combination of non-porphyrinic iron catalysts and hydrogen peroxide to perform epoxidation reactions in preparative scale had remained underrepresented. One of the first examples with potential applicability in organic synthesis was reported by Jacobsen and co-workers in 2001.[130] The complex prepared in situ from iron perchlorate and bpmen ligand (figure I.6) was able to epoxidize aliphatic alkenes in short reaction times with high isolated yields by using only 1.5 equiv. of H_2O_2, in the presence of substoichiometric amounts of acetic acid (scheme I.11).

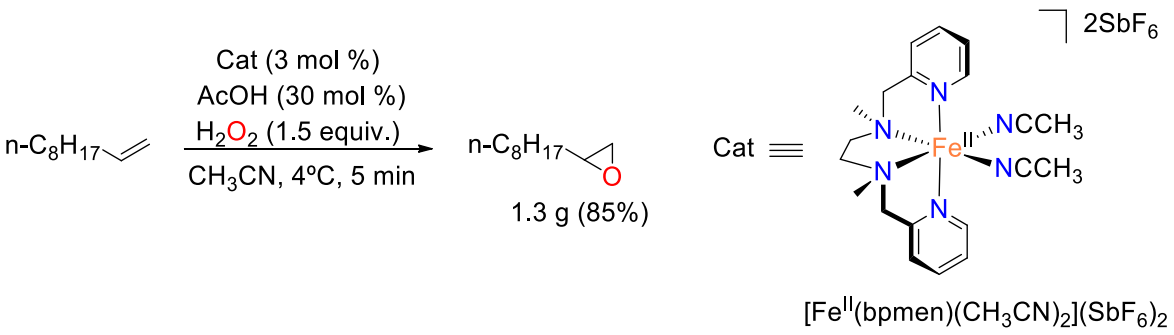

Scheme I.11. Epoxidation of 1-decene catalyzed by $[Fe(bpmen)(CH_3CN)_2](SbF_6)_2$.

A major breakthrough was made by Beller and co-workers in 2007 who reported a practical method to epoxidize alkenes at room temperature and under aerobic conditions.[131] The catalyst is generated *in situ* by the combination of commercially available $FeCl_3{\cdot}6H_2O$ as iron source, pyridine-2,6-dicarboxylic acid as additive and simple amines, such as benzylamine, 4-methylimidazole, and pyrrolidine, acting as ligands. The system can activate H_2O_2 to epoxidize a wide array of aromatic alkenes and through the use of a enantiomerically enriched 1,2-diphenyl-ethylene-1,2-diamine the authors have extended their approach to asymmetric epoxidations (scheme I.12).[132] Indeed, *trans*-stilbene derivatives are epoxidized with moderate to excellent yields and enantioselectivities (up to 92% and 97% ee, respectively). However, the steric factors are more important than electronic factors in controlling the enantioselectivity, therefore, the stereoselectivity depends mainly on substrate symmetry and bulkiness.

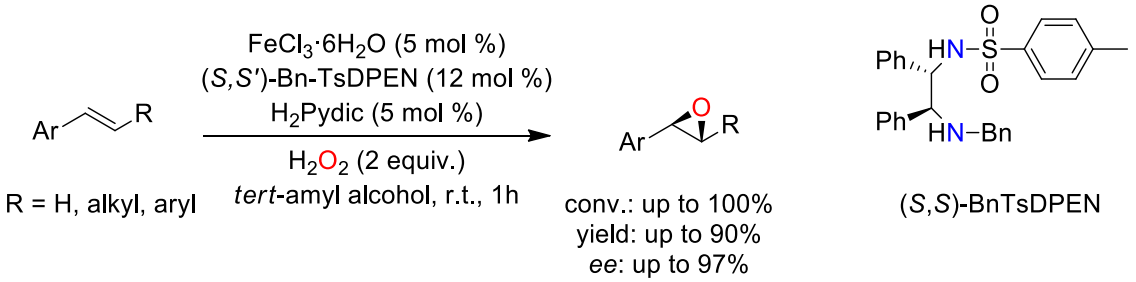

Scheme I.12. Asymmetric epoxidation of aromatic alkenes using a enantiomerically enriched diamine, $FeCl_3{\cdot}6H_2O$, H_2O_2 and dipicolinic acid.

It is important to notice, that this system is a clear example of a simple biomimetic approach by mixing basic type ligands (carboxylic acids and amines) present in non-heme iron oxygenases with a metal salt.

In 2011, Sun described for the first time the use of the chiral iron(II) complex based on the *N,N'*-dimethyl-*trans*-1,2-cyclohexanediamine backbone (scheme I.6) in the epoxidation of α,β-enones with remarkable levels of enantioselectivity employing H_2O_2 as oxidant.[133] The authors also developed and studied more structurally elaborated catalysts by introducing some modifications in the mcp scaffold (scheme I.13). The addition of two chiral groups in pseudo-benzylic

position of the pyridines leads to a more robust catalyst with increased activity and, more interestingly, enantioselectivity, displaying up to 87% ee for substituted *trans*-chalcones. The principal limitation is that the system appears to be applicable only for epoxidation of aromatic *trans*-α,β-enones.

One year later, the same group developed a tetradentate N-ligand based on a more rigid enantiopure diamine template derived from L-proline and two benzimidazole donors instead of pyridines .[134] The corresponding iron(II) complex was an active catalyst for the highly enantioselective epoxidation (up to 98% ee) of a broad range of di- and trisubstituted enones (scheme I.13). Taking advantage of the improved results obtained with the benzimidazole moiety, in 2013, Sun reported the adaptation of the mcp ligand with the replacement of the pyridines by 1-methylbenzimidazoles.[135] The resulting iron(II) catalyst exhibited much higher enantioselectivity when compared to the pyridine substituted one and similar results to the L-proline derived one.

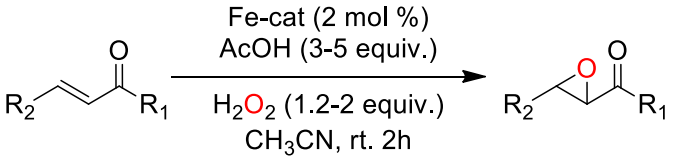

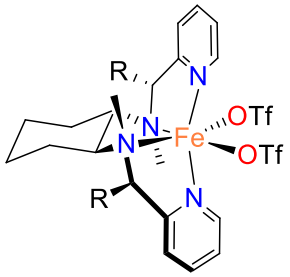

Selected examples

R_1 = Ph, R_2 = Ph, 53%, 77% ee
R_1 = Ph, R_2 = *p*-Cl-Ph, 90%, 84% ee
R_1 = Ph, R_2 = *p*-F-Ph, 73%, 87% ee
R_1 = *p*-Me-Ph, R_2 = Ph, 61%, 82% ee

R = H; (*R,R'*)-[Fe(OTf)$_2$(mcp)]
R = Ph; (*R,R,R,R'*)-[Fe(OTf)$_2$ (pmcp)]
R = 4-*t*-Bu-C$_6$H$_4$; (*R,R,R,R'*)-[Fe(OTf)$_2$(bpmcp)]

R_1 = Ph, R_2 = Ph, 89%, 92% ee
R_1 = Ph, R_2 = *p*-Cl-Ph, 97%, 94% ee
R_1 = *o*-Cl-Ph, R_2 = Ph, 78%, 91% ee
R_1 = *p*-Me-Ph, R_2 = *p*-F-Ph, 93%, 92% ee

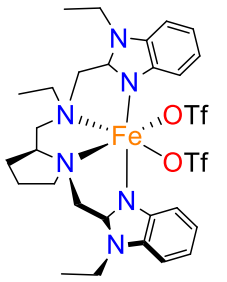

(*S*)-[Fe(OTf)$_2$(peb)]

R_1 = Ph, R_2 = Ph, 94%, 93% ee
R_1 = Ph, R_2 = *p*-Me-Ph, 71%, 87% ee
R_1 = Ph, R_2 = *p*-Cl-Ph, 81%, 93% ee
R_1 = *p*-F-Ph, R_2 = Ph, 85%, 87% ee

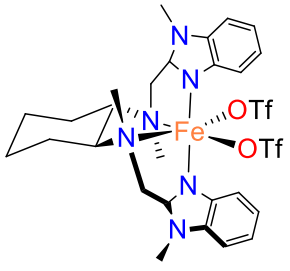

(*R,R'*)-[Fe(OTf)$_2$(mcmb)]

Scheme I.13. Asymmetric epoxidation of substituted *trans*-chalcones using the iron catalysts reported by Sun and co-workers.[133-135]

In 2011, Yamamoto designed a mononuclear iron catalyst bearing phenanthroline ligands derivatized with binaphthyl moieties (scheme I.14).[136] The catalyst can either be prepared *in situ* or isolated, and is capable to epoxidize acyclic β,β-disubstituted enones. These substrates appeared very difficult to epoxidize with stereoselectivity due to the steric congestion at the β carbon. The usually Weitz-Scheffer-type methods used for their epoxidation lead to diastereomeric mixtures. The β-substituents generate steric repulsions that cause breaking of the conjugation. Thus, the electrophilicity of the double bond in those substrates is thought to be weak and the reactivity toward electrophilic epoxidation should be increased, as it is in the case of Yamamoto's system.

The epoxidation proceeds with good yields (61-88%) and excellent enantioselectivities (90-92% ee), by using peracetic acid or mCPBA as terminal oxidants, but unfortunately H_2O_2 was not a suitable oxidant (scheme I.14). This system is also competent for the epoxidation of trisubstituted α,β-unsaturated esters, providing epoxide products with high enantioselectivities (63-99% ee), although only in moderate yields in most cases (16-69%).[137]

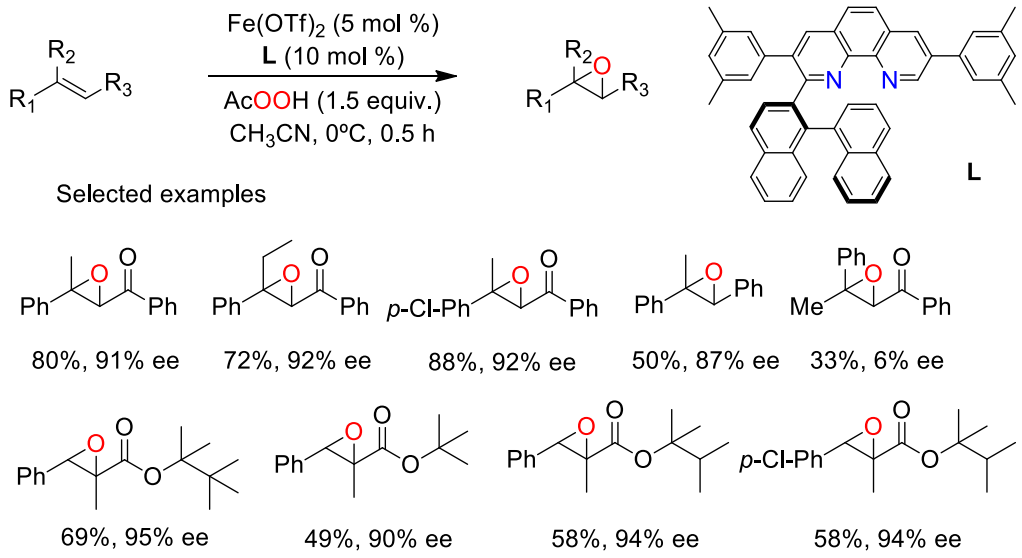

Scheme I.14. Asymmetric epoxidation of β,β-disubstituted chalcones and trisubstituted α,β-unsaturated esters with the system reported by Yamamoto.

In 2012, the chiral iron(II) pdp based complex (figure I.6) was used by Talsi and co-workers for the first time in the asymmetric epoxidation of various olefins with hydrogen peroxide as oxidant.[138] The use of the 2,2'-bipyrrolidine backbone instead of the *N,N'*-dimethyl-*trans*-1,2-cyclohexanediamine led to improved enantioselectivities in the epoxidation of chalcones. The authors also examined the effect of different carboxylic acids and the enantioselectivity of the epoxide product increased with growing steric demand of acidic additives, obtaining the best results with 2-ethylhexanoic acid (scheme I.15). The system exhibited high efficiency (up to 1000 TON) and selectivity (up to 100%), and presented good to high

enantioselectivity (up to 93% ee). Although *trans*-chalcone derivatives exhibit the best results, the system can be also applied to other substrates such as chromene derivatives, *trans*-cinnamate and styrene derivatives, still obtaining only moderate enantioselectivities.

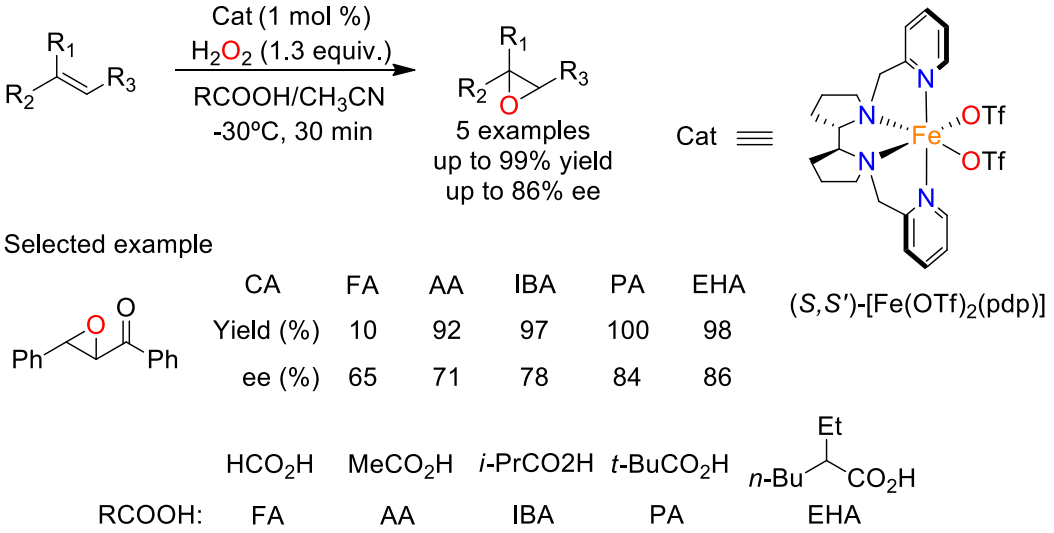

Scheme I.15. Asymmetric epoxidation of olefins with the (*S,S*)-[Fe(OTf)$_2$(pdp)] complex, H_2O_2 and different carboxylic acids.

An alternative methodology for manipulating the catalytic properties of iron aminopyridine complexes was reported in 2013 by our group.[139] Selecting the pdp complex as base, an in deep screening of the substitution in the pyridine moiety resulted in a series of complexes, the enantioselectivity of which increased with increasing electron-donating properties of the substituents. Taking *cis*-β-methylstyrene as a model substrate and H_2O_2 as oxidant, the dimethylamino substituted pyridine appeared to form the best catalyst (scheme I.16). To ensure the best enantioselection, different carboxylic acid where tested (including several optically pure chiral compounds). The most effective additives selected were 2-ethylhexanoic acid and (*S*)-ibuprofen. Moreover, when the best catalyst is use, the carboxylic acid can be added in catalytic amounts without alteration of the chemo- and stereoselectivity of the reaction.

Interestingly, these acid additives can be successfully replaced by protected amino acids as synergistical coligands, broadening the scope of epoxidation to α-alkyl-substituted styrenes, which are challenging substrates for asymmetric epoxidation.[140] Proper matching of the chiralities of the additives and [Fe(OTf)$_2$(^{Me2N}pdp)] catalyst was shown to improve the enantioselectivity, showing that the best result in terms of yield and enantioselectivity was obtained using *N*-NPha-Ileu-OH with the (*R,R*') catalyst (scheme I.16).

One year later, the synthesis of a C_1-symmetric tetradentate N-based complex was developed for the enantioselective epoxidation of cyclic aliphatic enones and dienones with hydrogen peroxide in the presence of 2-ethylhexanoic

acid.[141] The chiral ligand is based on the 2,2'-bipyrrolidine backbone in combination with a bulky pyridine (tips substituted) and a benzimidazole ring (scheme I.16). The epoxidation of cyclic enones provided in short reaction times good to excellent yields and enantioselectivities (up to 99% yield, and 95% ee).

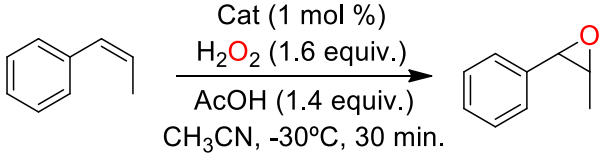

Cat	Yield (%)	ee (%)
^{H}pdp	38	21
^{Cl}pdp	33	15
^{CO2Et}pdp	22	19
^{Me}pdp	27	31
^{MeO}pdp	37	39
^{dMM}pdp	81	40
^{Me2N}pdp	82	60

Cat ≡

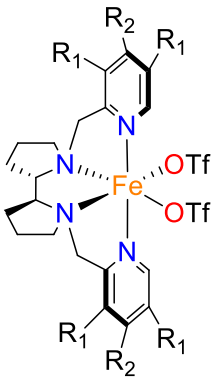

^{X}pdp	R_1	R_2
^{Me2N}pdp	-H	-NMe_2
^{dMM}pdp	-Me	-OMe
^{MeO}pdp	-H	-OMe
^{Me}pdp	-H	-Me
^{H}pdp	-H	-H
^{Cl}pdp	-H	-Cl
^{CO2Et}pdp	-H	-CO_2Et

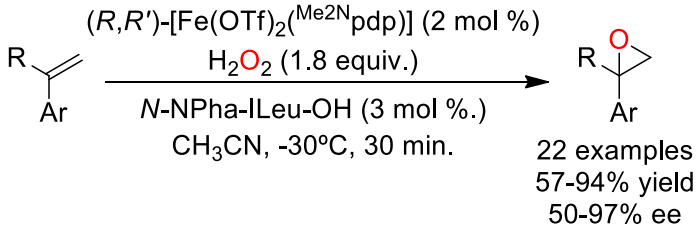

Selected examples:

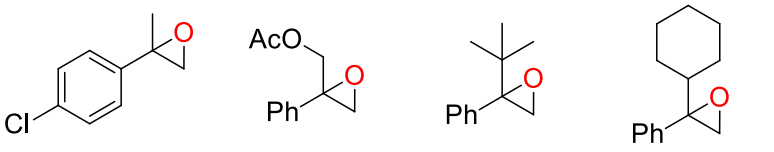

90%, 63% ee | 80%, 83% ee | 85%, 91% ee | 52%, 75% ee

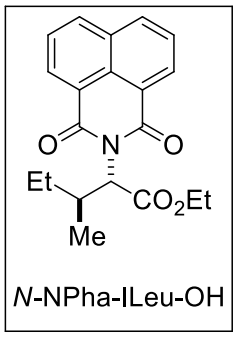

N-NPha-ILeu-OH

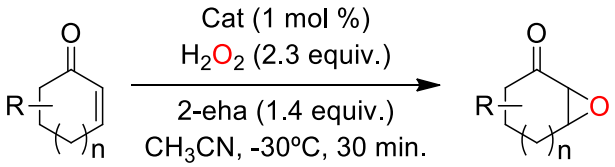

Cat ≡

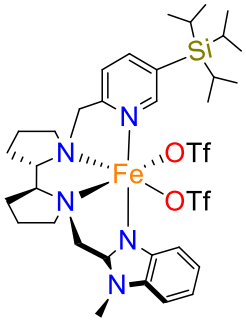

Scheme I.16. Asymmetric epoxidation of various types of olefins with the iron(II) systems reported by Costas and co-workers.[139-141]

I.3.4 Epoxidation of alkenes (C=C double bonds) by non-porphyrinic manganese complexes

The development of manganese-salen complexes by Katsuki and co-workers.[142, 143] and Jacobsen and co-workers[144] for the epoxidation of certain unfunctionalised alkenes was the starting point of biomimetic non-porphyrinic manganese complexes (figure I.9). Since their milestone discoveries manganese-salen complexes have attracted great attention for many years as asymmetric epoxidation catalysts.[145]

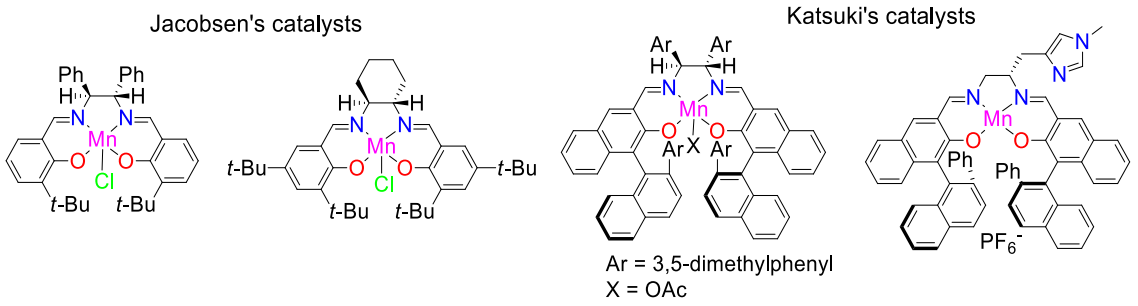

Figure I.9. Selected Jacobsen and Katsuki's manganese-salen complexes.

During the last fifteen years, a parallel line of research has been developed involving the use of manganese complexes based on tetradentate N-donor ligands. This new era commenced in 2003 when Stack and co-workers reported their pioneer work in this field.[146] They developed manganese complexes based on the ethylendiamine and *N,N'*-dimethylcyclohexane-1,2-diamine backbones (figure I.6), which efficiently catalyze epoxidation of terminal and electron-deficient alkenes with peracetic acid by only using 0.1 mol % of catalyst (scheme I.17). Unfortunately, hydrogen peroxide disproportionation in presence of those complexes precluded its use as terminal oxidant. In subsequent contributions, the same group, screened various Mn(II) complexes as catalysts in the epoxidation of 1-octene with peracetic acid.[147] The originally designed Mn(II) mcp based catalyst demonstrated the highest efficiency, achieving over 900 TON over 5 min and giving 1-octeneoxide in 92% yield. Although the catalysts were chiral, the enantioselectivities of these reactions were not reported.

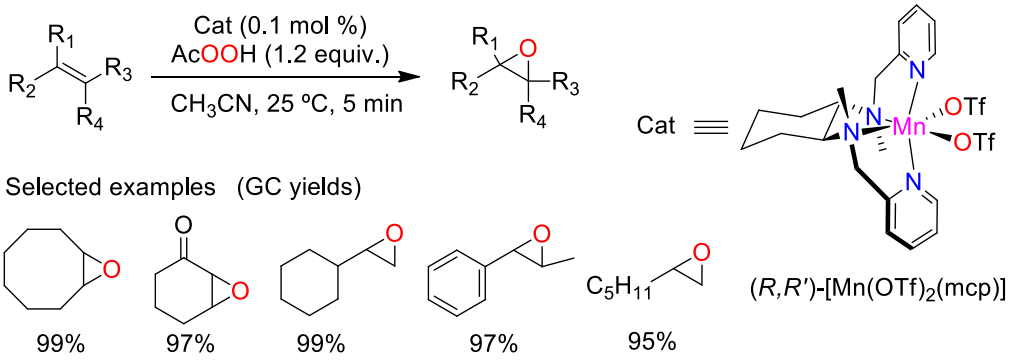

Scheme I.17. Epoxidation with (*R,R*)-[Mn(OTf)$_2$(mcp)] complex and AcOOH.

The first example of asymmetric epoxidations of these Mn aminopyridine catalysts (with AcOOH as terminal oxidant) came from Costas and co-workers in 2007, who synthesized a modified mcp ligand by introducing pinene rings fused to the 4 and 5 positions of the two pyridine moieties (scheme I.18).[148] With this modification, two effects were devised: 1) an increase in the enantioselectivity of the reactions, as the two labile binding sites of the manganese ion are confined in a better-defined chiral pocket and 2) an increase in the robustness of the catalyst, as the electron donating effect of the pinenes would stabilize the high oxidation state of the active species. The complexes exhibit comparable catalytic activity to the parent manganese mcp catalyst and a remarkable stereoselectivity (up to 46% ee) in the epoxidation of selected substrates.

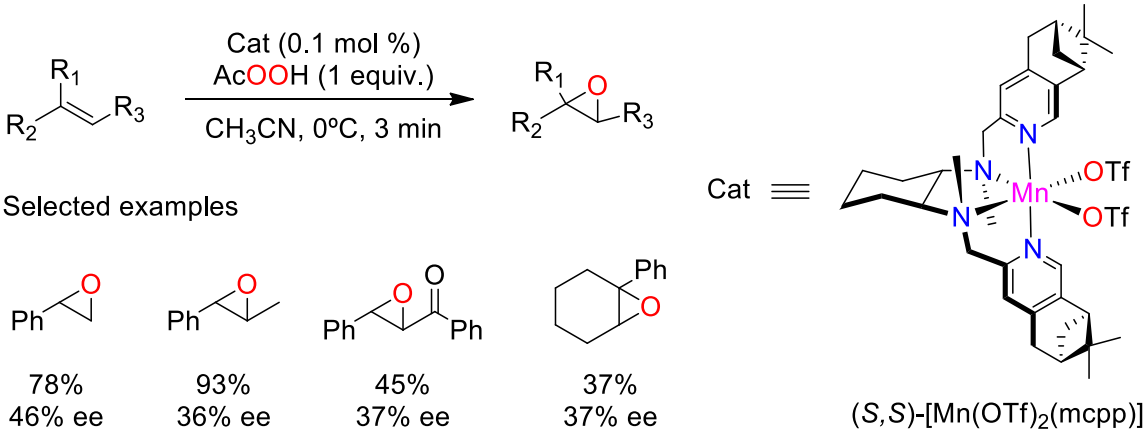

Scheme I.18. Asymmetric epoxidation of aromatic olefins with (*S*,*S*)-[Mn(OTf)$_2$(mcpp)] complex and AcOOH.

Two years later, the same group reported similar systems which are able to use H_2O_2 as oxidant.[149] Only 1.2 equiv. of hydrogen peroxide was sufficient for achieving high yields through the use of appropriate co-catalyst (AcOH, 14 equiv. with respect to substrate). The manganese complexes are based in ^{H}Pytacn, bpmen and mcp ligands (figure I.6 and scheme I.19), which leads to a fast epoxidation of a wide range of olefins in good yields and quite unusual chemoselectivity properties that allow regioselective monoepoxidation of diolefins.

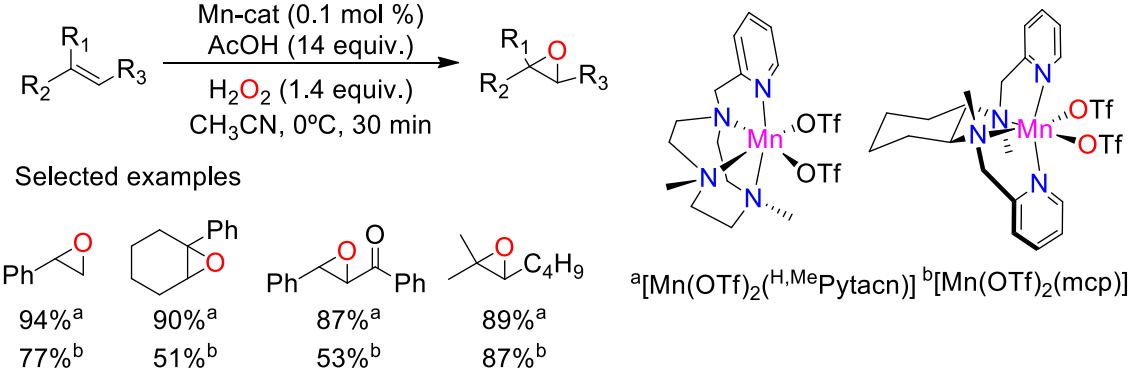

Scheme I.19. Epoxidation of various olefins with [Mn(OTf)$_2$(^{H}Pytacn)] and [Mn(OTf)$_2$(mcp)] complexes and H_2O_2/AcOH mixture.

Sun and co-workers synthesized three novel ligands based on the structure of mcp ligand, and the corresponding complexes exhibited an enhanced enantioselectivity in their epoxidation reactions (figure I.6 and scheme I.20).[150] Chiral aromatic groups were introduced into the 2-pyridylmethyl pseudo-benzylic positions of the ligand, closer to the reaction center. The corresponding manganese(II) triflate complexes proved to be more effective than the previously reported examples by Stack or Costas groups. However, the oxidant of choice was a combination of hydrogen peroxide and acetic acid, inspired by the previously mentioned method. The enantioselective epoxidation of olefins proceeds with nearly full conversion and enantiomeric excess values that range from 18% ee (for nonconjugated vinylcyclohexane) to 89% ee (for α,β-enones) in a wide array of substrates, such as unfunctionalized and conjugated olefins (scheme I.20).

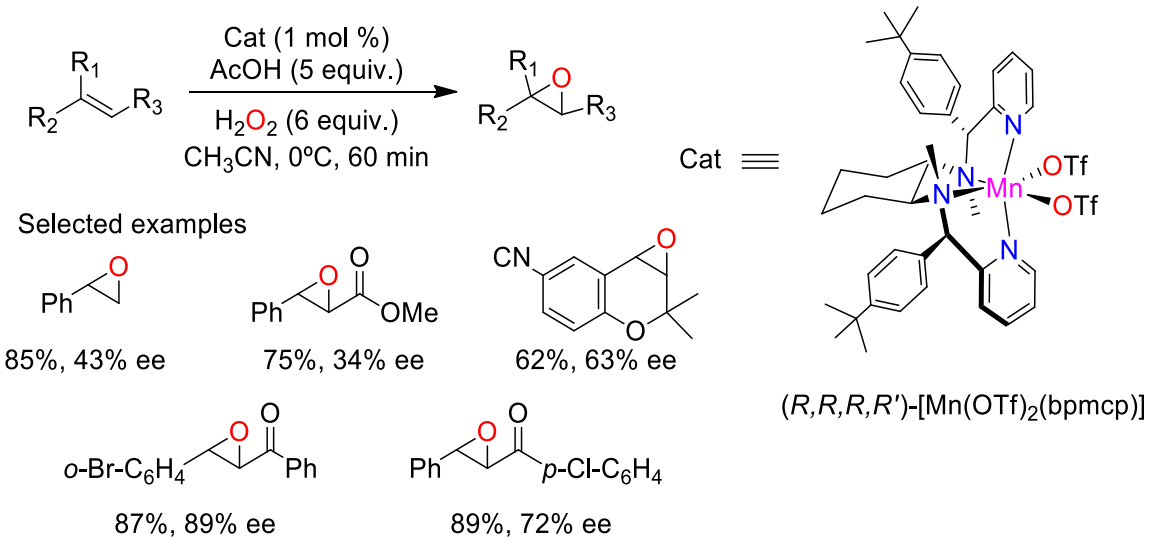

Scheme I.20. Asymmetric epoxidation of various olefins with the manganese complex reported by Sun and co-workers.[150]

In 2011, Bryliakov and co-workers developed a more efficient and selective manganese catalyst based in the pdp ligand derived from the enantiomerically enriched 2,2'-bipyrrolidine (figure I.6 and scheme I.21).[151] The authors compared the activity and stereoselectivity of the manganese complex based on mcp (*N*,*N*'-dimethylcyclohexane-1,2-diamine as backbone) and pdp (biyrrolidine as backbone) ligands, appearing the latter a better catalyst for most of the substrates tested. They also compared the peracetic acid with the hydrogen peroxide/acetic acid combination as oxidants, being the former slightly better. In general, the asymmetric epoxidation of various olefins proceeds with moderate to good yields and enantioselectivities (up to 89% ee, AcOOH and up to 84%, H_2O_2). Furthermore, the authors also observed that the enantioselectivity increases with growing steric demand of the acid, which was further studied in another report.[138] Obtaining high efficiency (up to 1000 TON), selectivity (up to 100%), and with good to high enantioselectivity (up to 93% ee with 2-ethylhexanoic acid).

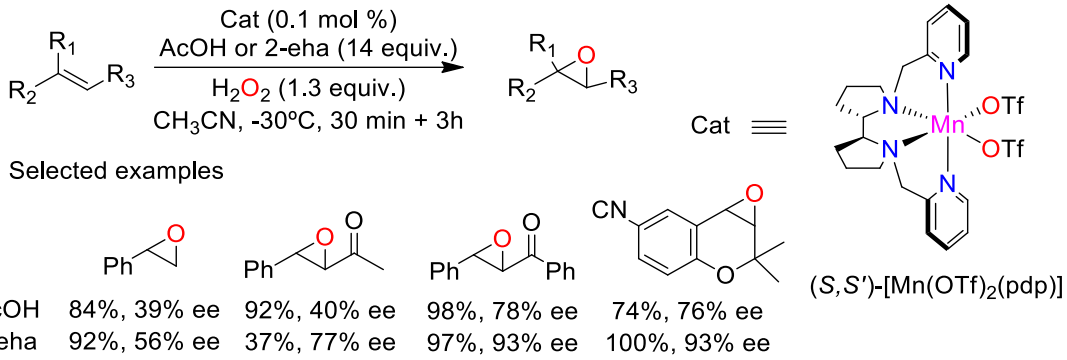

Scheme I.21. Asymmetric epoxidation of various olefins with (*S,S*)-[Mn(OTf)$_2$(pdp)].

Further modification of these ligand architecture came in 2012 from Costas and co-workers who synthesized new bipyrrolidine derived ligands bearing already described 4,5-pinene-appended pyridine rings (scheme I.22).[152] The two complexes afforded in short reaction times good to excellent yields (80–100%, TON up to 1000) in the asymmetric epoxidation of various olefins by H_2O_2 (1.2 equiv.) in the presence of acetic acid (14 equiv. vs substrate), demonstrating generally moderate enantioselectivities (66–73% ee) for some substrates (scheme I.22).

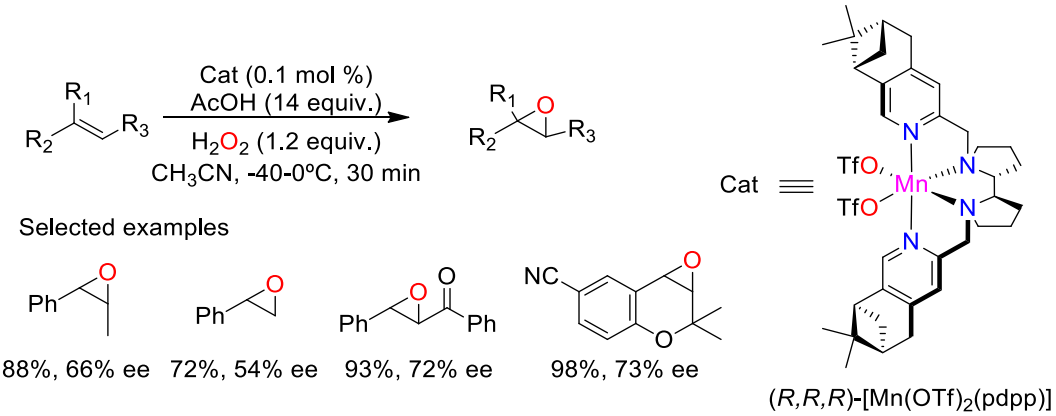

Scheme I.22. Asymmetric epoxidation of various olefins with (*R, R, R*)-[Mn(OTf)$_2$(pdpp)].

Sun and co-workers developed a new family of Mn(II) complexes with N_4-donor ligands bearing benzimidazole units instead of pyridines. In 2012, the backbone used in those ligands consists in a more rigid enantiopure diamine derived from proline (scheme I.23).[153] The corresponding manganese complex could efficiently catalyze asymmetric epoxidation of olefins with 0.01-0.2 mol % catalyst loadings furnishing 60-99% isolated yield and up to 95% ee (72-79% ee for substituted chromenes, up to 95% in substituted chalcones) with hydrogen peroxide as oxidant (scheme I.23). Moreover, the system was also suitable for gram-scale production of epoxides.

One year later, the same group, used the *N,N'*-dimethylcyclohexane-1,2-diamine as backbone for the benzimidazole modification (scheme I.23).[135] The manganese(II) complex was active for the catalyzed asymmetric epoxidation of olefins with H_2O_2 as oxidant and acetic acid as additive. The new catalyst provides

much higher enantioselectivities when compared to its parent [Mn(mcp)]. Indeed, up to 96% ee was observed for the epoxidation of α,β-unsaturated ketones at -20°C.

Finally, in 2014 the same authors reported the synthesis of a manganese complex with a ligand containing the enantiomerically enriched 2,2-bipyrrolidine and benzimidazole moieties (scheme I.23).[154] It was compared with previously mentioned catalysts that bear different diamine backbones, showing improved asymmetric induction (up to 96% ee), especially for simple olefins such as styrene derivatives and substituted chromene. However, the enantioselectivities for simple aliphatic alkenes were very low, although the conversions and selectivities were excellent.

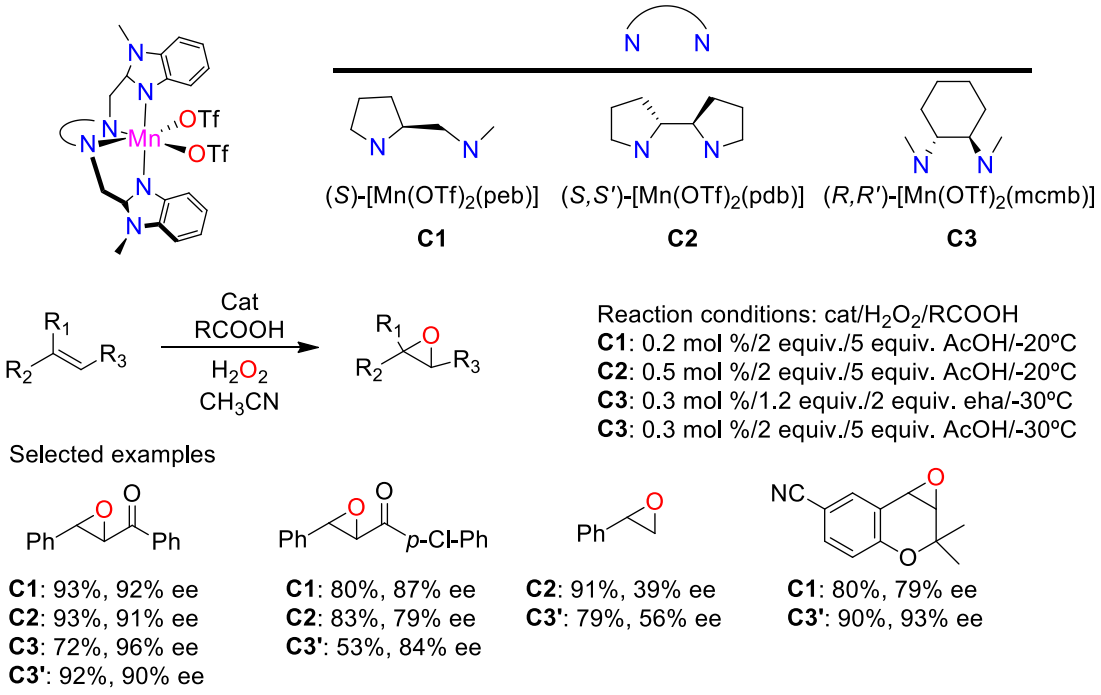

Scheme I.23. Asymmetric epoxidation of aromatic olefins with the manganese complexes reported by Sun and co-workers.[135, 153, 154]

Another important adjustment in the design of aminopyridine manganese catalysts was the variation of the steric and electronic characteristics by the introduction of substituents in the pyridine moieties of the ligand. In 2013, our group synthesized a series of Mn(II) complexes based on the 2,2'-bipyrrolidine backbone and systematic substitution at the pyridine for the asymmetric epoxidation with hydrogen peroxide as terminal oxidant (scheme I.24).[155] The enantioselectivity increased monotonously with an increase of the electron-donor properties of the substituents, obtaining the best ee (98% ee) with the complex containing -Me_2N- substituent at pyridine *para*-position. The catalytic reaction required 2 equiv. of H_2O_2 and 0.5 mol % of catalyst, affording the epoxide in 63–99% yield, and noticeably, substoichiometric amounts of the carboxylic acid are enough to efficiently activate the hydrogen peroxide. Moreover, this catalyst was

also employed in catalytic diastereoselective epoxidation of Δ^5-unsaturated steroids and displayed good yield with good selectivity towards β-epoxides which are considered as valuable biologically active compounds.

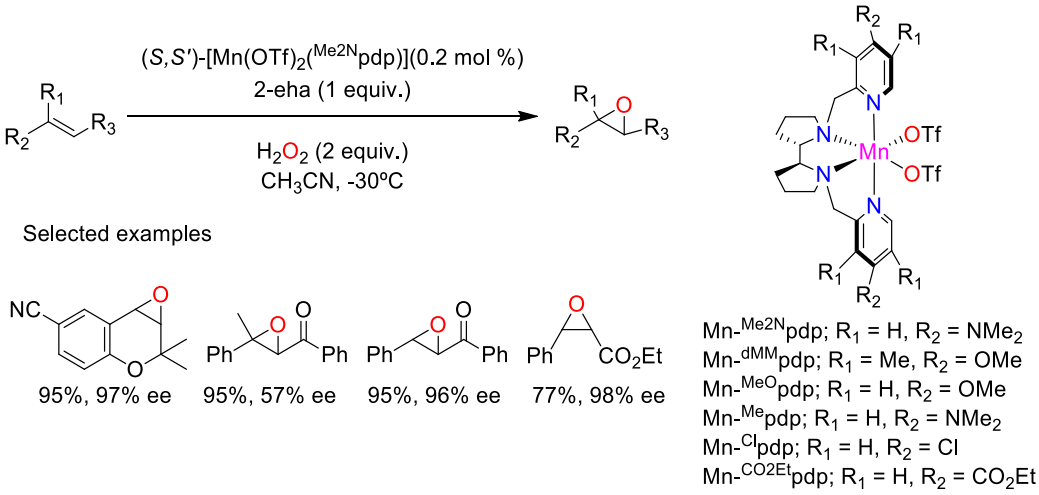

Scheme I.24. Schematic representation of the manganese complexes reported by Costas and co-workers and asymmetric epoxidation of various olefins with the best catalyst.[155]

One year later, Bryliakov and co-workers also reported the modification of the (*S,S*)-bipyrrolidine-derived manganese-based catalyst (scheme I.25).[156] The introduction of more sterically demanding substituents on the ligand (such as 3-phenyl substituted pyridine or isoquinolyl instead of pyridines) did not lead to obvious improvement of the optical yields (and the chemical yields dropped). However, the introduction of $-NH_2$ substituents at *para*-positions and –Me groups at *meta*-positions of the pyridine moieties increases enantioselectivity up to 99% ee in asymmetric epoxidations of electron-deficient olefins with H_2O_2.

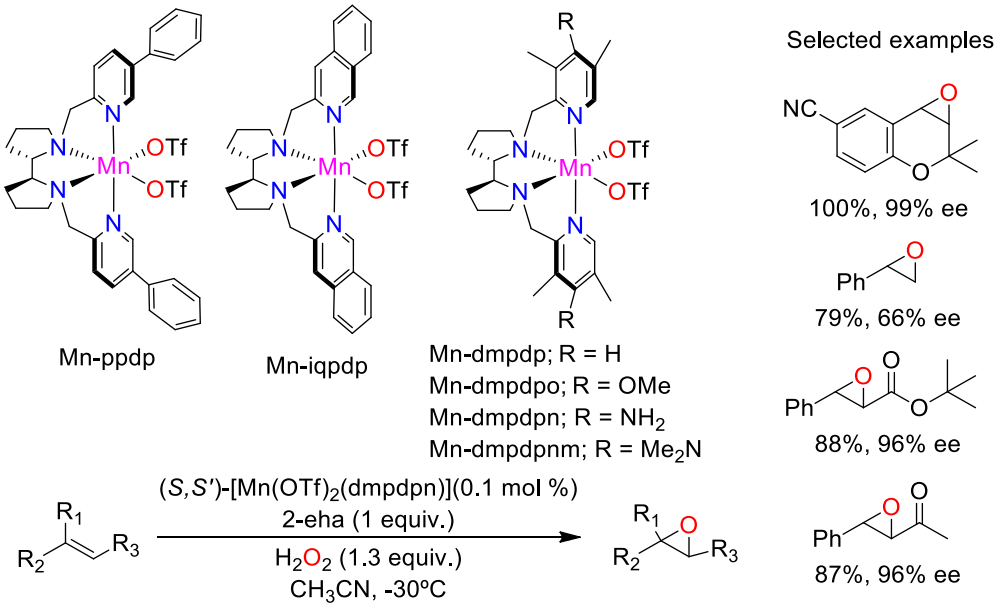

Scheme I.25. Schematic representation of the manganese complexes reported by Bryliakov and co-workers and asymmetric epoxidation of various olefins with the best catalyst.

Being the introduction of electron-donating groups into the pyridine rings of the ligands a simple way to improve the enantioselectivity, other previously reported manganese complexes were also modified. Sun and co-workers synthesized a ligand with the *N,N'*-dimethylcyclohexane-1,2-diamine as backbone that possessed additional aromatic groups at the pseudo-benzylic position of the pyridines and strong donating dimethylamino groups (scheme I.26).[157] The corresponding manganese(II) complex exhibited efficient and improved activities in the asymmetric epoxidation of various olefins, such as styrene derivatives (up to 93% ee with 2,2-dimethylbutyric acid (DMBA) as additive) with H_2O_2 as oxidant, even with a catalytic amount of carboxylic acid as additive.

Very recently, the same group, reported a new family of ligands derived from L-proline with the modification of the substituents on the pyridyl groups and on the nitrogen of the backbone (scheme I.26).[158] The corresponding manganese complexes were tested in asymmetric epoxidation of a variety of olefins using aqueous hydrogen peroxide as oxidant. With the best catalyst in hand, with only 0.2 mol % and 0.5 equiv. of 2,2-dimethylbutyric acid a variety of olefins, including styrenes, chromenes and cinnamamides were epoxidized with moderate to excellent enantioselectivities (yield up to 95%, ee up to 99%).

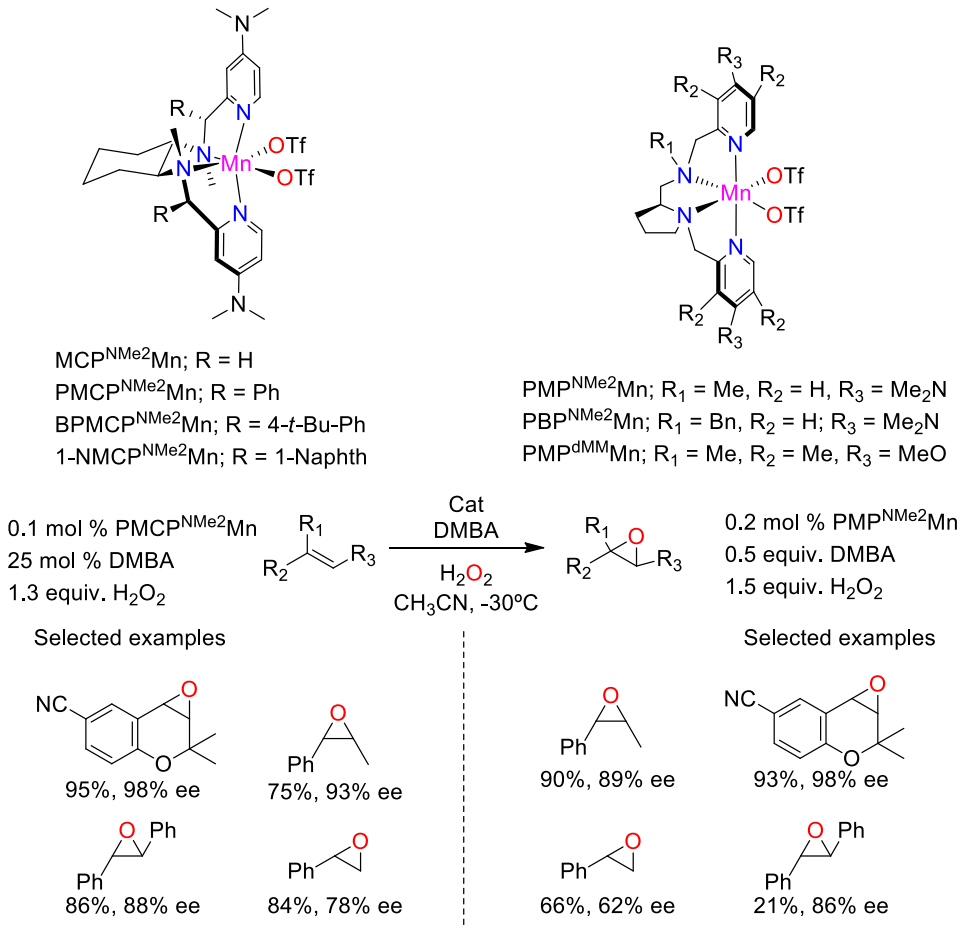

Scheme I.26. Schematic representation of the manganese complexes reported by Sun and co-workers and asymmetric epoxidation of various olefins with the best catalyst.[157, 158]

CHAPTER II

Main objectives

Inspired by the efficiency, selectivity and mild conditions of oxidation reactions that take place in nature and are catalyzed by metalloenzymes, we are interested in the development of small molecule catalysts capable to operate in a highly effective and selective manner in oxidation processes. Therefore, we target the development of new iron and manganese coordination complexes as oxidation catalysts.

As it can be seen in the literature, complexes based on aminopyridine and aminobenzimidazol tetradentate ligands are shown as one of the most successful catalysts for chemo-, regio- and enantioselective transformations with peroxide type oxidants. The starting point of the design would be established on the mentioned scaffolds. However, the novel catalysts should introduce new structural versatility to the ones previously reported, trying to broaden the substrate scope and to improve the selectivity in the oxidation reactions.

Looking at previously reported tetradentate N-donor ligands, we can recognize a clear limitation in the diamine backbones. Most of the ligands typically used on those reactions are based on three basic chiral diamines (*N*,*N*'-dimethylcyclohexane-1,2-diamine; 2,2-bipyrrolidine and L-(*S*)-pyrrolidin-2-ylmethanamine). Knowing full well that the structural properties and the nature of the backbone appeared to be an important factor in defining the catalytic performance, the research for novel diamine backbones become imperative. However, small modifications in the ligand scaffold can provoke important changes in the catalytic performance, thus, the selection of the new backbones should be carefully considered.

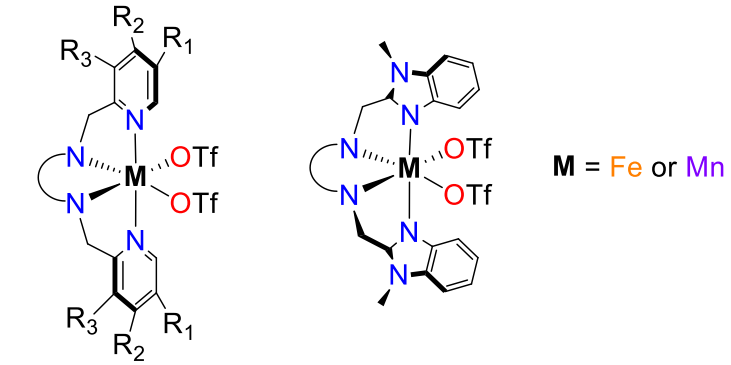

Figure II.1. Design of different iron and manganese complexes for oxidation reactions.

The strategy pursued in this thesis consists in the modification of the diamine backbone of tetradentate N-donor ligands by using structurally similar,

but at the same time, slightly distinct diamines, when compared to the reported ones. Moreover, as chirality is important in the oxidation reactions that we are interested in, we will focus on the synthesis of the diamines in a enantiopure fashion. Additionally, tuning the steric and electronic properties of the ligands would be performed, by modifying the substitution in the pyridine moiety.

Ideally, the corresponding iron and manganese complexes must efficiently activate hydrogen peroxide for their use in oxidation catalysis for substrates that remain difficult for current oxidation technologies. The catalytic performance of the active chiral complexes will be tested on a broad substrate scope of different olefins for their asymmetric epoxidation, including challenging substrates.

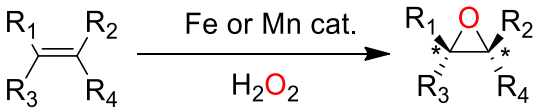

Scheme II.1. Asymmetric epoxidation reaction with iron and manganese complexes and hydrogen peroxide as oxidant.

In C-H oxidation catalysis, we will study the effect of the nature of the ligand diamine backbone, previously identified as a key structural aspect for the iron catalyst active site that have an impact on C-H site selectivity. Moreover, we envision that the influence of the introduction of bulky trialkylsilyl moieties at the pyridine will also modulate the regioselectivity.

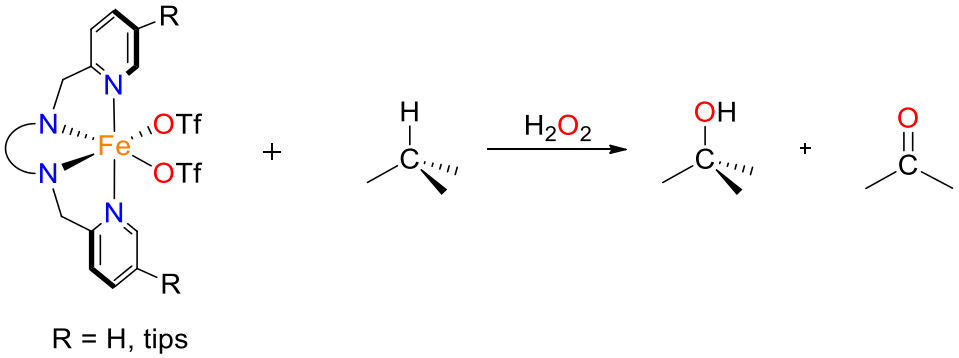

Scheme II.2. C-H oxidation reaction with selected iron complexes and hydrogen peroxide as oxidant.

CHAPTER III

Iron and manganese complexes based on the N^1,N^2-bis((*S*)-1-phenylethyl)ethane-1,2-diamine and (*R*,*R*)-1,5-diaza-*cis*-decalin backbones: synthesis, characterization and catalytic epoxidation activity

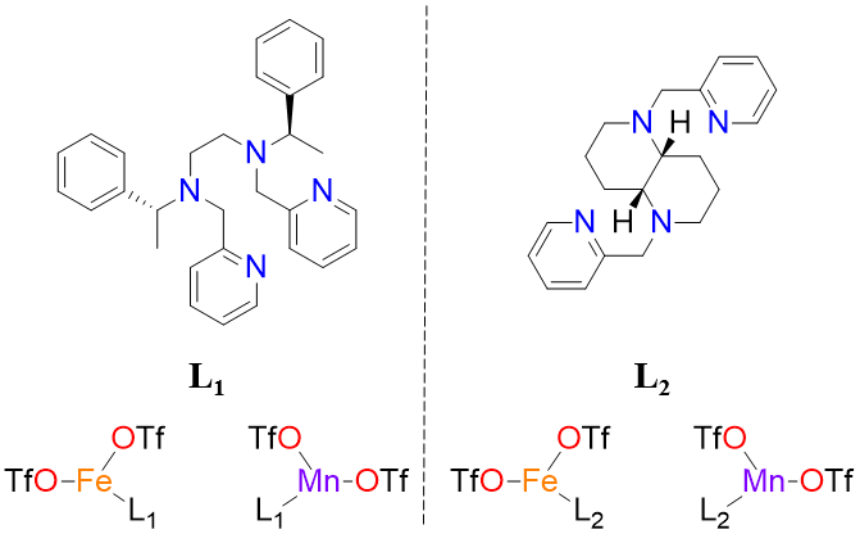

Abstract

Herein is described the synthesis of new iron and manganese complexes (**C1-C5**) based on tetradentate bis-pyridyl bis-amine ligands with (*S*,*S*)-1,5-diaza-*cis*-decalin and N^1,N^2-bis((*S*)-1-phenylethyl)ethane-1,2-diamine as chiral backbones. Preliminary studies in their use as catalysts in the epoxidation of some model substrates displayed modest results. Hence, the two chosen diamines are not suitable platforms for widening the structural versatility of these types of ligands.

III.1 Results and discussion

III.1.1 Synthesis of backbones

The first chiral diamine chose as backbone was the N^1,N^2-bis((*S*)-1-phenylethyl)ethane-1,2-diamine and it was synthesized following the procedure described in literature.[159] This diamine scaffold is very user-friendly in terms of simple and modular ligand modifications, as different substituents in the phenyl group can be introduced and the alkyl moiety can be easily modified (scheme III.1).

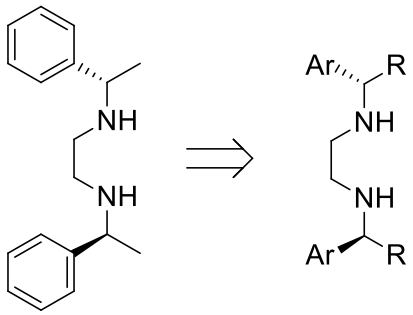

(*S*,*S*)-**BPhMeNH**

Scheme III.1. Modular modifications of (***S*,*S***)-**BPhMeNH** backbone.

It was originally expected that, after the synthesis of complexes with the ligand based on the simplest diamine (**BPhMeNH**), further modulation will be required on the backbone for the optimization of the reactivity of the corresponding complexes. However, these modifications were not performed due to the unsatisfactory results obtained in catalysis (see section III.5).

The second chiral diamine selected was 1,5-diaza-*cis*-decalin (**DCD**) (scheme III.2) due to the structural similarity to previously used backbones, such as *N,N'*-dimethyl-*trans*-1,2-cyclohexanediamine.[124, 160]

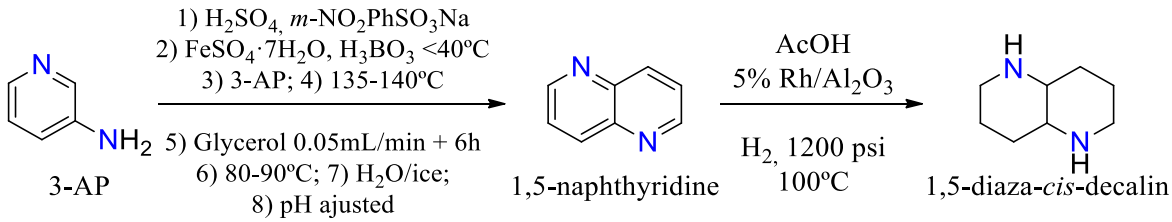

Scheme III.2. Synthesis of 1,5-diaza-cis-decalin backbone.

The synthesis of such diamine has been already reported in the literature[161] (scheme III.2) and it implies three-four straightforward steps. In the first step, commercially available 3-aminopyridine (3-AP) is readily converted to 1,5-naphthyridine via a Skraup reaction.[162] The next step consists in the hydrogenation

of the naphthyridine to the saturated diamine by employing acetic acid with rhodium/alumina as catalyst, to obtain 1,5-diaza-*cis*-decalin as the major isomer. At this point, the racemic diamine was resolved through the diastereomeric tartrate procedure.

The first step was accomplished in gram scale with a 57% yield. But the hydrogenation reaction was not reproducible. Following the previously mentioned synthesis, only the half-hydrogenated product, 1,2,3,4-tetrahydro-1,5-naphthyridine, was afforded (see figure III.1) in >99% of selectivity. Several attempts with slightly different reaction conditions were tested: a) 100°C, 10 bar, 12h; b) 120°C, 30 bar, 36h; c) 150°C, 100 bar, 12h. In all the cases the half-hydrogenated product was obtained. Also another reported synthesis have been proved[163] where a hydrochloric acid in AcOH solution was used at 80°C and 10 bar, during 8 days; however the same product was achieved.

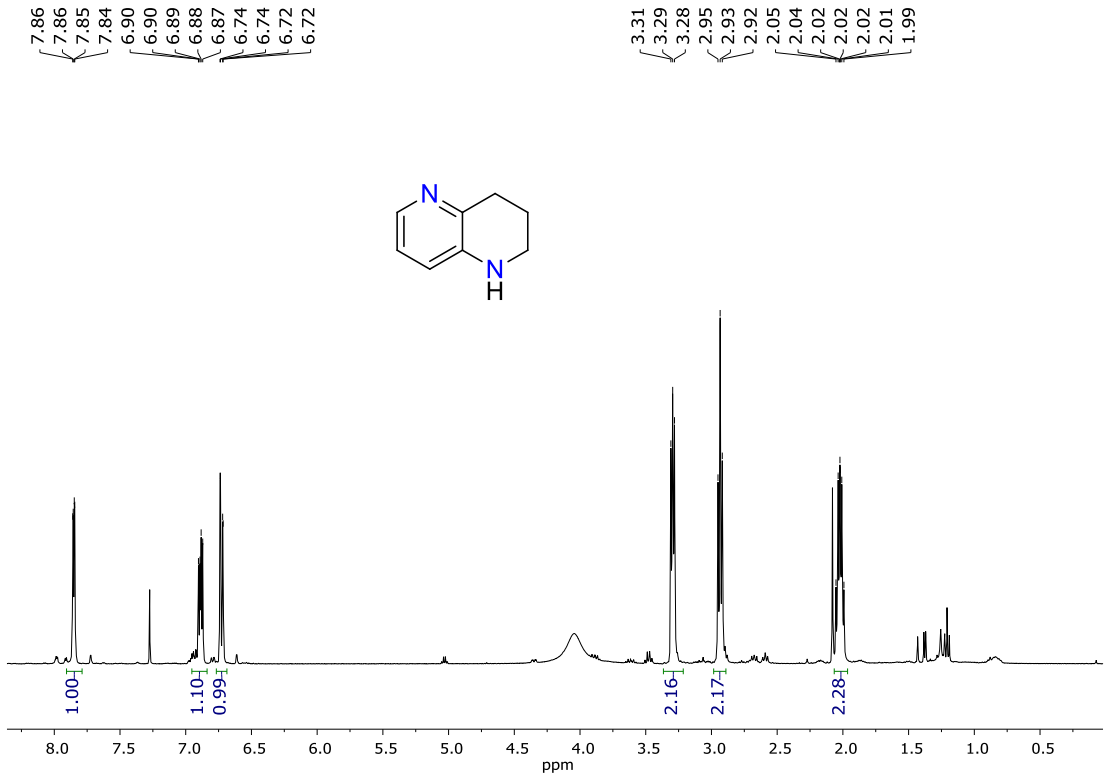

Figure III.1. ^{1}H-NMR spectra of the crude obtained in the hydrogenation of 1,5-naphthyridine.

Because of these results, we decided to obtain the backbone through a commercially available source. The chosen [(*R*,*R*)-1,5-diaza-*cis*-decalin]copper hydroxide iodide hydrate complex was submitted to NH_3 solution for the complexation of the copper and further release of the ligand. After extraction in CH_2Cl_2, the (*R*,*R*)-1,5-diaza-*cis*-decalin backbone was obtained pure in 58% yield.

III.1.2 Synthesis of ligands and complexes

Tetradentate ligands were prepared by alkylation of the corresponding enantiomerically enriched diamines with 2-picolyl chloride hydrochloride in acetonitrile under reflux using Na_2CO_3 as base. The unsubstituted pyridine was selected for the preparation of iron and manganese complexes to carry out a screening of their activity as epoxidation catalysts.

After chromatographic purification, **L1** was obtained as a pale orange solid, while **L2** was gotten as a brown oil (58 and 61% of yield respectively).

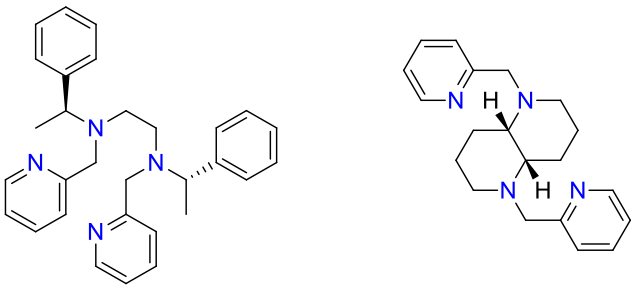

L1 **L2**

Figure III.2. Structures of the new bis-pyridyl bis-amine tetradentate based ligands.

Preparation of the complexes involved straightforward reaction of the corresponding tetradentate ligand in anhydrous solvents under anaerobic conditions with $[Fe(CF_3SO_3)_2(CH_3CN)_2]$, $[Mn(CF_3SO_3)_2]$ and $[FeCl_2]$ respectively to obtain **C1-C5** complexes (figure III.3). Slow diffusion of diethyl ether or hexane over saturated CH_2Cl_2 solutions afforded the corresponding complexes as solids or crystalline material in 33 to 54% yields.

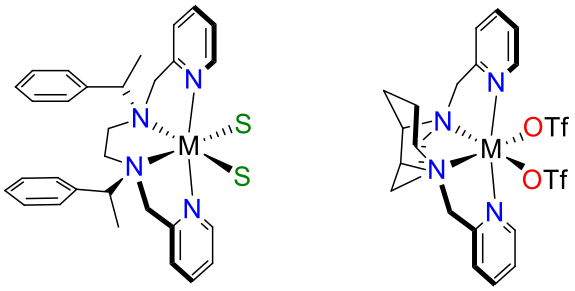

C1: **M**=Fe, S=CF_3SO_3
C2: **M**=Mn, S=CF_3SO_3
C3: **M**=Fe, S=Cl

C4: **M**=Fe
C5: **M**=Mn

Figure III.3. 3D chemical diagrams of **C1-C5** complexes.

III.1.3 Solid state characterization: X-ray crystallography

From the **BPhMeNH** based catalysts, only the iron chloride complex (**C3**) showed crystals suitable for X-ray diffraction analysis. While the two complexes obtained with **L2** ligand (**C4**, **C5**), crystalized properly. Their corresponding X-ray structures are depicted in figure III.1.4, experimental details of their crystal structure determination are collected in table III.1, and a list of selected bond distances and angles can be found in table III.2.

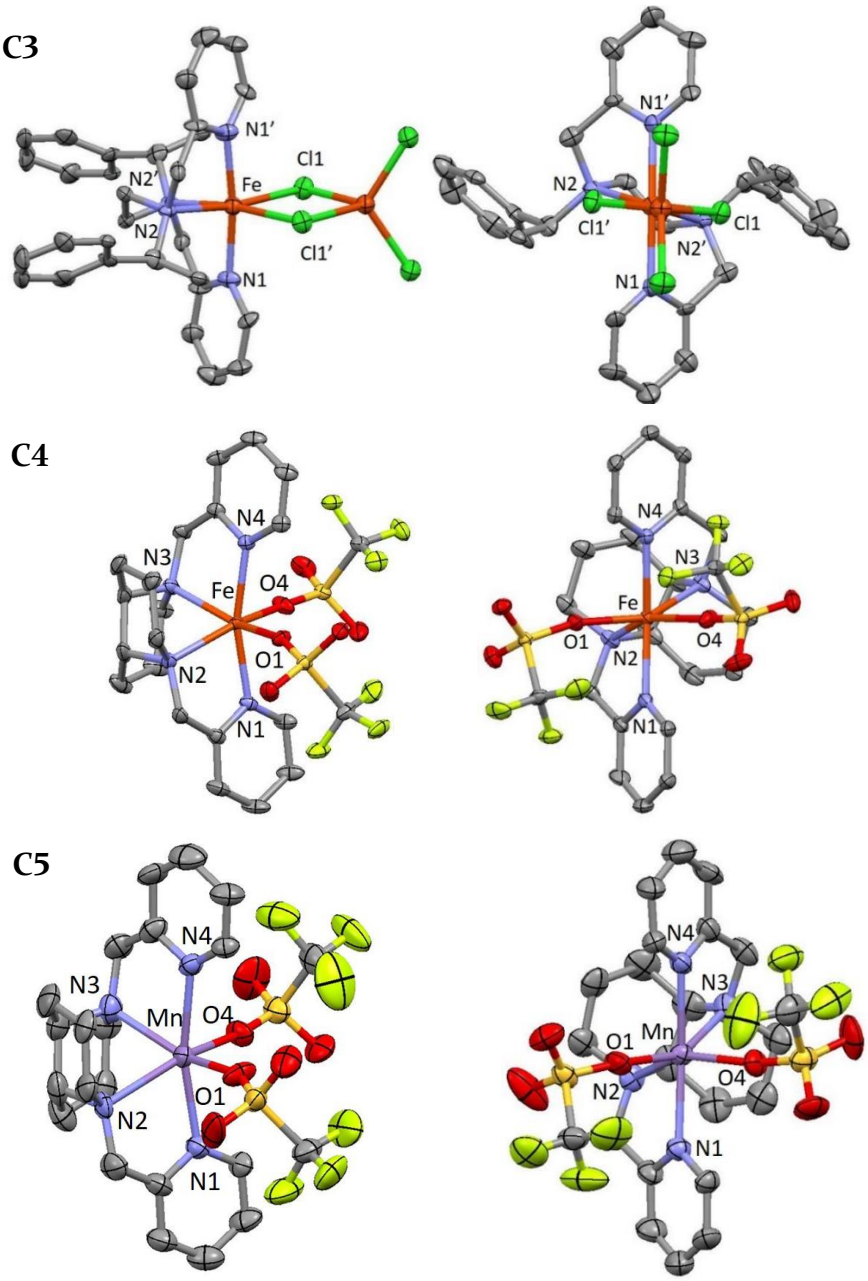

Figure III.4. Ellipsoid diagrams of **C3** and **C4** at a 50% of probability and **C5** at a 30% of probability. Hydrogen atoms were omitted for clarity.

Table III.1. Crystal data for **C3**-**C5** complexes.

Compound	C3	C4	C5
Empirical formula	$C_{30}H_{34}C_{l4}Fe_2N_4$	$C_{22}H_{26}F_6FeN_4O_6S_2$	$C_{22}H_{26}F_6MnN_4O_6S_2$
Formula weight	704.11	676.44	675.53
Temperature	293(2) K	100(2) K	298(2) K
Wavelength	0.71073 Å	0.71073 Å	0.71073 Å
Crystal system	Tetragonal	Monoclinic	Monoclinic
Space group	P 43 21 2	P 21	P 21
Unit cell dimensions	a = 15.960(9) Å; α = 90° b = 15.960(9) Å; β = 90° c = 14.426(11) Å; γ = 90°	a = 8.9855(15) Å; α = 90° b = 15.410(3) Å; β = 92.401(3)° c = 10.0702(17) Å; γ = 90°	a = 9.314(4) Å; α = 90° b = 18.343(8) Å; β = 117.386(7)° c = 9.550(4) Å; γ = 90°
Volume	3675(5) A^3	1393.2(4) A^3	1448.8(12) A^3
Z, Density (calculated)	4, 1.273Mg/m^3	2, 1.612 Mg/m^3	2, 1.549 Mg/m^3
Absorption coefficient	1.103 mm^{-1}	0.776 mm^{-1}	0.681 mm^{-1}
F(000)	1448	692	690
Crystal size	0.25 x 0.20 x 0.12 mm	0.35 x 0.10 x 0.10 mm	0.3 x 0.1 x 0.08 mm
Θ range for data collection	1.804 to 21.041°	2.269 to 28.422°	2.221 to 28.476°
Limiting indices	-9<=h<=16 -15<=k<=15 -14<=l<=14	-11<=h<=11 -20<=k<=20 -13<=l<=13	-12<=h<=12 -24<=k<=24 -12<=l<=12
Reflections collected/unique	12510 / 1981 [R(int) = 0.1990]	21649 / 6827 [R(int) = 0.0289]	21163 / 7082 [R(int) = 0.0958]
Completeness to Θ	99.5% (Θ = 25.242°)	99.9% (Θ = 25.242°)	99.9% (Θ = 25.242°)
Refinement method	Full-matrix least-squares on F^2	Full-matrix least-squares on F^2	Full-matrix least-squares on F^2
Data/restraints/parameters	1981 / 0 / 183	6827 / 1 / 370	7082 / 2 / 370
Goodness-of-fit on F2	1.034	1.028	0.973
Final R indices	R1 = 0.0597 wR2 = 0.1332	R1 = 0.0309 wR2 = 0.0759	R1 = 0.0673 wR2 = 0.0759
R indices (all data)	R1 = 0.1053 wR2 = 0.1550	R1 = 0.0331 wR2 = 0.0772	R1 = 0.1548 wR2 = 0.2074
Largest diff. peak and hole	0.670 and -0.550 $e.A^{-3}$	0.507 and -0.253 $e.A^{-3}$	1.069 and -0.533 $e.A^{-3}$

Table III.2. Selected bond lengths (Å) and angles (°) for **C3-C5** complexes.

	C3		C4		C5
Fe-N1	2.100(11)	Fe-N1	2.180(2)	Mn-N1	2.317(9)
Fe-N1'	2.100(11)	Fe-N2	2.255(2)	Mn-N2	2.316(11)
Fe-N2	2.295(11)	Fe-N3	2.250(2)	Mn-N3	2.364(9)
Fe-N2'	2.295(11)	Fe-N4	2.190(2)	Mn-N4	2.293(9)
Fe-Cl1	2.505(5)	Fe-O1	2.129(2)	Mn-O1	2.155(7)
Fe-Cl1'	2.505(5)	Fe-O4	2.137(2)	Mn-O4	2.161(8)
N1-Fe-N2	97.7(4)	N1-Fe-N2	77.04(10)	N1-Mn-N2	74.2(4)
N1-Fe-N1'	172.8(8)	N1-Fe-N4	164.48(10)	N1-Mn-N4	166.3(3)
N1-Fe-Cl1'	95.5(4)	N1-Fe-O4	88.36(9)	N1-Mn-O4	84.3(3)
N1-Fe-Cl1	89.9(3)	N1-Fe-O1	84.41(8)	N1-Mn-O1	86.9(3)
N2-Fe-N1'	76.8(4)	N2-Fe-N4	115.85(9)	N2-Mn-N4	118.4(4)
N2'-Fe-N1'	97.7(4)	N3-Fe-N4	76.94(9)	N3-Mn-N4	73.4(3)
N2-Fe-Cl1'	98.1(3)	N2-Fe-O4	153.26(10)	N2-Mn-O4	153.4(3)
N1'-Fe-Cl1	95.5(4)	N4-Fe-O1	86.88(9)	N4-Mn-O1	87.3(3)
N2'-Fe-Cl1	98.1(3)	N3-Fe-O1	153.40(9)	N3-Mn-O1	148.1(3)
N2-Fe-N2'	82.1(6)	N2-Fe-N3	78.57(9)	N2-Mn-N3	76.0(3)
N1'-Fe-Cl1'	89.9(3)	N3-Fe-O4	88.05(10)	N3-Mn-O4	100.8(4)
Cl1-Fe-Cl1'	82.8(2)	O1-Fe-O4	110.97(9)	O1-Mn-O4	102.4(4)

The X-ray structures disclose that the metal centers have a distorted octahedral geometry and the ligands coordinate in a *cis*-α-topology, as the nitrogen atoms of the pyridines are in *trans* to each other. This distortion is highly evidenced for **C4** and **C5** complexes when looking at their structures in figure III.2, where the dihedral angle between the plane of R'RN-M-NRR' and Npy-M-Npy is highly distorted from the expected orthogonality. The coordination sphere is completed by equatorial anions (chloride or triflate) that are in a relative *cis* configuration. The **C3** structure was further coordinated to another iron chloride moiety, maybe due to the use of an excess of it in the synthesis.

As the chirality of the backbone determine the topological chirality at the metal,[148] the main iron metal center for **C3** exhibits a Λ helical chirality because of the (*S*,*S*) chirality of the backbone, whereas the metal centers of **C4** and **C5** exhibit a Δ helical chirality resulting from the opposite (*R*,*R*) chirality of the backbone.

The M–N (M = Fe or Mn) distances reflect the different chemical nature of the donor atoms: the distance to the pyridyl nitrogens (average: 2.10, 2.19 and 2.32 Å for each complex), are noticeably shorter than to the amine nitrogens (average: 2.30, 2.25 and 2.34 Å for each complex). In general, M–N distances measured are

in good agreement with those reported in the literature for related high spin M^{II} complexes with N4 based ligands. [146, 148, 150-153, 155, 164]

The two nitrogen atoms of the pyridine rings are mutually *trans*, with the Npy-M-Npy angle ranging from 164.48(10)° for **C4** to 172.8(8)° for **C3**, while the two aliphatic nitrogen atoms (R'RN-M-NRR') are mutually *cis*. Because of the formation of five member chelate-rings, the R'RN-M-NRR' and R'RN-M-Npy angles are all smaller than 90°.

III.1.4 Characterization of the complexes in solution

III.1.4.1 ESI-MS

The solution behavior of the complexes was analyzed by ESI-MS in acetonitrile. The spectra of **C3** complex shows an unique cationic peak corresponding to the loss of one chloride $[LFe(Cl)]^+$ (L = **L1**). For the bis-triflate complexes **C1**, **C2** and **C4**, the spectra shows two cationic peaks, whose mass and isotopic pattern could be satisfactorily assigned to the monocationic $[LM(CF_3SO_3)]^+$ ion and to the dicationic $[LM]^{+2}$ (M = Fe or Mn and L = **L1** or **L2**). The spectra of **C5** complex shows, apart from the previous mentioned peaks for bis-triflate complexes, two more peaks assigned to the dicationic species and a molecule of acetonitrile or a water $[\mathbf{L2}Mn+S]^{+2}$ (S = CH_3CN or H_2O).

III.1.4.2 ^{1}H-NMR spectroscopy

The ^{1}H-NMR spectroscopy of manganese complexes were not performed, as it is known that Mn(II) induces very short electronic relaxation times and high nuclear line broadening due to dipolar relaxation in the FID of the protons, therefore no signals are able to be observed through this technique.[165]

^{1}H-NMR spectra of iron complexes **C1**, **C3** and **C4** in different deuterated solvents are depicted in figures III.5.-III.7. All the iron compounds exhibit spectral windows that expand from –90 to 195 ppm, which is indicative of octahedral t_{2g}^4 e_g^2 Fe^{II} paramagnetic species.

C1 spectra displays broad signals due to triflates counteranions lability[166], nonetheless the spectra is quite simple with a relatively small number of signals, suggesting a C_2-symmetry in solution. Assignment of the α-pyridine protons of the complex can be made because of the characteristic paramagnetic downfield shift of these protons arising from the near interaction between the proton and the ferrous center. Likewise, β-pyridine protons are highly characteristic and appear as narrow signals around 60 ppm. [166-169] In addition, in the diamagnetic region of the spectra, three signals with a 2:2:1 ratio can be tentatively assigned to the phenyl protons of the backbone and the signal near to 2 ppm should corresponds to the

methyl groups of the backbone too (figure III.6). Thanks to the integration, the pseudobenzylic protons of the pyridine are assigned to the lowest signal of the spectra and benzylic protons of the backbone to the signal close to 120 ppm.

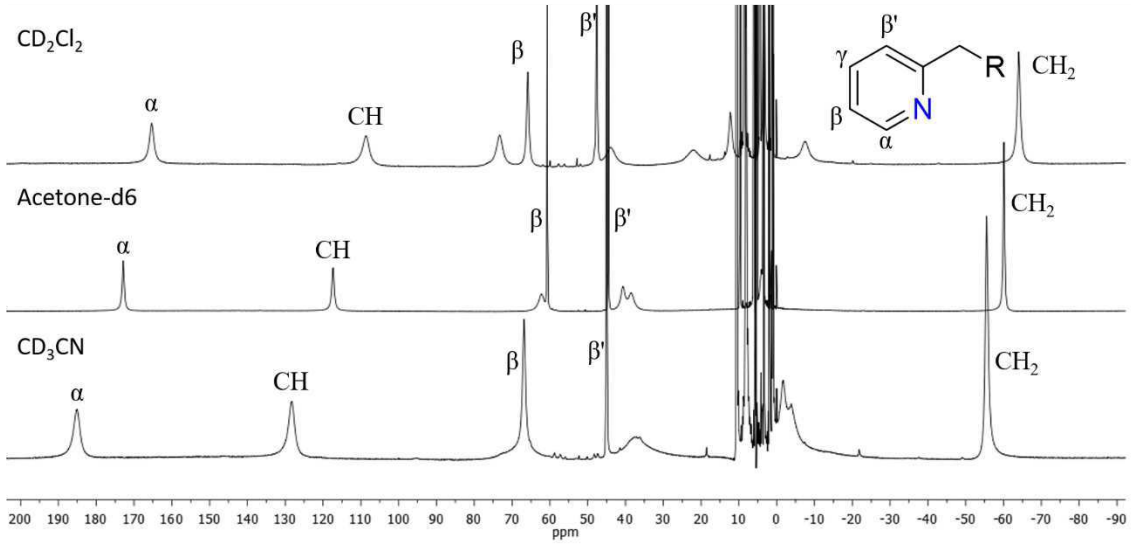

Figure III.5. ^{1}H-NMR spectra (400 MHz) of **C1** complex in different solvents at 298K.

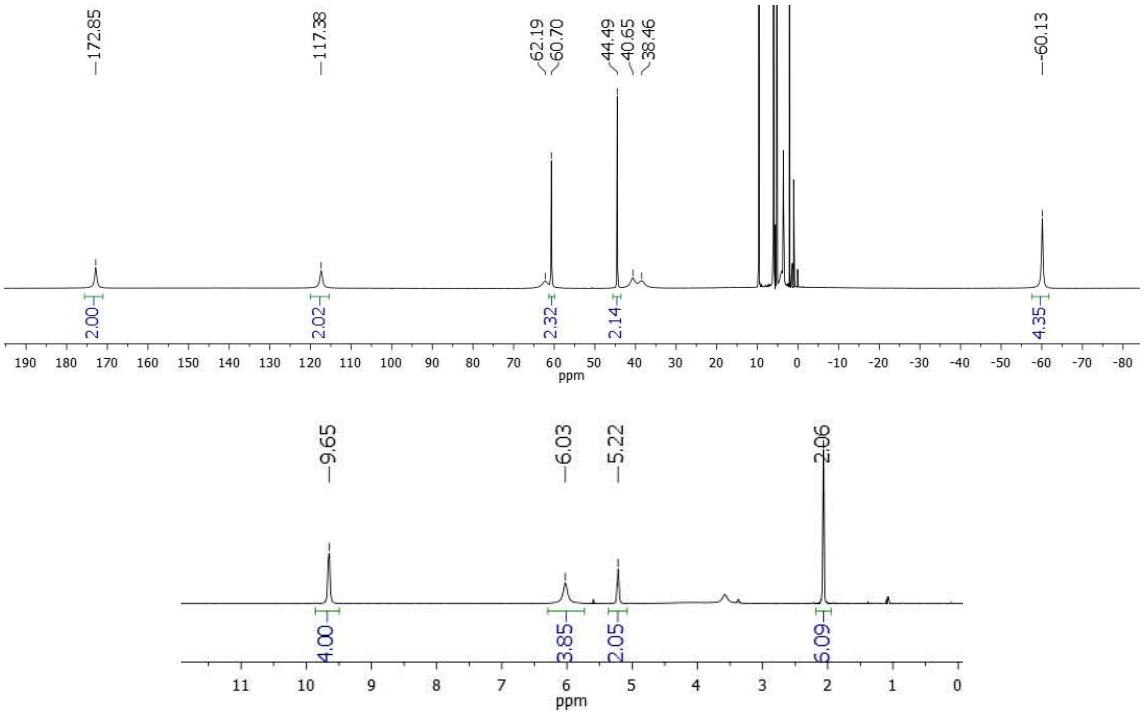

Figure III.6. ^{1}H-NMR integrated spectra (400 MHz) of **C1** complex in acetone-d_6 at 298K.

The **C3** structure of the solid state showed a perfect C_2-symmetry, which seems that is also retained in solution, as few signals appear in the spectra. When compared to **C1**, the spectral window is narrower; the highest signal appear at 95 ppm, while the lowest at -36 ppm (in front of 166 and -64 ppm respectively in CD_2Cl_2).

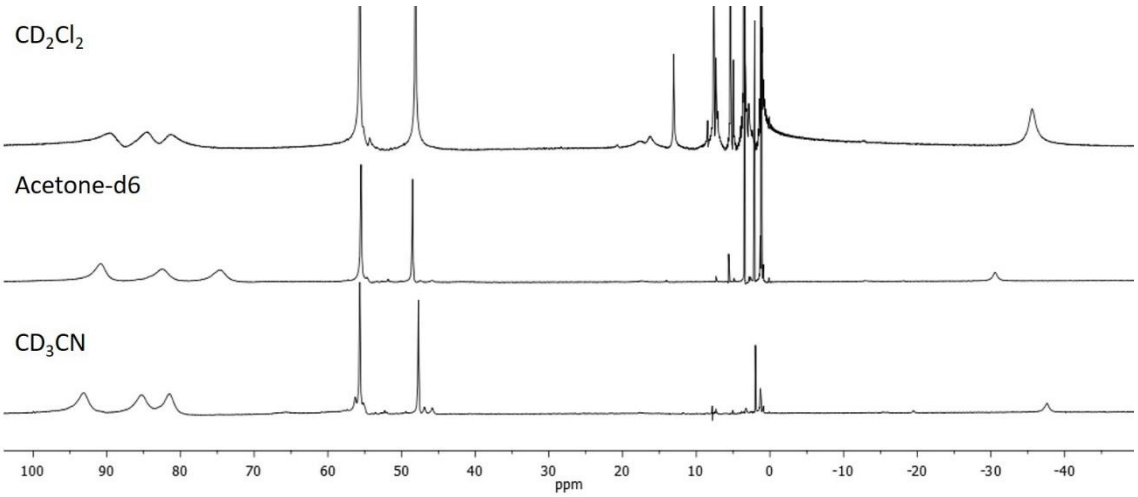

Figure III.7. ^{1}H-NMR spectra (400 MHz) of **C3** complex in different solvents at 298K.

The spectra of **C4** is complex (figure III.8), and contain multiple peaks. This can be explained because the cyclic diamine backbone contains several protons, which are difficult to assign, but the integration displayed in figure III.9 shows that the number of protons present in the spectra agrees with the number of protons present in the complex. α, β and β' protons of the pyridine are easily recognized, when compared to similar complexes.[166-169]

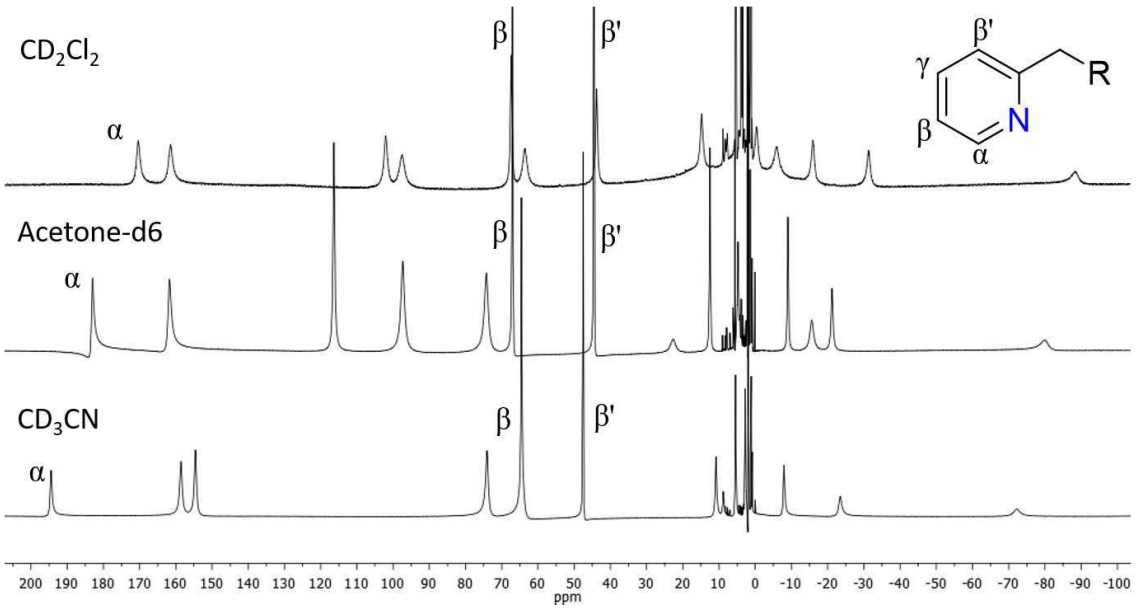

Figure III.8. ^{1}H-NMR spectra (400 MHz) of **C4** complex in different solvents at 298K.

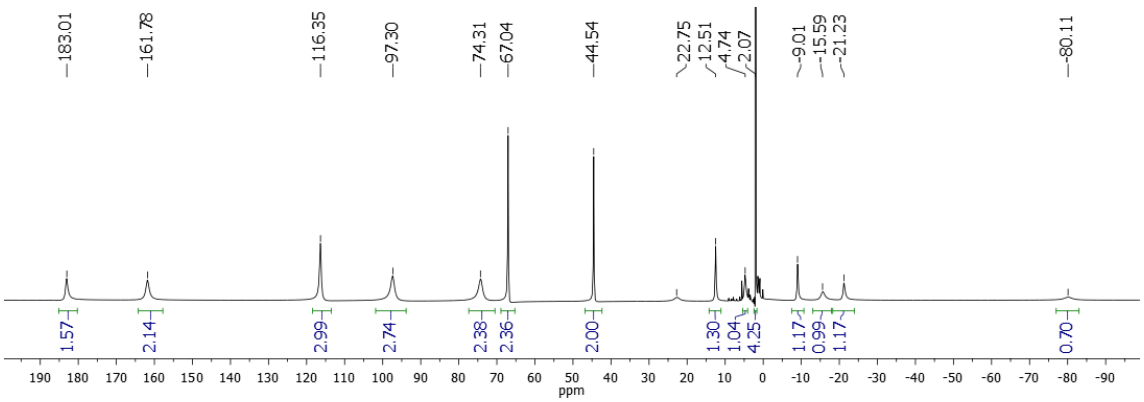

Figure III.9. ^{1}H-NMR integrated spectra (400 MHz) of **C4** complex in acetone-d_6.

When the ^{1}H-NMR spectra of the iron-triflate complexes were recorded in CD_3CN, the solvent can act as a coordinating ligand, displacing triflate groups to form solvato complexes $[Fe(L)(CH_3CN)_2]^{2+}$ (L = **L1-L2**) in which two acetonitrile molecules and the tetradentate ligands constitute the coordination sphere of the iron(II) center.

It is known that the substitution of the triflate anions by acetonitrile ligands can force the complex to be mainly low spin because acetonitrile ligand is a stronger ligand field than triflate anion. This effect is manifested by the reduction of the spectral window to the range expected for diamagnetic species. However, for complexes **C1** and **C4** the ^{1}H-NMR spectra in acetonitrile does not change in a significant way, indicating that the exchange of the mentioned ligands does not induce a spin change. Presumably, the rigid nature of the ligand makes energetically uphill the necessary compression of the Fe-N bonds associated with the low spin configuration.

III.1.4.3 UV-Vis spectroscopy

The UV–vis spectra of the complexes in acetonitrile solution at room temperature, were analyzed to obtain further information about their electronic structure.

The spectrum of all the complexes display a very strong absorption in the UV region (between 260 and 270 nm and ε between 5900 and 11000 $M^{-1}\cdot cm^{-1}$), which can be assigned to pyridine π–π* transitions. In the visible region, iron complexes exhibit less intense bands related to metal-to-ligand charge-transfer (MLCT) absorptions. The spectra at high concentrations (1 mM approx.), show bands between 310 and 360 nm respectively with extinction coefficients that go from 730 to 1800 $M^{-1}\cdot cm^{-1}$ (figures III.10-III.11, table III.3). These UV-Vis spectroscopic features are characteristic of high spin Fe^{II} centers.[170, 171]

On the other hand, manganese complexes, **C2** and **C5**, exhibit no bands in the visible region consistent with the lack of d–d transitions as expected for a d^5 metal ion high spin in an octahedral coordination environment.[172]

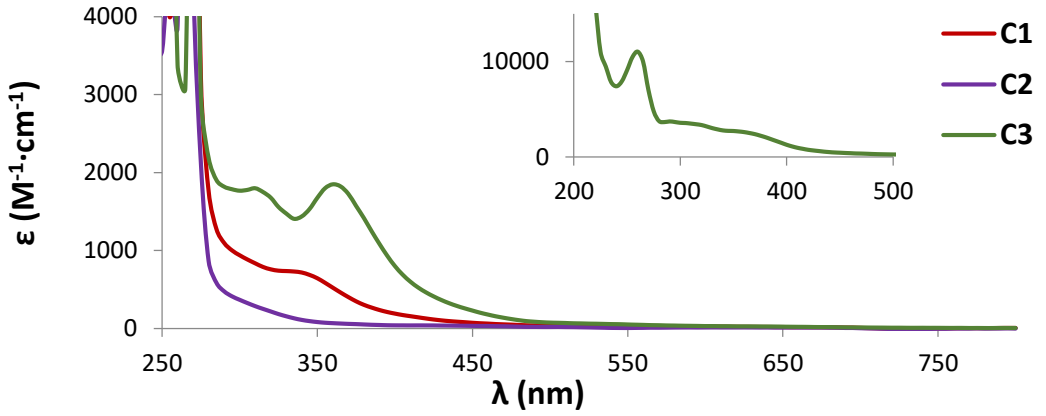

Figure III.10. UV-Vis spectra (298K) in acetonitrile of **BPhMeNH** based complexes.

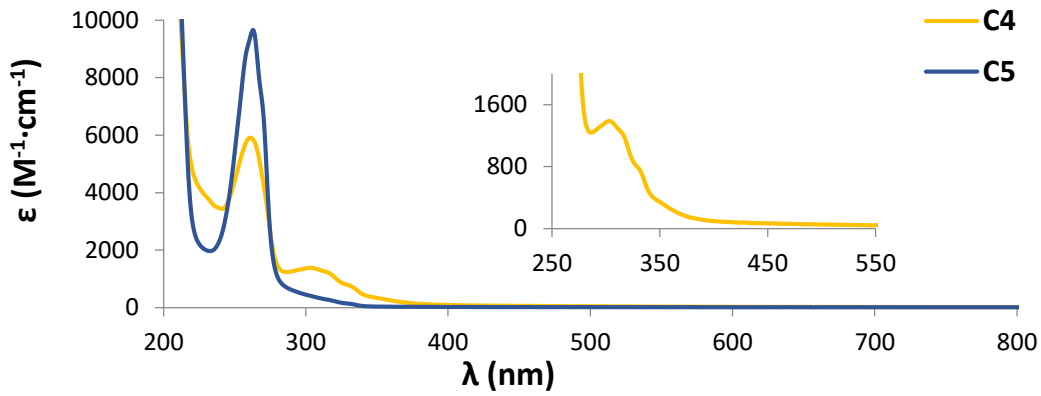

Figure III.11. UV-Vis spectra (298K) in acetonitrile of **DCD** based complexes.

Table III.3. Spectrophotometric data for **C1-C5** complexes in acetonitrile at room temperature.

	λ_{max} (ε, $M^{-1}\cdot cm^{-1}$)	
Complex	π–π*	MLCT
C1	270 (10600)	335 (730)
C2	265 (10600)	-
C3	260 (11000)	310 (1800), 360 (1800)
C4	261 (5900)	300 (1500), 330 (790)
C5	263 (7700)	-

III.1.4.4 Electrochemistry of the complexes

To complement the spectroscopic results presented in the preceding section, electrochemistry experiments were carried out on all the complexes to assess their redox properties. Cyclic voltammetry experiments were carried out in dry CH_3CN, sodium saturated calomel electrode was used as a reference and tetrabutylammonium hexafluorophosphate was used as supporting electrolyte. The cyclic voltammograms are depicted in figures III.12-III.13.

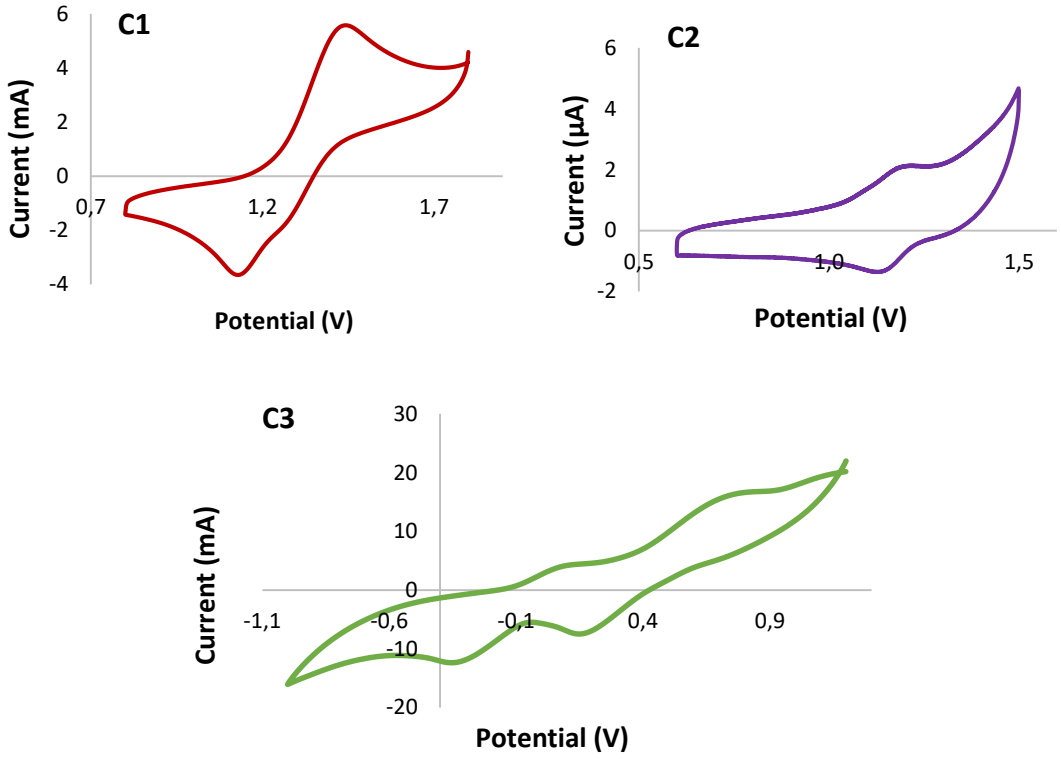

Figure III.12. Cyclic voltammograms of **BPhMeNH** based complexes at a scan rate of 50 mV s^{-1} for **C1**, 100 mV s^{-1} for **C2** and 500 mV s^{-1} for **C3** (2 mg of complex in 4 mL of CH_3CN).

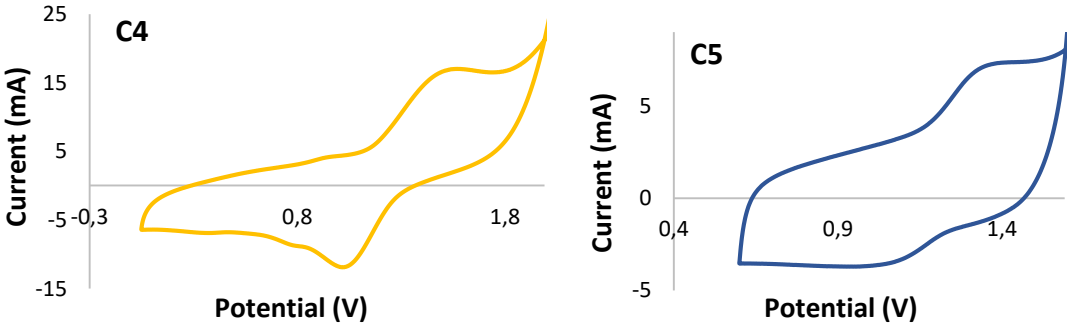

Figure III.13. Cyclic voltammograms of **DCD** based complexes at a scan rate of 500 mV s^{-1} for **C4** and **C5** (2 mg of complex in 4 mL of CH_3CN).

All the complexes showed a chemically reversible, electrochemically quasi-reversible wave, as ΔE range from 73 to 589 mV. The redox potentials of the iron triflate complexes are found around 1260 mV, meanwhile manganese triflate complexes appear around 1190 mV displaying a less defined redox process. It is reasonable to assign these signals to the M^{III}/M^{II} redox potential as compared with similar complexes.[122, 173-176]

Table III.4. Electrochemical data for **C1-C5** complexes in acetonitrile at room temperature.

Ligand		**L1**		**L2**
		$E_{½}$ (ΔEb, mV)		$E_{½}$ (ΔEb, mV)
Complex	**C1**	1286 (313)	**C4**	1246 (553)
	C2	~1174 (73)	**C5**	~1215 (326)
	C3	-121 (446) 445 (589)		

As expected, **C3** exhibits two redox potentials due to the presence of two iron centers, which are tentatively assigned to the to the Fe^{III}/Fe^{II} redox potential of each metal center. The processes are cathodically shifted with respect to **C1** due to the exchange of OTf^- counterions by CH_3CN in the latter, which leads to the formation of a dicationic complex that is more difficult to oxidize.

III.1.5 Catalytic epoxidation

III.1.5.1 Initial screening

To examine the catalytic efficiency of iron and manganese triflate complexes, some model substrates (**S1-S5**) were tested in epoxidation reaction using aqueous hydrogen peroxide as terminal oxidant. Model substrates included a *cis*- and *trans*-β-methyl substituted styrene, an aliphatic and an aromatic enone, and a *cis*-disubstituted aliphatic olefin (table III.5). In this first screening, reaction conditions were not optimized but slightly modified from some previous studies.[140, 141, 155] The reactions were carried out with 2 and 1 mol % of iron (**C1** and **C4**) and manganese (**C2** and **C5**) complexes respectively in acetonitrile at 0°C and acetic acid was used as additive (1.4 and 14 equiv. respectively).

Table III.5. Catalysts screening in the asymmetric epoxidation of conjugated and non-conjugated olefins under standard conditions.[a]

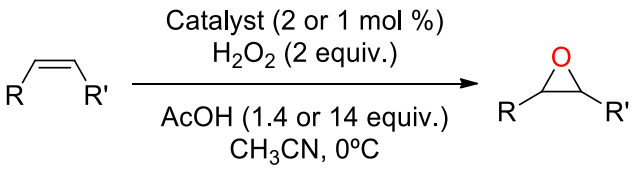

Substrate	Entry	Cat.	Conv. (%)	Yield (%)	ee (%)	Entry	Cat.	Conv. (%)	Yield (%)	ee (%)
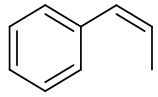 **S1**[b]	1	**C1**	42	12	6	5	**C2**	0	0	-
	2[c]	**C1**	39	14	3	6[c]	**C2**	20	10	25
	3	**C4**	0	0	-	7	**C5**	0	0	-
	4[c]	**C4**	30	5	6	8[c]	**C5**	44	19	6
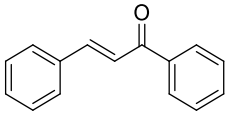 **S2**[d]	9	**C1**	20	6	-[e]	12	**C2**	0	0	-
	10	**C4**	0	0	-	13	**C5**	1	1	-[e]
	11[c]	**C4**	13	2	-[e]	14[c]	**C5**	15	3	-[e]
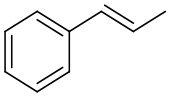 **S3**	15	**C1**	17	9	8	18	**C2**	0	0	-
						19[c]	**C2**	24	18	1
	16	**C4**	0	0	-	20	**C5**	0	0	-
	17[c]	**C4**	29	3	19	21[c]	**C5**	45	2	2
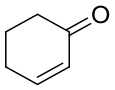 **S4**[b]	22	**C1**	0	0	-	25	**C2**	0	0	-
	23	**C4**	0	0	-	26	**C5**	0	0	-
	24[c]	**C4**	4	2	9	27[c]	**C5**	25	14	1
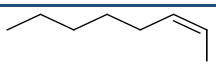 **S5**	28	**C1**	37	11	1	30	**C2**	0	0	-
	29	**C4**	0	0	-	31	**C5**	0	0	-

[a] Reaction conditions are as follow: **C1** and **C4** (2 mol %), **C2** and **C5** (1 mol %), H_2O_2 (2 equiv. as a 9.8 M H_2O_2 in acetonitrile solution added via syringe pump during 30 min), and AcOH (1.4 equiv. for **C1** and **C4**, and 14 equiv. for **C2** and **C5**) in CH_3CN at 0°C during 30 min. Substrate conversions, product yields, and ee's were determined by chiral GC-FID. [b] Absolute configuration of main epoxide product is (2*S*, 3*R*) for **S1** and (2*R*, 3*R*) for **S4** and were determined by comparison with catalysts previously described in the literature. [c] 1.2 equiv. of synthesized peracetic acid was used as oxidant and no acid was added. [d] Substrate conversions and product yields were determined by NMR. [e] Enantioselectivity cannot be calculated due to the low yield.

Surprisingly, all the complexes displayed very low or lacking activity, even for the epoxidation of electron-rich substrates, such as *cis*-*β*-methylstyrene (**S1**), and electron-deficient activated substrates such as *trans*-chalcone (**S2**). With hydrogen peroxide as oxidant, only **C1** presented some activity (entries 1, 9, 15 and 28, table III.5), except for the electron-deficient substrate cyclohexenone (**S4**, entry

22), which is even more difficult to undergo oxidation by an electrophilic reagent. Therefore, synthetic peracetic acid[147] was tested as oxidant, which exhibit less acidic conditions with respect to the commercial one (pH ~ 4 vs pH ~ 1). Slightly better activity was obtained, although still low (entries 4, 6, 8, 11, 14, 21, 24, 27). In all the cases, enantioselectivities observed are very poor.

As seen in the above shown results, catalyst stability under the oxidizing conditions required to epoxidize alkenes is the main problem. It is thought that the obstacle of **L1** based complex is the presence of benzylic positions in the backbone, that can be oxidized easier than the corresponding substrate. For **L2** based complexes, the low activity can be due to the rigidity of the diamine backbone, which is translated in a huge distortion of the complexes that prompt easy detachment of the metal from the ligand during the catalysis.

High-resolution mass spectrometry (HRMS) of the final catalysis crude were performed to obtain further information about this problem. The oxidation of **S5** with H_2O_2 (entries 28-31) were the catalysis chosen for this study. The spectra of iron's catalysis showed as a major peak the corresponding ligand, assigned to $[L+H^+]^+$ (L = **L1** or **L2**). For **C4**, the double protonated ligand was also found, $[\mathbf{L2}+2H^+]^{+2}$. But no trace of complexes have been observed, as the expected peaks would be the monocationic $[LFe(CF_3SO_3)]^+$ ion and the dicationic $[LFe]^{+2}$ (L = **L1** or **L2**) one. Nonetheless, the spectra of **C1** catalysis exhibits a little peak assigned to $[\mathbf{L1}Fe+O]^+$, that could correspond to the oxidation of the ligand.

The spectra of manganese's catalysis display likewise as major peak, the corresponding ligand, assigned to $[L+H^+]^+$ (L = **L1** or **L2**). Also, the double protonated ligand was observed in both spectra, $[L+2H^+]^{+2}$. Moreover the peak identified as $[LMn+AcO^-]^+$ (L = **L1** or **L2**) can be found, and another minor one that corresponds to the $[LMn(CF_3SO_3)]^+$ (L = **L1** or **L2**) was observed in both spectra.

III.2 Summary

The combination of two different aliphatic diamino backbonds, N^1,N^2-bis((*S*)-1-phenylethyl)ethane-1,2-diamine and (*R*,*R*)-1,5-diaza-*cis*-decalin, with the unsubstituted pyridine was used to synthesize two new N_4-donor aminopyridine ligands (**L1** and **L2**). The corresponding iron(II) triflate, manganese(II) triflate and iron(II) chloride (only for the former ligand) complexes (**C1**-**C5**) have been also synthesized and characterized. The catalytic performance of the triflate complexes was tested in the epoxidation of alkenes, giving very poor results. The oxidation of the benzylic positions of **BPhMeNH** backbone and the huge rigidity of the **DCD**

backbone may be the causes of the low or inexistent activity of those catalysts under oxidative conditions.

III.3 Experimental section

III.3.1 Materials

Reagents and solvents used were of commercially available reagent quality unless stated otherwise. Solvents were purchased from Carlo Erba and Scharlab. Solvents were purified and dried by passing through an activated alumina purification system (MBraun SPS-800). Substrates were filtered in basic alumina before performing the epoxidation reactions. HPLC quality acetonitrile was employed in the epoxidation reactions. Preparation and handling of air-sensitive materials were carried out in a N_2 dry box (Braun) with O_2 and H_2O concentrations < 1 ppm.

III.3.2 Instrumentation

IR spectra were taken in a Mattson-Galaxy Satellite FT-IR spectrophotometer using a MKII Golden Gate single reflection ATR system. NMR spectra were taken on a Bruker Ultrashiel DPX400 MHz spectrometer using standard conditions. NMR data are given in the δ scale and are referred to internal TMS. UV/Vis absorption spectra were performed on a diode-array Agilent Cary 60 spectrophotometer and temperature control was maintained with a cryostat from Unisoku Scientific Instruments. Cyclic voltammetry (CV) was performed by using a potentiostat from CHInstruments with a three-electrode cell. The working electrode was a glassy carbon disk from BAS (0.07 cm^2), the reference electrode was a sodium saturated calomel electrode, and the auxiliary electrode was a platinum wire. CV was carried out with nBu_4NPF_6 (TBAHP) as a supporting electrolyte (0.1M). Elemental analyses of C, H, and N were performed using a CHNS-O EA-1108 elemental analyser from Fisons. High resolution mass spectra (HRMS) were recorded on a Bruker MicroTOF-Q IITM instrument with an ESI source and a quadrupole analyser at Serveis Tècnics of the University of Girona. Samples were introduced into the mass spectrometer ion source by direct infusion through a syringe pump and were externally calibrated using sodium formate. Oxidation products were identified by ^{1}H and ^{13}C-NMR analyses. Chromatographic resolution of enantiomers was performed on HPLC 1200 series Agilent technologies using CHIRALPAK-IA and CHIRALPAK-IC columns. The configuration of the major enantiomer was determined by chemical correlation. The X-ray measurements were carried out on a BRUKER SMART APEX CCD

diffractometer using graphite-monochromated Mo Ka radiation (l = 0.71073 Å) from an X-ray Tube. Programs used: data collection, Smart Version 5.631, 1997-2002; data reduction, Saint+ Version 6.36A, 2001; absorption correction, SADABS Version 2.10, 2001. Structure solution and refinement was done using SHELXTL Version 6.14, 2000-2003 and SHELXL-2017. The structures were solved by direct methods and refined by full-matrix least-squares methods on F^2. The non-hydrogen atoms were refined anisotropically. The H-atoms were placed in geometrically optimized positions and forced to ride on the atom to which they are attached.

III.3.3 Synthesis of complexes

III.3.3.1 Synthesis of backbones

The *N*[1],*N*[2]-bis((*S*)-1-phenylethyl)ethane-1,2-diamine ((*S*,*S*)-**BPhMeNH**) was synthetized according to a described procedure.[159]

The (*R*,*R*)-1,5-diaza-cis-decalin ((*R*,*R*)-**DCD**) was obtained from a commercially available complex, [(*R*,*R*)-1,5-diaza-*cis*-decalin]copper hydroxide iodide hydrate.

To 250 mg of [(*R*,*R*)-1,5-diaza-*cis*-decalin] copper hydroxide iodide hydrate (0.72 mmol), ammonium hydroxide solution (5 mL) was added. The solution turned deep blue due to the formation of copper ammonia ion complex. The mixture was extracted with CH_2Cl_2 (3 x 10 mL). The combined organic layers were dried over anhydrous $MgSO_4$ and the solvent was removed under reduced pressure to obtain (*R*,*R*)-1,5-diaza-*cis*-decalin (115,7 mg, 58% yield). Spectral data match those previously reported.[161]

III.3.3.2 Synthesis of ligands

Synthesis of (*S*,*S*)-^{H}BPhMeN (L1)

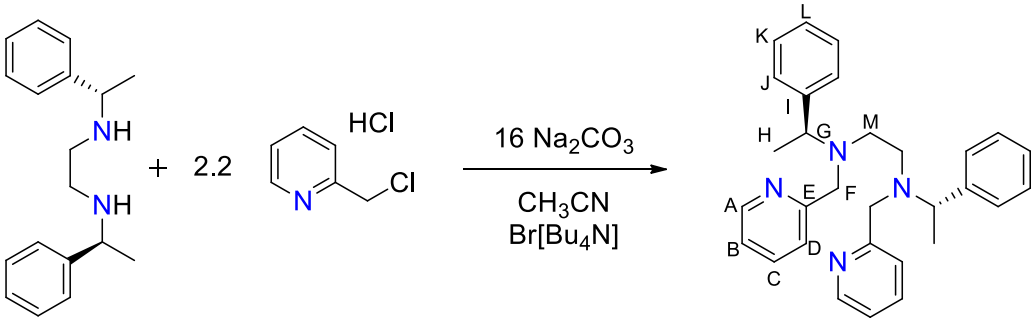

Scheme III.3. Synthesis of (*S*,*S*)-^{H}**BPhMeN**.

2-Picolyl chloride hydrochloride (218.21 mg, 1.30 mmol), **(*S*,*S*)-ohbiq** (156.7 mg, 0.59 mmol) and anhydrous acetonitrile (30 mL) were mixed in a 100 mL flask. Na_2CO_3 (1.01 g) and tetrabutylammonium bromide (20 mg) were added directly as solids and the resulting mixture was heated at reflux under N_2 for 18 hours. After cooling to room temperature, the resulting brown mixture was filtered and the filter cake was washed with CH_2Cl_2. The combined filtrates were evaporated under reduced pressure. To the resulting residue, 1M NaOH (20 mL) was added and the mixture was extracted with CH_2Cl_2 (3 x 15 mL). The combined organic layers were dried over anhydrous $MgSO_4$ and the solvent was removed under reduced pressure. The residue was purified by preparative chromatography (silica, CH_2Cl_2:MeOH:NH_3 96:3:1) to provide 152.2 mg (58% yield) of a pale orange solid. ^{1}H-NMR ($CDCl_3$, 400 MHz, 300K) δ, ppm: 8.44 (d, *J* = 4.8 Hz, 2H, H_A), 7.56 (t, *J* = 8.0 Hz, 2H, H_C), 7.42 (d, *J* = 7.8 Hz, 2H, H_D), 7.31-7.23 (m, 8H, $H_{J,K}$), 7.23-7.17 (m, 2H, H_L), 7.12-7.04 (m, 2H, H_B), 3.77 (q, *J* = 6.8 Hz, 2H, H_G), 3.72 (d, *J* = 15.4 Hz, 2H, H_F), 3.57 (d, *J* = 15.2 Hz, 2H, $H_{F'}$), 2.71-2.57 (m, 2H, H_M), 2.57-2.41 (m, 2H, $H_{M'}$), 1.29 (d, *J* = 6.7 Hz, 6H, H_H). ^{13}C-NMR ($CDCl_3$, 133 MHz, 300K) δ, ppm: 161.32 (E), 148.63 (A), 143.42 (I), 136.25 (C), 128.03 (J), 127.69 (N), 126.69 (L), 122.61 (D), 121.62 (B), 59.33 (G), 57.27 (F), 49.46 (O), 15.81 (H). HRMS (ESI-MS) m/z calculated for $C_{30}H_{35}N_4$ $[M+H]^+$: 451.2856, found: 451.2866; $C_{30}H_{34}N_4Na$ $[M+Na]^+$: 473.2676, found: 473.2672. FT-IR (ATR) ν, cm^{-1}: 3082-2830 (C-H)sp^3 , 1669, 1589, 1568, 1492, 1432, 1372, 1146, 1117, 1084, 994, 757, 731, 698, 579.

Synthesis of (*R*,*R*)-^{H}DCD (L2)

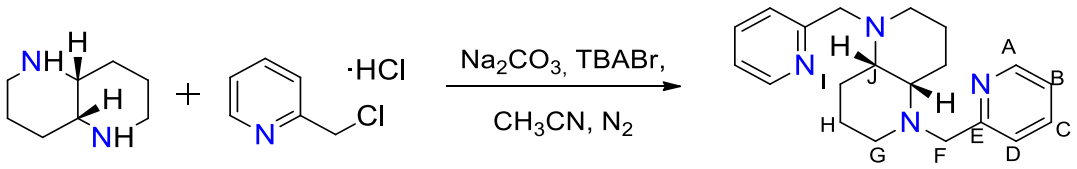

Scheme III.4. Synthesis of (*R*,*R*)-^{H}**DCD**.

It was prepared in analogous manner to **L1** starting from **(*R*,*R*)-DCD** (78.3 mg, 415.7 μmol) and 2-picolyl chloride hydrochloride (205.6 mg, 8.93 mmol) to provide 109.8 mg (61% yield) of a yellow oil. ^{1}H-NMR ($CDCl_3$, 400 MHz, 300K) δ, ppm: 8.49 (ddd, *J* = 4.9, 1.8, 0.9 Hz, 2H, H_A), 7.60 (td, *J* = 7.6, 1.8 Hz, 2H, H_C), 7.45 (d, *J* = 7.8 Hz, 2H, H_D), 7.10 (ddd, *J* = 7.5, 4.9, 1.2 Hz, 2H, H_B), 3.84 (d, *J* = 14.5 Hz, 2H, H_F), 3.74 (d, J = 14.4 Hz, 2H, $H_{F'}$), 3.12-3.01 (m, 2H, H_J), 2.50 (t, *J* = 11.5 Hz, 2H, H_G), 2.41 (d, *J* = 10.9 Hz, 2H, $H_{G'}$), 1.70 (dd, *J* = 36.7, 10.2 Hz, 6H, $H_{I,H}$), 1.49 (dtt, *J* = 17.0, 8.5, 4.3 Hz, 2H, $H_{H'}$). ^{13}C-NMR($CDCl_3$, 133 MHz, 300K) δ, ppm: 160.17 (E), 148.95

(A), 136.40 (C), 122.64 (D), 121.75 (B), 60.57 (F), 59.17 (J), 46.14 (G), 24.27 (H), 16.51 (I). HRMS (ESI-MS) m/z calculated for $C_{20}H_{26}N_4Na$ $[M+Na]^+$: 345.2050, found: 345.2065, $C_{20}H_{27}N_4$ $[M+H]^+$: 323.2230, found: 323.2246. FT-IR (ATR) ν, cm^{-1}: 2923-2853 (C-H)sp^3 , 1665, 1590, 1470, 1431, 1143, 993, 755, 619.

III.3.3.3 Synthesis of complexes

Synthesis of (*S*,*S*)-^{H}BPhMeN based complexes

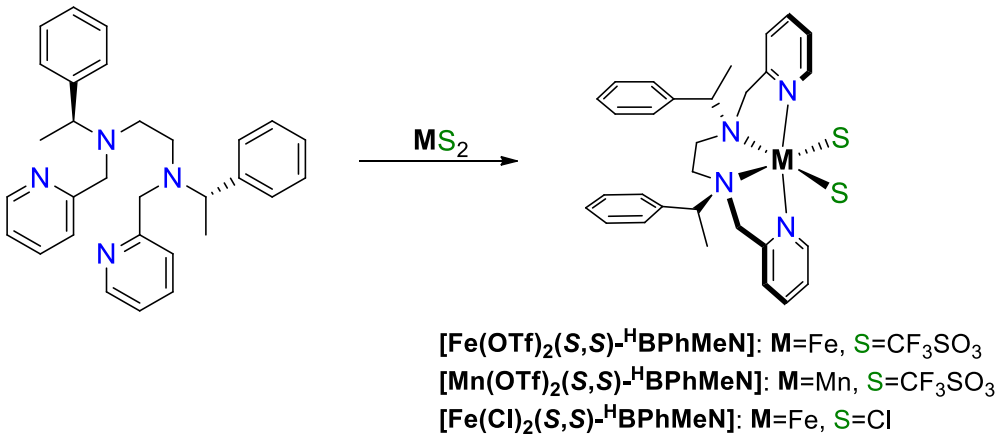

[Fe(OTf)$_2$(*S*,*S*)-^{H}BPhMeN]: **M**=Fe, S=CF_3SO_3
[Mn(OTf)$_2$(*S*,*S*)-^{H}BPhMeN]: **M**=Mn, S=CF_3SO_3
[Fe(Cl)$_2$(*S*,*S*)-^{H}BPhMeN]: **M**=Fe, S=Cl

Scheme III.5. Synthesis and nomenclature of (*S*,*S*)-^{H}**BPhMeN** based complexes.

[Fe(OTf)$_2$(*S*,*S*)-^{H}BPhMeN] (**C1**) was synthesized following a similar procedure described in literature for bipyrrolidine based complex.[139] Under a N_2 atmosphere, a suspension of $Fe(CF_3SO_3)_2(CH_3CN)_2$ (172.74 mg, 396.1 µmol) in anhydrous THF (1 mL) was added drop-wise to a vigorously stirred solution of **L1** (178.5 mg, 396.1 µmol) in anhydrous THF (1 mL). After stirring overnight, ether was added until complete precipitation. The orange solid was filtered, dried and solved in the minimum quantity of CH_2Cl_2 and the solution filtered off through celite©. Reiterative slow diethyl ether diffusion over the resultant solution afforded, in some days, 103.2 mg of pale yellow crystals (32% yield). HRMS (ESI-MS) m/z calculated for $C_{31}H_{34}F_3FeN_4O_3S$ $[M-OTf]^+$: 655.1648, found: 655.1668; $C_{30}H_{34}FeN_4$ $[M-2OTf]^{2+}$: 253.1061, found: 253.1062. FT-IR (ATR) ν, cm^{-1}: 1610, 1443, 1295, 1210, 1156, 1021, 920, 778, 707, 633, 571, 515, 416. Anal. Calcd. for $C_{32}H_{34}F_6FeN_4O_6S_2$: C, 47.77; H, 4.26; N, 6.96%; found: C, 47.75; H, 4.38; N, 7.09%.

[Mn(OTf)$_2$(*S*,*S*)-^{H}BPhMeN] (**C2**) was prepared in a similar manner to **C1,** starting from **L1** (50 mg, 111 µmol) and $Mn(CF_3SO_3)_2$ (39.2 mg, 111 µmol) in anhydrous CH_2Cl_2 (1 mL) to obtain 47.7 mg of a white solid (54% yield). HRMS (ESI-MS) m/z calculated for $C_{31}H_{34}F_3MnN_4O_3S$ $[M-OTf]^+$: 654.1679, found: 654.1668; $C_{30}H_{34}MnN_4$ $[M-2OTf]^{2+}$: 252.6076, found: 252.6065. FT-IR (ATR) ν, cm^{-1}: 1607,

1442, 1319, 1234, 1207, 1156, 923, 775, 705, 628, 570, 512, 413. Anal. Calcd. for $C_{32}H_{34}F_6MnN_4O_6S_2$: C, 47.82; H, 4.26; N, 6.97%; found: C, 47.83; H, 4.03; N, 6.89%.

[Fe(Cl)$_2$(*S,S*)-^{H}BPhMeN] (**C3**) was prepared in a similar manner to **C1,** starting from **L1** (82.5 mg, 183 µmol) and $FeCl_2$ (23.3 mg, 183 µmol) in anhydrous CH_3CN (1 mL) to obtain 52 mg of yellow crystals (49 % yield). HRMS (ESI-MS) m/z calculated for $C_{30}H_{34}FeN_4Cl$ $[M\text{-}Cl]^+$: 541.1817, found: 541.1833. FT-IR (ATR) ν, cm^{-1}: 3059-2875 (C-H)sp^3, 1605, 1442, 1303, 1020, 766, 705, 553, 419. X-ray analysis indicates that the complex adopts a Λ topological chirality. Anal. Calcd. for $C_{30}H_{34}Cl_2FeN_4{\cdot}0.8CH_2Cl_2$: C, 57.33; H, 4.25.56; N, 8.68%; found: C, 57.10; H, 5.31; N, 8.72%.

Synthesis of (*S,S*)-^{H}DCD based complexes

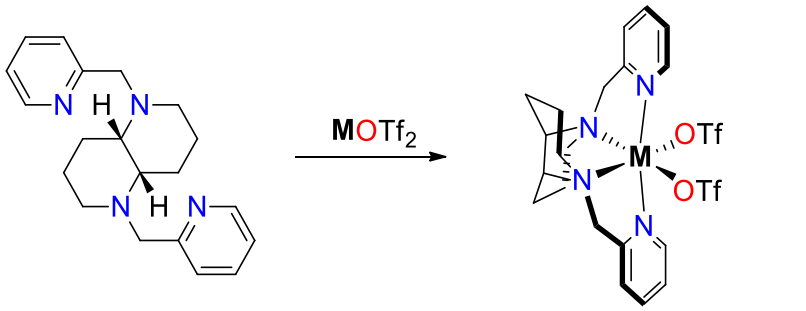

[Fe(OTf)$_2$(*S,S*)-^{H}DCD]: **M**=Fe
[Mn(OTf)$_2$(*S,S*)-^{H}DCD]: **M**=Mn

Scheme III.6. Synthesis and nomenclature of (*S,S*)-^{H}**DCD** based complexes.

[Fe(OTf)$_2$(*S,S*)-^{H}DCD] (**C4**) was prepared in a similar manner to **C1**, starting from **L2** (63 mg, 195.4 µmol) and $Fe(CF_3SO_3)_2(CH_3CN)_2$ (85.2 mg, 195.4 µmol) in anhydrous CH_2Cl_2 to obtain 71 mg of pale yellow crystals (52% yield). HRMS (ESI-MS) m/z calculated for $C_{21}H_{26}F_3FeN_4O_3S$ $[M\text{-}OTf]^+$: 527.1022, found: 527.1034; $C_{20}H_{26}FeN_4$ $[M\text{-}2OTf]^{2+}$: 189.0748, found: 189.0764. FT-IR (ATR) ν, cm^{-1}: 2957-2865 (C-H)sp^3 , 1608, 1302, 1222, 1157, 1080, 1034, 774, 633, 512, 425. Anal. Calcd. for $C_{22}H_{26}F_6FeN_4O_2S_2 \cdot 1H_2O$: C, 37.19; H, 3.97; N, 7.89%; found: C, 37.29; H, 4.14; N, 7.90%. X-ray analysis indicates that the complex adopts a Δ topological chirality.

[Mn(OTf)$_2$(*S,S*)-^{H}DCD] (**C5**) was prepared in a similar manner to **C1**, starting from **L2** (44.0 mg, 136.5 µmol) and $Mn(CF_3SO_3)_2$ (48.2 mg, 136.5 µmol) in anhydrous CH_2Cl_2 to obtain 46 mg of yellow crystals (50% yield). HRMS (ESI-MS) m/z calculated for $C_{21}H_{26}F_3MnN_4O_3S$ $[M\text{-}OTf]^+$: 526.1053, found: 526.1061; $C_{22}H_{29}MnN_5$ $[M\text{-}2OTf\text{+}CH_3CN]^{2+}$: 209.0896, found: 209.0896; $C_{20}H_{28}MnN_4O$

$[M\text{-}2OTf+H_2O]^{2+}$: 197.5816, found: 197.5817; $C_{20}H_{26}MnN_4$ $[M\text{-}2OTf]^{2+}$: 118.5763, found: 118.5776. FT-IR (ATR) ν, cm^{-1}: 2969-2862 (C-H)sp^3 , 1606, 1306, 1210, 1165, 1080, 1031, 769, 633, 5132, 423. Anal. Calcd. for $C_{22}H_{26}F_6MnN_4O_2S_2$: C, 39.12; H, 3.88; N, 8.29%; found: C, 39.33; H, 3.90; N, 8.36%. X-ray analysis indicates that the complex adopts a Δ topological chirality.

III.3.4 Catalytic reactions conditions

Hydrogen peroxide solutions employed in the reactions were prepared by diluting commercially available hydrogen peroxide (32%, unless indicated, H_2O_2 solution in water, Aldrich) in acetonitrile (1:3 v:v).

III.3.4.1 Reaction protocol

Table III.5:

An acetonitrile solution (750 µL) of the corresponding substrate (**S1**-**S5**) (88 µmols) and the corresponding complex (2 mol % for iron, and 1 mol % for manganese) was prepared in a vial (10 mL) equipped with a stir bar cooled at 0°C, in an ice bath. A 7 µL (neat, 1.4 equiv. 0.12 mmols) for iron catalysis and 70 µL (neat, 14 equiv. 1.2 mmols) for manganese ones of acetic acid was added directly to the solution. Then, 70 µL of 3:1 v:v acetonitrile:hydrogen peroxide solution 30% (2 equiv. 0.18 mmols) was added by syringe pump over a period of 30 min. The solution was further stirred at 0°C for 30 minutes. At this point an internal standard (biphenyl) was added and the solution was quickly filtered through a basic alumina plug, which was subsequently rinsed with 2 x 1 mL AcOEt. GC analysis of the solution provided substrate conversions and product yields relative to the internal standard integration.

For **S2** substrate, the internal standard used was 1,3,5-trimethoxybenzene. After its addition, 5 mL of a saturated aqueous solution of $NaHCO_3$ were added, and the resulting mixture was extracted with 2 mL of CH_2Cl_2 (3 times). Then, organic layers were dried over $MgSO_4$ and the solvent was removed under reduced pressure. The resultant product was dissolved in $CDCl_3$ and the yield and conversion were calculated by NMR. As the yields were very low, the HPLC analysis was not performed.

III.3.4.2 Calibration curves and epoxide determination

GC analysis of the catalysis provided substrate conversions and product yields relative to the internal standard integration. Substrates calibration curves

were obtained from commercially available substrates. Epoxides calibration curves used are those of the corresponding substrates.

Epoxides were identified by comparison to the GC retention time of authentic samples, and by their GC-MS spectrum. Commercially not available epoxides were identified by a combination of ^{1}H, ^{13}C-NMR analyses, and GC-MS. The epoxide product was identified by comparison to the GC retention time of racemate epoxide and by its GC-MS spectrum.

The racemic epoxides were synthetized with an achiral catalyst ([$Mn(OTf)_2(^{H}pytacn)$]) that has been already reported for epoxidation reactions.[177]

CHAPTER IV

Iron and manganese complexes based on the 1,1',2,2',3,3',4,4'-octahydro-1,1'-biisoquinoline backbone: synthesis, characterization and catalytic epoxidation activity

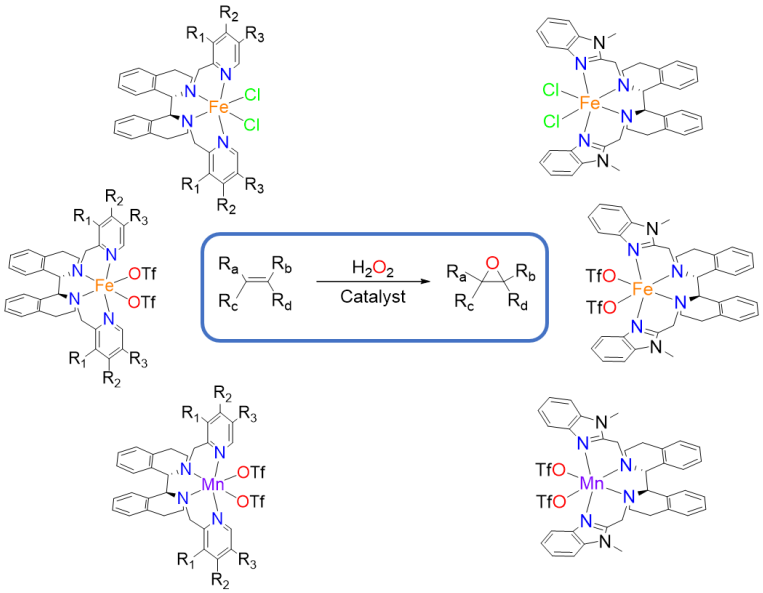

Abstract

In this chapter a new family of iron and manganese complexes (**C6-C20**) based on bis(aminopyridine) and bis(aminobenzimidazol) tetradentate ligands is described. 1,1',2,2',3,3',4,4'-octahydro-1,1'-biisoquinoline is used as an aliphatic diamine backbone and different substituents are introduced in the pyridine moiety for the modification of the electronic and steric properties of those ligands. The corresponding iron and manganese triflate complexes are used as catalysts in the epoxidation of alkenes with H_2O_2, achieving moderate to good yields in some model substrates, and good to excellent enantioselectivities.

MANUSCRIPT IN PREPARATION. EMBARGOED UNTIL PUBLICATION DATE

CHAPTER V

Manganese catalysed highly enantioselective epoxidation of β,β-disubstituted enamides with aqueous H_2O_2. Stereoselectivity reversal with catalysts having the same chirality at the metal

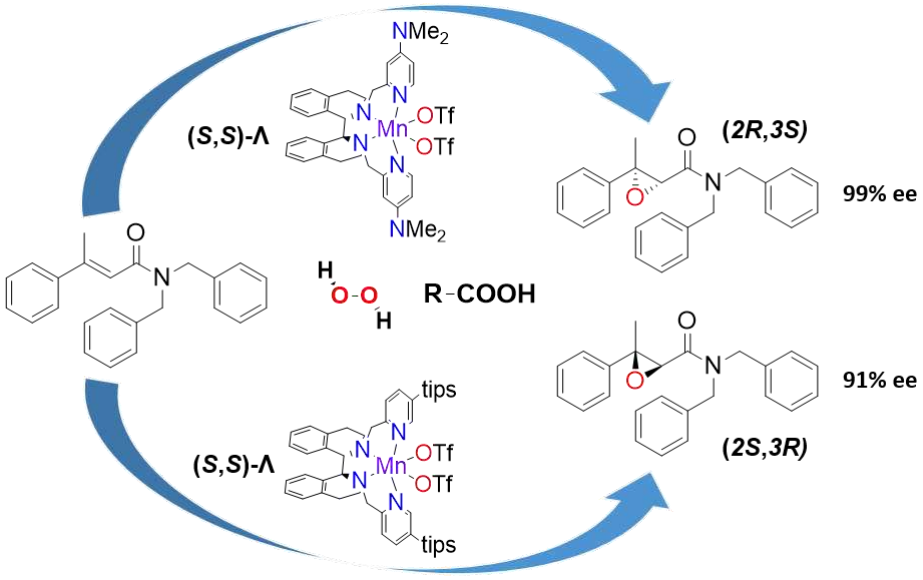

Abstract

In this chapter we take advantage of **L5** and **L6** ligands described in chapter III.2, where dimethylamino and triisopropylsilyl groups are respectively used as substituents in the pyridine moiety. When the corresponding manganese complex of the former ligand is used as catalyst, highly enantioselective epoxidation of β,β-disubstituted enamides with aqueous H_2O_2 can be accomplished. Surprisingly, complexes **C18** and **C19**, sharing the same chirality at the diamine and the same chirality at the metal, produce epoxide products with opposite absolute configuration.

MANUSCRIPT IN PREPARATION. EMBARGOED UNTIL PUBLICATION DATE

CHAPTER VI

Iron and manganese complexes based on the 2,2-bipiperidine backbone: synthesis, characterization and catalytic C-H oxidation activity

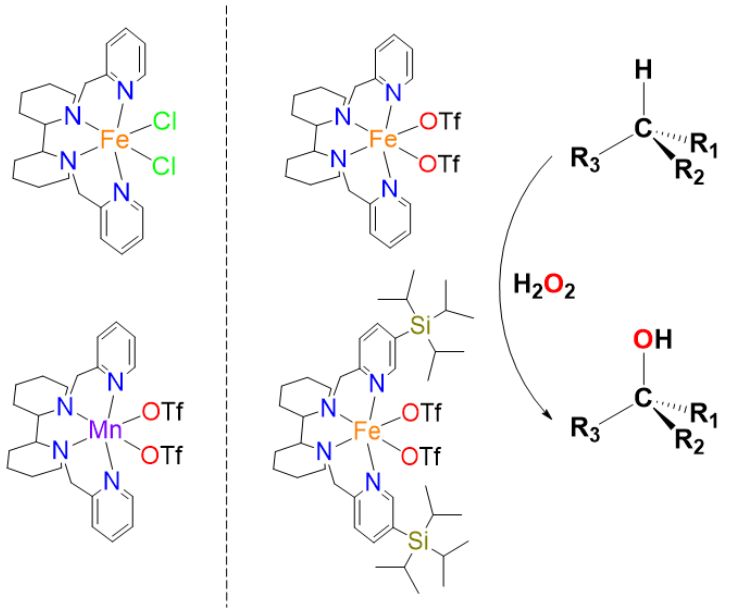

Abstract

Herein, 2,2'-bipiperidine was used as diamine backbone for the synthesis of new iron and manganese complexes (C21-C27). The iron triflate complexes C24 and C27 (bearing the unsubstituted and the tips substituted pyridine respectively) have been tested as catalysts in the oxidation of alkanes and compared with the analogous complexes that contain N,N'-dimethyl-trans-1,2-cyclohexanediamine, 2,2'-bipyrrolidine, 1,1'-biisoindoline and 1,1',2,2',3,3',4,4'-octahydro-1,1'-biisoquinoline (C11 and C14) as backbones. C27 exhibit stereospecific and selective oxidation of alkanes, affording very promising results.

VI.1 Results and discussion

VI.1.1 Synthesis of the backbone

The diamine used in this chapter is the 2,2'-bipiperidine. Its synthesis through different pathways has been already reported in the literature.[244-246] The first procedure followed was the one described by Rybak-Akimova and co-workers,[244] where 2,2′-bipyridine was reduced by Raney nickel and after work up, the crude obtained was a mixture of initial reagent and product (scheme VI.1, a). Then, HBr was added to precipitate the desired compound, and the solid residue was directly used in the next step, which is the formation of the aminopyridine ligand in its racemic version.

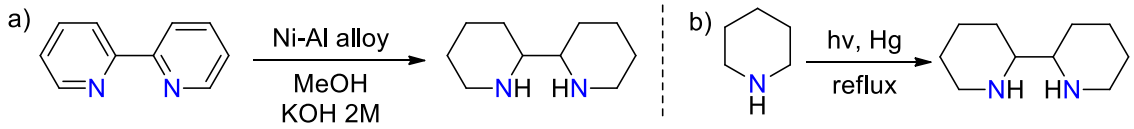

Scheme VI.1. Possible methods to prepare 2,2'-bipiperidine.

As we are interested in the enantiopure version of the backbone, after removal of the HBr, the racemic diamine obtained was submitted to chiral resolution with tartaric acid.[246] This methodology should be straightforward, as it only consists in mixing the diamine with the desired enantiomerically enriched tartaric acid in water/methanol, and after heating, let it slowly crystallize in an ice bath (scheme VI.2, a), but all our attempts were completely unsuccessful. Maybe this was due to the low quantity of material that we are working with.

At this point, two incongruences arose. The first one is that after reduction of 2,2′-bipyridine with Ni-Al alloy, a mixture of racemic and *meso* forms should be obtained, a question that was not noted in the original report. Indeed, another publication by Hoffmann that follows the same starting procedure, describe separation of *meso* and racemic forms taking advantage of the different solubility of their corresponding hydrobromic salts (scheme VI.2, b).[245] The second issue is about the resolution. In the aforementioned paper, the use of tartaric acid as resolving chiral reagent proved unsuccessful to achieve chiral resolution. Instead, the authors propose and alternative method by forming diastereoisomers with PCl_3, *N*,*N*-dimethylaniline and 1-menthol, that could be separated by crystallizations. So, the resolution with tartaric acid appears not to be a straightforward procedure.

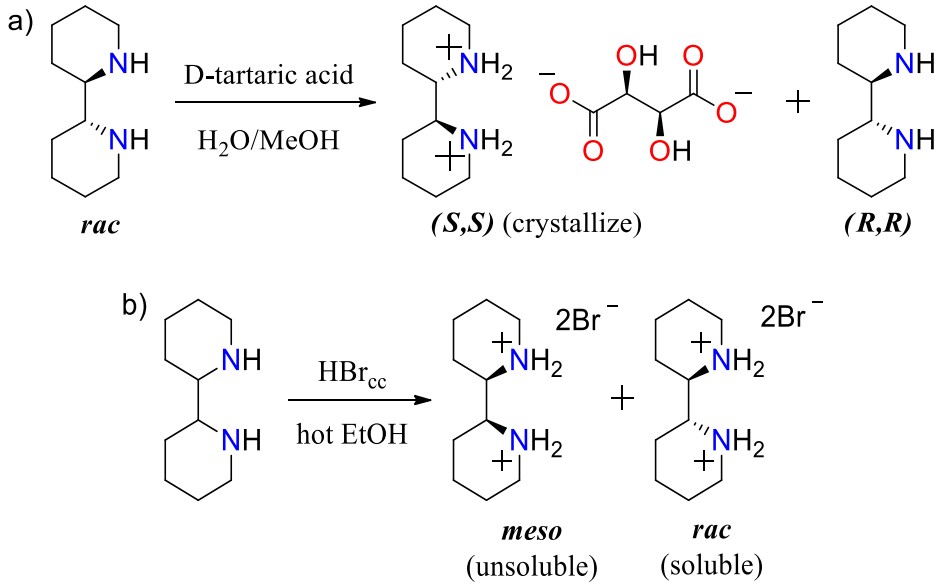

Scheme VI.2. Optical chiral resolution of 2,2'-bipiperidine according to ref. 148b and 148c.

Consequently, an alternative method was used to obtain the isomeric mixture of 2,2'-bipiperidine in a larger amount (scheme VI.1, b). A combination of piperidine and a drop of mercury, under photochemical irradiation and reflux was pursued.[246] After 7 days under reflux, distillation under vacuum provided a clear colorless liquid, containing a mixture of 2,2'-bipiperidines. Then, hydrobromic acid was added carefully and the two diastereoisomers were separated by their different solubility in hot ethanol, following the Hoffmann's reported procedure (scheme VI.2, b).

At this point, resolution of the chiral 2,2'-bipiperidines was attempted with the tartrate procedure, but all the attempts were ineffective.

VI.1.2 Synthesis of ligands and complexes

As the enantiopure version of the diamine could not be obtained, different bis(aminopyridine) tetradentate ligands (**L8-L10**, figure VI.1), based on the racemic and *meso* forms of 2,2'-bipiperidine (**bpp**) have been prepared.

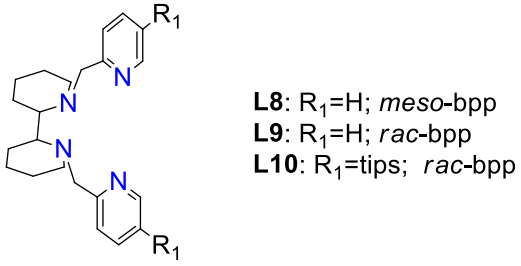

Figure VI.1. Structures of the new **bpp** based ligands.

Tetradentate ligands were prepared by alkylation of the **bpp** with the corresponding picolyl chloride in acetonitrile under reflux using Na_2CO_3 as base. After chromatographic purification, the ligands with the unsubstituted pyridine were obtained as brown oils in 50 and 74% yield for **L8** and **L9** ligands respectively. While for tips substituted pyridine ligand, a solid material was achieved, still with very poor yield (only 10% for **L10**).

Preparation of the complexes involved straightforward reaction of the corresponding tetradentate ligands in THF or CH_3CN under anaerobic conditions with [$FeCl_2$], [$Fe(CF_3SO_3)_2(CH_3CN)_2$] and [$Mn(CF_3SO_3)_2$] respectively to obtain **C21-C23** and **C25-C26** complexes (figure VI.2).

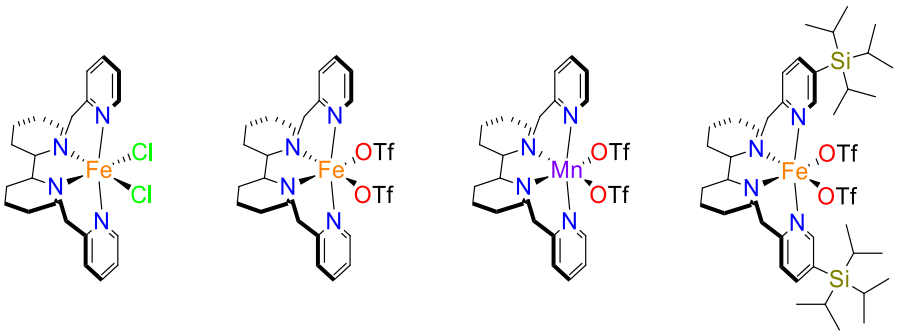

C21: *meso*-bpp
C22: *rac*-bpp

C23: *meso*-bpp
C24: *rac*-bpp

C25: *meso*-bpp
C26: *rac*-bpp

C27: *rac*-bpp

Figure VI.2. 3D chemical diagrams of **C21-C27** complexes.

Unexpectedly, the synthesis of **C24** following this strategy yielded a mixture of *cis*-α and *cis*-β isomers, as evidenced by ^{1}H-NMR, and their separation proved impossible. Our original target was the selective preparation of complexes adopting a *cis*-α topological geometry, because literature studies have demonstrated they are specially efficient oxidation catalysts.[108, 109, 130, 247] Therefore, a two-step route for the selective preparation of this isomer was followed via reaction of the tetradentate **L9** ligand with iron(II) chloride (**C22** was obtained) and subsequent reaction with 2 equiv. of AgOTf. As the same output was expected for **C27** complex, the two-step synthesis in one pot was also used.

VI.1.3 Solid state characterization: X-ray crystallography

The solid-state molecular structure of **C21-C26** complexes, were established by X-ray diffraction analysis. Figure VI.3 shows the X-ray structures of all of them and table VI.1 gathers selected bond lengths and angles for **C22**, **C24**, and **C26** crystallographically determined structures. For the other complexes, this data can be found in the table VI.13 in the experimental section of this chapter, and the

experimental details of the crystal structure determination of all the complexes are collected in the annex.

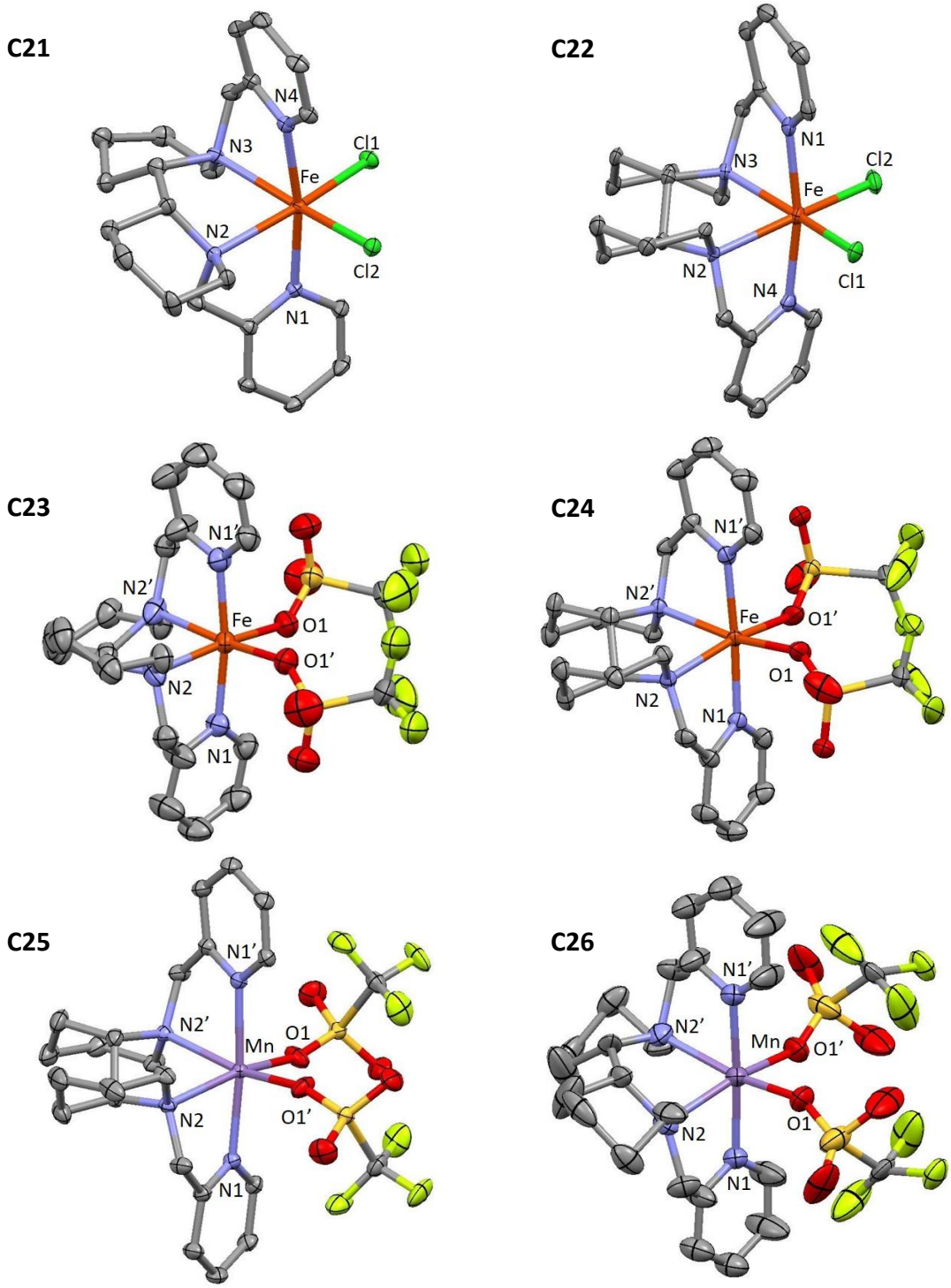

Figure VI.3. Ellipsoid diagrams of **C21-C26** complexes at a 50% of probability. Hydrogen atoms were omitted for clarity.

Table VI.1. Selected bond lengths (Å) and angles (°) for **C22**, **C24**, and **C26** complexes.

	C22		**C24**		**C26**
Fe-N1	2.214(4)	Fe-N1	2.149(2)	Mn-N1	2.2255(15)
Fe-N2	2.311(4)	Fe-N2	2.242(2)	Mn-N2	2.2760(16)
Fe-N3	2.305(3)	Fe-N2'	2.242(2)	Mn-N2'	2.2760(16)
Fe-N4	2.214(4)	Fe-N1'	2.149(2)	Mn-N1'	2.2255(15)
Fe-Cl1	2.4451(14)	Fe-O1	2.139(2)	Mn-O1	2.1380(15)
Fe-Cl2	2.4230(13)	Fe-O1'	2.139(2)	Mn-O1'	2.1380(15)
N1-Fe-N2	75.23(14)	N1-Fe-N2	77.80(8)	N1-Mn-N2	76.11(6)
N1-Fe-N4	168.81(13)	N1-Fe-N1'	176.64(10)	N1-Mn-N1'	174.60(8)
N1-Fe-Cl2	94.28(10)	N1-Fe-O1'	88.57(9)	N1-Mn-O1'	94.85(6)
N1-Fe-Cl1	94.43(11)	N1-Fe-O1	93.78(9)	N1-Mn-O1	88.75(6)
N2-Fe-N4	96.89(13)	N2-Fe-N1'	99.56(8)	N2-Mn-N1'	99.66(6)
N3-Fe-N4	75.26(14)	N2'-Fe-N1'	77.80(8)	N2'-Mn-N1'	76.11(6)
N2-Fe-Cl2	90.92(9)	N2-Fe-O1'	164.67(8)	N2-Mn-O1'	94.00(6)
N4-Fe-Cl1	91.53(10)	N1'-Fe-O1	88.57(9)	N1'-Mn-O1	94.85(6)
N3-Fe-Cl1	92.30(10)	N2'-Fe-O1	164.67(8)	N2'-Mn-O1	94.00(6)
N2-Fe-N3	77.20(12)	N2-Fe-N2'	79.18(11)	N2-Mn-N2'	79.66(8)
N3-Fe-Cl2	162.50(10)	N2'-Fe-O1'	96.45(9)	N2'-Mn-O1'	162.21(6)
Cl1-Fe-Cl2	101.73(5)	O1-Fe-O1'	91.36(15)	O1-Mn-O1'	96.58(10)

As expected, all the X-ray structures exhibit a distorted octahedral geometry. For *meso* compounds (**C23** and **C25**) a *cis*-β-topology was expected, because the solid structure of the analogous iron triflate complex based on the 2,2'-bipyrrolidine backbone, has been reported to adopt this topology.[186] However, complexes **C23** and **C25** display a *cis*-α-topology, like the racemic isomers, suggesting a higher flexibility of the 2,2'-bipiperidine diamine in comparison with the 2,2'-bipyrrolidine.

In all the complexes, four coordination sites are occupied by the N atoms of the ligand and the coordination environment is completed by two anionic ligands, either Cl^- or triflate, that are in a relative *cis* configuration. Although the structures shown in the figures reveal all a Λ topological chirality, the crystallographic point groups are not enantiopure, and crystals contain racemic mixtures of complexes with Λ and Δ chirality.

For the iron chloride complexes the Fe–N bond distance are between 2.17-2.37 Å, and for the iron bis-triflato complexes the Fe–N bond distances are between

2.14–2.24 Å, characteristic of high-spin Fe^{II} complexes.[119, 134, 183-186] For the manganese ones the Mn-N distances are between 2.21-2.30 Å, which fall in the range of distances observed in related complexes, also high-spin.[146, 148, 150-153, 155, 164] A close inspection in their structures, evidences that the metal bonds length of the N-atom of the pyridine are systematically shorter (0.1 Å approx.) than those to the N-atom of the amines.

Moreover, the two nitrogen atoms of the pyridine rings are mutually *trans*, with the Npy-M-Npy (M = Fe or Mn) angle ranging from 168.81(13)° for **C22** to 176.69(16)° for **C25**, while the two aliphatic nitrogen atoms (R'RN-M-NRR') (M = Fe or Mn) are mutually *cis*. The R'RN-M-NRR' and R'RN-M-Npy (M = Fe or Mn) angles are all smaller than 90°, because of the formation of five member chelate-rings.

Peculiarly, in the **C22** crystallization, slow diffusion of ethyl ether in a CH_2Cl_2 solution of the compound, afforded crystals with two distinguishable colors. The orange crystals, found as the main material, correspond to the structure previously shown (figure VI.3), while a second group of yellow crystals, obtained in small amounts, correspond to a different complex that is depicted in figure VI.4 (a) (**C22'**). The structure displays a bis(μ-halo)di-iron core, with two bridging chlorides binding symmetrically. Each iron adopts a distorted octahedral environment coordinated to one ligand, which only contains one methylenepyridine attached to the diamine backbone (figure VI.4, b). The complex appears neutral, as two more chlorides were bound to the respective iron(II) centers. It is important to note that the crystals of this compound were obtained in minor amounts, and the incomplete ligand appears also as an impurity present in **L9** ligand, resulting from incomplete alkylation of the 2,2'-bipiperidine.

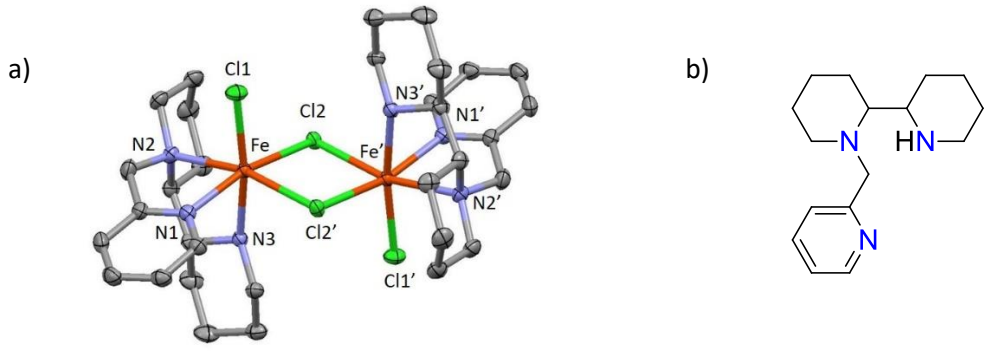

Figure VI.4. a) Ellipsoid diagram of **C22'** at a 50% of probability. Hydrogen atoms were omitted for clarity. b) 3D chemical diagram of the ligand impurity.

VI.1.4 Characterization of the complexes in solution

VI.1.4.1 ESI-MS

The solution behavior of the complexes was analyzed by ESI-MS in acetonitrile. The spectra of iron chloride complexes show an unique cationic peak corresponding to the loss of one chloride $[LFe(Cl)]^+$ (L = **L8-L9**). For the bis-triflate complexes the spectra show two cationic peaks, whose mass and isotopic pattern could be satisfactorily assigned to the monocationic $[LM(CF_3SO_3)]^+$ and to the dicationic $[LM]^{+2}$ (M = Fe or Mn and L = **L8-L10**) ions. For manganese complexes, other peaks are observed corresponding to the dicationic species with water or acetonitrile ligands. These observations strongly suggest that all the complexes retain in solution the mononuclear nature determined in the solid state.

VI.1.4.2 ^{1}H-NMR spectroscopy

As discussed in previous chapters, the ^{1}H-NMR spectra of manganese complexes were not collected.

^{1}H-NMR spectra of iron chloride complexes **C21** and **C22** in CD_2Cl_2 are depicted in figure VI.5. As previously mentioned, the **C22** solid consists of a mixture of two type of crystals, and the orange ones seemed insoluble at CD_2Cl_2; so the shown spectrum should belong mostly to **C22'**. As seen in the solid state, **C22'** structure contains an inversion center that relates the two metal ions, and the ligand has only one pyridine, therefore, the spectrum presents few signals. On the other hand, **C21** has no symmetry, consequently, the spectrum displays one signal per proton. A plausible assignment for some of the protons is illustrated in the spectra. The assignment of the γ-protons is doubtful, but α, β and benzylic protons are comparable to similar complexes (see chapter III, IV and references 98 and 99).

The same complexes in acetone presented poor solubility, that made it difficult to obtain ^{1}H-NMR spectra with a good signal-to-noise ratio. All detectable broad signals appear within the compact 10-0 ppm range. By contrast, in acetonitrile, the complexes were a little bit more soluble exhibiting paramagnetically shifted signals between δ = -14 and δ = 220 ppm for **C21**, while among δ = -20 and δ = 150 ppm for **C22** (^{1}H-NMR spectra in such solvents are depicted in figure VI.8 and in the annex).

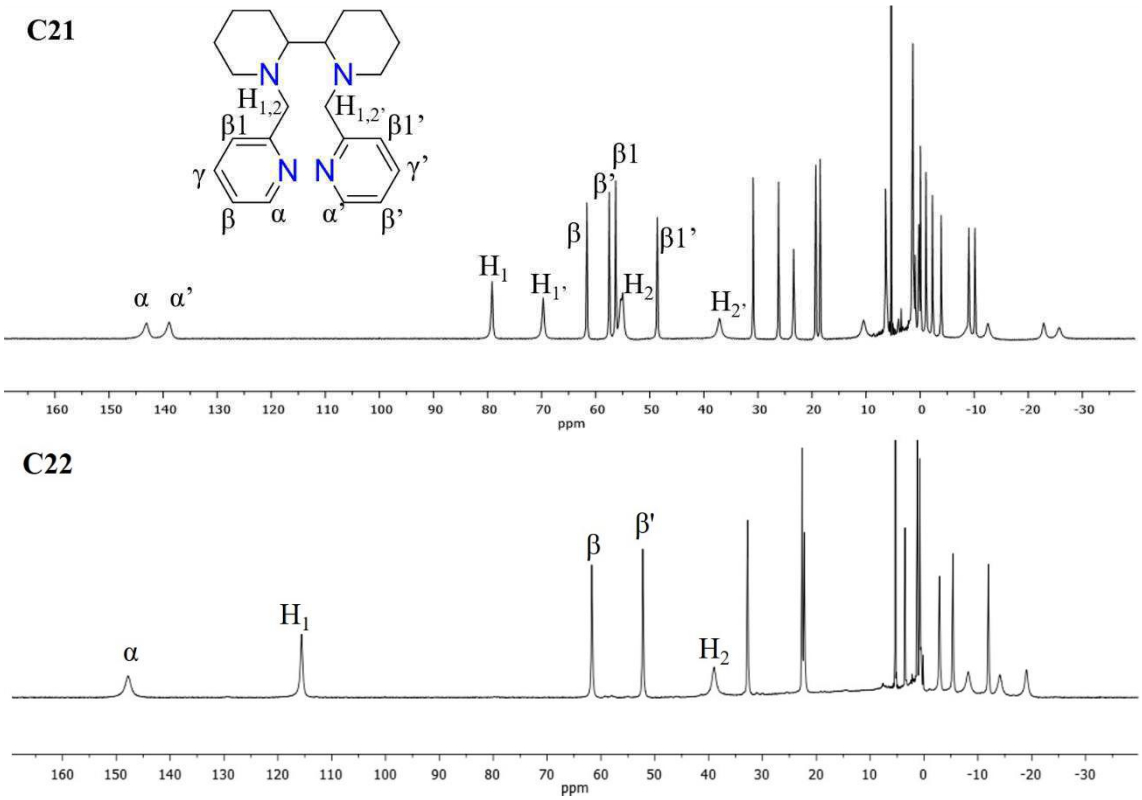

Figure VI.5. ^{1}H-NMR spectra (400 MHz) of iron chloride complexes **C21-C22'** in CD_2Cl_2 at 298K and a plausible assignment.

^{1}H-NMR spectra of iron triflate complexes **C23**, **C24** and **C27** in CD_2Cl_2 are depicted in figure VI.6. All the iron compounds display spectral windows that expand from –35 to 185 ppm with broad signals. This is indicative of octahedral high spin Fe^{II} paramagnetic species.

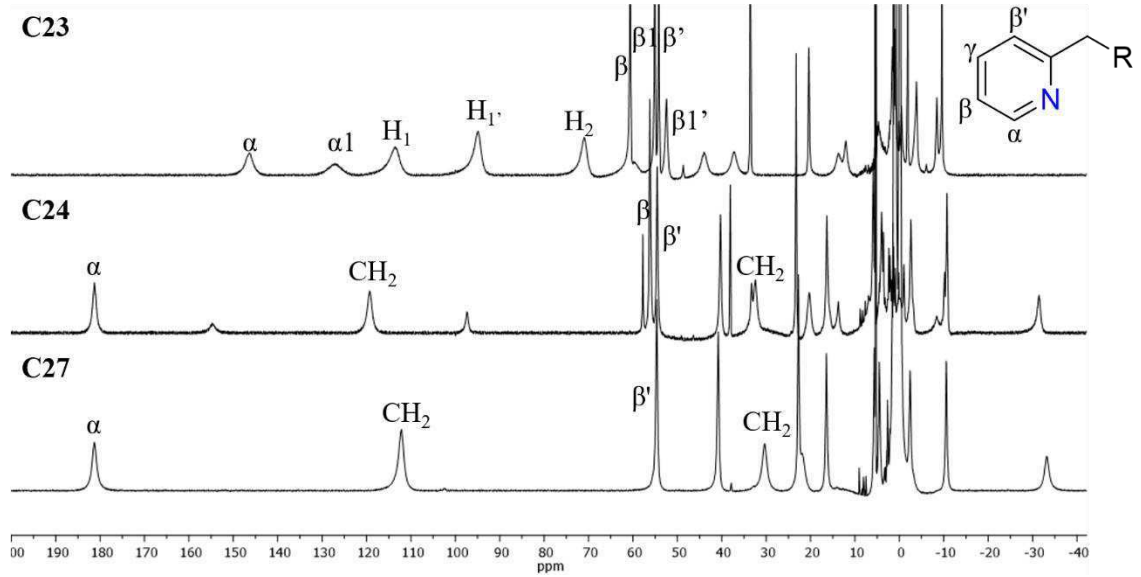

Figure VI.6. ^{1}H-NMR spectra (400 MHz) of iron triflate complexes **C23**, **C24** and **C27** in CD_2Cl_2 at 298K and some plausible assignments.

When compared to the previous spectra, the signals of iron triflate complexes appear broader due to the increased lability of the triflate anions compared to the chloride ones. Nonetheless, assignment of the α-pyridine protons of the iron triflate complexes can also be made because of the characteristic paramagnetic downfield shift of these protons arising from the near interaction between the proton and the paramagnetic ferrous center.

Once again, the spectrum of the *meso* complex (**C23**) exhibits one signal per each chemically different proton due to the lack of symmetry, while for **C24** and **C27,** having C_2-symmetry, the spectra become simpler. It is important to note that the spectra of **C24** presents some little signals coming from an impurity, probably from its precursor, **C22**.

As mention before, the direct synthesis of **C24** from $[Fe(CF_3SO_3)_2(CH_3CN)_2]$ precursor, lead to a mixture of isomers with *cis*-α and *cis*-β topologies, while a two-step synthesis through the formation of the iron chloride analogous conducts to the formation of the *cis*-α topology exclusively. Those spectra are compared in figure VI.7.

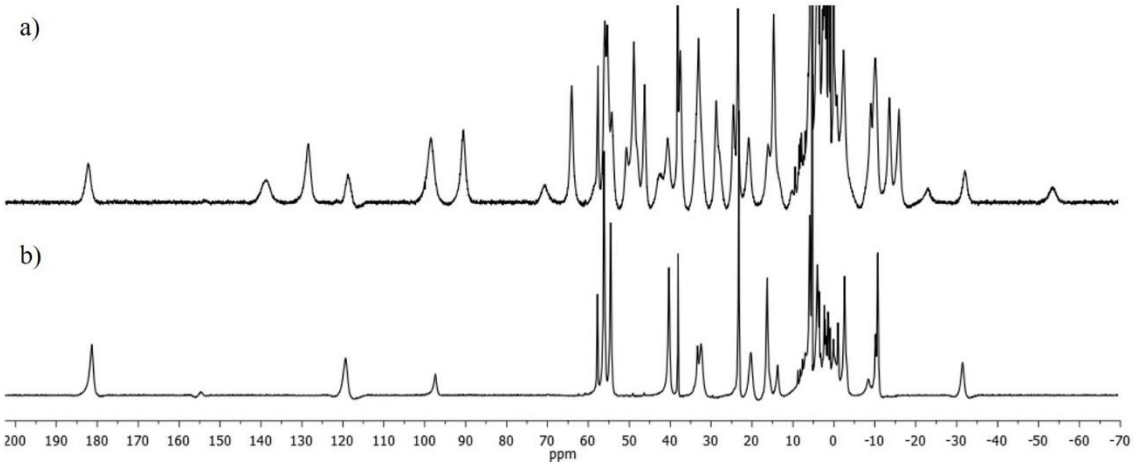

Figure VI.7. ^{1}H-NMR spectra (400 MHz) of iron triflate complex **C24** in CD_2Cl_2 at 298K in a a) *cis*-α and *cis*-β mixture, b) *cis*-α topology.

^{1}H-NMR spectra of iron complexes were also measured in CD_3CN (figure VI.8). In the case of iron triflate complexes, this solvent acts as a coordinating ligand, and it displaces triflate groups to form complexes with the general formula $[Fe(L)(CH_3CN)_2]^{2+}(OTf)_2$ (L = **L8**-**L10**) in which two acetonitrile molecules and the tetradentate ligands constitute the coordination sphere of the iron(II) center.

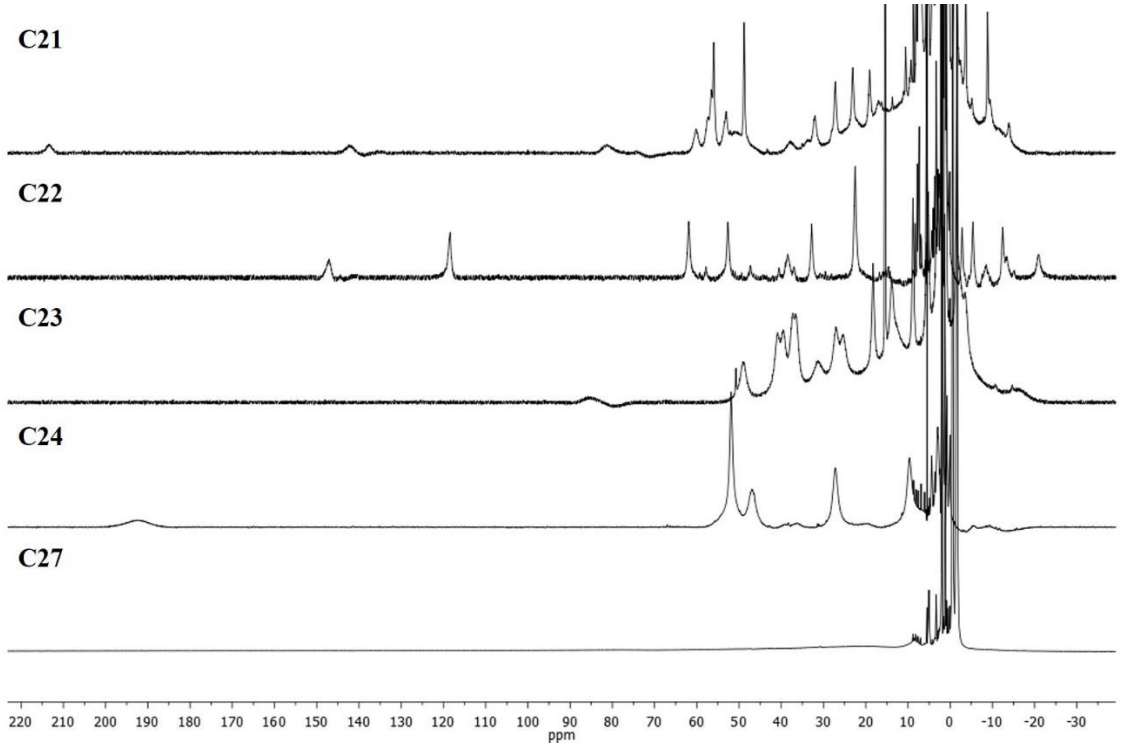

Figure VI.8. ^{1}H-NMR spectra of iron complexes **C21-C24** and **C27** in CD_3CN.

As previously mentioned, acetonitrile ligand is a stronger ligand field than triflate anion, therefore, upon substitution of triflates anions by CD_3CN ligands, the complex can become mainly LS, which is reflected in the reduction of the spectral window. From all the complexes, only **C27** signals appear in the compact spectral window, from -3 to 10 ppm, although the signals were still broad, suggesting some degree of paramagnetism. The chloride complexes, as expected, remain high spin.

VI.1.4.3 UV-Vis spectroscopy

The UV–vis spectra of the complexes in acetonitrile solution at room temperature, were analyzed to obtain further information about their electronic structure.

The spectrum of each iron complex exhibits a very strong absorption in the UV, corresponding to pyridine π-π* transitions, and a less intense one in the visible related to metal to ligand charge transfer (table VI.2 and figure VI.9).

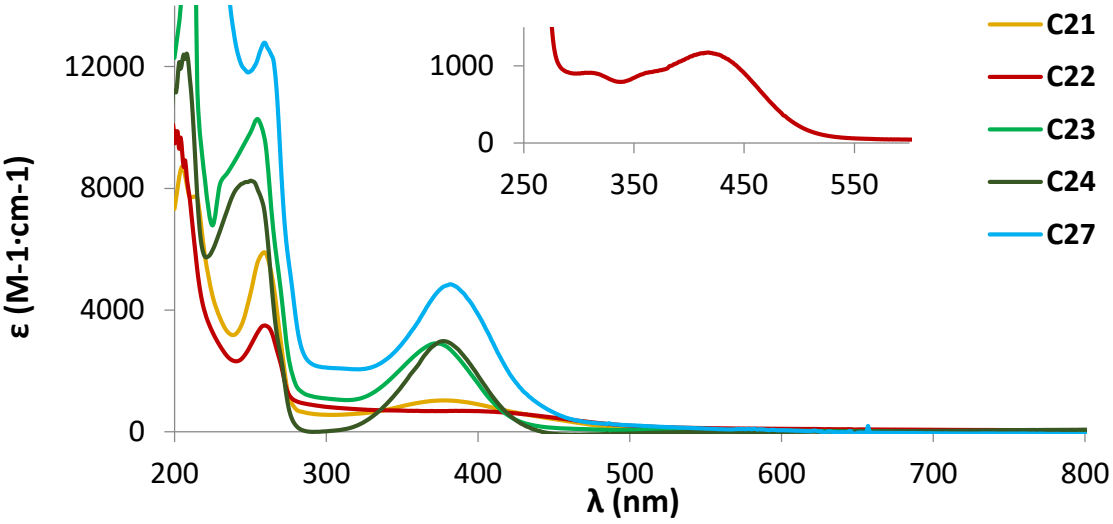

Figure VI.9. UV-Vis spectra (298K) in acetonitrile of iron complexes **C21**-**C24** and **C27**.

Table VI.2. Spectrophotometric data for **C21**, **C23-C26** and **C27** complexes in acetonitrile at room temperature.

	λ_{max} (ε, $M^{-1}\cdot cm^{-1}$)			λ_{max} (ε, $M^{-1}\cdot cm^{-1}$)
Complex	π–π*	MLCT	Complex	π–π*
C21	260 (5900)	380 (1000)	**C25**	262 (940)
C22	260 (3500)	310 (910), 417 (1174)	**C26**	262(7000)
C23	255 (10000)	375 (2900)		
C24	250 (8300)	377 (3000)		
C27	259 (12800)	382 (4900)		

All the MLCT bands of the complexes appear in a narrow range around 373 nm (being **C22** the most diverted and exhibiting two λ_{max}). As the position of the MLCT bands is directly related to the electronic properties of the ligand, it can be assumed that all the complexes present similar electronic properties.

The UV-vis region of the electronic spectra of manganese complexes (table VI.2 and figure VI.10), also exhibit an intense band, due to the already mentioned π-π* transitions of the ligand. As expected, the visible region shows no d-d bands because of the octahedral coordination environment of a d^5 metal ion, for which all d-d bands are spin-forbidden.[172]

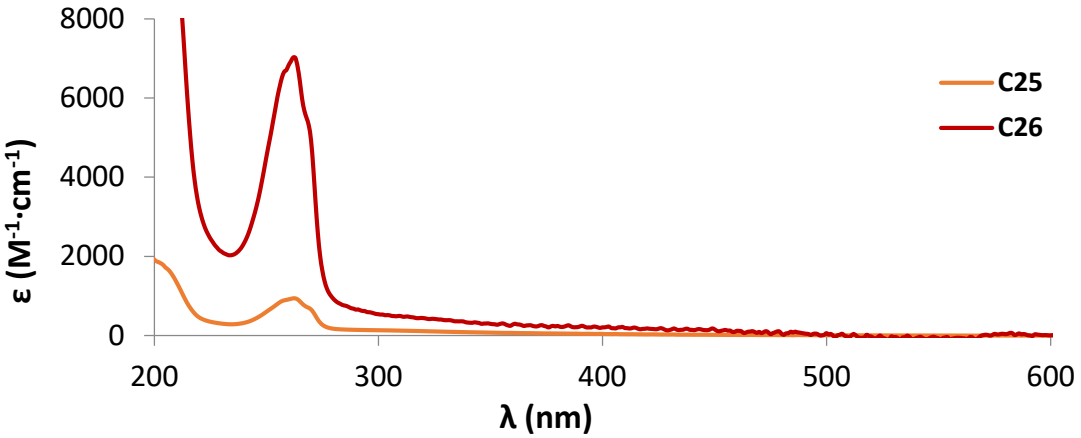

Figure VI.10. UV-Vis spectra (298K) in acetonitrile of manganese triflate complexes **C25** and **C26**.

VI.1.4.4 Electrochemistry of the complexes

To complement the spectroscopic results presented in the preceding section, electrochemistry experiments were carried out on all the complexes to assess their redox properties. Cyclic voltammetry experiments were carried out in dry CH_3CN, sodium saturated calomel (SSC) electrode was used as a reference and tetrabutylammonium hexafluorophosphate (TBAHP) was used as supporting electrolyte. The cyclic voltammograms are depicted in figures VI.9- VI.11.

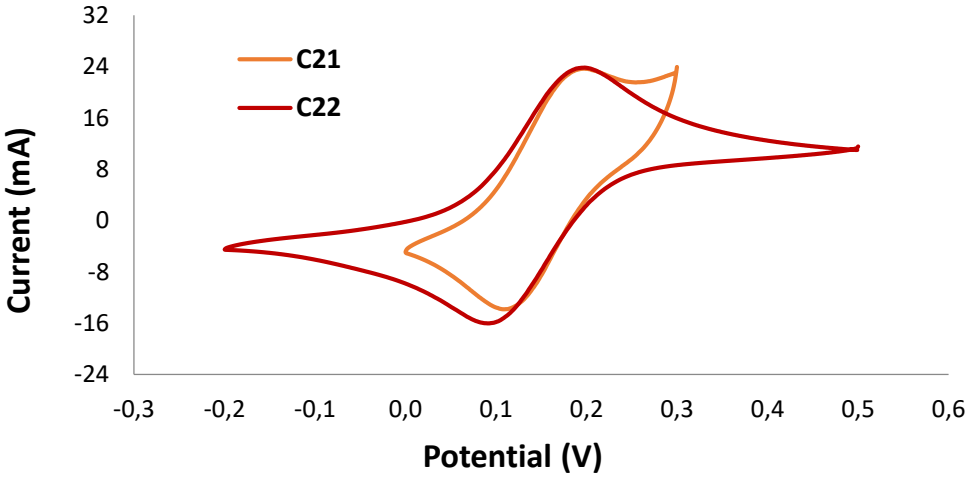

Figure VI.11. Cyclic voltammograms of iron chloride complexes at a scan rate of 100 mV s^{-1} for **C21** and 50 mV s^{-1} for **C22** (2 mg of complex in 4 mL of CH_3CN).

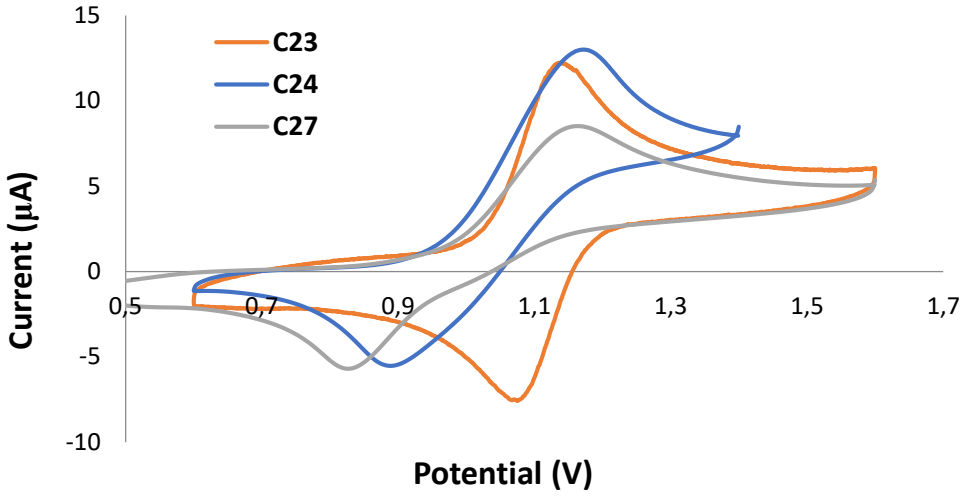

Figure VI.12. Cyclic voltammograms of iron triflate complexes at a scan rate of 100 mV s^{-1} for **C23** and 50 mV s^{-1} for **C24** and **C27** (2 mg of complex in 4 mL of CH_3CN).

All the complexes showed a chemically reversible, electrochemically quasi-reversible wave, as ΔE range from 65 to 341 mV. The redox potentials of the iron chloride complexes were found to fall around 149 mV. While, for iron triflate complexes, the $E_{1/2}$ values appear around 1045 mV. It is reasonable to assign these signals to the Fe^{III}/Fe^{II} redox potential as compared with similar complexes.[122, 173, 174, 176]

Table VI.3. Electrochemical data for **C21-C26** and **C27** complexes in acetonitrile at room temperature.

Fe-Cl		Fe-OTf		Mn-OTf	
	$E_{½}$ (ΔEb, mV)		$E_{½}$ (ΔEb, mV)		$E_{½}$ (ΔEb, mV)
C21	153 (88)	**C23**	1107 (65)	**C25**	981 (83)
C22	144 (106)	**C24**	1032 (286)	**C26**	~950 (165)
		C27	997 (341)		

As previously mentioned, iron triflate complexes in acetonitrile, exchange the OTf^- counterions by CH_3CN ligands. Therefore, dicationic complexes were formed in solution, which are more difficult to oxidize, and consequently, the redox potentials of those complexes are higher when compared to iron chloride analogous.

The cyclic voltammograms of the manganese triflate complexes display less defined redox processes (figure VI.13). The $E_{½}$ values were found to fall around 965 mV, although **C26** exhibit another non-defined irreversible redox process at 705 mV.

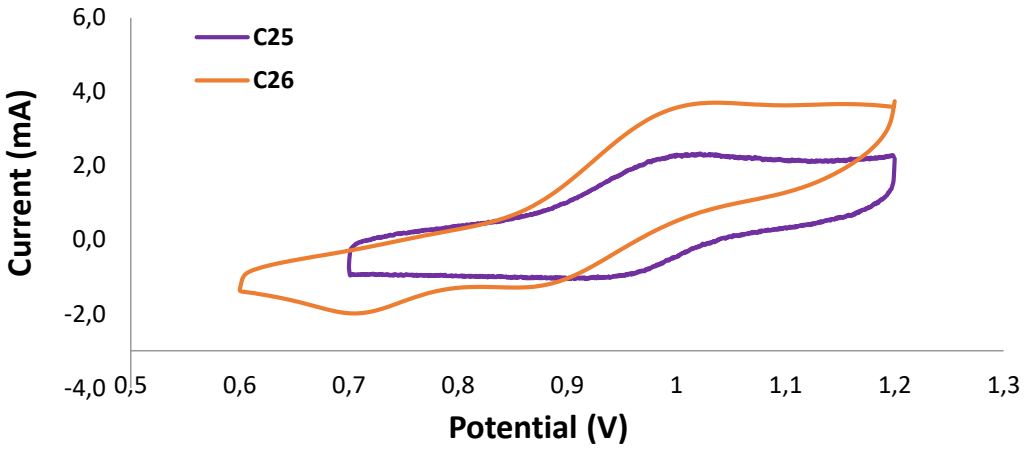

Figure VI.13. Cyclic voltammograms of manganese triflate complexes at a scan rate of 100 mV s^{-1} for **C25** and **C26** (2 mg of complex in 4 mL of CH_3CN).

Further scans to higher potentials up to +1.6 V under the dry solvent conditions did not elicit any other features in the CVs that could be correlated to the formation of M^{IV} (M = Fe or Mn) species. This result should not be surprising, since formation of this species may be prevented by the lack of an oxygen-atom source to form an oxo ligand, under the solvent conditions used.

As seen in the previous section (UV-Vis) the tips group has virtually no effect on terms of electronic properties, as the redox potential of **C27** with respect to saturated calomel electrode (SCE) is very similar when compared to the complex that has no substituent in the pyridine, **C24**.

VI.1.5 Catalytic C-H oxidation

One of the most attractive strategies in organic synthesis is the development of methodologies that allow for the site selective oxidation of alkyl sp^3 C-H groups. In the absence of directing groups, the strength of the C-H bond commonly dominates selectivity. Therefore, tertiary C-H are preferred over methylene sites. The search of catalysts that could bias this inherent reactivity are particularly valuable.

It has been reported that non-heme iron catalysts, based on *N,N'*-dimethyl-*trans*-1,2-cyclohexanediamine and 2,2'-bipyrrolidine backbones that introduce steric bulkiness at the ligand scaffold, were more active and selective in the oxidation of simple substrates when compared to their analogous complexes without any substituent in the pyridine moiety.[129] The catalysts bearing the more sterically crowded triisopropylsilyl groups create a cavity-like space around the

metal site that leads to a preferred oxidation of methylenic sites over tertiary C-H, due to the steric demand on the catalyst and on the substrate.

Moreover, the nature of the ligand diamine backbone has been identified as a key structural aspect of the iron catalyst active site that have an impact in C-H site selectivity. We envisioned that the different diamines used in this thesis could have a distinct influence in the selectivity in C-H oxidation catalysis.

VI.1.5.1 Comparative regioselectivity among iron catalysts

In order to test the effect of the nature of the diamine backbone on the oxidation activity of these catalysts in C-H oxidation reaction; different iron complexes based on *N,N'*-dimethyl-*trans*-1,2-cyclohexanediamine, 2,2'-bipyrrolidine, 2,2'-bipiperidine, 1,1'-biisoindoline and 1,1',2,2',3,3',4,4'-octahydro-1,1'-biisoquinoline diamine backbones were studied (scheme VI.3). 1,1-Dimethylcyclohexane (**S43**), *trans*-1,2-dimethylcyclohexane (**S44**) and *trans*-decalin (**S45**) were used as model substrates. Taking in consideration the precedents, the working conditions used for their oxidation consisted in a single syringe pump addition of H_2O_2 (17 min) over a CH_3CN solution containing the catalyst (3 mol %), AcOH (1.5 equiv., commonly used as a beneficial additive in iron catalyzed oxidation reactions[130, 138, 248]) and substrate at 0°C. This simple protocol was already reported in the literature and was used for a comparative purpose.[129]

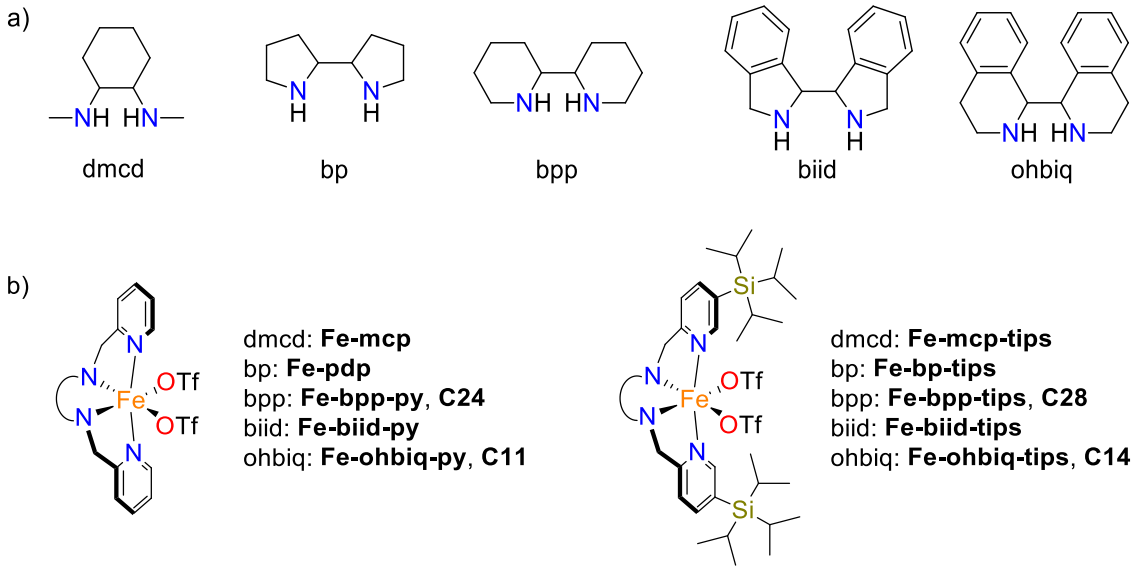

Scheme VI.3. a) Diamine backbones and b) structures of the catalysts used in C-H oxidation. (dmcd, bp, biid and ohbiq are used in their enantiopure version, while bpp was used as *meso* and racemic forms).

Cyclohexanes constitute common basic frameworks in organic molecules and may be regarded as informative substrate probes. When they are subjected to

the standard oxidation procedure, cyclohexane derivatives in general provide moderate to good product yields (28%-70%; tables VI.4- VI.6). The oxidation of the methylenic sites yields the corresponding ketones as the main product, presumably via a two-step oxidation of the C-H bond into the corresponding alcohol, which is rapidly further oxidized to the corresponding ketone. Mass balance in these reactions ranges from 50-80%, which should be regarded as good considering the complexity of the substrates and the difficulty of the reaction. Part of it, is observed as several little peaks in the GC spectra corresponding to over-oxidized products.

Table VI.4. Oxidation of 1,1-dimethylcyclohexane, **S43**.

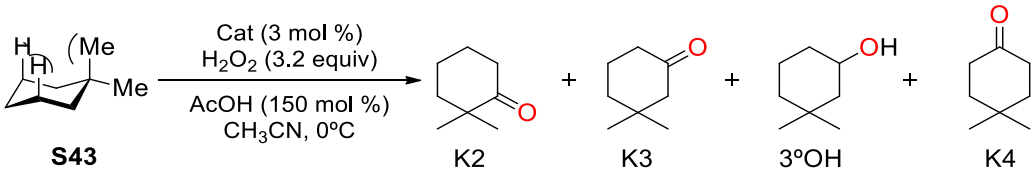

S43 K2 K3 3ºOH K4

Entry	Cat.	Yield (%, conversion)[a]	K2/C3/K4[b]
1	**Fe-mcp**	42 (61)	19/59/22
2	**Fe-mcp-tips**	67 (97)	16/57/27
3	**Fe-pdp**	56 (80)	33/46/21
4	**Fe-bp-tips**	68 (98)	25/50/25
5a	**Fe-bpp-py (*rac*)**	56 (75)	23/54/23
5b	**Fe-bpp-py (*meso*)**	47 (61)	24/54/22
6	**Fe-bpp-tips**	70 (99)	16/57/27
7	**Fe-biid-py**	30 (47)	31/53/16
8	**Fe-biid-tips**	56 (79)	26/52/22
9	**Fe-ohbiq-py**	22 (40)	23/63/14
10	**Fe-ohbiq-tips**	52 (80)	18/60/21

[a] Product yield and substrate conversion determined by GC-FID [b] Normalized (100) ratio of products. C3 includes K3 and 3°OH.

In the oxidation of 1,1-dimethylcyclohexane (**S43**) (table VI.4), the statistically expected selectivity ratio of K2/C3/K4 (C3 includes K3 and 3°OH) would be [40/40/20] according to the number of C-H bonds present in the molecule. However, for all the iron catalysts tested, the major product obtained corresponds to the oxidation in the position C3 (46-63% of selectivity), and K2 and K4 were obtained as minor products (16-33% of selectivity). The preferred oxidation site leading to K3 and 3°OH should be understood as a compromise

between steric accessibility (K4 > C3 > K2) and electron richness of the oxidized methylene site (K4 < C3 < K2). Besides, K2 is further deactivated towards C-H oxidation via an initial hydrogen atom transfer because of torsional effects.[249] Irrespective of the diamine backbone employed, the introduction of the tips substituent provokes a reduction on the K2 selectivity, and increases the selectivity towards the oxidation of positions C3 and C4. The most remarkable results are obtained with **Fe-mcp-tips** and **Fe-bpp-tips** (**C27**), with which only a 16% of selectivity was obtained for K2 product. Moreover, the introduction of the silyl groups also leads to more robust catalysts exhibiting higher yields, when compared to the analogous naked complexes.

Noticeable, when the iron complex with a *meso* backbone was used (**C23**), similar activity and equal selectivity was observed when compared to the analogous iron complex with a racemic backbone **Fe-bpp-py** (**C24**) (entries 5a and 5b, table VI.4).

These results indicate that all iron complexes are able to discriminate among the three methylenic sites of **S43**, and this differentiation is increased by the use of tips substituted ligands, with a decrease in the relative amount of K2 (substantially lower than the 40% statistically expected value). Thus, we conclude that that steric interactions between the catalysts and substrate is a decisive aspect in defining the overall regioselectivity in these reactions. Therefore, C-H site selectivity is not only governed by the innate reactivity properties of C-H bonds, but instead, catalyst architecture is determinant.

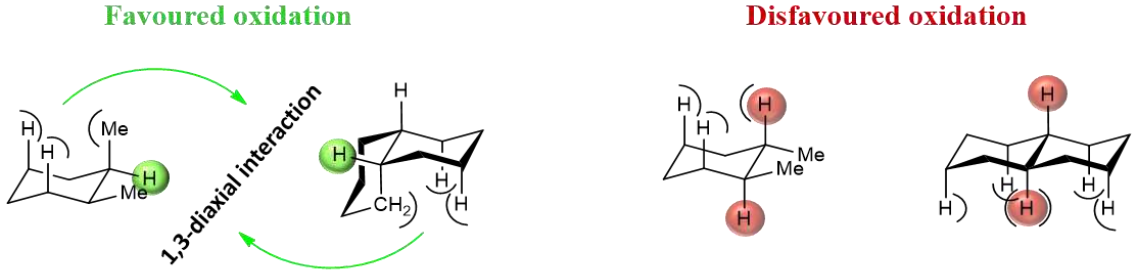

Figure VI.14. Influence of chair conformation orientation in C-H group oxidations of *cis* and *trans* cyclohexane-based substrates.

In cyclohexane derivatives, the orientation of the C-H group to be oxidized is determinant for the regioselective outcome of the oxidation reaction. Tertiary C-H groups in equatorial position are more prone to oxidation, because they are spatially more accessible and because a strain release of the 1,3-diaxial interactions occurs in the rate determining C-H bond-breaking step. Instead, breakage of tertiary C-H bonds in axial positions is not facilitated by strain release, and competitive oxidation between 3° and 2° sites can occur, because the latter are also spatially more accessible (figure VI.14). Therefore, *trans*-1,2-dimethylcyclohexane

(**S44**) and *trans*-decalin (**S45**) were chosen as test platforms to estimate the ability of the catalysts to differentiate among 2° and 3° C-H bonds (2°/3°), and also among different methylenic sites differing in their relative steric hindrance (K3/K2).

Table VI.5 presents the results of the performance of all the catalysts in the oxidation of *trans*-1,2-dimethylcyclohexane, **S44**. Once again, irrespective of the diamine backbone employed, the introduction of the silyl group at the pyridine systematically improves product yields. Moreover, discrimination between the two ketone products is enhanced (e.g. K3/K2 ratio from 1.8 with **Fe-bpp-py C24** to 3.1 with **Fe-bpp-tips C27**, entries 5a and 6), indicating a preference for the formation of the less sterically demanding ketone K3 upon increasing the bulk at the pyridine moiety of the ligand. According to this fact, secondary sites are more prone to be oxidized over tertiary sites with bulkier catalysts (e.g. 2°/3° ratio from 2 using **Fe-bpp-py C24** to 16 using **Fe-bpp-tips C27**, entries 5a and 6).

Table VI.5. Oxidation of *trans*-1,2-dimethylcyclohexane, **S44**.

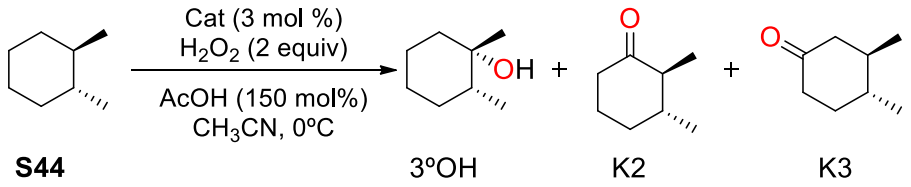

Entry	Cat.	Yield (%, conversion)[a]	3°OH/K2/K3[b]	K3/K2	2°/3°
1	**Fe-mcp**	43 (67)	27/26/47	1.8	3
2	**Fe-mcp-tips**	51 (70)	12/25/63	2.6	7
3	**Fe-pdp**	43 (63)	49/22/29	1.3	1
4	**Fe-bp-tips**	57 (91)	19/26/55	2.1	4
5a	**Fe-bpp-py (*rac*)**	45 (71)	33/24/43	1.8	2
5b	**Fe-bpp-py (*meso*)**	37 (51)	34/26/40	1.6	2
6	**Fe-bpp-tips**	62 (96)	6/23/71	3.1	16
7	**Fe-biid-py**	28 (47)	49/25/25	1.0	1
8	**Fe-biid-tips**	46 (74)	26/27/47	1.7	3
9	**Fe-ohbiq-py**	19 (37)	37/31/32	1.1	2
10	**Fe-ohbiq-tips**	47 (75)	11/25/64	2.6	8

[a] Product yield and substrate conversion determined by GC-FID [b] Normalized (100) ratio of products.

As expected the hydroxylation of **S44** to the corresponding tertiary alcohol affords almost exclusively the epimer with *trans*-dimethyl groups, indicating large degree of stereoretention of configuration (> 99%). This is indicative that metal centered species are responsible for the oxidation ability of these complexes and free diffusing radicals do not significantly operate in the reactions.[118, 250]

A similar analysis has been performed in the oxidation of *trans*-decalin (**S45**) by the same set of catalysts (table VI.6). In this case, the increase of the steric bulk of the ligand does not have such an important impact in terms of yield as in the oxidation of **S44**, but the selectivity toward methylenic sites is pleasantly increased as anticipated.

Table VI.6. Oxidation of *trans*-decalin, **S45**.

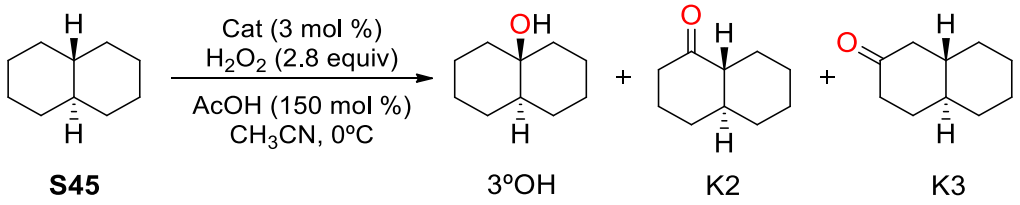

Entry	Cat.	Yield (%, conversion)[a]	3°OH/K2/K3[b]	K3/K2	2°/3°
1	**Fe-mcp**	53 (86)	3/37/59	1.6	28
2	**Fe-mcp-tips**	63 (93)	1/33/67	2.0	99
3	**Fe-pdp**	46 (81)	16/40/44	1.1	5.0
4	**Fe-bp-tips**	54 (93)	3/38/59	1.5	40
5a	**Fe-bpp-py (*rac*)**	49 (89)	5/39/56	1.4	20
5b	**Fe-bpp-py (*meso*)**	54 (77)	4/40/56	1.4	27
6	**Fe-bpp-tips**	48 (99)	0/31/69	2.3	423
7	**Fe-biid-py**	28 (48)	23/40/39	1.0	4
8	**Fe-biid-tips**	52 (87)	4/42/54	1.3	23
9	**Fe-ohbiq-py**	34 (49)	11/42/48	1.1	8
10	**Fe-ohbiq-tips**	44 (78)	1/34/65	2.0	95

[a] Product yield and substrate conversion determined by GC-FID [b] Normalized (100) ratio of products.

Surprisingly, the **Fe-ohbiq-tips** (**C14**) complex shows similar results to **Fe-mcp-tips** complex in terms of selectivity (entries 10 and 2 respectively, table VI.6), while **Fe-bpp-tips** (**C27**) selectivity towards methylenic sites appeared astonishingly (entry 6, table VI.6). Negligible amounts of 3°OH product were

obtained and a preference for the formation of the less sterically demanding ketone K3 was observed (K3/K2 = 2.3).

It is important to note that complex **C23**, which contains a *meso* backbone, exhibits once again, comparable activity and identical selectivity when compared to the analogous iron complex with a racemic backbone **C24** in the oxidation of **S44** and **S45** (entries 5a and 5b, table VI.5 and VI.6).

To confirm and improve the results obtained with complexes **C24** and **C27**, a little optimization is reported in table VI.7. For **Fe-ohbiq-tips C24**, increasing the amount of oxidant improves slightly the yield and the selectivity toward the methylenic sites. While, for **Fe-bpp-tips C27**, an increase in the quantity of oxidant does not result in an increase of the yield, yet the outstanding regioselectivity is confirmed (entries 3 and 8).

Table VI.7. Oxidation of *trans* isomers of 1,2-dimethylcyclohexane **S44** and decalin **S45**.

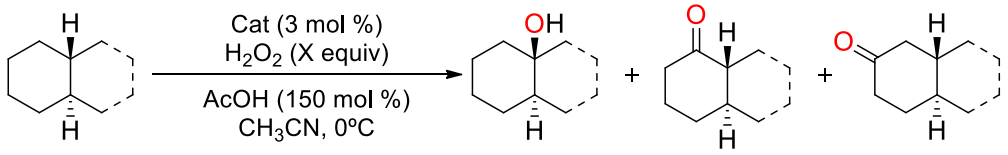

trans-1,2-dimethylcyclohexane, **S44**
trans-decalin, **S45**

3°OH K2 K3

Entry	Subst.	Cat.	Equiv. H_2O_2	Conv. (%)[a]	Yield (%)[a]	3°OH/K2/K3[b]	K3/K2	2°/3°
1	**S44**	**Fe-bpp-tips**	2	96	62	6/23/71	3.1	16
2	**S44**	**Fe-bpp-tips**	2.1	38	35	17/27/56	2.1	5
3	**S44**	**Fe-bpp-tips**	3.5	98	60	4/23/73	3.1	27
4	**S44**	**Fe-ohbiq-tips**	2	75	47	11/25/64	2.6	8
5	**S44**	**Fe-ohbiq-tips**	3.5	78	52	11/26/63	2.4	9
6	**S45**	**Fe-bpp-tips**	2.8	99	48[c]	0/31/69	2.3	423
7	**S45**	**Fe-bpp-tips**	2.1	85	51	1/33/66	2.0	99
8	**S45**	**Fe-bpp-tips**	3.5	100	40[d]	0/30/70	2.3	753
9	**S45**	**Fe-ohbiq-tips**	2.8	78	44	1/34/65	2.0	95
10	**S45**	**Fe-ohbiq-tips**	2.1	84	59	1/33/66	2.0	111
11	**S45**	**Fe-ohbiq-tips**	3.5	92	54	1/35/64	1.8	122

[a] Product yield and substrate conversion determined by GC-FID [b] Normalized (100) ratio of products. [c] ~28% of unidentified over-oxidized products. [c] ~35% of unidentified over-oxidized products.

VI.1.5.2 Oxidation of simple substrates

From the results of *trans*-1,2-dimethylcyclohexane and *trans*-decalin oxidation, it is clear that the new two backbones presented in this thesis together with the introduction of triisopropylsilyl groups at the ligand architecture gives rise to catalysts with enhanced selectivity toward the oxidation of methylenic sites. Therefore, **Fe-ohbiq-tips** (**C24**) and **Fe-bpp-tips** (**C27**) were used to be further studied in the oxidation of a set of structurally simple substrates (*cis*-1,2-dimethylcyclohexane **S46**, *cis*-decalin **S47**, *cis*-4-methylcyclohexyl pivalate **S48**, *trans*-4-methylcyclohexyl pivalate **S49**).

Reaction conditions taken from the previously described oxidation of **S44** and **S45** were employed. These also permit a fair comparison with literature precedents.

As mentioned previously, tertiary C-H groups in equatorial position are easy to oxidize. Therefore, the oxidation of **S46** (table VI.8) leads to the formation of 3°OH as the main product, in good yields (up to 61%) and high retention of configuration (>95%). The 2°/3° ratio observed (0.3 and 0.4 for **Fe-bpp-tips** and **Fe-ohbiq-tips** respectively) is slightly larger than the ones observed with mcp and pdp based pinene-containing non-heme iron catalysts reported in the literature (2°/3° ratio = 0.2 for dmcd backbone, 0.1 for bp backbone under the same reaction conditions);[126] and it is comparable to the one observed for 1-[2′-(pyridyl)methyl]-4,7-dialkyl-1,4,7-triazacyclononane (pytacn) based iron complexes (2°/3° ratio = 0.3), although 3.6 equiv. of H_2O_2 were used in the latter case.[123]

Table VI.8. Oxidation of *cis* isomers of 1,2-dimethylcyclohexane **S46** and decalin **S47**.

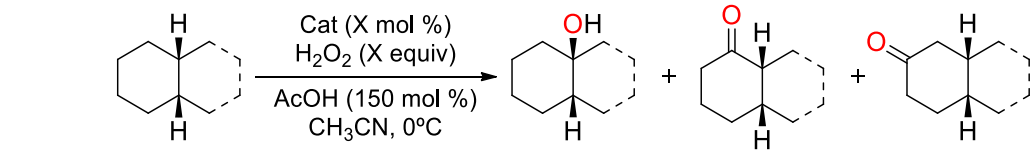

cis-1,2-dimethylcyclohexane, **S46**
cis-decalin, **S47**

3°OH K2 K3

Entry	Subst.	Cat. (Equiv.)	Equiv. H_2O_2	Conv. (%)[a]	Yield (%)[a]	3°OH/K2/K3[b]	K3/K2	2°/3°
1	**S46**	**Fe-bpp-tips** (1)	1.2	83	61	74/12/14	1.1	0.3
2	**S46**	**Fe-ohbiq-tips** (1)	1.2	66	47	74/13/14	1.1	0.4
3	**S47**	**Fe-bpp-tips** (3)	2	92	48	52/26/22	0.8	0.9
4	**S47**	**Fe-ohbiq-tips** (3)	2	98	39	36/36/28	0.8	1.8

[a] Product yield and substrate conversion determined by GC-FID [b] Normalized (100) ratio of products.

Interestingly, submitting **S47** to the standard oxidizing conditions provides, for **Fe-bpp-tips** an almost 1:1 ratio between 2° and 3° C-H, and for **Fe-ohbiq-tips**, the methylenic sites were oxidized preferentially (2°/3° ratio = 1.8). These selectivities are substantially higher than the ones reported by the previously mentioned catalysts, 2°/3° ratio = 0.4 for mcp based pinene catalyst (same reaction conditions),[126] 0.3 for bp based pinene catalyst (same reaction conditions),[126] 0.5 for pytacn based catalyst (3.6 equiv. of H_2O_2),[123] and 0.5 for mcp catalyst (5 equiv. of AcOH).[251] Nevertheless, the mass balance for this new catalysts is low and should be improved by optimizing the reaction conditions of the new system, before a definitive conclusion about the regioselectivity of the reactions can be reached.

Table VI.9. Oxidation of *cis*- (**S48**) and *trans*- (**S49**) 4-methylcyclohexyl pivalate.

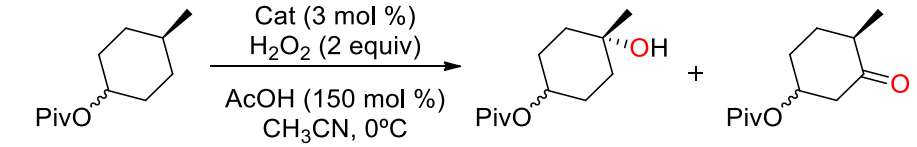

cis-pivalate, **S48**
trans-pivalate, **S49**

3ºOH

K2

Entry	Substrate	Cat.	Conv. (%)[a]	Yield (%)[a]	2°/3°
1	**S48**	**Fe-bpp-tips**	83	45	0.2
2	**S48**	**Fe-ohbiq-tips**	56	21	0.2
3	**S49**	**Fe-bpp-tips**	67	42	0.4
4	**S49**	**Fe-ohbiq-tips**	42	16	0.5

[a] Product yield and substrate conversion determined by GC-FID [b] Normalized (100) ratio of products.

In the oxidation of *cis*- and *trans*-4-methylcyclohexyl pivalate (table VI.9), two products are formed: ketone, K2, at the secondary site most remote from the electronwithdrawing pivalate group, and a tertiary alcohol, 3ºOH in carbon C4. The most significant difference between **S48** and **S49** influencing their reactivity in hydrogen atom transfer reactions is the presence on the axial 3° C-H bond in **S49**, but equatorial in **S48**. This makes this C-H bond more reactive in the case of **S48**, favoring selective oxidation at this site. Instead, in **S49** oxidation of this bond is competitive with the oxidation of a sterically less encumbered methylenic site.

S48 oxidation gives slightly larger 2°/3° ratios than the literature reported values, because in the later cases the oxidation of the 3° C-H is favored and no K2 product is usually obtained.[123, 126] Only a 2°/3° ratio = 0.1 was reported for mcp iron complex,[251] and it is slightly lower to the one observed for the new catalysts (0.2).

On the other hand, **S49** oxidation provides selectivities very similar to dmcd based complexes (with pinene or ligands with unsubstituted pyridines, 2°/3° ratio ranges from 0.41-0.45),[126, 160] higher than bp based pinene-containing iron catalysts but similar to the tips substituted analogous (2°/3° ratio = 0.25 and 0.45 respectively),[126, 129] and lower to the pytacn based complexes or mcp-tips iron catalyst (2°/3° ratio = 0.56 and 0.53 respectively).[123, 129]

VI.1.5.3 Oxidation of complex molecules

The potential utility of these new catalysts in organic synthesis is best illustrated in the oxidation of structurally more complex substrates, such as natural products. The selective oxidation of (-)-ambroxide (**S50**) can be regarded as a non-trivial problem. This terpenoid contains 14 methylene and 2 tertiary C-H bonds (table VI.10) but it can be selectively oxidized at the activated methylene site adjacent to the ether moiety to yield (+)-sclareolide (**S51**) in 52-53% yield (16-18% of over-oxidized product) employing **Fe-bpp-tips** and **Fe-ohbiq-tips**.

Table VI.10. Oxidation of (-)-ambroxide, **S50**.

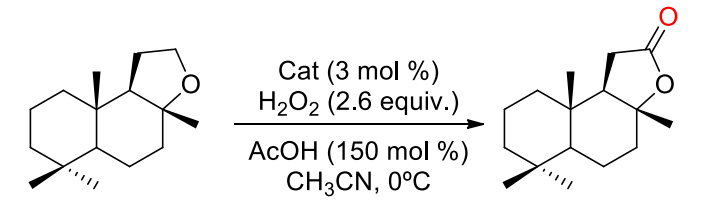

(-)-ambroxide, **S50** (+)-sclareolide, **S51**

Entry	Cat.	Conv. (%)[a]	Yield (%)[a]
1	Fe-*rac*-bpp-tips	99	52[b]
2	Fe-(*S*,*S*)-ohbiq-tips	100	53[c]

[a] Product yield and substrate conversion determined by GC-FID [b] ~18% of over-oxidized products. [c] ~16% of over-oxidized products.

When **S51** is subjected to oxidation, the carbonyl group deactivates the surrounding C-H bonds, directing the oxidation towards the most remote cyclohexane ring, which contains three chemically distinct methylene sites (table VI.11). Therefore, only ketone products (K1, K2 and K3) arising from oxidation at the three different methylene sites (C1, C2 and C3, respectively) are obtained.

Preferential functionalization at C2 was observed for both catalyst, but **Fe-rac-bpp-tips** exhibit higher activity when compared to **Fe-(S,S)-ohbiq-tips** (82% vs 24% yield respectively) and enhanced selectivity (64% vs 51% normalized ratio of products) towards this position. It is important to mention that, from previous

studies, chirality at the metal center can govern C-H regioselectivity in enantiopure molecules.[129] The use of Λ or Δ catalysts may allow to discriminate and to diverge the dominant regioselectivity among multiple methylene sites. Therefore, the enantiopure version of the diamine backbone, which in fact determines the chirality at the metal center, would be most convenient.

Table VI.11. Oxidation of (+)-sclareolide, **S51**.

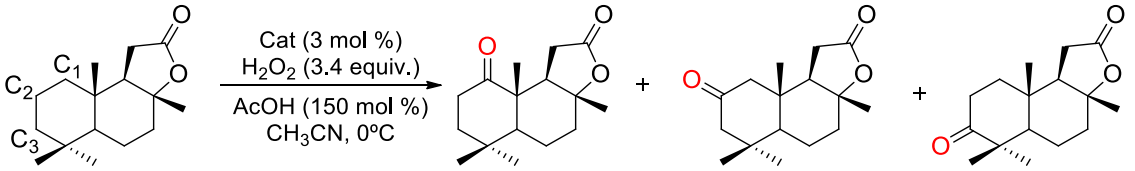

(+)-sclareolide, **S51** K1 K2 K3

Entry	Cat.	Conv. (%)[a]	Yield (%)[a]	K1/K2/K3[b]
1	**Fe-*rac*-bpp-tips**	83	82	3/64/33
2	**Fe-(*S*,*S*)-ohbiq-tips**	46	24	7/51/42
3	**Fe-(*R*,*R*)-bpp-tips**	86	85	0/62/38

[a] Product yield and substrate conversion determined by GC-FID [b] Normalized (100) ratio of products.

A small sample of the **(*R*,*R*)-bpp** backbone was provided by Rybak Akimova, and subsequent synthesis of the ligand and the corresponding iron triflate complex was accomplished to study the effect of the chirality in the oxidation of complex molecules. With the use of the new catalyst, **Fe-(*R*,*R*)-bpp-tips**, negligible amounts of K1 were obtained maintaining the high activity (85% yield) and K2 was furnished as the main product.

Steroids are interesting substrate platforms because of their elaborated structure, with several and different C-H groups that allows the possibility of studying the selectivity bases in C-H oxidation.[251] Moreover, steroids are also of biological relevance,[252] since their oxidation mediated by P450 enzymes is known to occur in living systems in the biosynthesis and biological degradation of steroidal hormones.[253, 254] Thus, the oxidation of *trans*-androsterone acetate (**S52**) and *cis*-androsterone acetate (**S53**) was evaluated.

These substrates contain 3 primary C-H sites, 9 secondary C-H sites and 5 tertiary C-H bonds potentially susceptible of being oxidized. Since rings A and D contain electron-withdrawing groups, it was envisioned that C-H bonds at rings B and C would be more prone to oxidation. Furthermore, considering the low reactivity of the tertiary bridgehead C-H bonds at *trans*-decalin (table VI.12), it was

also presumed that tertiary sites would also be disfavored. Indeed, when subjected to the standard experimental conditions, oxidation of **S52** and **S53** proceeds with moderate to good substrate conversion (45-82%), and three major oxidation products are obtained resulting from oxidation at three different methylenic sites (C7, C6, and C12, table VI.12) in low to good yields (28-70%), all of them belonging to rings B and C. Mass balance in these oxidations ranges from 53-76%, which should be considered as quite good for a C-H oxidation reaction of complex molecules.

Table VI.12. Oxidation of *trans*-androsterone acetate (**S52**) and *cis*-androsterone acetate (**S53**). [a]

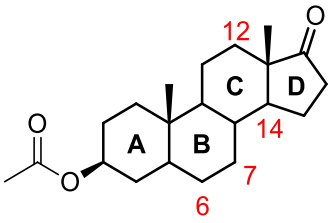

trans-androsterone acetate, **S52**

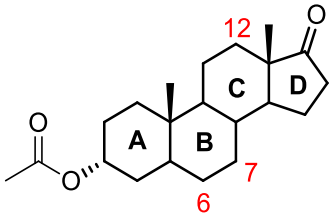

cis-androsterone acetate, **S53**

Entry	Substrate	Cat.	Conv. (%)	Yield (%)	C6/C7/C12/C14[b]
1	**S52**	**Fe-*rac*-bpp-tips**	74	56	37/4/58/1
2	**S52**	**Fe-(*S*,*S*)-ohbiq-tips**	45	29	68/8/22/2
3	**S52**	**Fe-(*R*,*R*)-bpp-tips**	82	70	18/3/79/0
Entry	**Substrate**	**Cat.**	**Conv. (%)**	**Yield (%)**	**C6/C7/C12[b]**
4	**S53**	**Fe-*rac*-bpp-tips**	82	53	42/1/57
5	**S53**	**Fe-(*S*,*S*)-ohbiq-tips**	53	28	71/3/26
6	**S53**	**Fe-(*R*,*R*)-bpp-tips**	51	39	17/0/83

[a] Reaction conditions are: Cat:H_2O_2:substrate:AcOH-3:250:100:150. Product yield and substrate conversion determined by GC-FID [b] Normalized (100) ratio of products.

Ketone at C12 is the dominant product when **Fe-*rac*-bpp-tips** is used as catalyst, accounting for 58% of the products in the oxidation of **S52**, and 57% for **S53**. A different selectivity pattern is observed for **Fe-(S,S)-ohbiq-tips** catalyst in the oxidation of those substrates, as the main product obtained consists in the oxidation of C6 (involving 68% of the product for the oxidation of **S52**, and up to 71% for **S53**). Ketones arising from oxidation at C7 and C14 are also obtained in the oxidation of **S52** in minor amounts, and no K14 product was observed in the oxidation of **S53**.

As mentioned previously, the chirality of the backbone is important in the outcome of the selectivity of those oxidation reactions. And this can be further supported by the results observed with **Fe-(*R*,*R*)-bpp-tips** catalyst, where the preference for the C12 position increases up to 79% (vs 58%) for **S52** and up to 83% (vs 57%) for **S53** when compared to the racemic version, **Fe-*rac*-bpp-tips**. Obtaining, with the latter substrate, no oxidation on the C7 position.

It has been already reported that changing from (*R*,*R*) to (*S*,*S*), which implies the modification of the chirality at the metal center (from Δ to Λ), can dictate the regioselectivity of the reaction providing a switch in methylene site selectivity oxidations.[129] Indeed, this behaviour is observed by using **Fe-(*R*,*R*)-bpp-tips** and **Fe-(*S*,*S*)-ohbiq-tips** which leads to the preferential oxidation of C6 or C12 positions respectively (compare entries 2 vs 3, and 5 vs 6).

Although the reaction conditions are not optimized, the robustness of **Fe-bpp-tips** is evidenced by the better mass balance obtained with this catalyst (64-99%).

VI.2 Summary

The work presented in this chapter shows the synthesis of new tetradentate aminopyridine ligands based on the 2,2'-bipiperidine backbone (**L8-L10**). The corresponding iron chloride, iron triflate and manganese triflate complexes were prepared and characterized.

A comparison between iron complexes based on different backbones was accomplished in C-H oxidation catalysis, confirming the importance of the diamine backbone used in the C-H site selectivity of the reactions. 1,1',2,2',3,3',4,4'-octahydro-1,1'-biisoquinoline (**ohbiq**) based catalysts exhibit similar results, in terms of selectivity, to the previous reported *N,N'*-dimethyl-*trans*-1,2-cyclohexanediamine (**dmcd**) and 2,2'-bipyrrolidine (**bp**) based analogous complexes. While, 2,2'-bipiperidine (**bpp**) based catalysts appear to be more selective for secondary site oxidation and more capable to discriminate among different secondary sites, compared to their bp- and dmcd-counterparts.

The presence of the tips group in the ligand afforded, in general, more active and more selective catalysts. Nevertheless, it should be noted that the mass balance of the reactions require improvement. This fact might be due to the difficultness of this type of oxidations, which involve highly oxidizing species, in which chemo- and regioselectivity is difficult to control.

In general, **bpp** based iron complexes appeared as very convenient catalysts for C-H oxidation reactions employing H_2O_2 as terminal oxidant. We envision that further studies of this new catalyst in C-H and C=C oxidation, which requires a deeper optimization of the reaction conditions of the system, may led to a novel family of catalysts with outstanding activity.

VI.3 Experimental section

VI.3.1 Materials

Reagents and solvents used were of commercially available reagent quality unless stated otherwise. Solvents were purchased from Carlo Erba and Scharlab. Solvents were purified and dried by passing through an activated alumina purification system (MBraun SPS-800). Substrates were filtered through basic alumina before performing the epoxidation reactions. HPLC quality acetonitrile was employed in the epoxidation reactions. Preparation and handling of air-sensitive materials were carried out in a N_2 dry box (Braun) with O_2 and H_2O concentrations < 1 ppm.

VI.3.2 Instrumentation

IR spectra were taken in a Mattson-Galaxy Satellite FT-IR spectrophotometer using a MKII Golden Gate single reflection ATR system. NMR spectra were taken on a Bruker Ultrashiel DPX400 MHz spectrometer using standard conditions. NMR data are given in the δ scale and are referred to internal TMS. UV/Vis absorption spectra were performed on a diode-array Agilent Cary 60 spectrophotometer and temperature control was maintained with a cryostat from Unisoku Scientific Instruments. Cyclic voltammetry (CV) was performed by using a potentiostat from CHInstruments with a three-electrode cell. The working electrode was a glassy carbon disk from BAS (0.07 cm^2), the reference electrode was a sodium saturated calomel electrode, and the auxiliary electrode was a platinum wire. CV was carried out with nBu_4NPF_6 (TBAP) as a supporting electrolyte (0.1 M). Elemental analyses of C, H, and N were performed using a CHNS-O EA-1108 elemental analyser from Fisons. High resolution mass spectra (HRMS) were recorded on a Bruker MicroTOF-Q IITM instrument with an ESI source and a quadrupole analyser at Serveis Tècnics of the University of Girona. Samples were introduced into the mass spectrometer ion source by direct infusion through a syringe pump and were externally calibrated using sodium formate. Oxidation products were identified by ^1H and ^{13}C-NMR analyses. Chromatographic resolution of enantiomers was performed on HPLC 1200 series Agilent

technologies using CHIRALPAK-IA and CHIRALPAK-IC columns. The configuration of the major enantiomer was determined by chemical correlation. The X-ray measurements were carried out on a BRUKER SMART APEX CCD diffractometer using graphite-monochromated Mo Ka radiation (l = 0.71073 Å) from an X-ray Tube. Programs used: data collection, Smart Version 5.631, 1997-2002; data reduction, Saint+ Version 6.36A, 2001; absorption correction, SADABS Version 2.10, 2001. Structure solution and refinement was done using SHELXTL Version 6.14, 2000-2003 and SHELXL-2017. The structures were solved by direct methods and refined by full-matrix least-squares methods on F^2. The non-hydrogen atoms were refined anisotropically. The H-atoms were placed in geometrically optimized positions and forced to ride on the atom to which they are attached.

VI.3.3 Synthesis of complexes

Iron complexes based on dmcd (*N,N'*-dimethyl-*trans*-1,2-cyclohexanediamine) and bp (2,2'-bipyrrolidine) backbones were synthesized according to the literature.[129] Iron complexes based on the biid (1,1'-biisoindoline) backbone were provided by Professor Robertus Klein Gebbink.[256]

VI.3.3.1 Synthesis of the backbone

The 2,2'-bipiperidine (**bpp**) was synthetized according to described procedures.[245, 246]

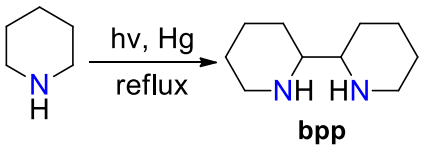

bpp

A 500-mL, 3-necked flask was equipped with three quartz condensers and three reflux condensers. It was then charged with 160 mL of piperidine and one drop of Hg. To avoid evaporation, all the joints were connected with Teflon gaskets. The apparatus was placed inside a photoreactor outfitted with 254 nm Hg lamps. Using a heating mantle, the piperidine was brought to a very gentle reflux. All exposed glass on the hood was covered with aluminum foil for eye protection and the lamps were turned on. After 7 days the lamps were turned off and the apparatus was allowed to cool. The reaction mixture was carefully decanted away from the mercury, which was then disposed. The liquid was then fractionally distilled at 85°C (0.15 mmHg) to give 40.26 g (30% yield) of *rac* and *meso* **bpp** as a clear colorless liquid.

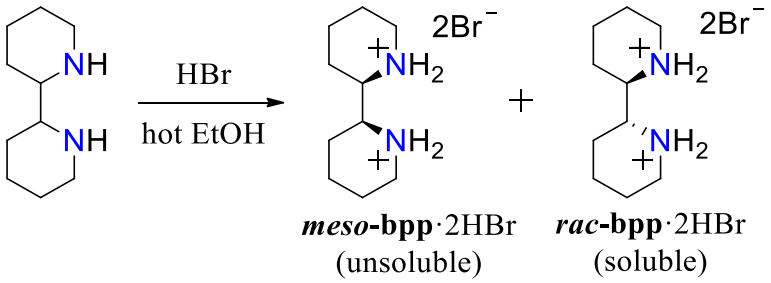

Concentrated hydrobromic acid was added to *rac* and *meso* **bpp** (7.8 g, 46.35 mmol) to reach a pH of about 2. After evaporation of water under reduced pressure, the resultant residue was dried under vacuum to obtain a mixture of the racemic (***rac*-bpp**·2HBr) and *meso* (***meso*-bpp**·2HBr) bishydrobromide salts. The crude was heated to boiling point in 90 mL of ethanol for 20 min and filtered hot. This washing was repeated three times to give ***meso*-bpp**·2HBr (4.49 g, 59% yield) as a white powder. Combined ethanol washings were allowed to cool and filtered to give ***rac*-bpp**·2HBr (1.96 g, 26% yield) as an off-white solid.

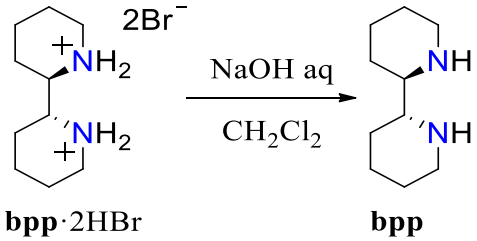

***rac* or *meso*-bpp**·2HBr was stirred in CH_2Cl_2 (25 ml) and 5 M NaOH (25 ml) at r.t. for 3 h. The organic layer was separated and dried over magnesium sulfate. Removal of drying agent and solvent gave ***rac* or *meso*-bpp** (quantitative yield) as a colourless oil.

VI.3.3.2 Synthesis of pyridine synthons

Pyridine synthon 2-chloromethylpyridine hydrochloride, **^{H}PyCH$_2$Cl·HCl** was purchased from Aldrich. 2-chloromethyl-5-triisopropylpyridine hydrochloride, **^{tips}PyCH$_2$Cl·HCl** was synthesized following a previously described procedure.[197]

VI.3.3.3 Synthesis of ligands

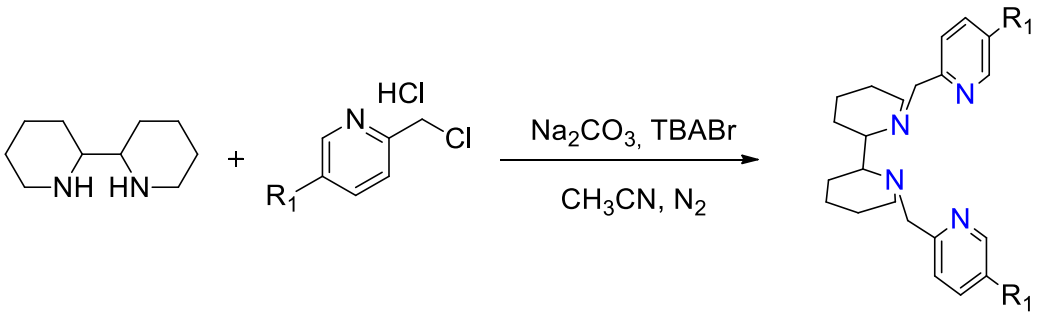

L8, *meso*-^{H}bpp: R_1=H
L9, *rac*-^{H}bpp: R_1=H
L10, *rac*-^{tips}ohbiq: R_1= tips
L11, *meso*-^{tips}ohbiq: R_1= tips

Scheme VI.4. Synthesis and nomenclature of the ligands.

Synthesis of *meso*-^{H}bpp (L8)

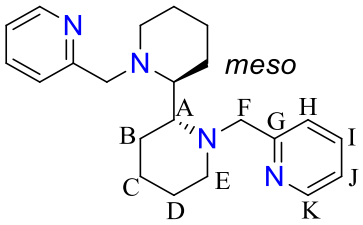

2-Picolyl chloride hydrochloride (1.088 g, 6.50 mmol), ***meso*-bpp** (975.3 mg, 2.96 mmol) and anhydrous acetonitrile (50 mL) were mixed in a 100 mL flask. Na_2CO_3 (5.03 g) and tetrabutylammonium bromide, TBABr (20 mg) were added directly as solids and the resulting mixture was heated at reflux under N_2 for 18 hours. After cooling to room temperature, the resulting brown mixture was filtered and the filter cake was washed with CH_2Cl_2. The combined filtrates were evaporated under reduced pressure. To the resulting residue, 1 M NaOH (30 mL) was added and the mixture was extracted with CH_2Cl_2 (3 x 20 mL). The combined organic layers were dried over anhydrous $MgSO_4$ and the solvent was removed under reduced pressure. After, the residue was purified by preparative chromatography (silica CH_2Cl_2:MeOH:NH_3 96:3:1) to provide 521.1 mg (50% yield) of a brown oil. ^{1}H-NMR ($CDCl_3$, 400 MHz, 300K) δ, ppm: 8.50 (ddd, J = 4.9, 1.8, 0.9 Hz, 2H, H_K), 7.67-7.60 (m, 2H, H_I), 7.55-7.49 (m, 2H, H_H), 7.14-7.07 (m, 2H, H_J), 4.92 (d, J = 14.9 Hz, 2H, H_F), 3.29 (d, J = 14.9 Hz, 2H, $H_{F'}$), 2.78 (d, J = 12.3 Hz, 2H, H_E), 2.60 (s, 2H, H_A), 1.98 (t, J = 11.1 Hz, 2H, $H_{E'}$), 1.79-1.59 (m, 6H, $H_{B,D}$), 1.51-1.42 (m, 2H, H_D), 1.38-1.24 (m, 4H, H_C). ^{13}C-NMR ($CDCl_3$, 133 MHz, 300K) δ, ppm: 161.06 (G), 148.80 (K), 136.44 (I), 122.37 (H), 121.51 (J), 63.62 (A), 60.09 (F), 54.14 (E), 27.54 (B), 24.71 (C,D). HRMS (ESI-MS) m/z calculated for $C_{22}H_{31}N_4$ $[M+H]^+$:

351.2543, found: 351.2538. FT-IR (ATR) ν, cm^{-1}: 3060, 3007 (C-H)sp^2, 2932-2719 (C-H)sp^3, 1588, 1568, 1430, 1365, 1101, 994, 753, 731, 611, 471.

Synthesis of *rac*-^{H}bpp (L9)

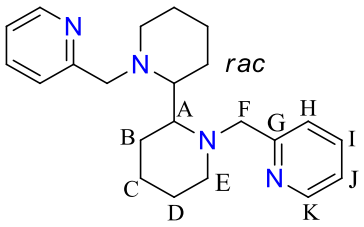

It was prepared in analogous manner to **L8** starting from ***rac*-bpp** (990.0 mg, 3.00 mmol) and 2-picolyl chloride hydrochloride (1.104 g, 6.60 mmol) to provide 776.4 mg (74% yield) of a brown oil. ^{1}H-NMR ($CDCl_3$, 400 MHz, 300K) δ, ppm: 8.52 (ddd, *J* = 4.9, 1.8, 0.9 Hz, 1H, H_K), 7.61 (td, *J* = 7.6, 1.9 Hz, 2H, H_I), 7.45 (d, *J* = 7.8 Hz, 2H, H_H), 7.12 (ddd, *J* = 7.5, 4.8, 1.2 Hz, 2H, H_J), 4.25 (d, *J* = 14.4 Hz, 2H, H_F), 3.24 (d, *J* = 14.7 Hz, 2H, $H_{F'}$), 2.86-2.78 (m, 2H, H_E), 2.73 (d, *J* = 13.3 Hz, 2H, H_A), 2.09-1.88 (m, 4H, $H_{E',D}$), 1.79-1.66 (m, 2H, H_C), 1.61-1.36 (m, 6H, $H_{B,D'}$), 1.25-1.12 (m, 2H, $H_{C'}$). ^{13}C-NMR ($CDCl_3$, 133 MHz, 300K) δ, ppm: 160.23 (G), 148.99 (K), 136.30 (I), 122.69 (H), 121.64 (H), 62.21 (J), 59.45 (A), 54.69 (F), 25.54 (E), 24.82 (B), 24.68 (C,D). HRMS (ESI-MS) m/z calculated for $C_{22}H_{31}N_4$ $[M+H]^+$: 351.2543, found: 351.2551; $C_{22}H_{31}NaN_4$ $[M+Na]^+$: 373.2363, found: 373.2355. FT-IR (ATR) ν, cm^{-1}: 3051, 3012 (C-H)sp^2, 2930-2718 (C-H)sp^3 , 1589, 1567, 1472, 1431, 1303, 1202, 1119, 1064, 987, 891, 827, 794, 759, 613, 488, 412.

Synthesis of *rac*-^{tips}bpp (L10)

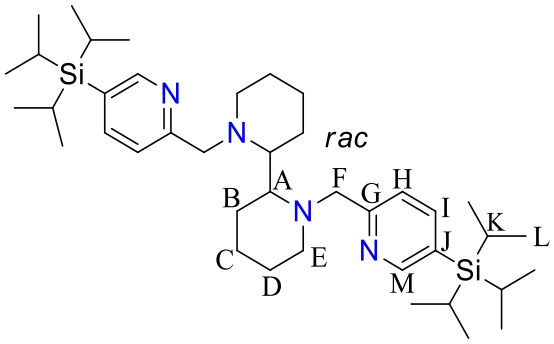

It was prepared in analogous manner to **L8** starting from ***rac*-bpp** (150.0 mg, 0.89 mmol) and **^{tips}PyCH$_2$Cl·HCl** (531.5 mg, 1.87 mmol) to provide 60.0 mg (10% yield) of a pale orange solid. ^{1}H-NMR ($CDCl_3$, 400 MHz, 300K) δ, ppm: 8.59 (d, *J* = 1.7 Hz, 2H, H_M), 7.71 (dd, *J* = 7.7, 1.8 Hz, 2H, H_I), 7.43 (d, *J* = 7.7 Hz, 2H, H_H), 4.26 (d, *J* = 14.2 Hz, 2H, H_F), 3.18 (d, *J* = 14.2 Hz, 2H, $H_{F'}$), 2.86 (d, *J* = 11.6 Hz, 2H, H_E), 2.69 (d, *J* = 10.3 Hz, 2H, H_A), 2.06-1.90 (m, 4H, $H_{C,E'}$), 1.73 (d, *J* = 12.1 Hz, 2H, H_D), 1.54-1.43 (m, *J* = 25.8 Hz, 8H, $H_{B,C',D'}$), 1.38 (app sext., *J* = 14.6, 7.4 Hz, 6H, H_K),

1.07 (d, J = 7.6 Hz, 36H, H_L). ^{13}C-NMR ($CDCl_3$, 133 MHz, 300K) δ, ppm: 160.25 (G), 154.78 (M), 143.30 (I), 122.09 (H), 62.59 (A), 59.85 (F), 55.03 (E), 25.66 (B), 24.79 (C,D), 18.47 (L), 10.64 (K). HRMS (ESI-MS) m/z calculated for $C_{40}H_{71}N_4Si_2$ $[M+H]^+$: 663.5212, found: 663.5193.

VI.3.3.4 Synthesis of complexes

Synthesis of iron chloride complexes

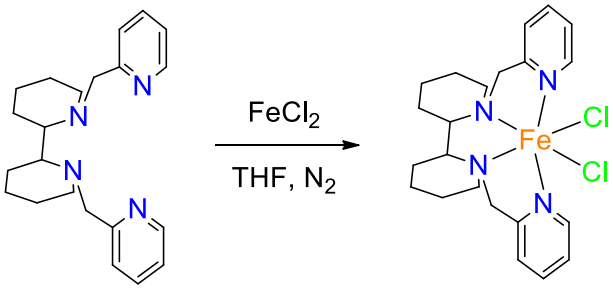

C21: *meso*-bpp
C22: *rac*-bpp

Scheme VI.5. Synthesis and nomenclature of the iron chloride complexes.

[Fe(Cl)$_2$(*meso*-^{H}bpp)] (**C21**) was synthesized following a similar procedure to the one described in literature. Under a N_2 atmosphere, a suspension of $FeCl_2$ (17.8 mg, 139.8 µmol) in anhydrous THF (1 mL) was added drop-wise to a vigorously stirred solution of **L8** (49.0 mg, 139.8 µmol) in anhydrous THF (1 mL). After a few seconds the solution became orange and started to precipitate an orange solid. After stirring overnight, the precipitate was filtered and dried under vacuum. The obtained solid was solved in the minimum quantity of CH_2Cl_2 and the solution filtered off through celite©. Slow diethyl ether diffusion over the resultant solution afforded, in a few days, orange crystals. HRMS (ESI-MS) m/z calculated for $C_{22}H_{30}ClFeN_4$ $[M-Cl]^-$: 441.1503, found: 441.1506. FT-IR (ATR) ν, cm^{-1}: 2959-2863 (C-H)sp^3 , 1602, 1570, 1477, 1443, 1307, 1157, 1083, 1048, 1017, 868, 725, 588, 417. Anal. Calcd. for $C_{22}H_{30}Cl_2FeN_4 \cdot 0.1CH_2Cl_2$: C, 54.65; H, 6.27; N, 11.53%; found: C, 54.85; H, 6.30; N, 11.37%.

[Fe(Cl)$_2$(*rac*-^{H}bpp)] (**C22**) was prepared in a similar manner to **C21**, starting from **L9** (100.0 mg, 285.3 µmol) and $Fe(Cl)_2$ (36.3 mg, 285.3 µmol) in anhydrous CH_3CN. After a few seconds the solution became red. After stirring overnight, an orange precipitate appeared. The solution was removed and the solid dried under vacuum. This solid was solved in CH_3CN and the solution filtered off through Celite©. Slow diethyl ether diffusion over the resultant solution afforded, in a few days, 78.9 mg (58% yield) of orange crystals. HRMS (of the crystals) (ESI-MS) m/z calculated for $C_{22}H_{30}ClFeN_4$ $[M-Cl]^-$: 441.1503, found: 441.1593; $C_{22}H_{30}FeN_4$ $[M-2Cl]^{-2}$: 203.0905, found: 203.0889.

When the solid was solved in CD_2Cl_2, slow diethyl ether diffusion over the resultant solution gave also yellow crystals of complex **C22'**.

FT-IR (of the whole sample) (ATR) ν, cm^{-1}: 3511-3433 (N-H), 2953-2860 (C-H)sp^3, 1602, 1568, 1441, 1314, 1153, 1092, 1050, 1013, 987, 851, 775, 736, 637, 554, 420.

Synthesis of iron triflate complexes

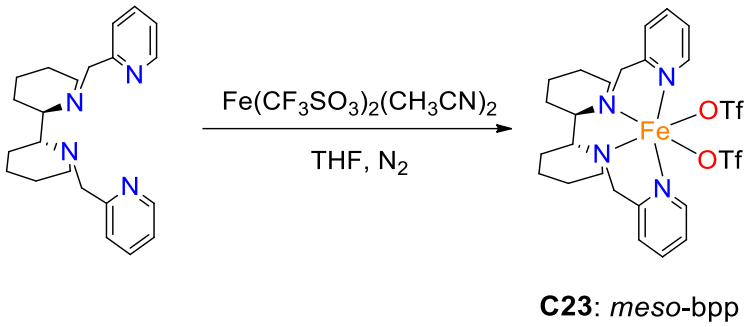

C23: *meso*-bpp

Scheme VI.6. Synthesis and nomenclature of the iron triflate complex with *meso*-bpp.

[Fe(CF$_3$SO$_3$)$_2$(*meso*-^{H}bpp)] (**C23**) was prepared in a similar manner to **C21**, starting from **L8** and $Fe(CF_3SO_3)_2(CH_3CN)_2$ in anhydrous THF. After stirring overnight, a yellow precipitate appeared. The solution was removed and the solid dried under vacuum. This solid was solved in CH_2Cl_2 and the solution filtered off through Celite©. Slow diethyl ether diffusion over the resultant solution in the freezer afforded, in a few days, yellow crystals. HRMS (ESI-MS) m/z calculated for $C_{23}H_{30}F_3FeN_4O_3S$ [M-OTf]$^+$: 555.1335, found: 555.1355; $C_{22}H_{30}FeN_4$ [M-2OTf]$^+$: 203.0905, found: 203.0906. FT-IR (ATR) ν, cm^{-1}: 2955-2853 (C-H)sp^3, 1606, 1573, 1442, 1368, 1304, 1235, 1208, 1157, 1019, 982, 920, 773, 632, 572, 514, 414. Anal. Calcd. for $C_{24}H_{30}F_6FeN_4O_6S_2 \cdot 0.22C_4H_{10}O$: C, 41.46; H, 4.50; N, 7.77%; found: C, 41.75; H, 4.22 N, 7.60%.

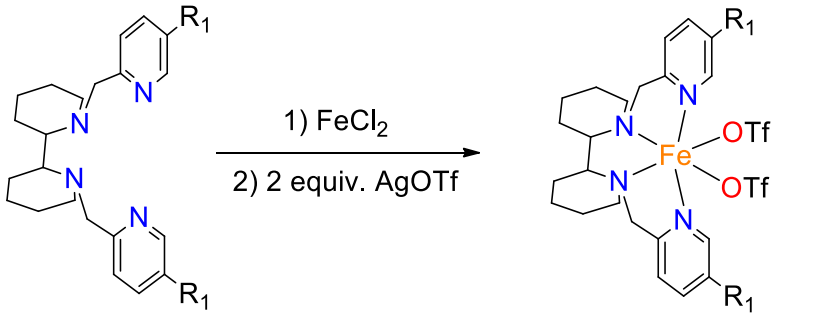

C24: *rac*-bpp; R_1 = H
C27: *rac*-bpp; R_1 = tips

Scheme VI.7. Synthesis and nomenclature of the iron triflate complexes with *rac*-bpp.

[Fe(CF_3SO_3)$_2$(*rac*-^{H}bpp)] (**C24**) was synthesized following a similar procedure to the one described in literature. Under a N_2 atmosphere, a suspension of AgOTf (47.0 mg, 179.36 µmol) in anhydrous CH_3CN (1 mL) was added drop-wise to a vigorously stirred solution of **C22** (42.8 mg, 89.68 µmol) in CH_3CN (1 mL). After stirring overnight, the solution was filtered through Celite© to remove AgCl precipitated. The solvent was evaporated under reduced pressure and the solid was redissolved in CH_2Cl_2 and the solution filtered off through Celite©. Slow diethyl ether diffusion over the resultant solution afforded, in a few days, yellow crystals. HRMS (ESI-MS) m/z calculated for $C_{23}H_{30}F_3FeN_4O_3S$ [M-OTf]$^-$: 555.1335, found: 555.1325; $C_{22}H_{30}FeN_4$ [M-2OTf]$^{-2}$: 203.0905, found: 203.0911. FT-IR (ATR) ν, cm^{-1}: 2959-2863 (C-H)sp^3, 1445, 1304, 1215, 1160, 852, 769, 633, 514, 415. Anal. Calcd. for $C_{24}H_{30}F_6FeN_4O_6S_2$·: C, 40.92; H, 4.29; N, 7.95%; found: C, 41.04; H, 4.44 N, 8.02%.

[Fe(CF_3SO_3)$_2$(*rac*-^{tips}bpp)] (**C27**) was prepared in a similar manner to **C24**, but the two step synthesis was performed in one pot. Under a N_2 atmosphere, a suspension of $FeCl_2$ (11.3 mg, 88.5 µmol) in anhydrous CH_3CN (1 mL) was added drop-wise to a vigorously stirred solution of **L10** (49.0 mg, 139.8 µmol) in anhydrous THF (1 mL). After stirring all night, a suspension of AgOTf (46.4 mg, 177.0 µmol) in anhydrous CH_3CN (1 mL) was added drop-wise. After stirring overnight, the solution was filtered through Celite© to remove AgCl precipitated. The solvent was evaporated under reduced pressure and the solid was redissolved in CH_2Cl_2 and the solution filtered off through Celite©. Slow diethyl ether diffusion over the resultant solution afforded, in a few days, yellow crystals. HRMS (ESI-MS) m/z calculated for $C_{41}H_{70}F_3FeN_4O_3SSi_2$ [M-OTf]$^-$: 867.4004, found: 867.4009; $C_{40}H_{70}N_4Si_2Fe$ [M-2OTf]$^{-2}$: 359.2239, found: 359.2246. Anal. Calcd. for $C_{42}H_{70}F_{36}FeN_4O_6S_2Si_2$·0.1$CH_2Cl_2$: C, 49.30; H, 6.90; N, 5.46%; found: C, 49.2; H, 7.16 N, 5.70%.

Synthesis of manganese triflate complexes

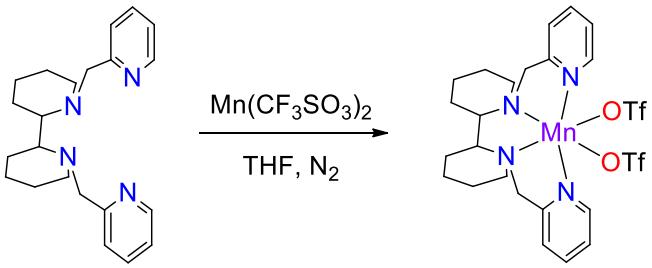

C25: *meso*-bpp
C26: *rac*-bpp

Scheme VI.8. Synthesis and nomenclature of the manganese triflate complexes.

[Mn(CF$_3$SO$_3$)$_2$(*meso*-^{H}bpp)] (**C25**) was prepared in a similar manner to **C21**, starting from **L8** (47.9 mg, 136.7 µmol) and Mn(CF$_3$SO$_3$)$_2$ (48.3 mg, 136.7 µmol) in anhydrous THF. After stirring overnight, a pale yellow precipitate appeared. The solution was removed and the solid dried under vacuum. This solid was solved in CH_2Cl_2 and the solution filtered off through Celite©. Slow diethyl ether diffusion over the resultant solution in the freezer afforded, in a few days, colourless crystals. HRMS (ESI-MS) m/z calculated for $C_{23}H_{30}F_3MnN_4O_3S$ [M-OTf]$^-$: 554.1366, found: 554.1356; $C_{24}H_{33}MnN_5$ [M-2OTf+CH$_3$CN]$^{-2}$: 223.1053, found: 223.1044; $C_{22}H_{32}MnN_4O$ [M-2OTf+H$_2$O]$^{-2}$: 211.5973, found: 211.5964; $C_{22}H_{30}MnN_4$ [M-2OTf]$^{-2}$: 202.5920, found: 202.5915. FT-IR (ATR) ν, cm^{-1}: 2953-2876 (C-H)sp^3, 1606, 1573, 1305, 1236, 1209, 1158, 1019, 981, 772, 633, 581, 514, 410. Anal. Calcd. for $C_{24}H_{30}F_6MnN_4O_6S_2$: C, 40.97; H, 4.30; N, 7.96%; found: C, 40.88; H, 4.17; N, 7.72%.

[Mn(CF$_3$SO$_3$)$_2$(*rac*-^{H}bpp)] (**C26**) was prepared in a similar manner to **C21**, starting from **L9** (100.0 mg, 285.3 µmol) and Mn(CF$_3$SO$_3$)$_2$ (100.7 mg, 285.3 µmol) in anhydrous THF. After stirring overnight, a white precipitate appeared. The solution was removed and the solid dried under vacuum. This solid was solved in CH_2Cl_2 and the solution filtered off through Celite©. Slow diethyl ether diffusion over the resultant solution afforded, in a few days, 60.7 mg (30% yield) of colorless crystals. HRMS (ESI-MS) m/z calculated for $C_{23}H_{30}F_3MnN_4O_3S$ [M-OTf]$^-$: 554.1366, found: 554.1359; $C_{22}H_{32}MnN_4O$ [M-2OTf+H$_2$O]$^{-2}$: 211.5973, found: 211.5963; $C_{22}H_{30}MnN_4$ [M-2OTf]$^{-2}$: 202.5920, found: 202.5916. FT-IR (ATR) ν, cm^{-1}: 2958-2868 (C-H)sp^3, 1445, 1306, 1213, 1160, 1031, 991, 850, 769, 634, 514. Anal. Calcd. for $C_{24}H_{30}F_6MnN_4O_6S_2$: C, 40.97; H, 4.30; N, 7.96%; found: C, 40.68; H, 4.33; N, 7.98%.

VI.3.4 Catalytic conditions

Hydrogen peroxide solutions employed in the reactions were prepared by diluting commercially available hydrogen peroxide (32%, unless indicated, H_2O_2 solution in water, Aldrich) in acetonitrile (HPLC grade).

VI.3.4.1 Reaction protocol for catalysis

Table VI.4-VI.12:

A 5 mL vial was charged with: catalyst (1.2 µmol, 3 mol %), substrate (40 µmol, 1 equiv.), CH$_3$CN (0.8 mL) and a magnetic stir bar. A 1.74 M CH_3CO_2H solution in CH$_3$CN was added (35 µL, 60 µmol, 150 mol %) and the vial was placed on an ice bath and stirred. The necessary amount of a 1.5 M (X equiv, see each table) H_2O_2 solution (diluted from a 32% H_2O_2 aqueous solution) was delivered by

syringe pump over 17 minutes at 0°C. After syringe pump addition, the resulting solution was stirred for another 10 min. Biphenyl was added at this point as internal standard. The iron complex was removed by passing the solution through a short path of silica followed by elution with 2 mL of AcOEt. Finally, the solution was subjected to GC analysis.

VI.3.4.2 Calibration curves and products determination

GC analysis of the catalysis provided substrate conversions and product yields relative to the internal standard integration. Calibration curves were obtained from commercial substrates. Products were identified by comparison to the GC retention time of authentic samples, and by their GC-MS spectrum. Products calibration curves used are those of the corresponding substrates.

IV.3.5 X-ray data

Table VI.13. First coordination sphere bond lengths (Å) and angles (°) for **C21, C23** and **C25** complexes.

Distances (Å) ***Complex***	**M-O / M-Cl**	**M-N_{sp2}**	**M-N_{sp3}**
C21	2.438, 2.412	2.193, 2.167	2.374, 2.321
C23	2.139, 2.139	2.137, 2.137	2.257, 2.257
C25	2.166, 2.166	2.213, 2.213	2.298, 2.298

Angles (°) ***Complex***	**O-M-O** **Cl-M-Cl**	**N_{sp2}-M-N_{sp2}**	**N_{sp3}-M-N_{sp3}**	**N_{sp2}-M-N_{sp3}**
C7	96.60	170.10	74.29	74.47
C9	92.05	171.53	79.58	80.50
C12	92.23	176.69	78.57	75.57

CHAPTER VII

General conclusions

- Two new enantiopure N_4-donor aminopyridine ligands (**L1** and **L2**) based on the N^1,N^2-bis((*S*)-1-phenylethyl)ethane-1,2-diamine (**BPhMeNH**) and (*R*,*R*)-1,5-diaza-*cis*-decalin (**DCD**) backbones have been developed. The corresponding iron(II) triflate, manganese(II) triflate and iron(II) chloride (only for the former ligand) complexes (**C1-C5**) have been also synthesized and characterized. These complexes contained a metal(II) center in a distorted octahedral coordination geometry with two *cis* labile sites available for the coordination of oxidant and additives. This distortion is more evidenced in the complexes based on the **DCD** backbone.

- The catalytic performance of these triflate complexes was tested in the epoxidation of alkenes, giving very poor results. Our hypothesis is that the complexes based on the **BPhMeNH** backbone are rapidly degraded, presumably self-oxidized at the benzylic positions of such diamine under the catalytic oxidative conditions. On the other hand, the complexes based on the **DCD** backbone present a huge rigidity (confirmed with the distortion observed in the X-Ray) that may prompt the complex to release the metal during the catalysis. Both pathways deactivated the catalyst inhibiting the catalytic cycle.

- We have also developed a novel family of enantiopure bis(aminopyridine) and bis(aminobenzimidazol) tetradentate ligands based on the 1,1',2,2',3,3',4,4'-octahydro-1,1'-biisoquinoline (**ohbiq**) backbone (**L3-L7**). Different substituents were introduced in the pyridine moiety for the modification of the electronic and steric properties of those ligands. The corresponding iron(II) chloride, iron(II) triflate and manganese(II) triflate complexes (**C6-C20**) have been also synthetized and characterized. The complexes present a distorted octahedral geometry and the ligand coordinates in a *cis*-α-topology. As expected, the metal center exhibits a Λ helical chirality for all the complexes, as the used backbone presents (*S*,*S*) chirality.

- The catalytic performance of these triflate complexes in the epoxidation of alkenes has been evaluated. In general, the electron-rich complexes provided the best enantioselectivities and yields with hydrogen peroxide as oxidant. The reaction conditions (including which catalyst and its amount, quantity of oxidant, which acid and its amount, and temperature) were optimized for some interesting substrates, achieving higher yields and enantioselectivities.

- For bulky substrates, we discover an inversion in the enantiocontrol of this reaction by the use of sterically demanding groups in the ligand, that has no precedents. Even if the absolute configuration of the epoxide product is expected to be determined by the chirality of the backbone (or the chirality at

the metal), the sterically bulky catalysts (that bear a tips group in the pyridine) are able to reverse it. Some mechanistically studies are being performed to understand the basis of this effect.

- We found that, **C19** manganese catalyst, which bears dimethylamino groups in the *para*-positions of the pyridines, accomplished highly enantioselective epoxidation of β,β-disubstituted enamides with aqueous hydrogen peroxide (up to 99% ee). The epoxidation of these substrates is very interesting as equal to difficult. We determine that the amide moiety is crucial in acquiring high enantioselectivities, being the dibenzyl substituted the best choice. The broad substrate scope of the system is truly remarkable, including electron-donating and electron-withdrawing groups, and exhibits good functional group tolerance, including pyridine moiety. In most cases, the epoxidation proceeds with stereoretention with moderate to excellent yields (65-90%) and excellent enantioselectivities (91-99% ee).

- Finally, we have synthesized new racemic tetradentate aminopyridine ligands based on the 2,2'-bipiperidine backbone (**L8-L10**). The corresponding iron chloride, iron triflate and manganese triflate complexes were prepared and characterized. All the X-ray structures exhibit a distorted octahedral geometry and, more interestingly, in a *cis*-α-topology, although a *cis*-β-topology was expected for *meso* compounds.

- We performed a comparison between iron complexes based on different backbones in C-H oxidation catalysis, confirming the importance of the diamine nature. *N,N'*-dimethyl-*trans*-1,2-cyclohexanediamine, 2,2'-bipyrrolidine, 2,2'-bipiperidine, 1,1'-biisoindoline and 1,1',2,2',3,3',4,4'-octahydro-1,1'-biisoquinoline diamine were the backbones studied. **Ohbiq** based catalysts exhibit similar results, in terms of selectivity, to the previous reported *N,N'*-dimethyl-*trans*-1,2-cyclohexanediamine (**mcp**) and 2,2'-bipyrrolidine (**bp**) based analogous complexes. While, 2,2'-bipiperidine (**bpp**) based catalysts appear to be more selective for secondary site oxidation and more capable to discriminate among different secondary sites, compared to their bp- and mcp-counterparts.

- We confirmed that the presence of the tips group in the ligand furnish more active and more selective catalysts. Nevertheless, it should be noted that the reaction conditions require further optimization for the improvement of the results. The mass balance is not complete, and this might be due to the difficultness of this type of oxidations, which involve highly oxidizing species and chemo- and regioselectivity is difficult to control.

- In general, **bpp** based iron complexes appeared as very convenient catalysts for C-H oxidation reactions employing H_2O_2 as terminal oxidant. The oxidation of enantiopure complex molecules, such as terpenoids or steroids, is highly dependent on the chirality of the complex. Thus, we envision that further studies of this new catalysts, in an enantiopure fashion, in C-H and C=C oxidation may let to a novel family of catalysts with outstanding activity. However, a deeper optimization of the reaction conditions of the system is required.

References

1. Singh, H. S., Organic Synthesis by Oxidation with Metal Compounds. In *Organic Synthesis by Oxidation with Metal Compounds*, Mijs, W. J.; de Jonge, C. R. H. I., Eds. Plenum Press: New York, **1986**; 633-693.

2. Sheldon, R. A.; Kochi, J. A., *Metal-Catalyzed Oxidations of Organic Compounds*, Academic Press: New York, **1981**.

3. Hudlicky, M., *Oxidations in Organic Chemistry*, American Chemical Society: Washington DC, 1990.

4. Bäckvall, J.-E., *Modern oxidation Methods*, Wiley-VCH: Weinheim, **2004**.

5. Sheldon, R. A., Biocatalytic and Biomimetic Oxidations from an Industrial Perspective. In *Biomimetic Oxidations Catalyzed by Transition Metal Complexes*, Meunier, B., Ed. Imperial College Press: London, **2000**; 613-662.

6. Noyori, R.; Aoki, M.; Sato, K. *Chem. Commun.* **2003**, *16*, 1977.

7. Damodar, B. D. K., Epoxides and Oxetanes. In *Heterocycles in Natural Product Synthesis*, Chattopadhyay, K. C. M. a. S. K., Ed. **2011**; 63-95.

8. Miyashita, K.; Imanishi, T. *Chem. Rev.* **2005**, *105*, 4515.

9. Zhou, Z.-L.; Yang, Y.-X.; Ding, J.; Li, Y.-C.; Miao, Z.-H. *Nat. Prod. Rep.* **2012**, *29*, 457.

10. Kolb, H. C.; Finn, M. G.; Sharpless, K. B. *Angew. Chem. Int. Ed.* **2001**, *40*, 2004.

11. Katsuki, T., Asymmetric Epoxidation of Unfunctionalized Olefins and Related Reactions. In *Catalytic Asymmetric Synthesis*, 2nd ed.; Ojima, I., Ed. Wiley-VCH: New York, **2000**; 287-325.

12. De Faveri, G.; Ilyashenko, G.; Watkinson, M. *Chem. Soc. Rev.* **2011**, *40*, 1722.

13. Chatterjee, D. *Coord. Chem. Rev*. **2008**, *252*, 176.

14. Wong, O. A.; Shi, Y. *Chem. Rev.* **2008**, *108*, 3958.

15. Diez, D.; Nunez, M. G.; Anton, A. B.; Garcia, P.; Moro, R. F.; Garrido, N. M.; Marcos, I. S.; Basabe, P.; Urones, J. G. *Curr. Org. Synth.* **2008**, *5*, 186.

16. Zhu, Y.; Wang, Q.; Cornwall, R. G.; Shi, Y. *Chem. Rev.* **2014**, *114*, 8199.

17. Davis, R. L.; Stiller, J.; Naicker, T.; Jiang, H.; Jørgensen, K. A. *Angew. Chem. Int. Ed.* **2014**, *53*, 7406.

18. Dyker, G., *Handbook of C-H Transformations*, Wiley-VCH: Weinheim, **2005**; Vol. 1-2.

19. Shilov, A. E.; Shul'pin, G. B., *Activation and Catalytic Reactions of Saturated Hydrocarbons in the Presence of Metal Complexes*, Springer-Verlag: Boston, **2000**.

20. Cernak, T.; Dykstra, K. D.; Tyagarajan, S.; Vachal, P.; Krska, S. W. *Chem. Soc. Rev.* **2016**, 45, 546.

21. Newhouse, T.; Baran, P. S. *Angew. Chem. Int. Ed.* **2011**, *50*, 3362.

22. Barton, D. H. R.; Doller, D. *Acc. Chem. Res.* **1992**, *25*, 504.

23. Zheng, C.; You, S.-L. *RSC Advances* **2014**, *4*, 6173.

24. Brückl, T.; Baxter, R. D.; Ishihara, Y.; Baran, P. S. *Acc. Chem. Res.* **2012**, *45*, 826.

25. Mayer, J. M. *Acc. Chem. Res.* **2011**, *44*, 36.

26. Salamone, M.; Bietti, M. *Acc. Chem. Res.* **2015**, *48*, 2895.

27. Chowdhury, R.; Hardy, A.; Schofield, C. J. *Chem. Soc. Rev.* **2008**, *37*, 1308.

28. Bruijnincx, P. C. A.; Koten, G. v.; Gebbink, R. J. M. K. *Chem. Soc. Rev.* **2008**, *12*, 2716.

29. Krebs, C.; Galonić Fujimori, D.; Walsh, C. T.; Bollinger, J. M. *Acc. Chem. Res.* **2007**, *40*, 484.

30. Costas, M.; Mehn, M. P.; Jensen, M. P.; Que, L., Jr. *Chem. Rev.* **2004**, *104*, 939.

31. Vaillancourt, F. H.; Yeh, E.; Vosburg, D. A.; Garneau-Tsodikova, S.; Walsh, C. T. *Chem. Rev.* **2006**, *106*, 3364.

32. Stillman, M. *Angew. Chem. Int. Ed.* **2007**, *46*, 8741.

33. McQuarters, A. B.; Wolf, M. W.; Hunt, A. P.; Lehnert, N. *Angew. Chem. Int. Ed.* **2014**, *53*, 4750.

34. Strieker, M.; Nolan, E. M.; Walsh, C. T.; Marahiel, M. A. *J. Am. Chem. Soc.* **2009**, *131*, 13523.

35. Hudlicky, T.; Reed, J. W. *Synlett* **2009**, 685.

36. Hudlicky, T.; Reed, J. W. *Chem. Soc. Rev.* **2009**, *38*, 3117.

37. Boyd, D. R.; Sharma, N. D.; Allen, C. C. R. *Curr. Opin. Biotechnol.* **2001**, *12*, 564.

38. Gibson, D. T.; Parales, R. E. *Curr. Opin. Biotechnol.* **2000**, *11*, 236.

39. Que, L.; Tolman, W. B. *Nature* **2008**, *455*, 333.

40. Cotton, F. A.; Carlos, M.; Brochman, M., *Advanced Inorganic Chemistry*, 6th ed.; John Wiley & Sons: New York, **1999**.

41. Groves, J. T., Models and Mechanisms of Cytochrome P450 Action. In *Cytochrome P450: Structure, Mechanism and Biochemistry*. 3rd ed., Ortiz de Montellano, P. R., Ed. Kluwer Academic/Plenum Publishers: New York, **2005**; 1-42.

42. Ortiz de Montellano, P. R. *Chem. Rev.* **2010**, *110*, 932.

43. Meunier, B.; Bernadou, J. *Struct. Bonding* **2000**, *97*, 1.

44. Meunier, B.; de Visser, S. P.; Shaik, S. *Chem. Rev.* **2004**, *104*, 3947.

45. Schlichting, I.; Berendzen, J.; Chu, K.; Stock, A. M.; Maves, S. A.; Benson, D. E.; Sweet, R. M.; Ringe, D.; Petsko, G. A.; Sligar, S. G. *Science* **2000**, *287*, 1615.

46. Li, H.; Narasimhulu, S.; Havran, L. M.; Winkler, J. D.; Poulos, T. L. *J. Am. Chem. Soc*. **1995**, *117*, 6297.

47. Yano, J. K.; Wester, M. R.; Schoch, G. A.; Griffin, K. J.; Stout, C. D.; Johnson, E. F. *J. Biol. Chem.* **2004**, *279*, 38091.

48. Kells, P. M.; Ouellet, H.; Santos-Aberturas, J.; Aparicio, J. F.; Podust, L. M. *Chem. Biol.* **2010**, *17*, 841.

49. Shah, M. B.; Jang, H.-H.; Zhang, Q.; David Stout, C.; Halpert, J. R. *Arch. Biochem. Biophys.* **2013**, *530*, 64.

50. Poulos, T. L.; Finzel, B. C.; Gunsalus, I. C.; Wagner, G. C.; Kraut, J. *J. Biol. Chem.* **1985**, *260*, 16122.

51. Sono, M.; Roach, M. P.; Coulter, E. D.; Dawson, J. H. *Chem. Rev.* **1996**, 96, 2841.

52. Dawson, J. H.; Sono, M. *Chem. Rev.* **1987**, *87*, 1255.

53. J. Mueller, E.; J. Loida, P.; Sligar, S., T*wenty-five Years of P450cam Research*, **1995**; 83-124.

54. Hrycay, E. G.; Bandiera, S. M. *Adv. Exp. Med. Biol.* **2015**, *851*, 1.

55. Denisov, I. G.; Makris, T. M.; Sligar, S. G.; Schlichting, I. *Chem. Rev.* **2005**, *105*, 2253.

56. I C Gunsalus; T C Pederson, a.; Sligar, S. G. *Annu. Rev. Biochem* **1975**, *44*, 377.

57. Munro, A. W.; Girvan, H. M.; Mason, A. E.; Dunford, A. J.; McLean, K. J. *Trends Biochem. Sci.* **2013**, *38*, 140.

58. Whitehouse, C. J. C.; Bell, S. G.; Wong, L.-L. *Chem. Soc. Rev.* **2012**, *41*, 1218.

59. Rittle, J.; Green, M. T. *Science* **2010**, *330*, 933.

60. Meunier, B.; Bernadou, J. *Top. Catal.* **2002**, *21*, 47.

61. Dunford, H. B.; Stillman, J. S. *Coord. Chem. Rev.* **1976**, *19*, 187.

62. King, N.; Winfield, M. *Aust. J. Chem.* **1959**, *12*, 47.

63. Groves, J. T.; McCluskey, G. A. *J. Am. Chem. Soc.* **1976**, *98*, 859.

64. Groves, J. T.; McClusky, G. A.; White, R. E.; Coon, M. *J. Biochem. Biophys. Res. Commun.* **1978**, *81*, 154.

65. Groves, J. T. *Proc. Nat. Acad. Sci. USA* **2003**, *100*, 3569.

66. Visser, S.; Kumar, D., *Iron-containing enzymes: versatile catalysts of hydroxylation reactions in nature*, **2011**.

67. Abu-Omar, M. M.; Loaiza, A.; Hontzeas, N. *Chem. Rev.* **2005**, *105*, 2227.

68. Gibson, D. T.; Resnick, S. M.; Lee, K.; Brand, J. M.; Torok, D. S.; Wackett, L. P.; Schocken, M. J.; Haigler, B. E. *J. Bacteriol.* **1995**, *177*, 2615.

69. Wolfe, M. D.; Parales, J. V.; Gibson, D. T.; Lipscomb, J. D. *J. Biol. Chem.* **2001**, *276*, 1945.

70. Ferraro, D. J.; Gakhar, L.; Ramaswamy, S. *Biochem. Biophys. Res. Commun.* **2005**, *338*, 175.

71. Bugg, T. D. H.; Ramaswamy, S. *Curr. Op. Chem. Biol.* **2008**, *12*, 134.

72. Wackett, L. P. *Enzyme Microb. Technol.* **2002**, *31*, 577.

73. E. Parales, R.; M. Resnick, S., *Aromatic Ring Hydroxylating Dioxygenases*, **2006**; Vol. 4, 287-340.

74. R. Boyd, D.; N. Sheldrake, G. *Nat. Prod. Rep.* **1998**, *15*, 309.

75. Sydor, P. K.; Barry, S. M.; Odulate, O. M.; Barona-Gomez, F.; Haynes, S. W.; Corre, C.; Song, L.; Challis, G. L. *Nat. Chem.* **2011**, *3*, 388.

76. Han, J.; Kim, S.-Y.; Jung, J.; Lim, Y.; Ahn, J.-H.; Kim, S.-I.; Hur, H.-G. *Appl. Environ. Microbiol.* **2005**, *71*, 5354.

77. Ensley, B. D.; Gibson, D. T. *J. Bacteriol.* ***1983***, *155*, 505.

78. Parales, R. E.; Lee, K.; Resnick, S. M.; Jiang, H.; Lessner, D. J.; Gibson, D. T. *J. Bacteriol.* **2000**, *182*, 1641.

79. Kauppi, B.; Lee, K.; Carredano, E.; Parales, R. E.; Gibson, D. T.; Eklund, H.; Ramaswamy, S. *Structure* **1998**, *6*, 571.

80. Parales, R. E.; Parales, J. V.; Gibson, D. T. *J. Bacteriol.* **1999**, *181*, 1831.

81. Perry, C.; de los Santos, Emmanuel L. C.; Alkhalaf, L. M.; Challis, G. L. *Nat. Prod. Rep.* **2018**, *35*, 622.

82. Koehntop, K., D.; Emerson, J. P.; Que Jr., L. *J. Biol. Inorg. Chem.* **2005**, *10*, 87.

83. Martins, B. M.; Svetlitchnaia, T.; Dobbek, H. *Structure* **2005**, *13*, 817.

84. Hsueh, K.-L.; Westler, W. M.; Markley, J. L. *J. Am. Chem. Soc.* **2010**, *132*, 7908.

85. Karlsson, A.; Parales, J. V.; Parales, R. E.; Gibson, D. T.; Eklund, H.; Ramaswamy, S. *Science* **2003**, *299*, 1039.

86. Wolfe, M. D.; Altier, D. J.; Stubna, A.; Popescu, C. V.; Münck, E.; Lipscomb, J. D. *Biochemistry* **2002**, *41*, 9611.

87. Abu-Omar, M. M.; Loaiza, A.; Hontzeas, N. *Chem. Rev.* **2005**, *105*, 2227.

88. Kal, S.; Que, L. JBIC, *J. Biol. Inorg. Chem.* **2017**, *22*, 339.

89. O'Neal, S. L.; Zheng, W. *Curr. Environ. Health. Rep.* **2015**, *2*, 315.

90. Finley, J. W.; Davis, C. D. *BioFactors* **1999**, *10*, 15.

91. Kaim, W.; Schwederski, B., *Bioinorganic Chemistry: Inorganic Elements in the Chemistry of Life*, John Wiley & Sons: Chichester, **1995**.

92. Umena, Y.; Kawakami, K.; Shen, J.-R.; Kamiya, N. *Nature* **2011**, 55.

93. Yano, J.; Kern, J.; Sauer, K.; Latimer, M. J.; Pushkar, Y.; Biesiadka, J.; Loll, B.; Saenger, W.; Messinger, J.; Zouni, A.; Yachandra, V. K. *Science* **2006**, *314*, 821.

94. Renger, G. *Biochim. Biophys. Acta-Bionergetics* **2012**, *1817*, 1164.

95. Fridovich, I. *Arch. Biochem. Biophys.* **1986**, *247*, 1.

96. Abreu, I. A.; Cabelli, D. E. *Biochim. Biophys. Acta-Proteins and Proteomics* **2010**, *1804*, 263.

97. Edwards, R. A.; Baker, H. M.; Whittaker, M. M.; Whittaker, J. W.; Jameson, G. B.; Baker, E. N. JBIC, *J. Biol. Inorg. Chem.* **1998**, *3*, 161.

98. Whiting, A. K.; Boldt, Y. R.; Hendrich, M. P.; Wackett, L. P.; Que, L., Jr. *Biochemistry* **1996**, *35*, 160.

99. Vetting, M. W.; Wackett, L. P.; Que, L.; Lipscomb, J. D.; Ohlendorf, D. H. *J. Bacteriol.* **2004**, *186*, 1945.

100. Meunier, B., *Biomimetic Oxidations Catalyzed by Transition Metal Complexes*, **2000**.

101. Sheldon, R.; Arends, I.; Hanefeld, U., *Green Chemisty and Catalysis*, **2007**; 1-433.

102. Gopalaiah, K. *Chem. Rev.* **2013**, *113*, 3248.

103. Oloo, W. N.; Que, L. *Acc. Chem. Res.* **2015**, *48*, 2612.

104. Talsi, E. P.; Bryliakov, K. P. *Coord. Chem. Rev.* **2012**, *256*, 1418.

105. Aldrich-Wright, J. R.; Vagg, R. S.; Williams, P. A. *Coord. Chem. Rev.* **1997**, *166*, 361.

106. Ulrich, K.; Alex, v. Z. *Angew. Chem. Int. Ed.* **1999**, *38*, 302.

107. Britovsek, G. J. P.; England, J.; White, A. J. P. *Dalton Trans.* **2006**, *11*, 1399.

108. Mas-Ballesté, R.; Costas, M.; Berg, T. v. d.; Que, L. *J. Chem. Eur. J.* **2006**, *12*, 7489.

109. England, J.; Britovsek, G. J. P.; Rabadia, N.; White, A. J. P. *Inorg. Chem.* **2007**, *46*, 3752.

110. Gavrilova, A. L.; Bosnich, B. *Chem. Rev.* **2004**, *104*, 349.

111. Costas, M.; Que Jr., L. *Angew. Chem. Int. Ed.* **2002**, *12*, 2179.

112. Hong, S.; Lee, Y.-M.; Cho, K.-B.; Sundaravel, K.; Cho, J.; Kirn, M. J.; Shin, W.; Nam, W. *J. Am. Chem. Soc.* **2011**, *133*, 11876.

113. Peter, S.; Vital, Y.; A., B. P. C.; M., W. B.; M., K. G. R. J. *Chem. Eur. J.* **2013**, *19*, 15012.

114. Chen, K.; Costas, M.; Que, L., Jr. *J. Chem. Soc., Dalton Trans.* **2002**, 672.

115. Mekmouche, Y.; Ménage, S.; Pécaut, J.; Lebrun, C.; Reilly, L.; Schuenemann, V.; Trautwein, A.; Fontecave, M. Eur. J. *Inorg. Chem.* **2004**, 3163.

116. Kim, C.; Chen, K.; Kim, J.; Que, L., Jr. *J. Am. Chem. Soc.* **1997**, *119*, 5964.

117. Chen, K.; Que, L., Jr. *Chem. Commun.* **1999**, 1375.

118. Chen, K.; Que, L., Jr. *J. Am. Chem. Soc.* **2001**, *123*, 6327.

119. Costas, M.; Tipton, A. K.; Chen, K.; Jo, D.-H.; Que Jr., L. *J. Am. Chem. Soc.* **2001**, *123*, 6722.

120. Company, A.; Gómez, L.; Güell, M.; Ribas, X.; Luis, J. M.; Que, L., Jr; Costas, M. *J. Am. Chem. Soc.* **2007**, *129*, 15766.

121. Company, A.; Gómez, L.; Fontrodona, X.; Ribas, X.; Costas, M. *Chem. Eur. J.* **2008**, *14*, 5727.

122. Prat, I.; Company, A.; Postils, V.; Ribas, X.; Lawrence Que, J.; Luis, J. M.; Costas, M. *Chem. Eur. J.* **2013**, *19*, 6724.

123. Prat, I.; Gomez, L.; Canta, M.; Ribas, X.; Costas, M. *Chemistry (Weinheim an der Bergstrasse, Germany) 2013*, **19**, 1908.

124. Chen, M. S.; White, M. C. *Science* **2007**, *318*, 783.

125. Chen, M. S.; White, M. C. *Science* **2010**, *327*, 566.

126. Gómez, L.; Canta, M.; Font, D.; Prat, I.; Ribas, X.; Costas, M. J. *Org. Chem.* **2013**, *78*, 1421.

127. Gómez, L.; Garcia-Bosch, I.; Company, A.; Benet-Buchholz, J.; Polo, A.; Sala, X.; Ribas, X.; Costas, M. *Angew. Chem. Int. Ed.* **2009**, *48*, 5720.

128. Gormisky, P. E.; White, M. C. *J. Am. Chem. Soc.* **2013**, *135*, 14052.

129. Font, D.; Canta, M.; Milan, M.; Cussó, O.; Ribas, X.; Klein Gebbink, R. J. M.; Costas, M. *Angew. Chem. Int. Ed.* **2016**, *55*, 5776.

130. White, M. C.; Doyle, A. G.; Jacobsen, E. N. *J. Am. Chem. Soc.* **2001**, *123*, 7194.

131. Anilkumar, G.; Bitterlich, B.; Gelalcha, F. G.; Tse, M. K.; Beller, M. *Chem. Commun.* **2007**, 289.

132. Gelalcha, F. G.; Anilkumar, G.; Tse, M. K.; Brückner, A.; Beller, M. *Chem. Eur. J.* **2008**, *14*, 7687.

133. Wu, M.; Miao, C.-X.; Wang, S.; Hu, X.; Xia, C.; Kühn, F. E.; Sun, W. *Adv. Synth. & Catal.* **2011**, *353*, 3014.

134. Wang, B.; Wang, S.; Xia, C.; Sun, W. *Chem. Eur. J.* **2012**, *18*, 7332.

135. Wang, X.; Miao, C.; Wang, S.; Xia, C.; Sun, W. *ChemCatChem* **2013**, *5*, 2489.

136. Nishikawa, Y.; Yamamoto, H. *J. Am. Chem. Soc.* **2011**, *133*, 8432.

137. Luo, L.; Yamamoto, H. *Eur. J. Org. Chem* **2014**, 7803.

138. Lyakin, O. Y.; Ottenbacher, R. V.; Bryliakov, K. P.; Talsi, E. P. *ACS Catal.* **2012**, *2*, 1196.

139. Cussó, O.; Garcia-Bosch, I.; Ribas, X.; Lloret-Fillol, J.; Costas, M. *J. Am. Chem. Soc.* **2013**, *135*, 14871.

140. Cussó, O.; Ribas, X.; Lloret-Fillol, J.; Costas, M. *Angew. Chem. Int. Ed.* **2015**, *54*, 2729.

141. Cussó, O.; Cianfanelli, M.; Ribas, X.; Klein Gebbink, R. J. M.; Costas, M. *J. Am. Chem. Soc.* **2016**, *138*, 2732.

142. Irie, R.; Noda, K.; Ito, Y.; Matsumoto, N.; Katsuki, T. *Tetrahedron Lett.* **1990**, *31*, 7345.

143. Katsuki, T. *Coord. Chem. Rev.* **1995**, *140*, 189.

144. Zhang, W.; Loebach, J. L.; Wilson, S. R.; Jacobsen, E. N. *J. Am. Chem. Soc.* **1990**, *112*, 2801.

145. McGarrigle, E. M.; Gilheany, D. G. *Chem. Rev.* **2005**, *105*, 1563.

146. Murphy, A.; Dubois, G.; Stack, T. D. P. *J. Am. Chem. Soc.* **2003**, *125*, 5250.

147. Murphy, A.; Pace, A.; Stack, T. D. P. *Org. Lett.* **2004**, *6*, 3119.

148. Gomez, L.; Garcia-Bosch, I.; Company, A.; Sala, X.; Fontrodona, X.; Ribas, X.; Costas, M. *Dalton Trans.* **2007**, 5539.

149. Garcia-Bosch, I.; Ribas, X.; Costas, M. *Adv. Synth. Catal.* **2009**, *351*, 348.

150. Wu, M.; Wang, B.; Wang, S.; Xia, C.; Sun, W. *Org. Lett.* **2009**, *11*, 3622.

151. Ottenbacher, R. V.; Bryliakov, K. P.; Talsi, E. P. *Adv. Synth. Catal.* **2011**, *353*, 885.

152. Garcia-Bosch, I.; Gómez, L.; Polo, A.; Ribas, X.; Costas, M. *Adv. Synth. Catal.* **2012**, *354*, 65.

153. Wang, B.; Miao, C.; Wang, S.; Xia, C.; Sun, W. *Chem. Eur. J.* **2012**, *18*, 6750.

154. Shen, D.; Miao, C.; Wang, S.; Xia, C.; Sun, W. *Eur. J. Inorg. Chem.* **2014**, 5777.

155. Cussó, O.; Garcia-Bosch, I.; Font, D.; Ribas, X.; Lloret-Fillol, J.; Costas, M. *Org. Lett.* **2013**, *15*, 6158.

156. Ottenbacher, R. V.; Samsonenko, D. G.; Talsi, E. P.; Bryliakov, K. P. *ACS Catal.* **2014**, *4*, 1599.

157. Shen, D.; Qiu, B.; Xu, D.; Miao, C.; Xia, C.; Sun, W. *Org. Lett.* **2016**, *18*, 372.

158. Wang, W.; Sun, Q.; Xia, C.; Sun, W. *Chin. J. Catal.* **2018**, *39*, 1463.

159. Donets, P. A.; Cramer, N. *J. Am. Chem. Soc.* **2013**, *135*, 11772.

160. Canta, M.; Font, D.; Gómez, L.; Ribas, X.; Costas, M. *Adv. Synth. Catal.* **2014**, *356*, 818.

161. Li, X.; Schenkel, L. B.; Kozlowski, M. C. *Org. Lett.* **2000**, *2*, 875.

162. Conlon, D. A.; Drahus-Paone, A.; Ho, G.-J.; Pipik, B.; Helmy, R.; McNamara, J. M.; Shi, Y.-J.; Williams, J. M.; Macdonald, D.; Deschênes, D.; Gallant, M.; Mastracchio, A.; Roy, B.; Scheigetz, J. *Org. Process Res. Dev.* **2006**, *10*, 36.

163. Gil de Oliveira Santos, A.; Klute, W.; Torode, J.; P. W. Bohm, V.; Cabrita, E.; Runsink, J.; W. Hoffmann, R. *New J. Chem.* **1998**, *22*, 993.

164. Ottenbacher, R. V.; Samsonenko, D. G.; Talsi, E. P.; Bryliakov, K. P. *Org. Lett.* **2012**, *14*, 4310.

165. Drago, R. S., *Physical Methods for Chemists*, 2nd ed.; Saunders: Philadelphia, **1992**; 626-649.

166. Prat, I.; Company, A.; Corona, T.; Parella, T.; Ribas, X.; Costas, M. *Inorg. Chem.* **2013**, *52*, 9229.

167. Britovsek, G. J. P.; England, J.; White, A. J. P. *Inorg. Chem.* **2005**, *44*, 8125.

168. England, J.; Gondhia, R.; Bigorra-Lopez, L.; Petersen, A. R.; White, A. J. P.; Britovsek, G. J. P. *Dalton Trans.* **2009**, 5319.

169. Petzold, H.; Djomgoue, P.; Horner, G.; Speck, J. M.; Ruffer, T.; Schaarschmidt, D. *Dalton Trans.* **2016**, *45*, 13798.

170. Mialane, P.; Nivorojkine, A.; Pratviel, G.; Azéma, L.; Slany, M.; Godde, F.; Simaan, A.; Banse, F.; Kargar-Grisel, T.; Bouchoux, G.; Sainton, J.; Horner, O.; Guilhem, J.; Tchertanova, L.; Meunier, B.; Girerd, J. J. *Inorg. Chem.* **1999**, *38*, 1085.

171. Balland, V.; Banse, F.; Anxolabéhère-Mallart, E.; Nierlich, M.; Girerd, J.-J. *Eur. J. Inorg. Chem.* **2003**, 2529.

172. Greenwood, N. N.; Earnshaw, A. *24-Manganese, Technetium and Rhenium*. In Chemistry of the Elements (Second Edition), Butterworth-Heinemann: Oxford, **1997**; 1040-1069.

173. Arulsamy, N.; Hodgson, D. J.; Glerup, J. *Inorg. Chim. Acta* **1993**, *209*, 61.

174. Simaan, J.; Poussereau, S.; Blondin, G.; Girerd, J.-J.; Defaye, D.; Philouze, C.; Guilhem, J.; Tchertanov, L. *Inorg. Chim. Acta* **2000**, *299*, 221.

175. Gómez, L., PhD Thesis. University of Girona, **2010**.

176. Olivo, G.; Nardi, M.; Vìdal, D.; Barbieri, A.; Lapi, A.; Gómez, L.; Lanzalunga, O.; Costas, M.; Di Stefano, S. *Inorg. Chem.* **2015**, *54*, 10141.

177. Garcia-Bosch, I.; Company, A.; Fontrodona, X.; Ribas, X.; Costas, M. *Org. Lett.* **2008**, *10*, 2095.

178. Elliott, M. C.; Williams, E. *Org. Biomol. Chem* **2003**, *1*, 3038.

179. Arai, S.; Takita, S.; Nishida, A. Eur. *J. Org. Chem* **2005**, 5262.

180. Yang, W.; Liu, Y.; Zhang, S.; Cai, Q. *Angew. Chem. Int. Ed.* **2015**, *54*, 8805.

181. Zhang, Y.; Wang, Q.; Wang, T.; He, H.; Yang, W.; Zhang, X.; Cai, Q. J. *Org. Chem*. **2017**, *82*, 1458.

182. Cussó, O.; Garcia-Bosch, I.; Ribas, X.; Lloret-Fillol, J.; Costas, M. *J. Am. Chem. Soc.* **2013**, *135*, 14871.

183. Suzuki, K.; Oldenburg, P. D.; Que Jr., L. *Angew. Chem. Int. Ed.* **2008**, *47*, 1887.

184. He, Y.; Gorden, J. D.; Goldsmith, C. R. *Inorg. Chem.* **2011**, *50*, 12651.

185. Gomez, L.; Canta, M.; Font, D.; Prat, I.; Ribas, X.; Costas, M. *J. Org. Chem* **2013**, *78*, 1421.

186. Yazerski, V. A.; Spannring, P.; Gatineau, D.; Woerde, C. H. M.; Wieclawska, S. M.; Lutz, M.; Kleijn, H.; Klein Gebbink, R. J. M. *Org. Biomol. Chem.* **2014**, *12*, 2062.

187. Diebold, A.; Hagen, K. S. *Inorg. Chem.* **1998**, *37*, 215.

188. Chen, K.; Costas, M.; Kim, J.; Tipton, A. K.; Que Jr., L. *J. Am. Chem. Soc.* **2002**, *124*, 3026.

189. Mazlan, N. A.; Ravoof, T. B. S. A.; Tiekink, E. R. T.; Tahir, M. I. M.; Veerakumarasivam, A.; Crouse, K. A. *Transition Met. Chem.* **2014**, *39*, 633.

190. Dayan, O.; Yunus İnan, M. M *Synth. React. Inorg. M.* **2015**, *45*, 1018.

191. Blakesley, D. W.; Payne, S. C.; Hagen, K. S. *Inorg. Chem.* **2000**, *39*, 1979.

192. Yeung, H.-L.; Sham, K.-C.; Tsang, C.-S.; Lau, T.-C.; Kwong, H.-L. *Chem. Commun.* **2008**, 3801.

193. Anna, L.; M., R. C.; Benjamin, L. *Adv. Synth. Catal.* **2012**, *354*, 1701.

194. Uteuliyev, M. M.; Nguyen, T. T.; Coltart, D. M. *Nat. Chem.* **2015**, *7*, 1024.

195. Larrow, J. F.; Jacobsen, E. N. *J. Am. Chem. Soc.* **1994**, *116*, 12129.

196. Zhang, C. X.; Kaderli, S.; Costas, M.; Kim, E.-i.; Neuhold, Y.-M.; Karlin, K. D.; Zuberbuehler, A. D. *Inorg. Chem.* **2003**, *42*, 1807.

197. Milan, M.; Bietti, M.; Costas, M. *ACS Cent. Sci.* **2017**, *3*, 196.

198. Wang, X.; Miao, C.; Wang, S.; Xia, C.; Sun, W. *ChemCatChem* **2013**, *5*, 2489.

199. Sankararaman, S.; E. Nesakumar, J. *J. Chem. Soc., Perkin Trans. 1* **1999**, 3173.

200. Olson, R. E.; Sielecki, T. M.; Wityak, J.; Pinto, D. J.; Batt, D. G.; Frietze, W. E.; Liu, J.; Tobin, A. E.; Orwat, M. J.; Di Meo, S. V.; Houghton, G. C.; Lalka, G. K.; Mousa, S. A.; Racanelli, A. L.; Hausner, E. A.; Kapil, R. P.; Rabel, S. R.; Thoolen, M. J.; Reilly, T. M.; Anderson, P. S.; Wexler, R. R. J. *Med. Chem.* **1999**, *42*, 1178.

201. Porter, M. J.; Skidmore, J. *Chem. Commun.* **2000**, 1215.

202. Ojima, I., *Catalytic Asymmetric Synthesis*. 2nd ed.; Wiley-VCH: New York, **2000**.

203. Pruitt, J. R.; Pinto, D. J.; Estrella, M. J.; Bostrom, L. L.; Knabb, R. M.; Wong, P. C.; Wright, M. R.; Wexler, R. R. *Bioorg. Med. Chem. Lett.* **2000**, *10*, 685.

204. Lauret, C. *Tetrahedron: Asymmetry* **2001**, *12*, 2359.

205. Xia, Q. H.; Ge, H. Q.; Ye, C. P.; Liu, Z. M.; Su, K. X. *Chem. Rev.* **2005**, *105*, 1603.

206. Dai, W.; Li, G.; Chen, B.; Wang, L.; Gao, S. *Org. Lett.* **2015**, *17*, 904.

207. Alessandra, L. *Curr. Org. Synth.* **2008**, *5*, 117.

208. Chu, Y.; Liu, X.; Li, W.; Hu, X.; Lin, L.; Feng, X. *Chem. Sci.* **2012**, *3*, 1996.

209. Srour, H.; Le Maux, P.; Chevance, S.; Simonneaux, G. *Coord. Chem. Rev.* **2013**, *257*, 3030.

210. Wang, C.; Yamamoto, H. *Chem. Asian J.* **2015**, *10*, 2056.

211. Ottenbacher, R. V.; Talsi, E. P.; Bryliakov, K. P. *Catal. Today* **2016**, *278*, 30.

212. Karaman, H. S.; Kılıç, H.; Şahin, E. *Tetrahedron: Asymmetry* **2017**, *28*, 1626.

213. Bérubé, C.; Voyer, N. *Supramol. Chem.* **2018**, *30*, 184.

214. Waldemar, A.; Paraselli Bheema, R.; Hans-Georg, D.; Chantu R., S. M. Eur. *J. Org. Chem* **2002**, 630.

215. Cuibao, L.; Xiaomin, S.; Liang, L.; Genwei, Z.; Ronghua, J.; Tanyu, C.; Guohua, L. *Chem. Asian J.* **2016**, *11*, 2072.

216. Adam, W.; Rao, P. B.; Degen, H.-G.; Levai, A.; Patonay, T.; Saha-Möller, C. R. *J. Org. Chem* **2002**, *67*, 259.

217. Kawai, H.; Okusu, S.; Yuan, Z.; Tokunaga, E.; Yamano, A.; Shiro, M.; Shibata, N. *Angew. Chem. Int. Ed.* **2013**, *52*, 2221.

218. Wu, S.; Pan, D.; Cao, C.; Wang, Q.; Chen, F.-X. *Adv. Synth. Catal.* **2013**, *355*, 1917.

219. Lu, S.-M.; Bolm, C. *Chem. Eur. J.* **2008**, *14*, 7513.

220. Yan, Q.; Kong, D.; Zhao, W.; Zi, G.; Hou, G. *J. Org. Chem*. **2016**, *81*, 2070.

221. Liu, L.; Du, L.; Zhang-Negrerie, D.; Du, Y.; Zhao, K. *Org. Lett.* **2014**, *16*, 5772.

222. Saito, Y.; Ouchi, H.; Takahata, H. *Tetrahedron* **2008**, *64*, 11129.

223. Bigi, M. A.; Liu, P.; Zou, L.; Houk, K. N.; White, M. C. *Synlett* **2012**, *23*, 2768.

224. Cusso, O.; Ribas, X.; Costas, M. *Chem. Commun.* **2015**, *51*, 14285.

225. Jacobsen, E. N.; Deng, L.; Furukawa, Y.; Martínez, L. E. *Tetrahedron* **1994**, *50*, 4323.

226. Pigott, A. J.; Lepage, R. J.; White, J. M.; Coster, M. J. *Tetrahedron Lett.* **2014**, *55*, 6864.

227. G., G. J. *Polym. Sci., Part A: Polym. Chem.* **1991**, *29*, 1223.

228. Szewczyk, M.; Bezłada, A.; Mlynarski, J. *ChemCatChem* **2016**, *8*, 3575.

229. Metternich, J. B.; Gilmour, R. *J. Am. Chem. Soc.* **2015**, *137*, 11254.

230. Tsuchiya, Y.; Hamashima, Y.; Sodeoka, M. *Org. Lett.* **2006**, *8*, 4851.

231. Nishikawa, K.; Fukuda, H.; Abe, M.; Nakanishi, K.; Tazawa, Y.; Yamaguchi, C.; Hiradate, S.; Fujii, Y.; Okuda, K.; Shindo, M. *Phytochemistry* **2013**, *96*, 223.

232. Bush, A. G.; Jiang, J. L.; Payne, P. R.; Ogilvie, W. W. *Tetrahedron* **2009**, *65*, 8502.

233. Bernasconi, M.; Ramella, V.; Tosatti, P.; Pfaltz, A. *Chem. Eur. J.* **2014**, *20*, 2440.

234. Comito, R. J.; Finelli, F. G.; MacMillan, D. W. C. *J. Am. Chem. Soc.* **2013**, *135*, 9358.

235. Lempenauer, L.; Duñach, E.; Lemière, G. *Chem. Eur. J.* **2017**, *23*, 10285.

236. Hennum, M.; Odden, H. H.; Gundersen, L.-L. *Eur. J. Org. Chem* **2017**, 846.

237. Metternich, J. B.; Gilmour, R. *J. Am. Chem. Soc.* **2016**, *138*, 1040.

238. Gao, P.; Guo, W.; Xue, J.; Zhao, Y.; Yuan, Y.; Xia, Y.; Shi, Z. *J. Am. Chem. Soc.* **2015**, *137*, 12231.

239. Liu, R.; Yang, Z.; Ni, Y.; Song, K.; Shen, K.; Lin, S.; Pan, Q. *J. Org. Chem* **2017**, *82*, 8023.

240. Wang, D.; Wang, Y.; Zhao, J.; Shen, M.; Hu, J.; Liu, Z.; Li, L.; Xue, F.; Yu, P. *Org. Lett.* **2017**, *19*, 984.

241. Rudler, H.; Comte, V.; Garrier, E.; Bellassoued, M.; Chelain, E.; Vaissermann, J. *J. Organomet. Chem.* **2001**, *621*, 284.

242. Kitanosono, T.; Xu, P.; Kobayashi, S. *Chem. Asian J.* **2014**, *9*, 179.

243. Chen, Y.; Turlik, A.; Newhouse, T. R. *J. Am. Chem. Soc.* **2016**, *138*, 1166.

244. Mikhalyova, E. A.; Makhlynets, O. V.; Palluccio, T. D.; Filatov, A. S.; Rybak-Akimova, E. V. *Chem. Commun.* **2012**, *48*, 687.

245. Herrmann, W. A.; Baskakov, D.; Herdtweck, E.; Hoffmann, S. D.; Bunlaksananusorn, T.; Rampf, F.; Rodefeld, L. *Organometallics* **2006**, *25*, 2449.

246. Denmark, S. E.; Fu, J.; Lawler, M. J. *J. Org. Chem* **2006**, *71*, 1523.

247. Ryu, J. Y.; Kim, J.; Costas, M.; Chen, K.; Nam, W.; Que Jr., L. *Chem. Commun.* **2002**, *12*, 1288.

248. Mas-Balleste, R.; Que, L., Jr. *J. Am. Chem. Soc.* **2007**, *129*, 15964.

249. Milan, M.; Bietti, M.; Costas, M. *Org. Lett.* **2018**, *20*, 2720.

250. Costas, M.; Chen, K.; Que, L., Jr. *Coord. Chem. Rev.* **2000**, *200-202*, 517.

251. Kille, S.; Zilly, F. E.; Acevedo, J. P.; Reetz, M. T. *Nat. Chem.* **2011**, *3*, 738.

252. Salvador, J. A. R.; Silvestre, S. M.; Moreira, V. M. *Curr. Org. Chem.* **2012**, *16*, 1243.

253. Zhang, Y. Y.; Yang, L. *Expert. Opin. Drug Metab. Toxicol.* **2009**, *5*, 621.

254. Monostory, K.; Dvorak, Z. *Curr. Drug Metab.* **2011**, *12*, 154.

255. Chen, J.; Lutz, M.; Milan, M.; Costas, M.; Otte, M.; Klein Gebbink, R. J. M. *Adv. Synth. Catal.* **2017**, *359*, 2590.

Annex

Annex chapter III

^{1}H and ^{13}C-NMR spectra of ligands

^{1}H-NMR of **L1** in $CDCl_3$

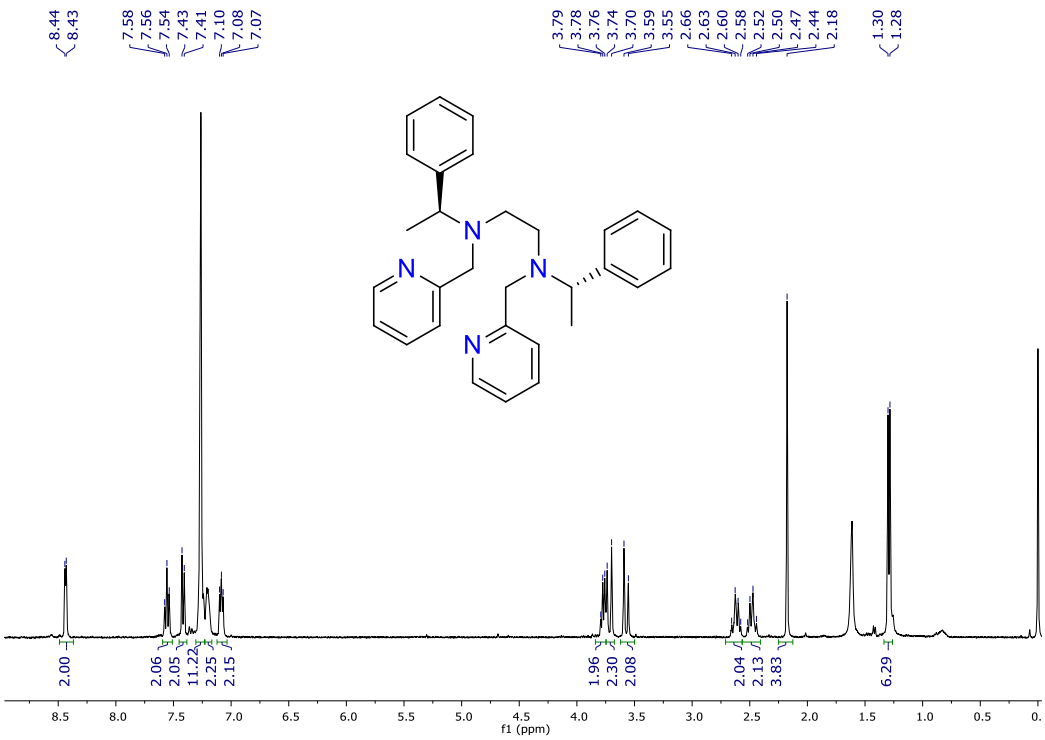

^{13}C-NMR of **L1** in $CDCl_3$

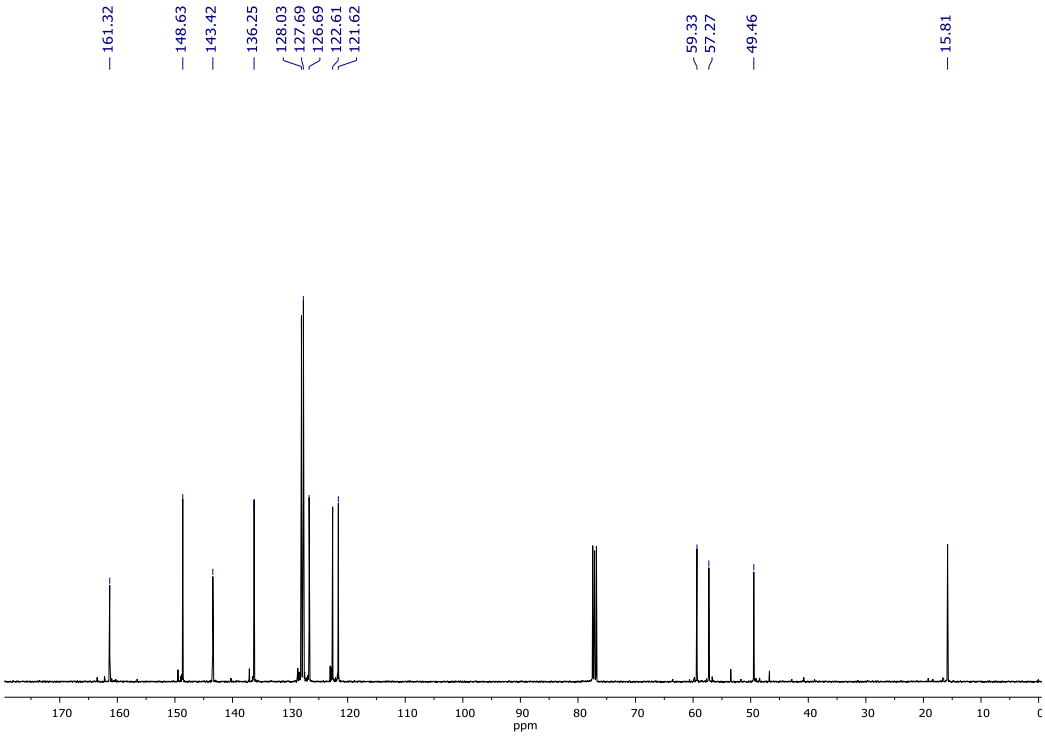

^{1}H-NMR of **L2** in $CDCl_3$

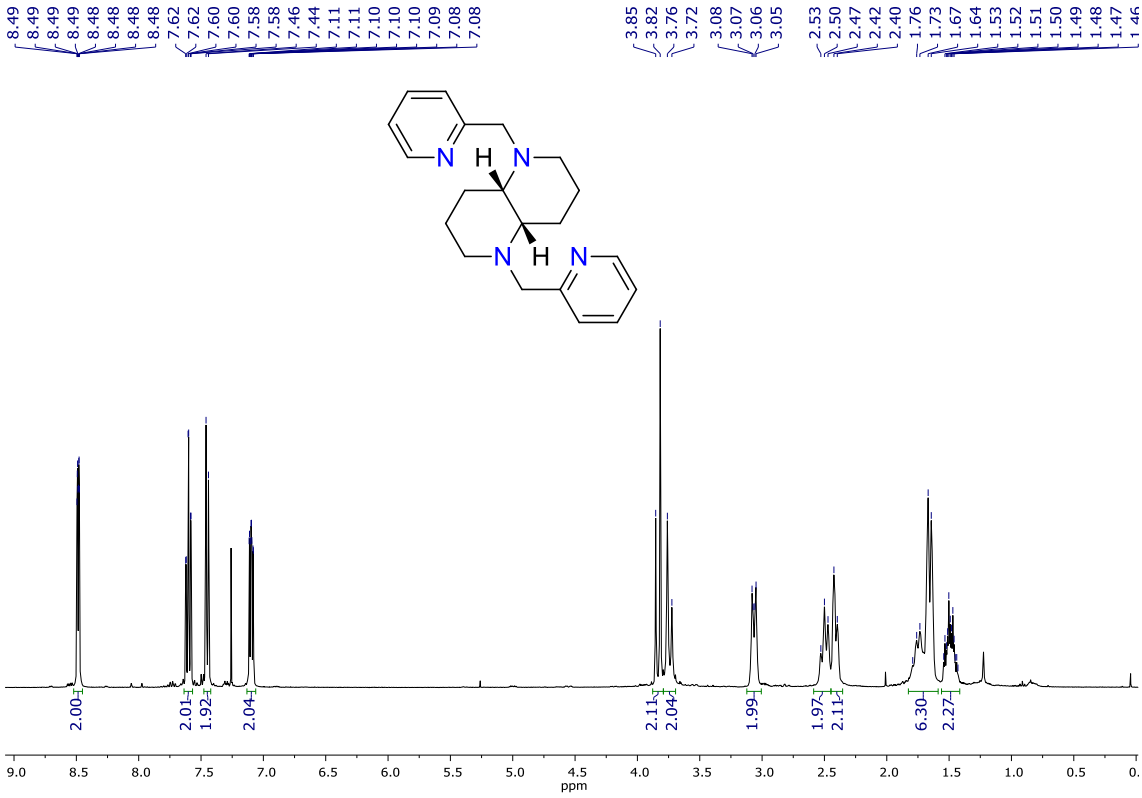

^{13}C-NMR of **L2** in $CDCl_3$

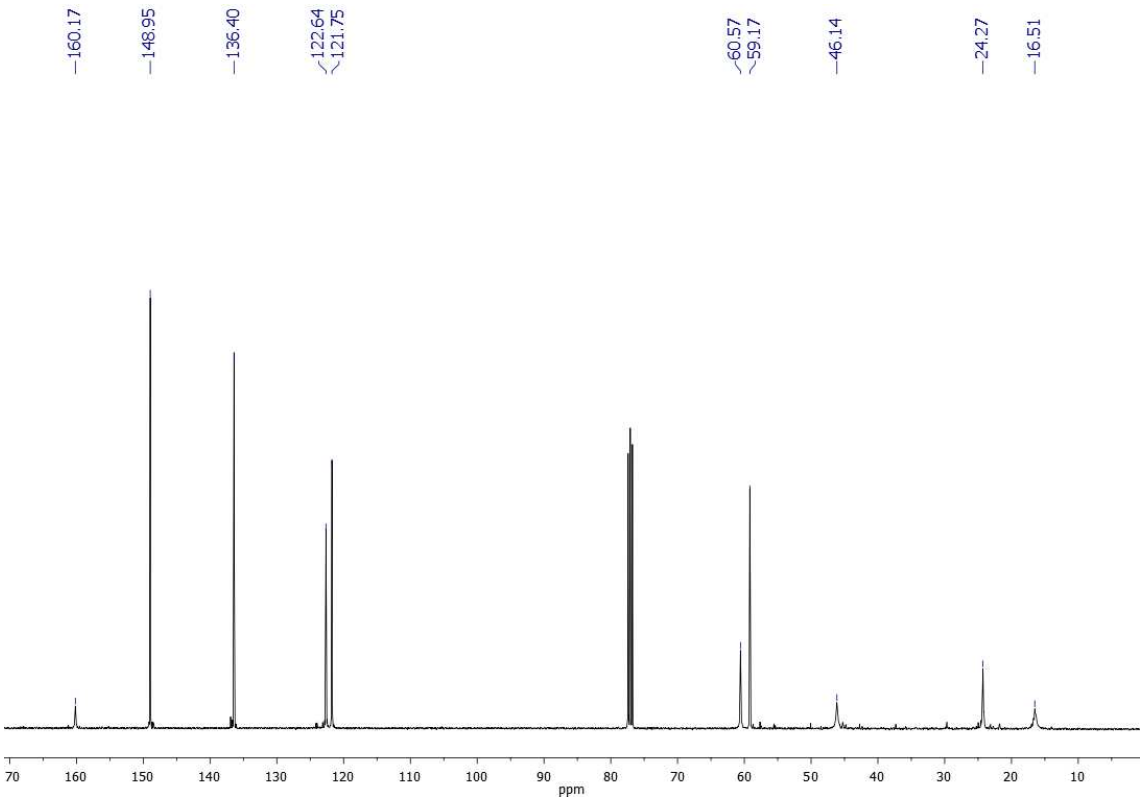

Annex chapter IV

^{1}H and ^{13}C-NMR spectra of ligands

^{1}H-NMR of **L3** in $CDCl_3$

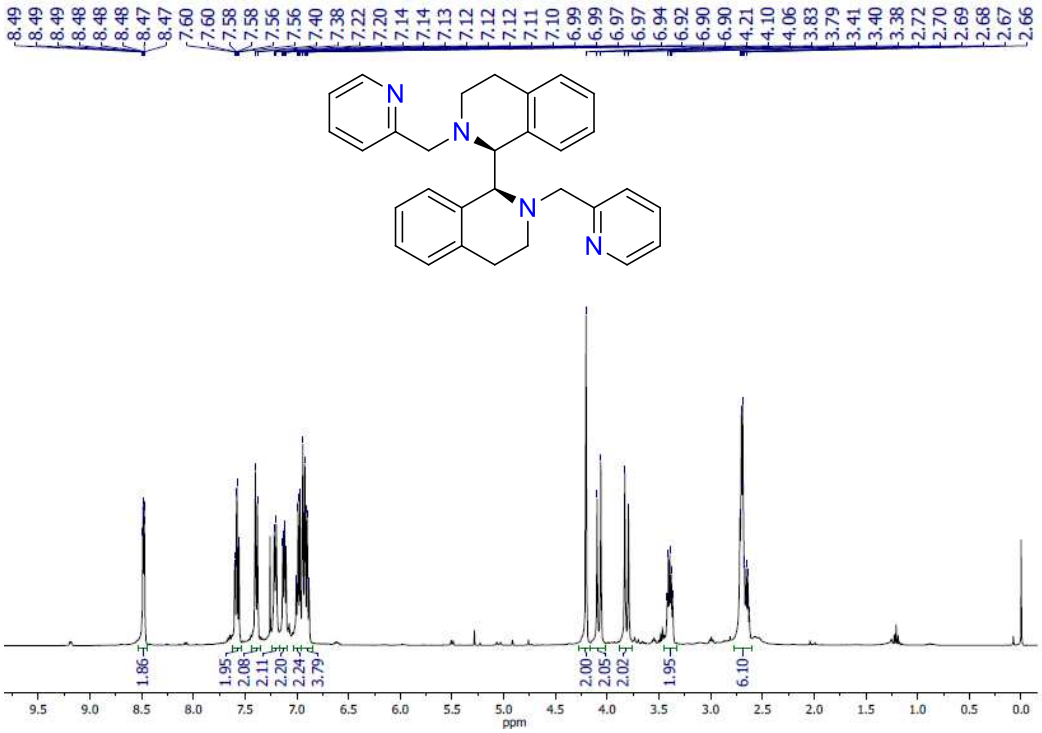

^{13}C-NMR of **L3** in $CDCl_3$

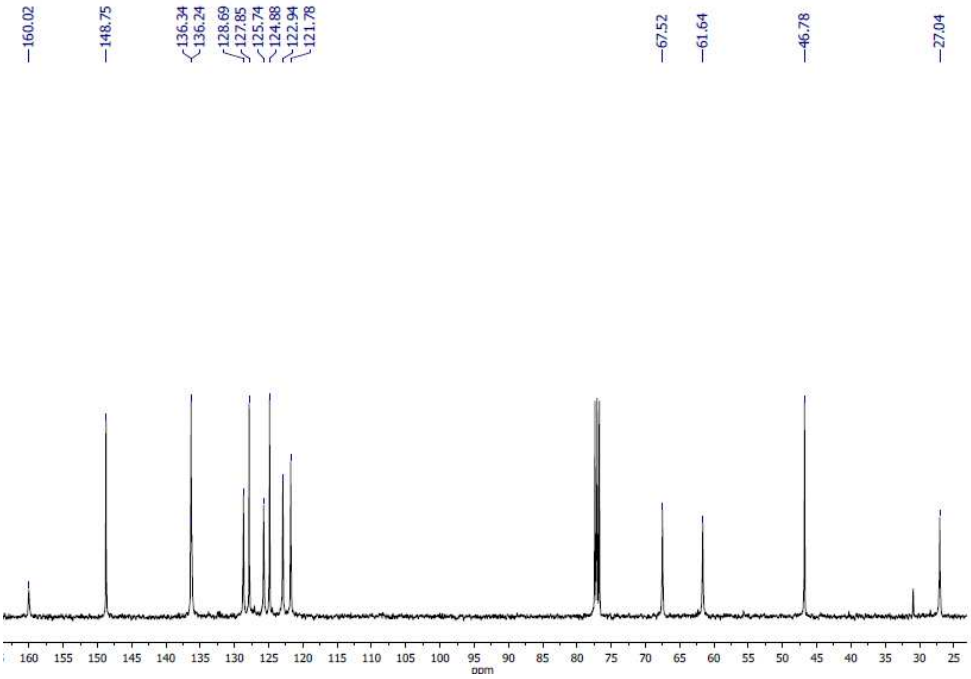

^{1}H-NMR of **L4** in $CDCl_3$

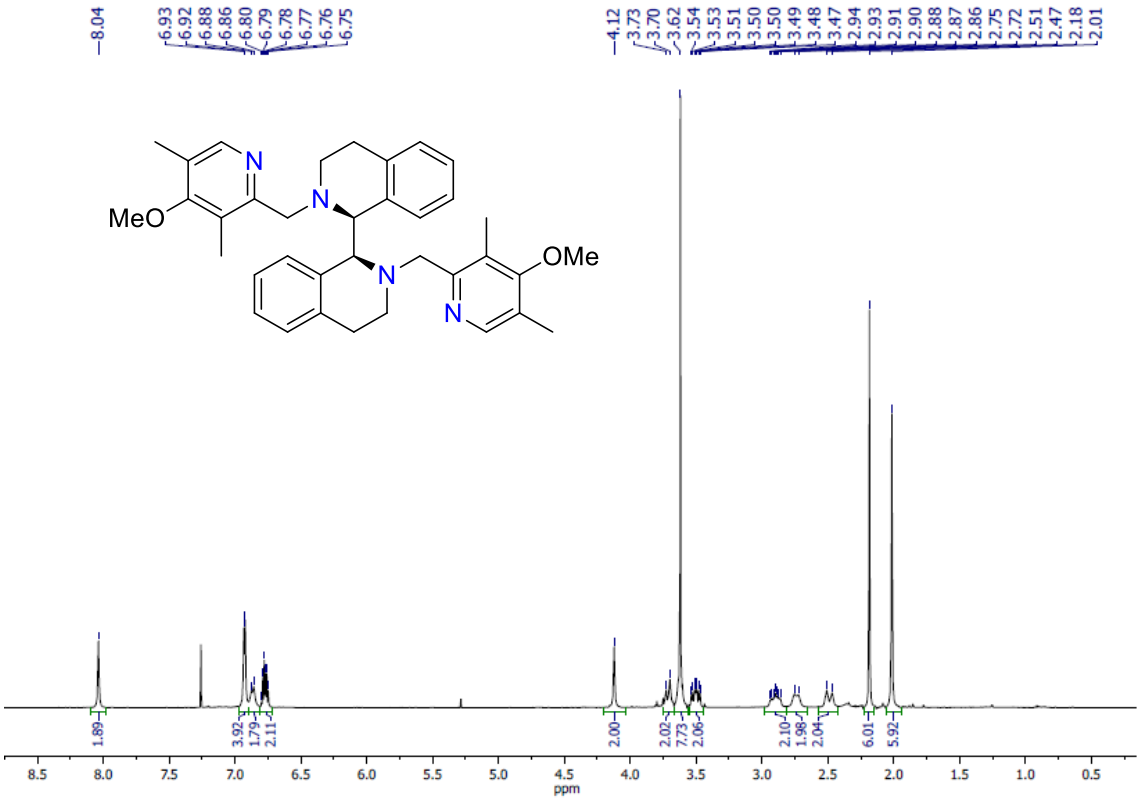

^{13}C-NMR of **L4** in $CDCl_3$

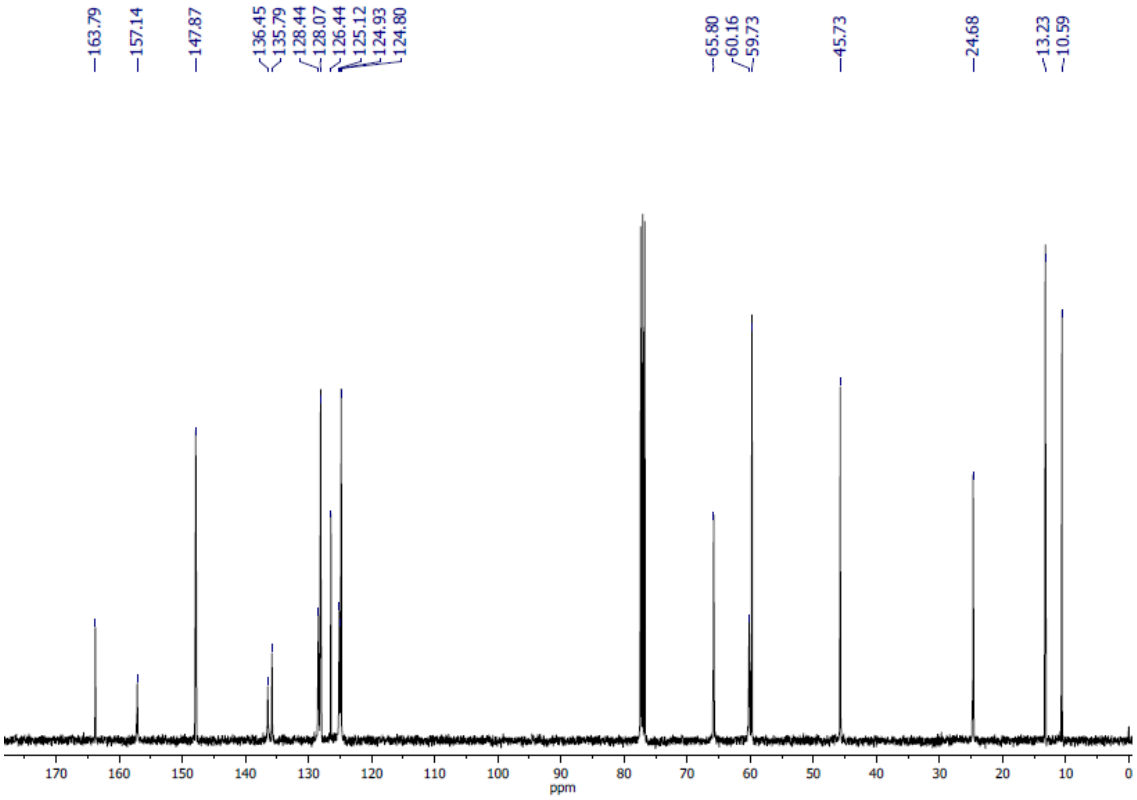

^{1}H-NMR of **L5** in $CDCl_3$

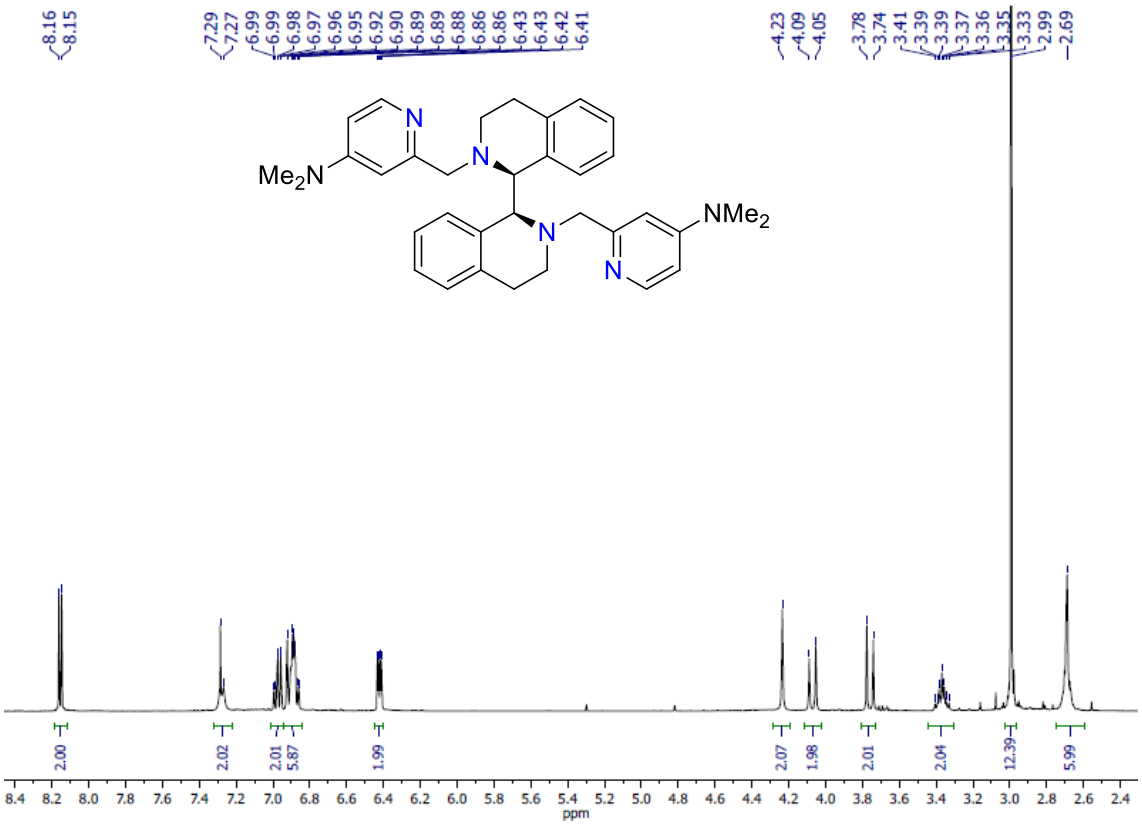

^{13}C-NMR of **L5** in $CDCl_3$

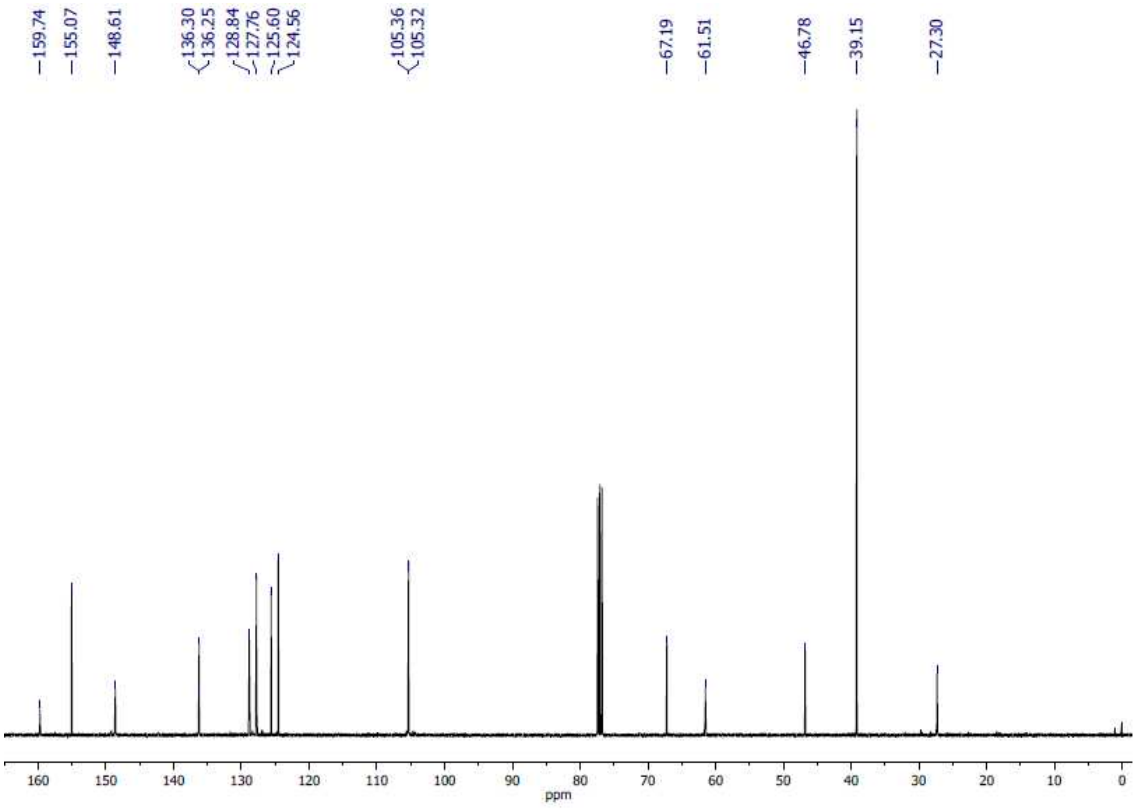

^{1}H-NMR of **L6** in $CDCl_3$

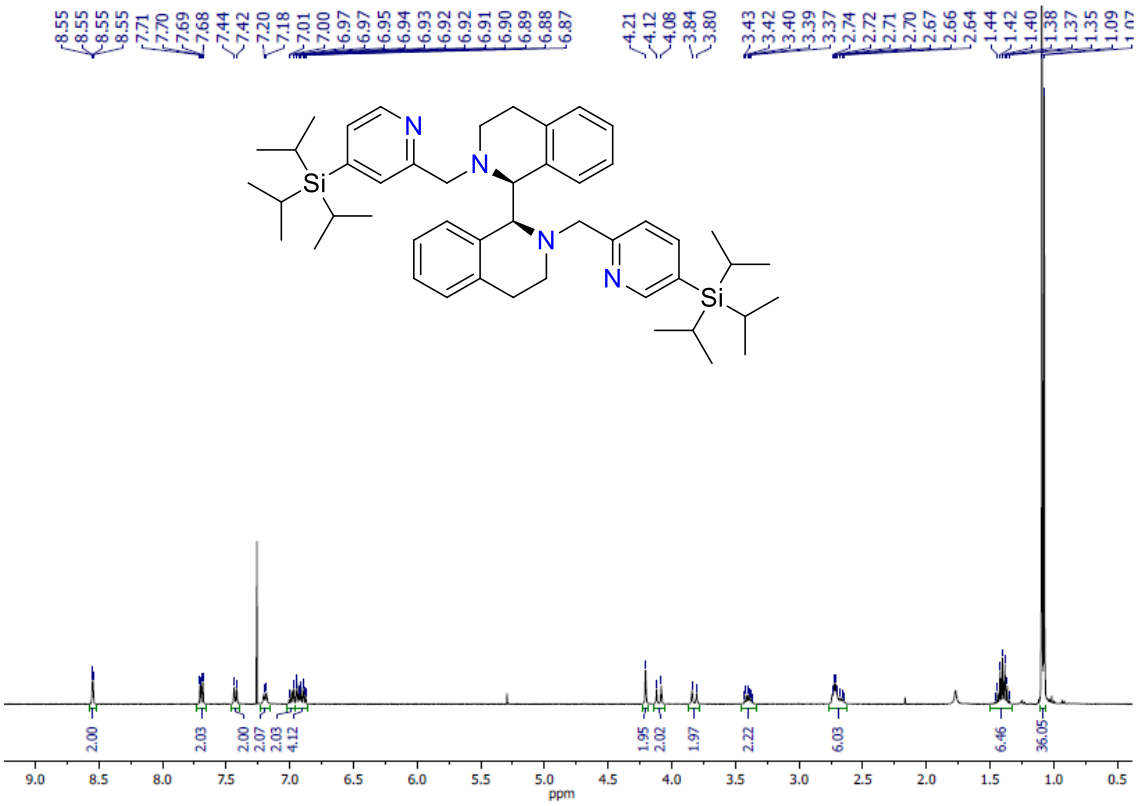

^{13}C-NMR of **L6** in $CDCl_3$

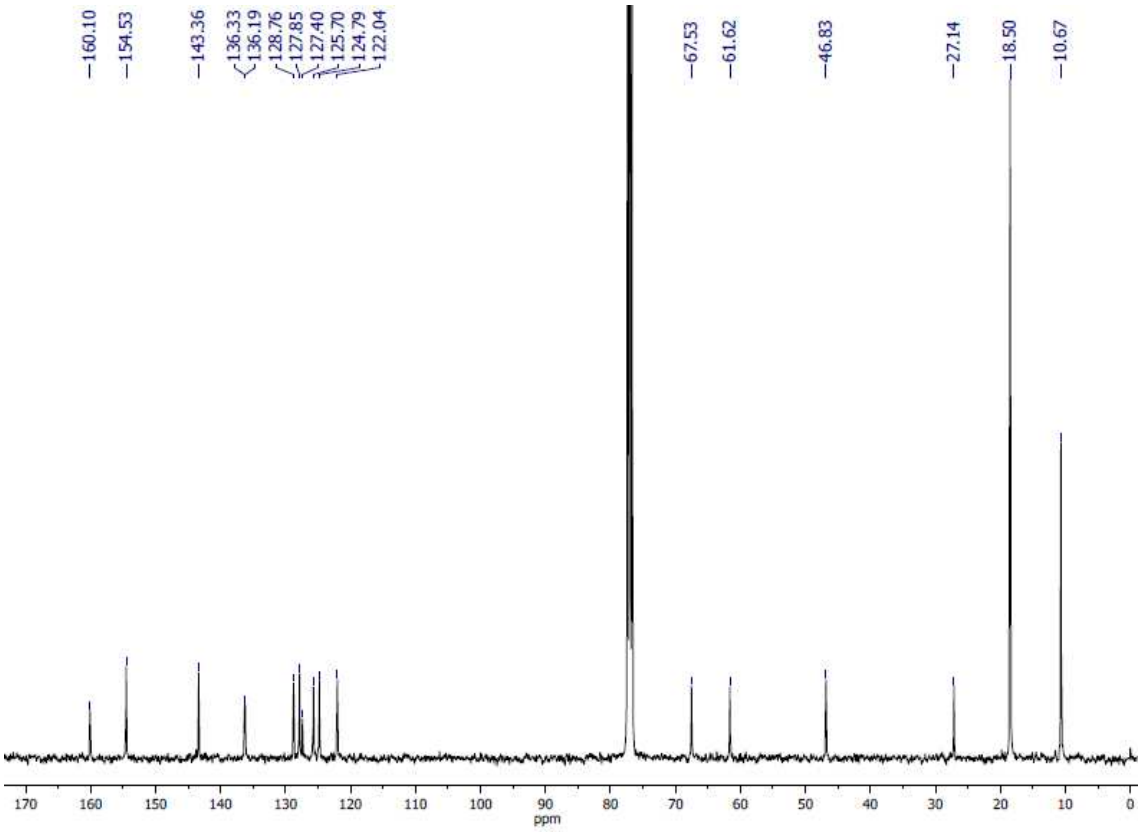

^{1}H-NMR of **L7** in $CDCl_3$

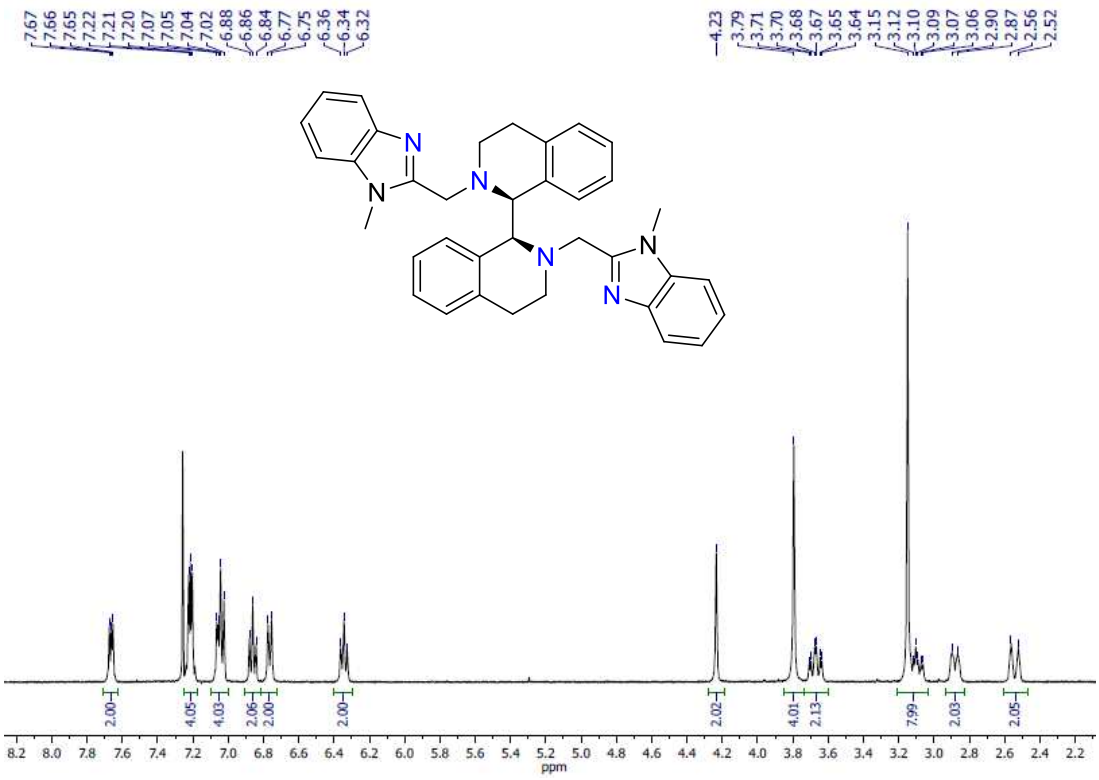

^{13}C-NMR of **L7** in $CDCl_3$

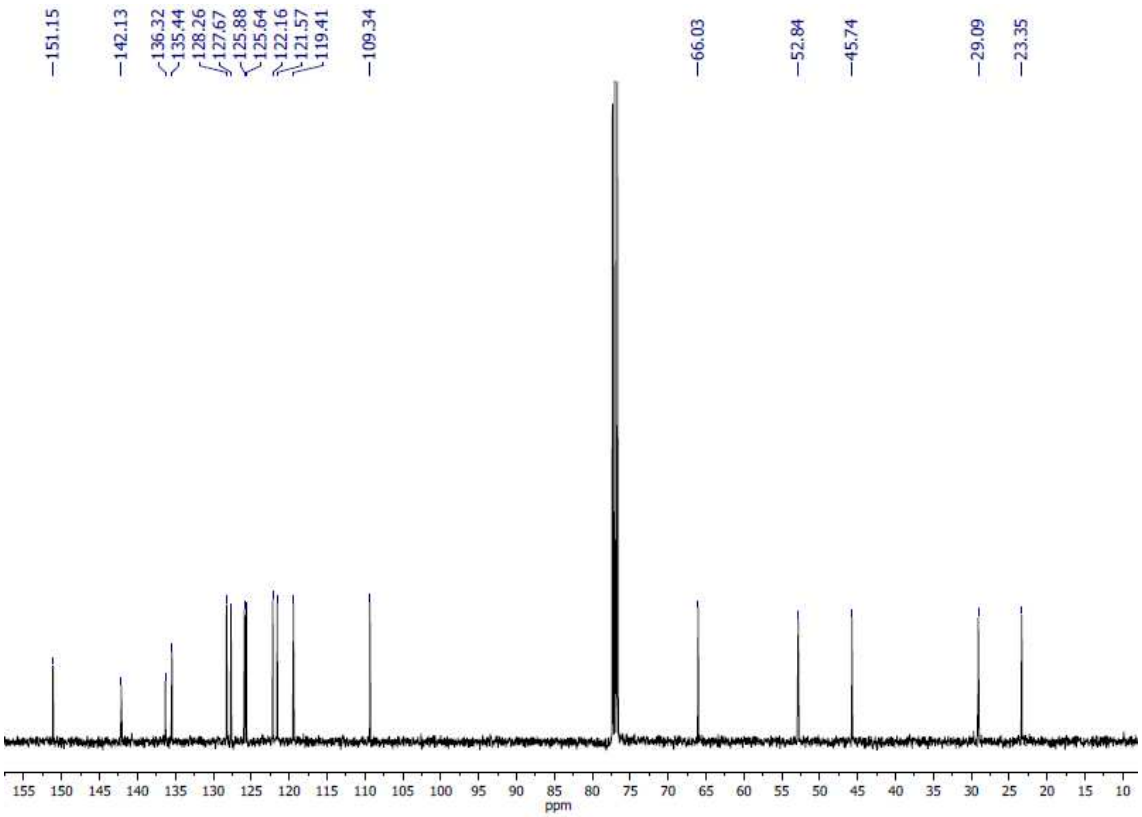

Paramagnetic ^{1}H-NMR spectra of Fe(II) complexes

^{1}H-NMR of **C6** in CD_2Cl_2

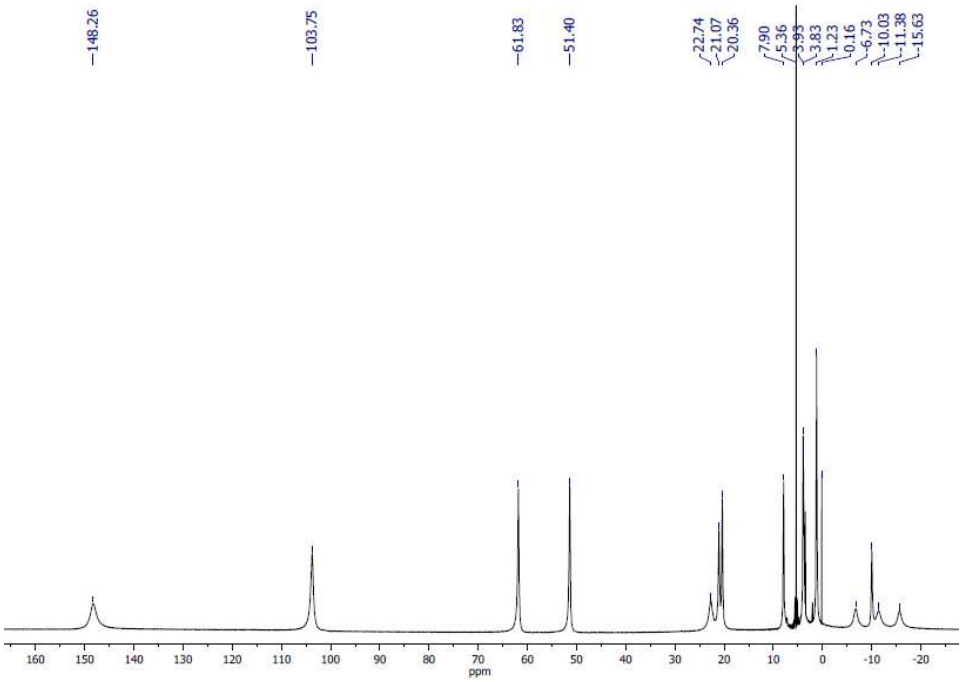

^{1}H-NMR of **C6** in acetone-d6

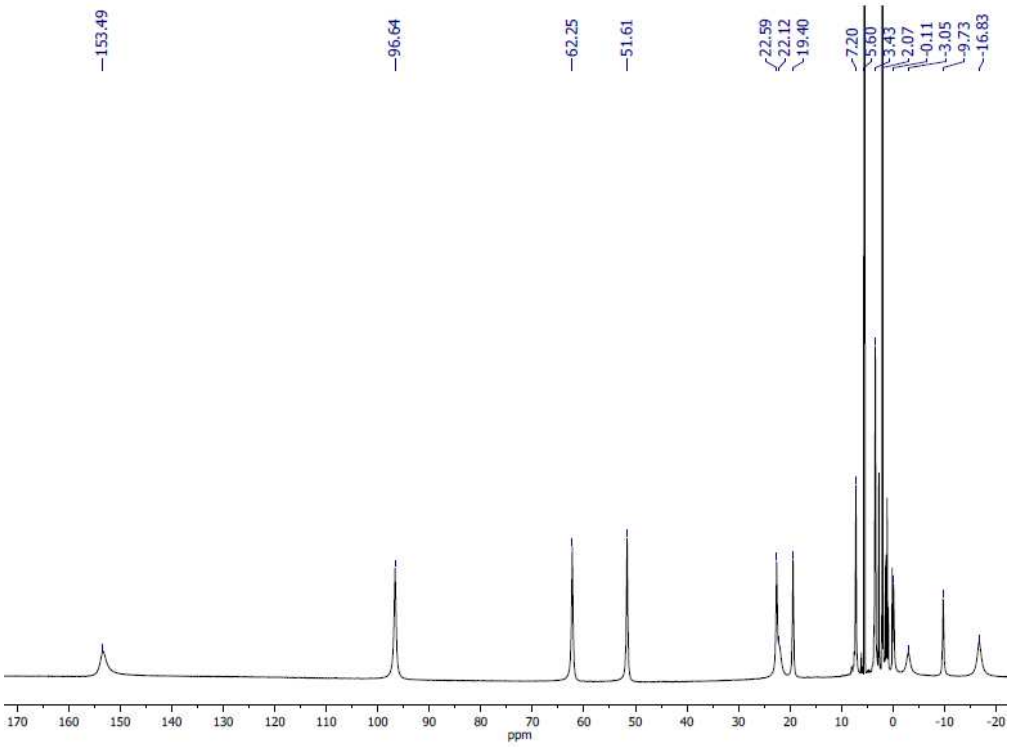

^{1}H-NMR of **C6** in CD_3CN

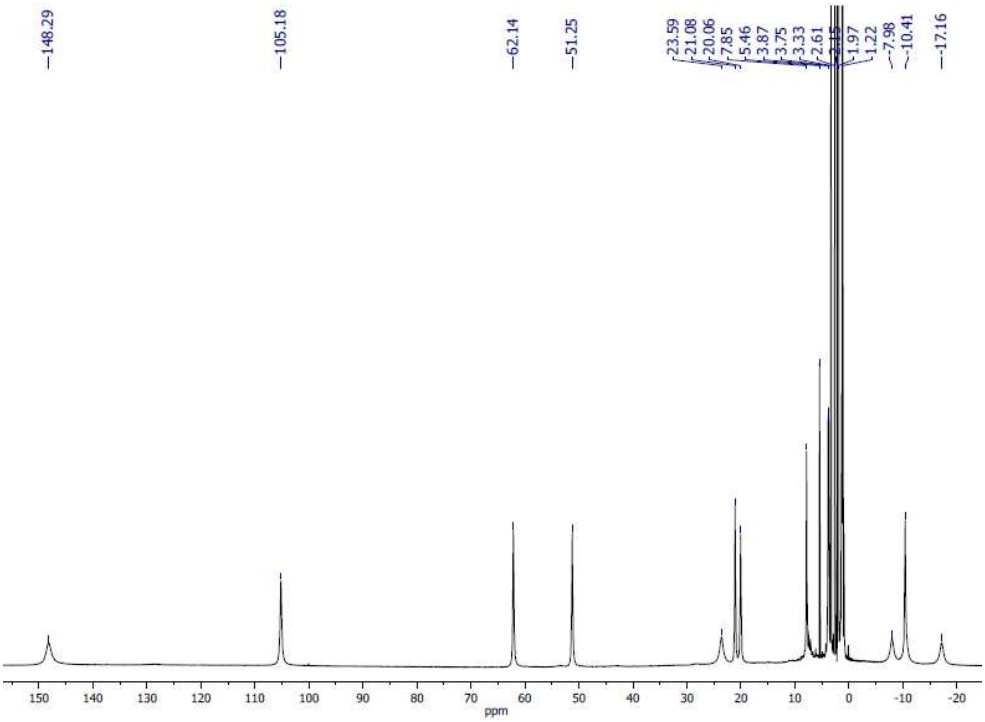

^{1}H-NMR of **C7** in CD_2Cl_2

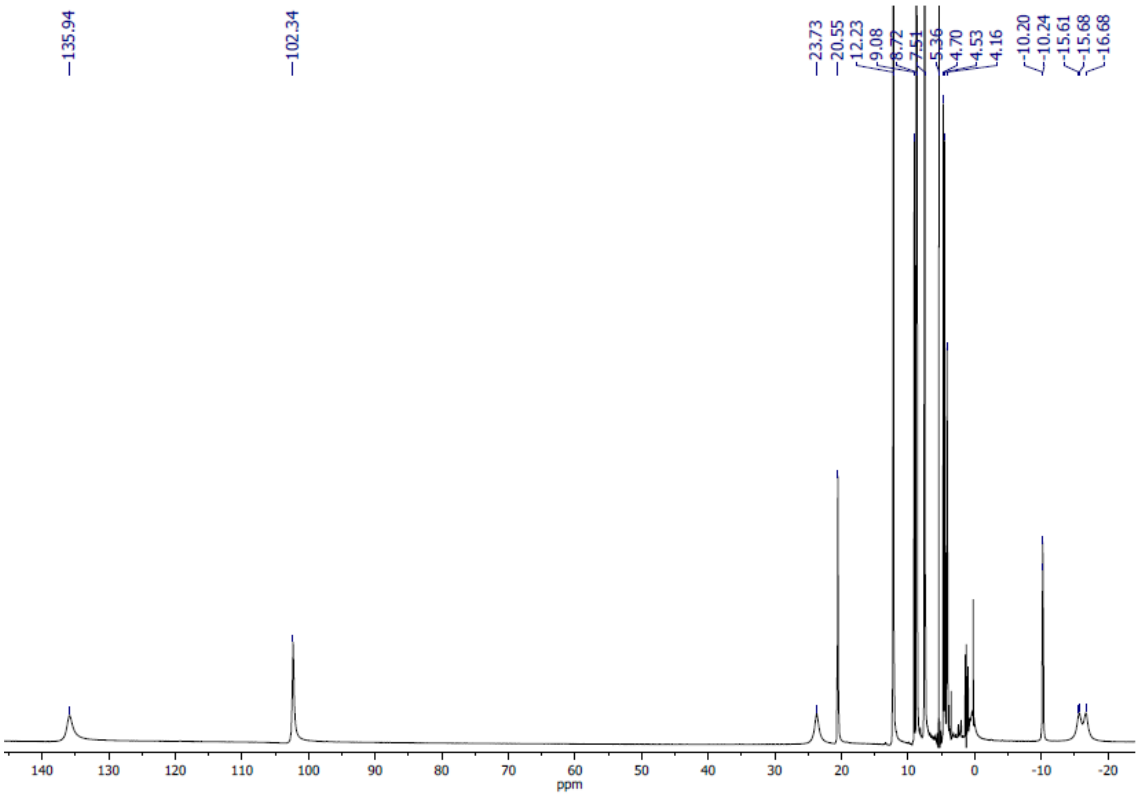

^{1}H-NMR of **C7** in acetone-d6

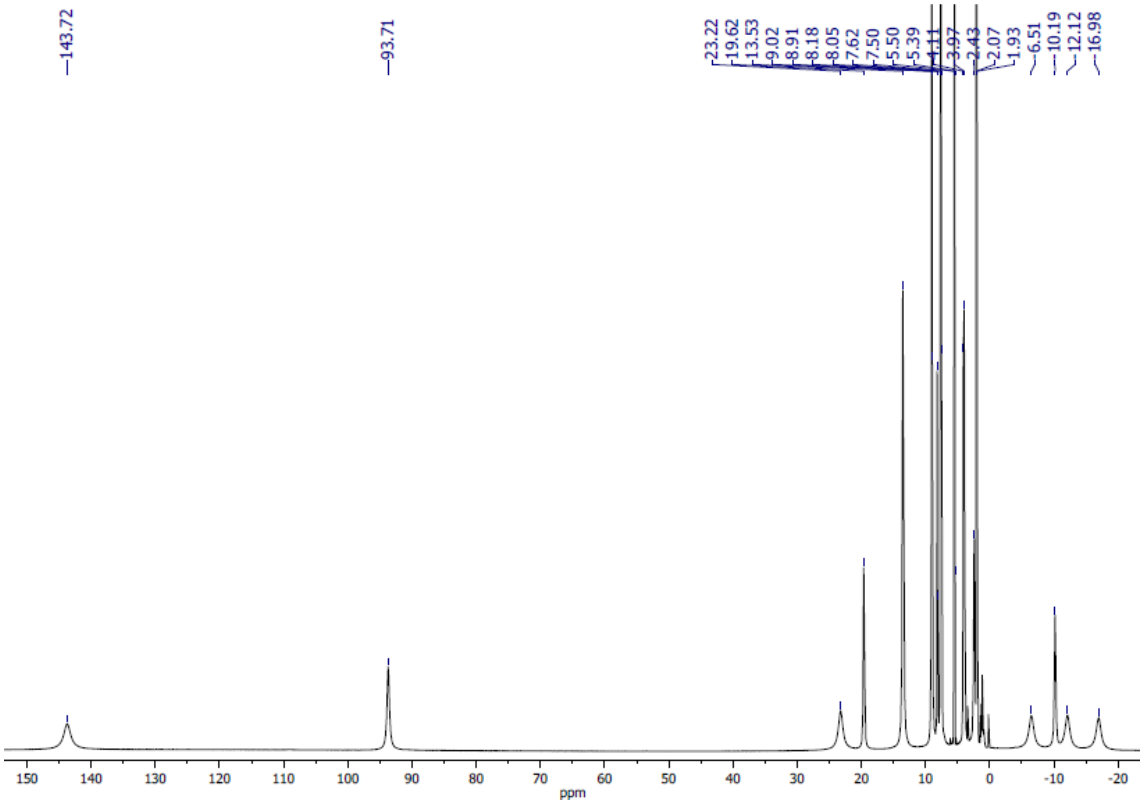

^{1}H-NMR of **C7** in CD_3CN

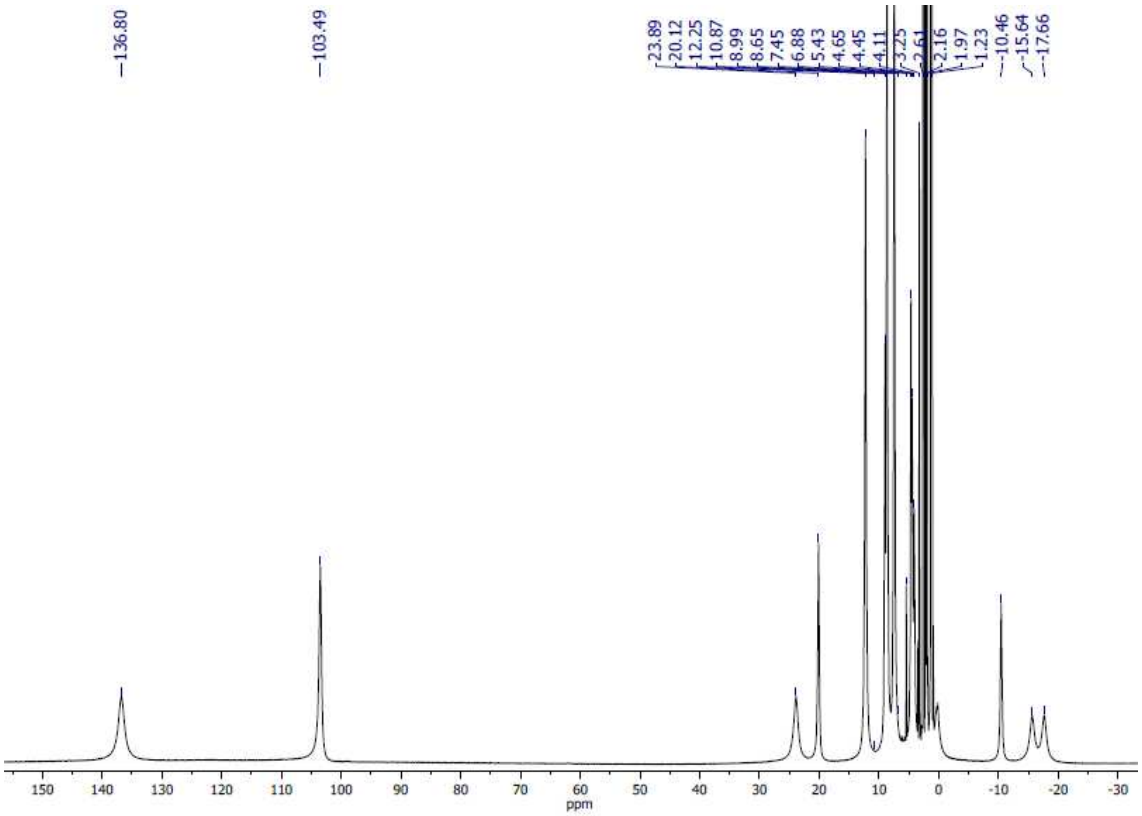

^{1}H-NMR of **C8** in CD_2Cl_2

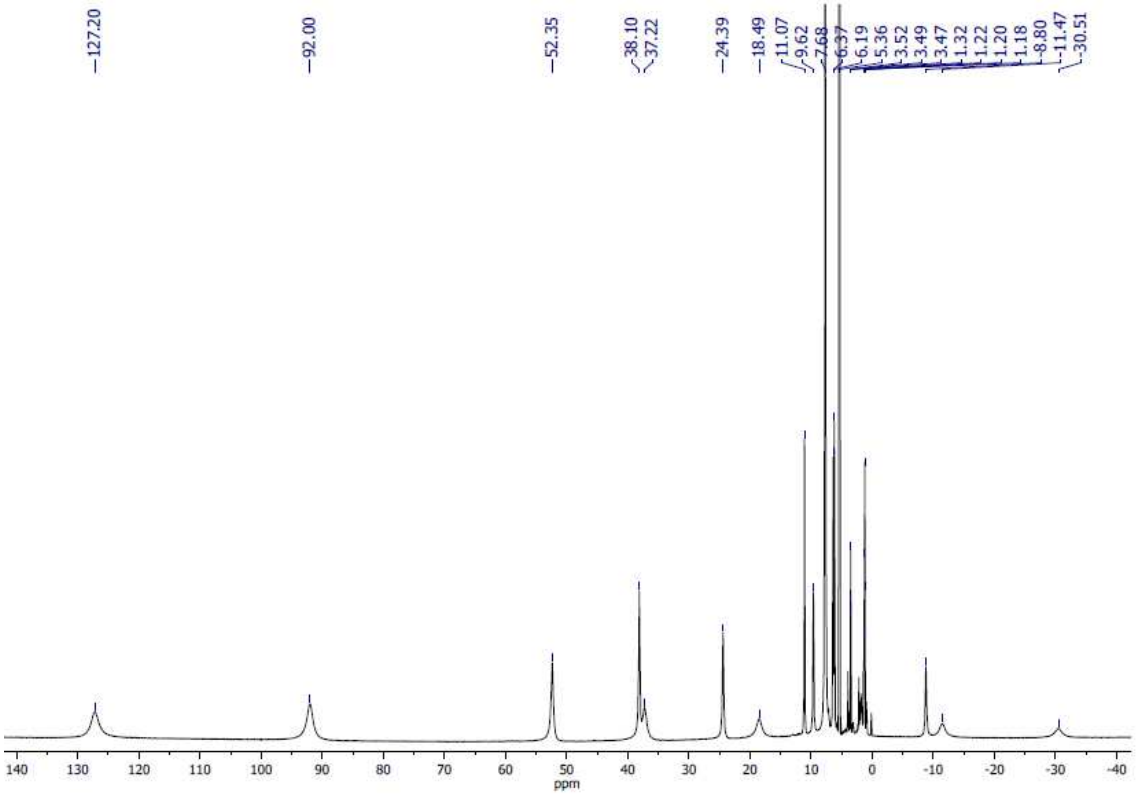

^{1}H-NMR of **C8** in acetone-d6

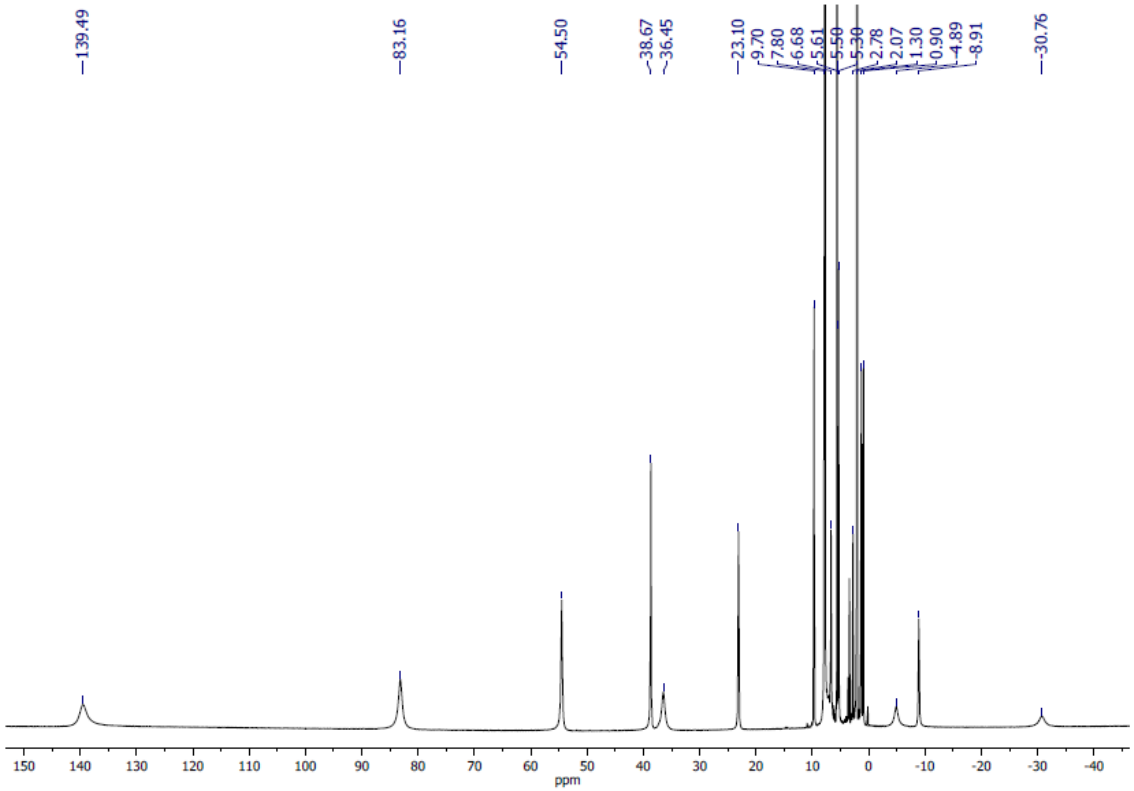

^{1}H-NMR of **C8** in CD_3CN

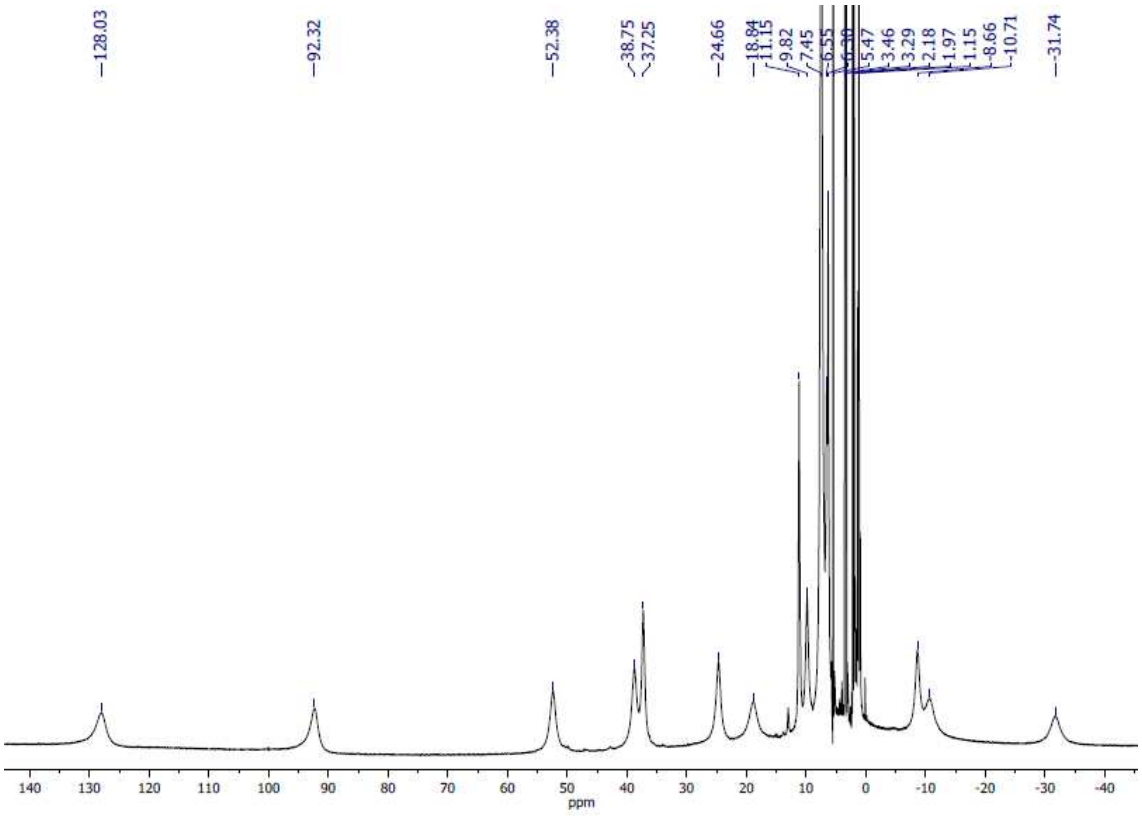

^{1}H-NMR of **C9** in CD_2Cl_2

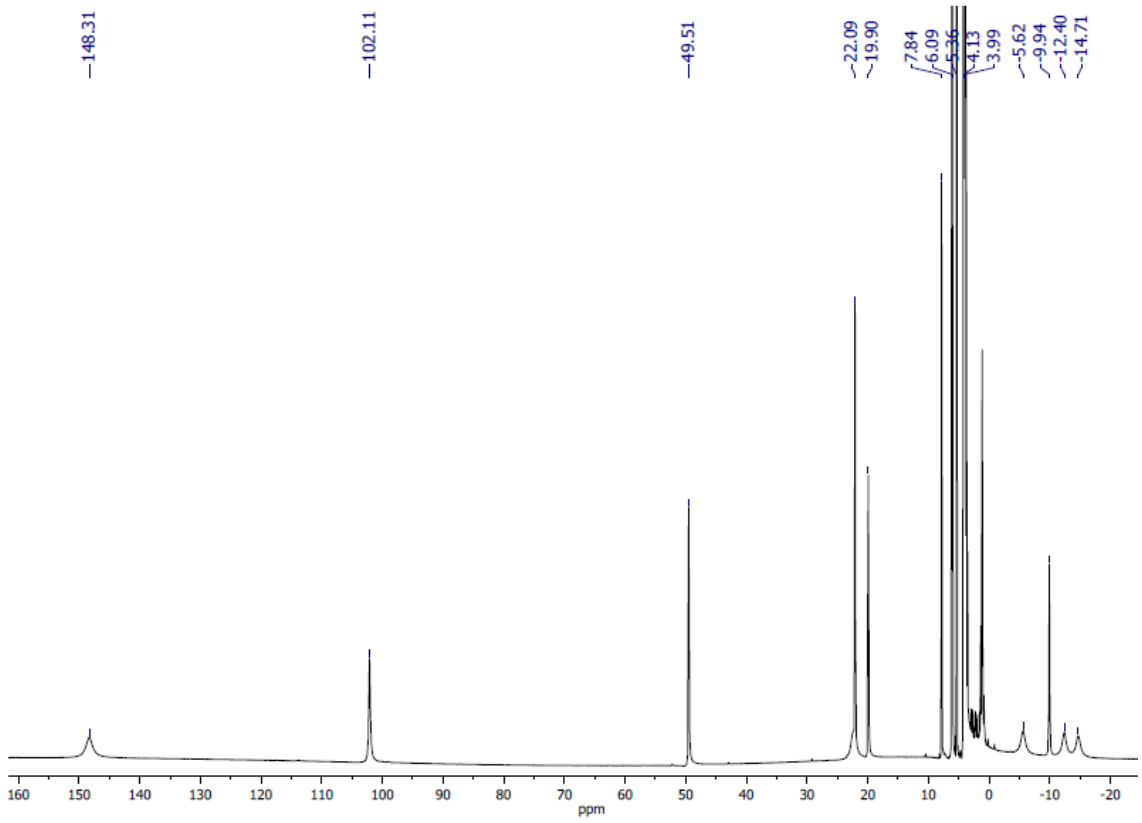

^{1}H-NMR of **C9** in acetone-d6

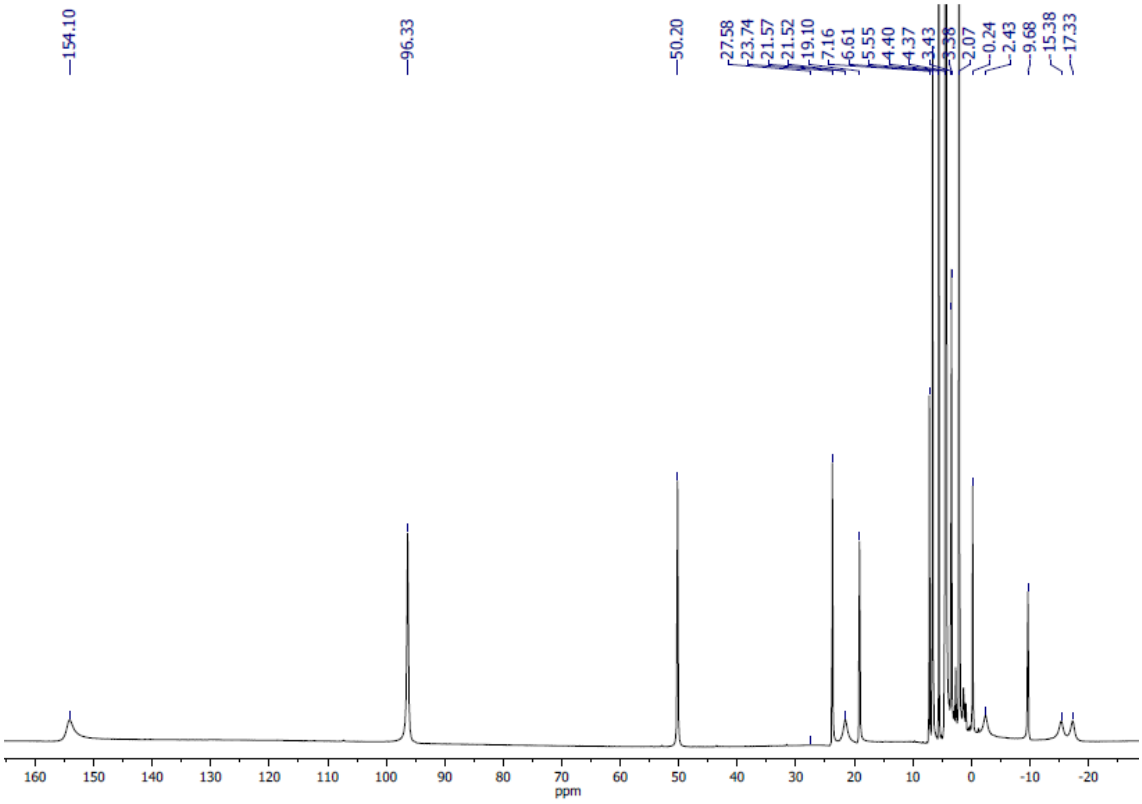

^{1}H-NMR of **C9** in CD_3CN

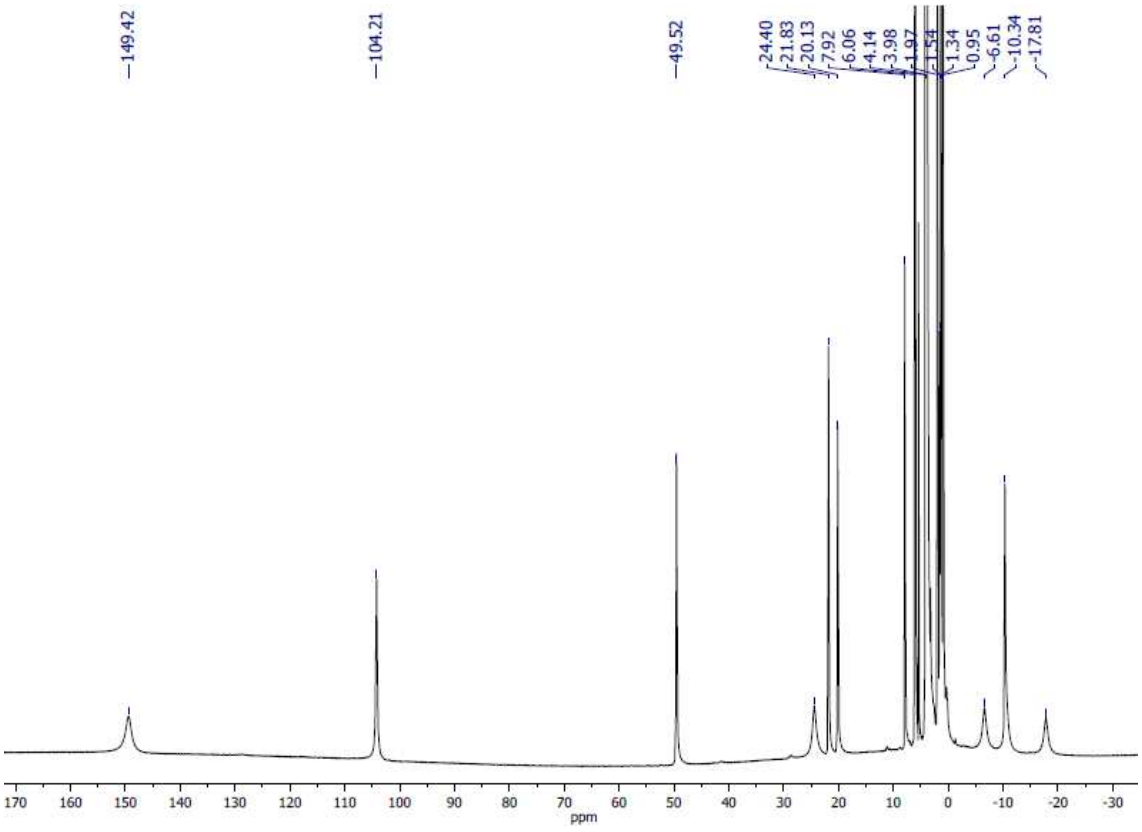

^{1}H-NMR of **C10** in CD_2Cl_2

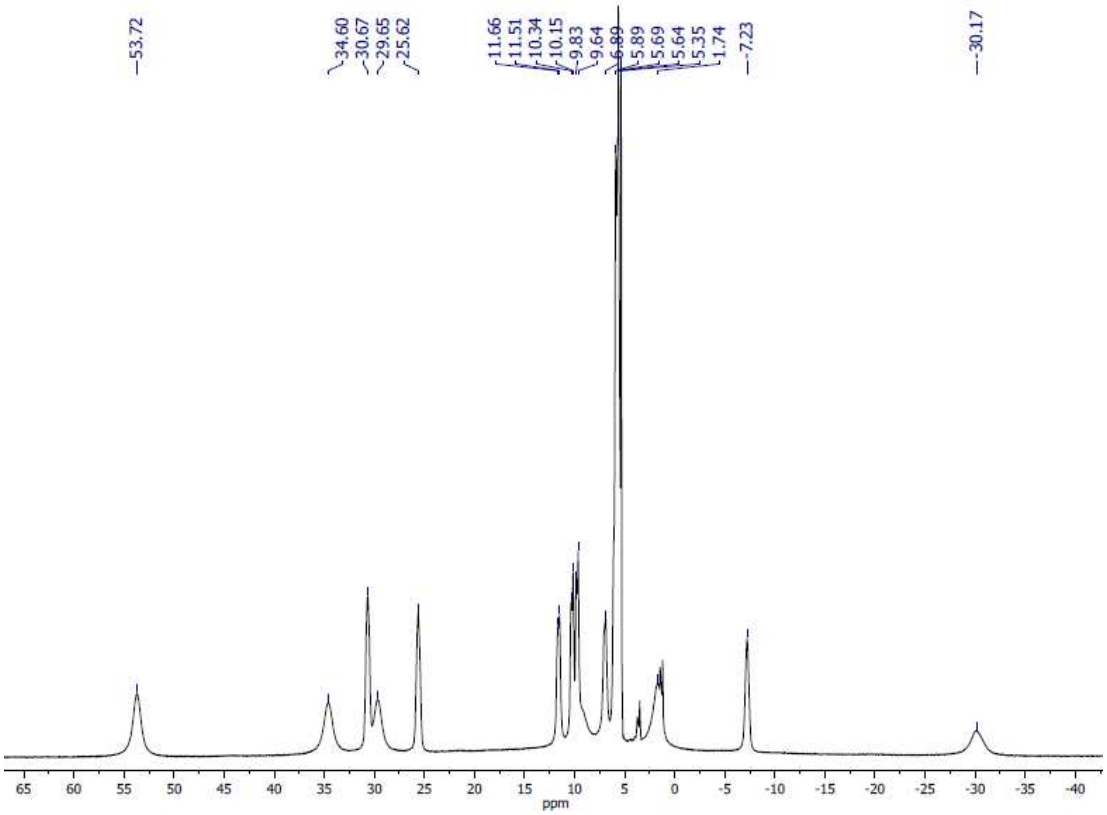

^{1}H-NMR of **C10** in acetone-d6

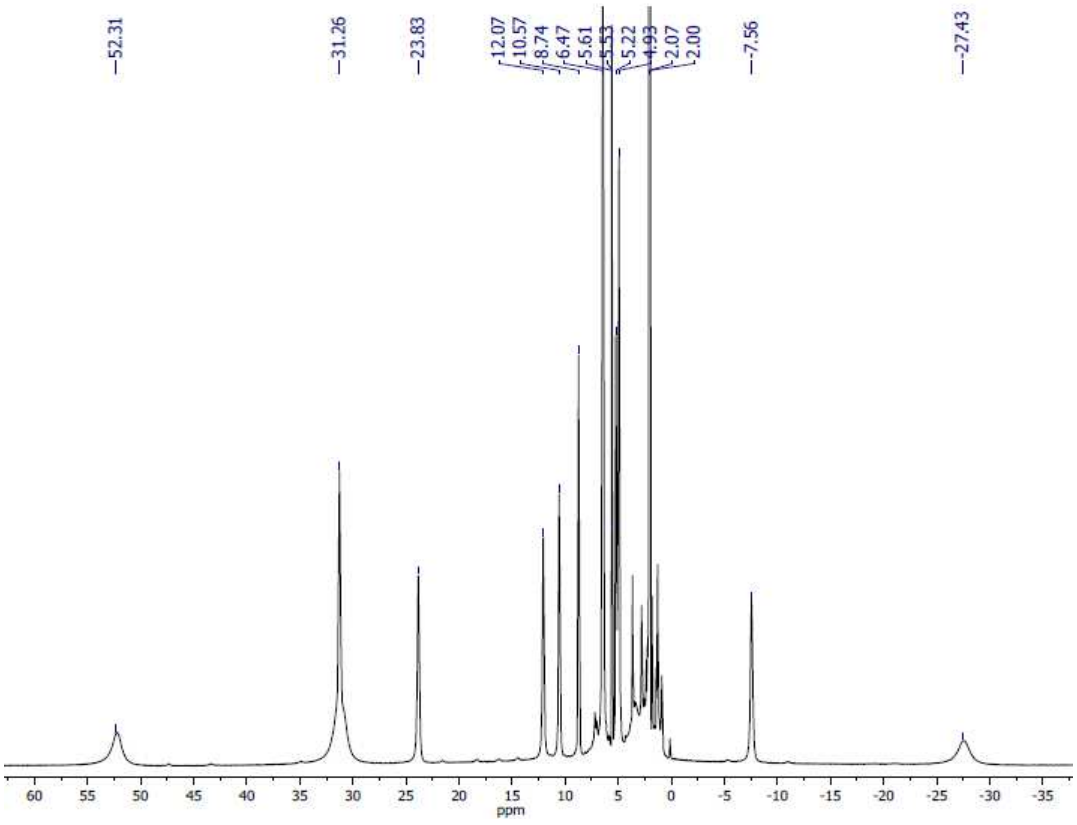

^{1}H-NMR of **C10** in CD_3CN

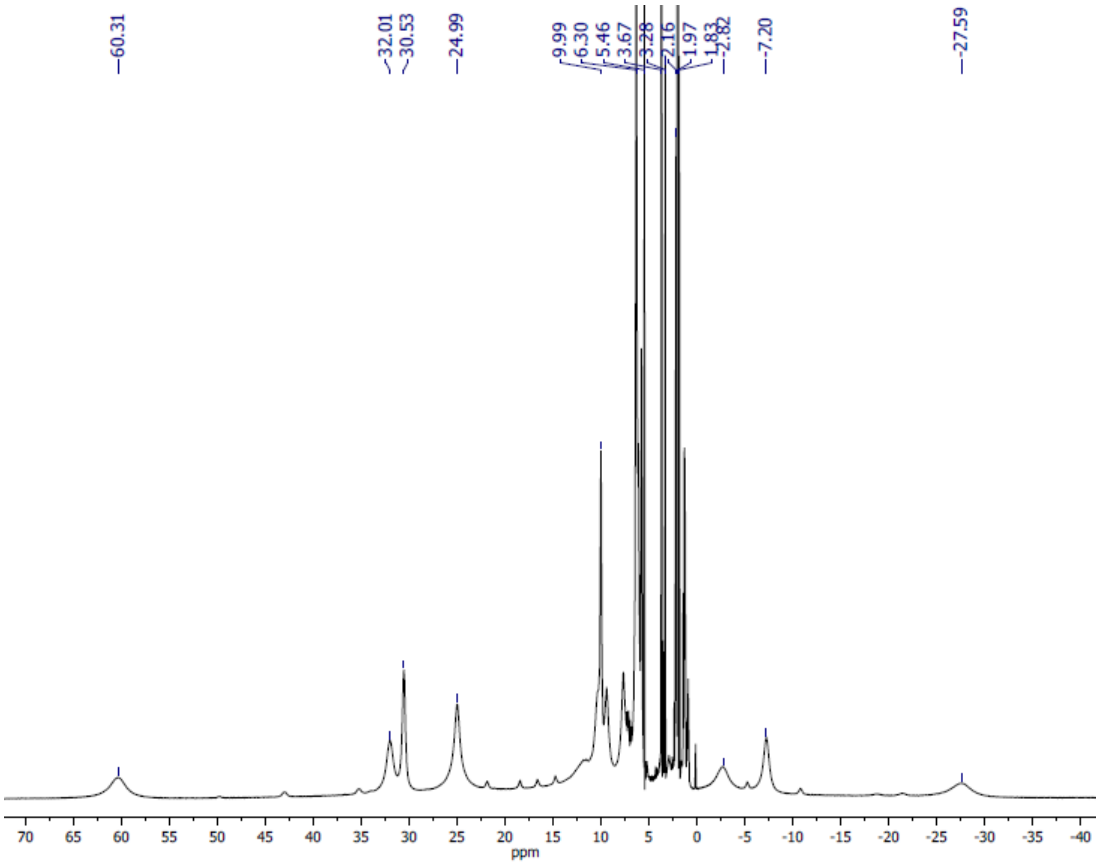

^{1}H-NMR of **C11** in CD_2Cl_2

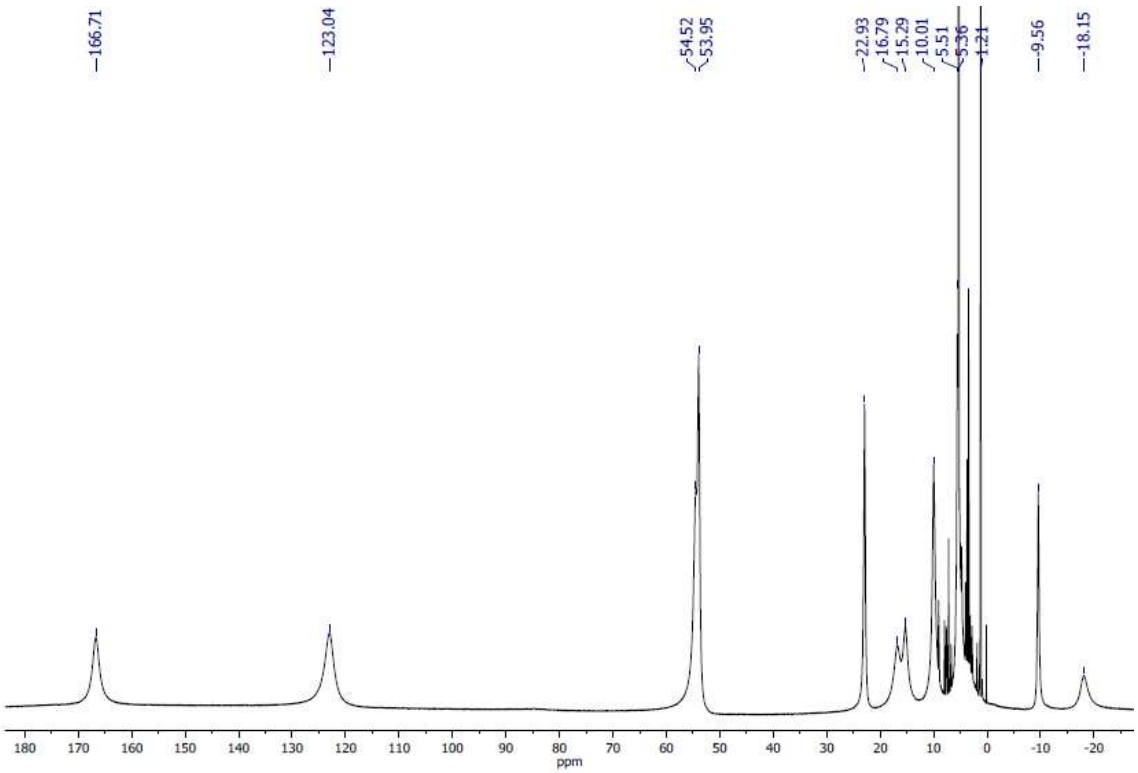

^{1}H-NMR of **C11** in acetone-d6

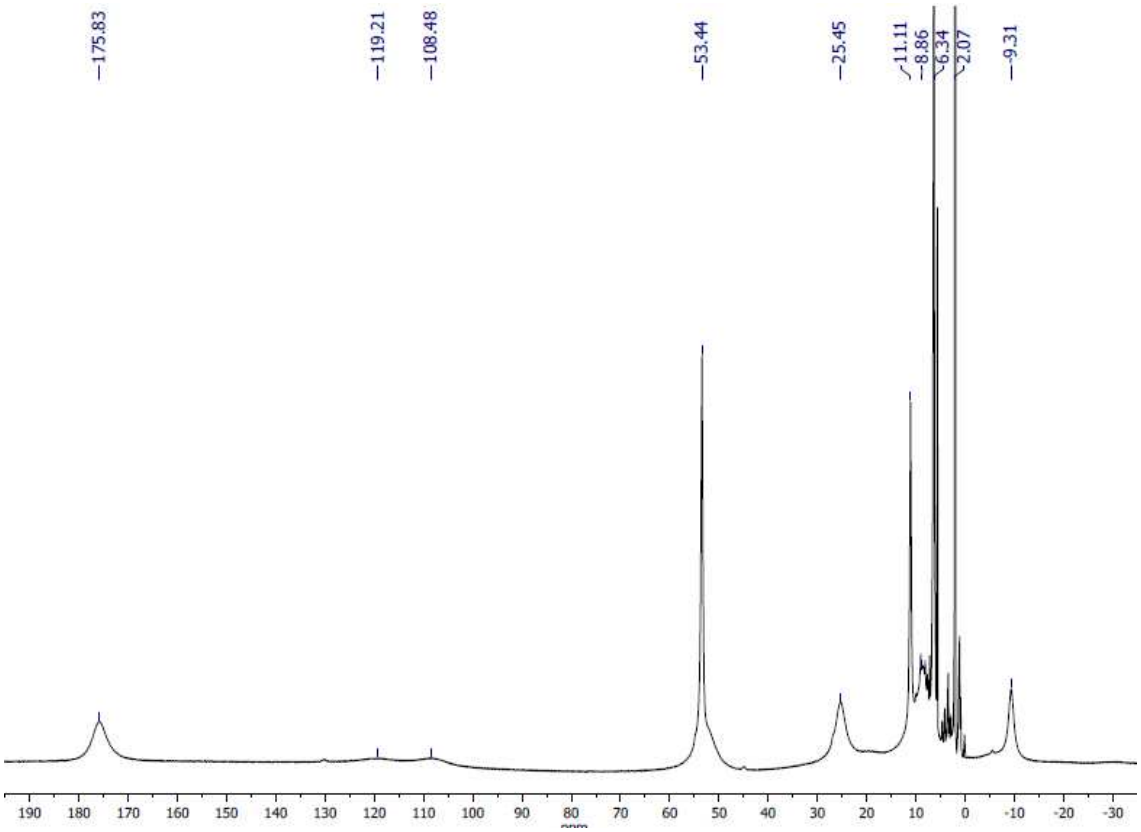

^{1}H-NMR of **C11** in CD_3CN

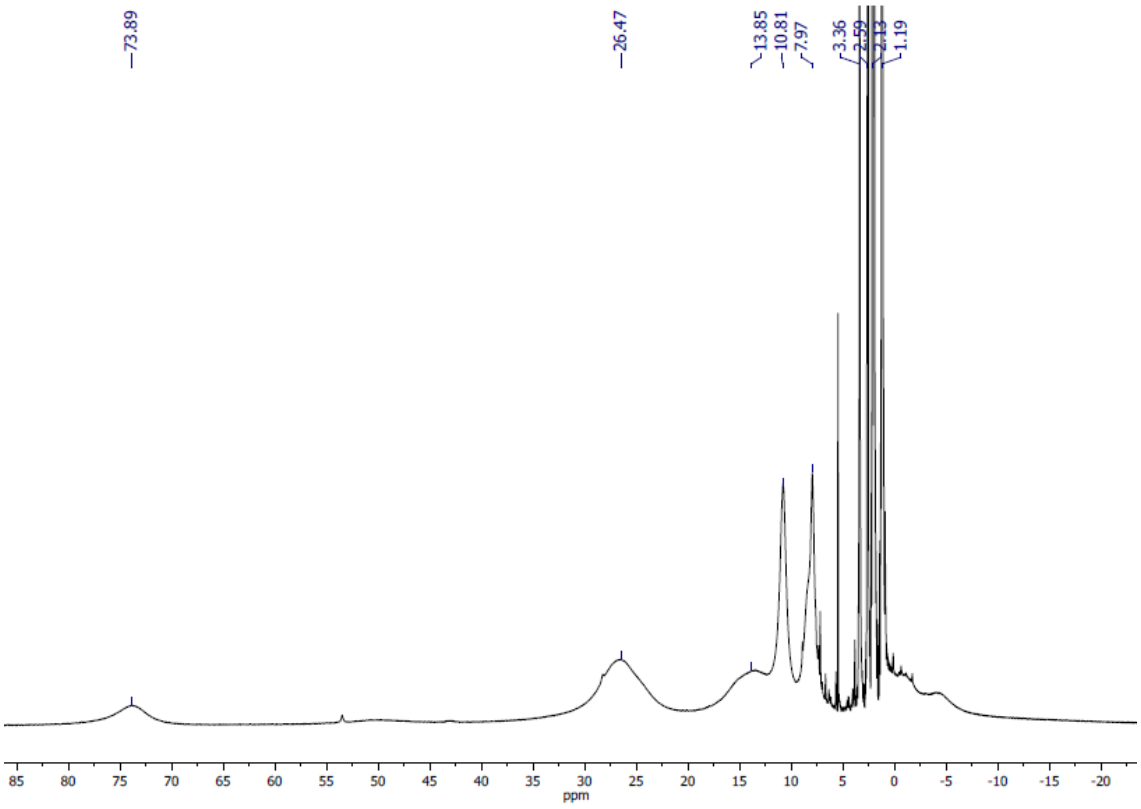

^{1}H-NMR of **C12** in CD_2Cl_2

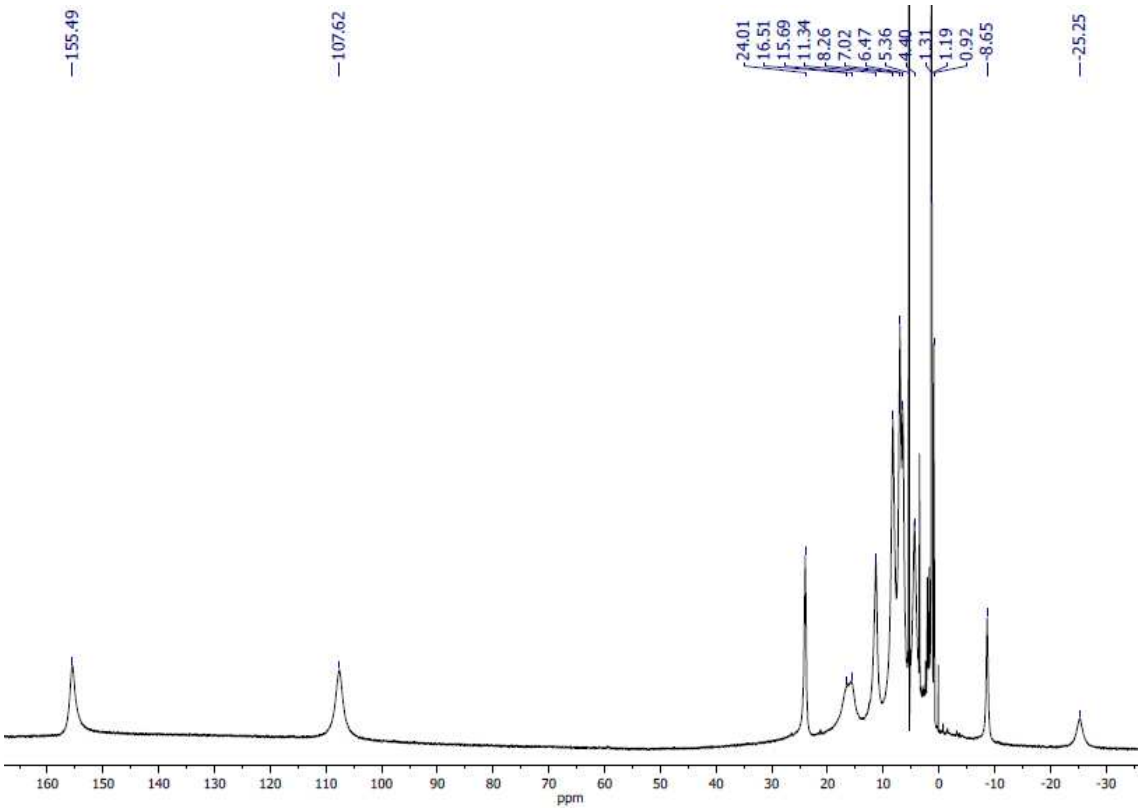

^{1}H-NMR of **C12** in acetone-d6

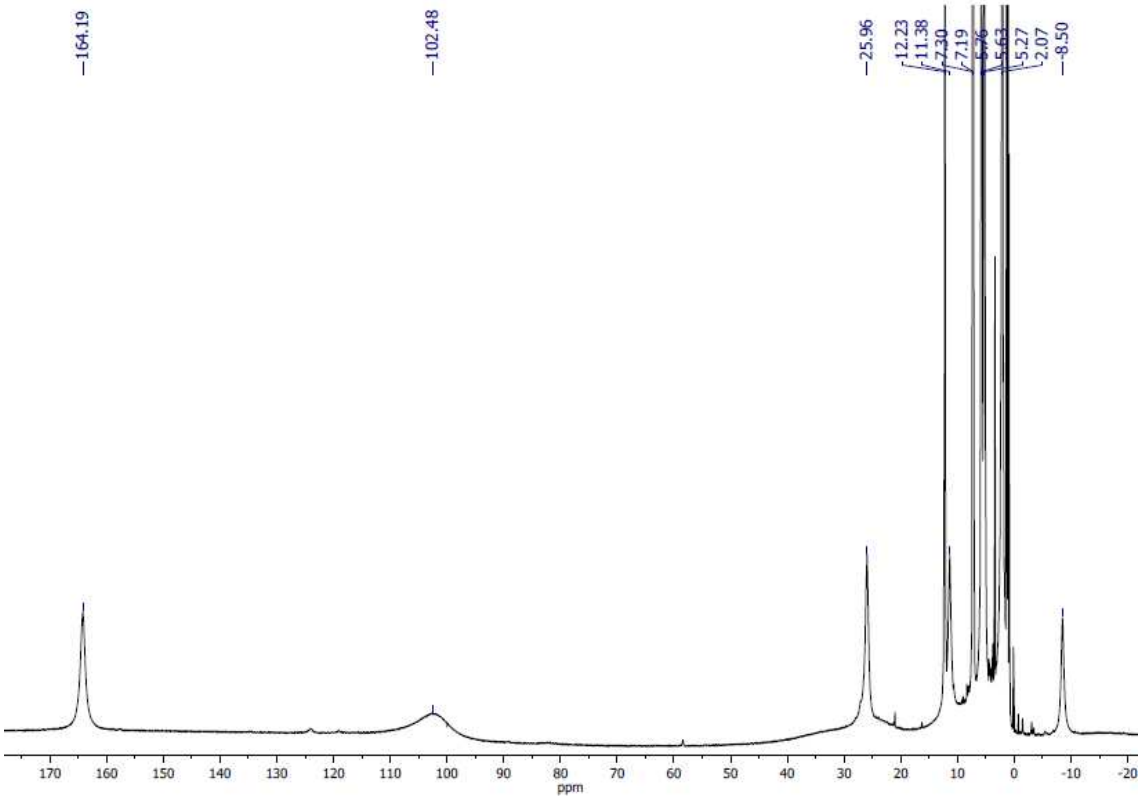

^{1}H-NMR of **C12** in CD_3CN

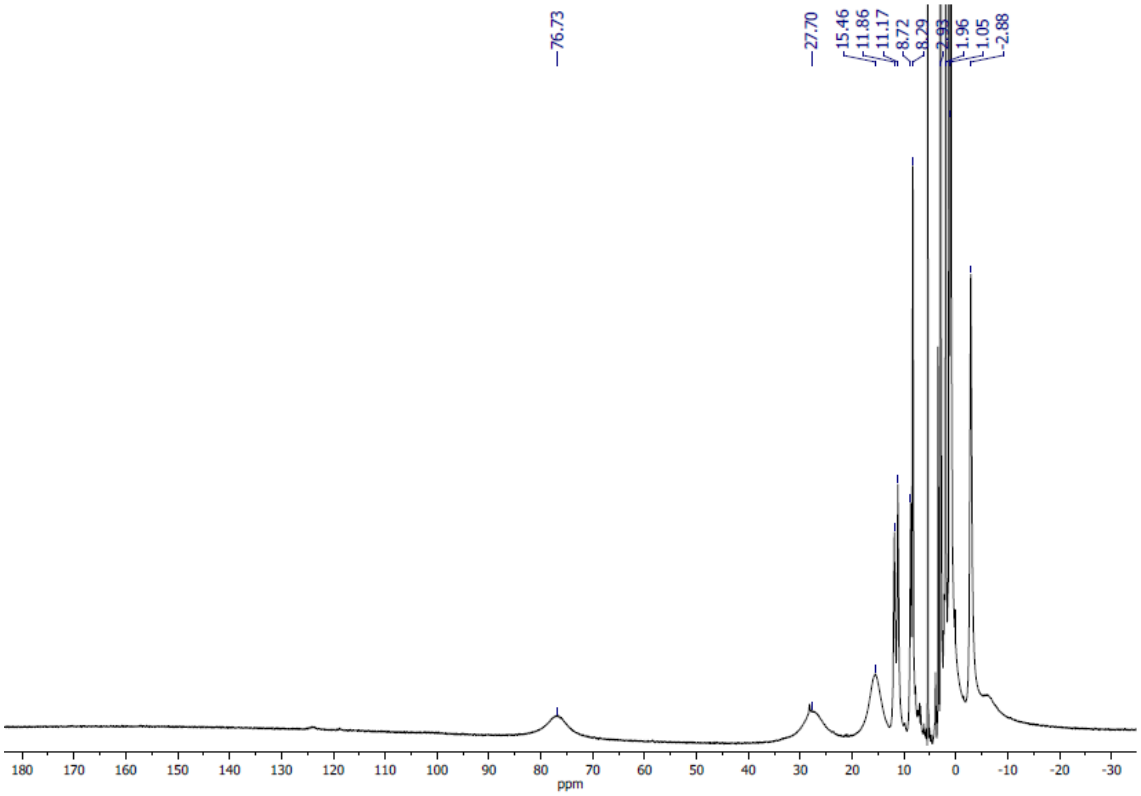

^{1}H-NMR of **C13** in CD_2Cl_2

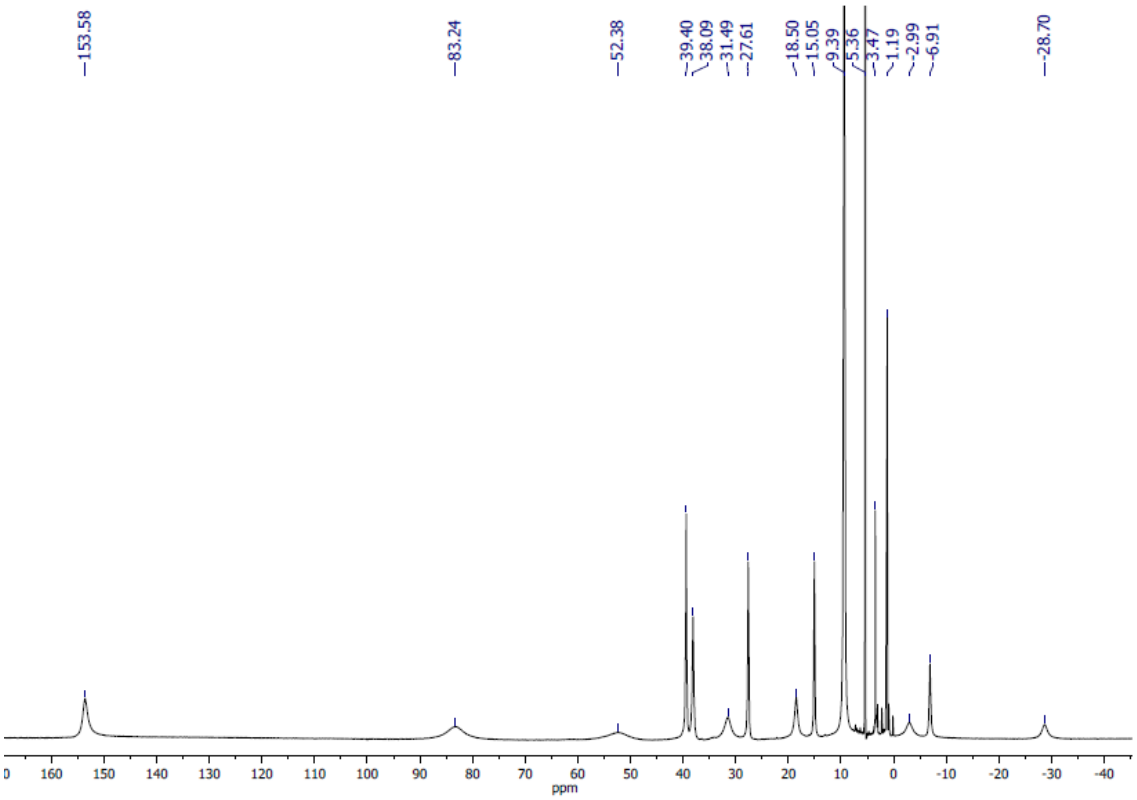

^{1}H-NMR of **C13** in acetone-d6

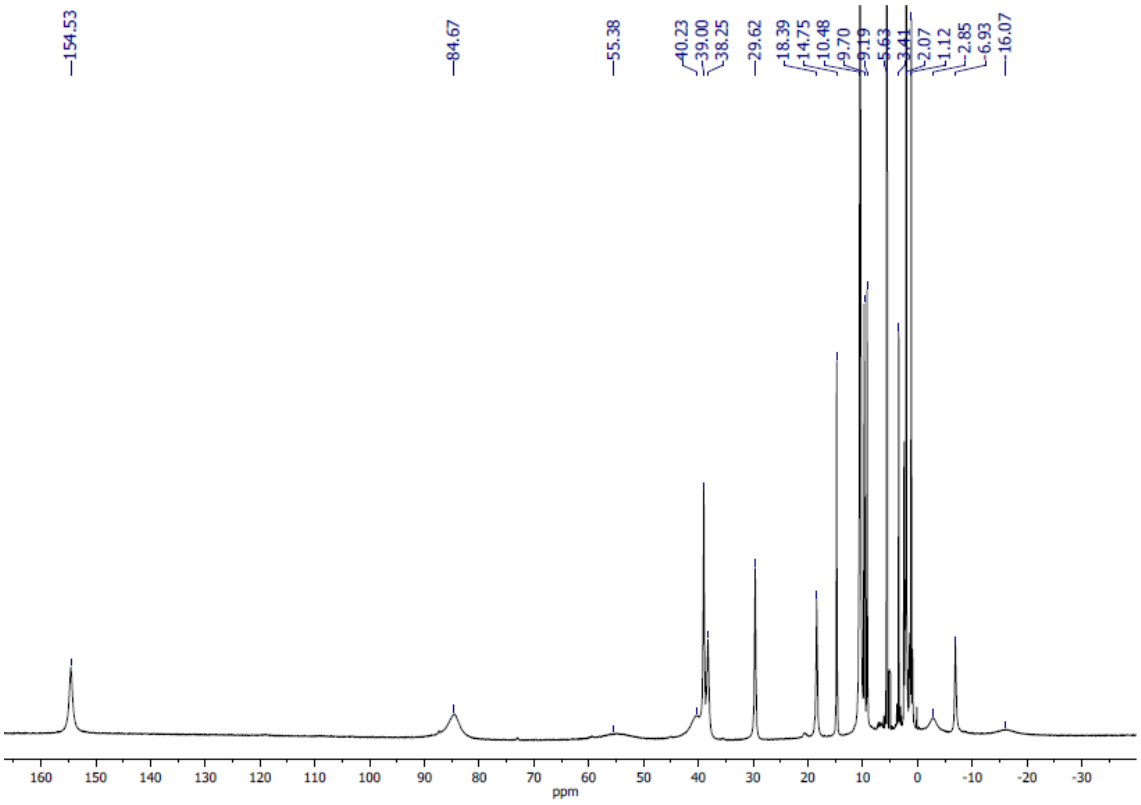

^{1}H-NMR of **C13** in CD_3CN

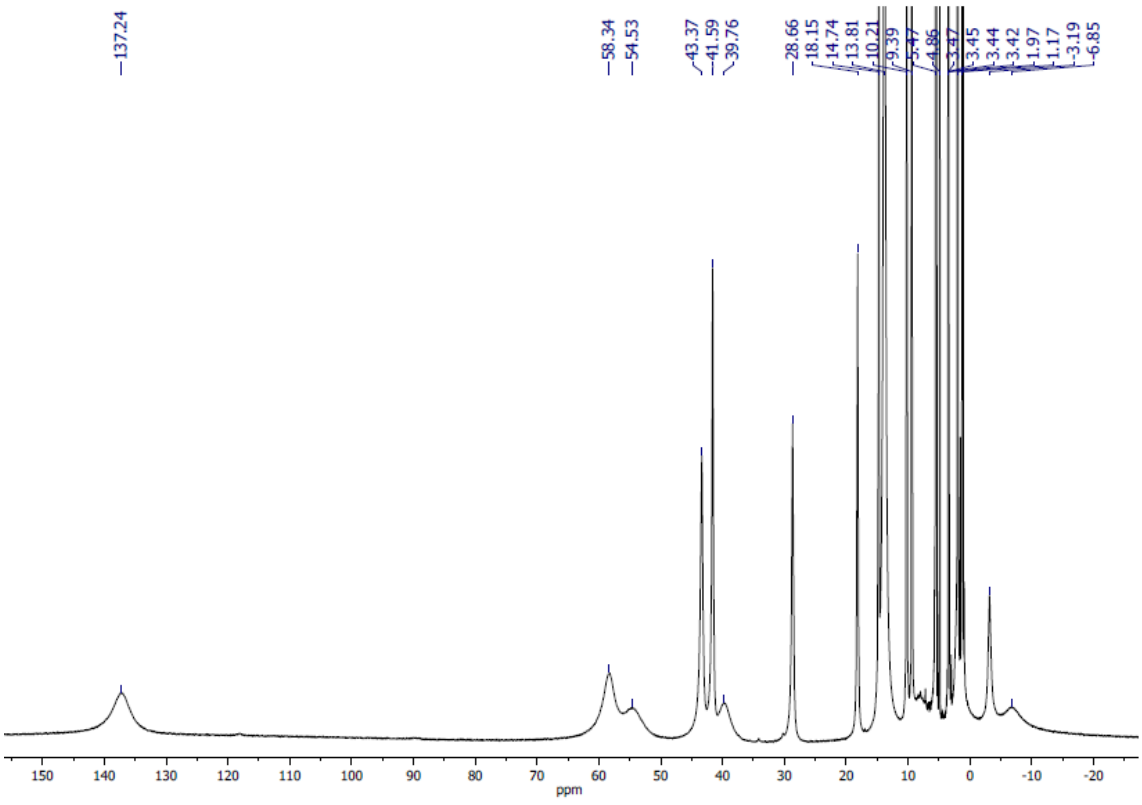

^{1}H-NMR of **CI4** in CD_2Cl_2

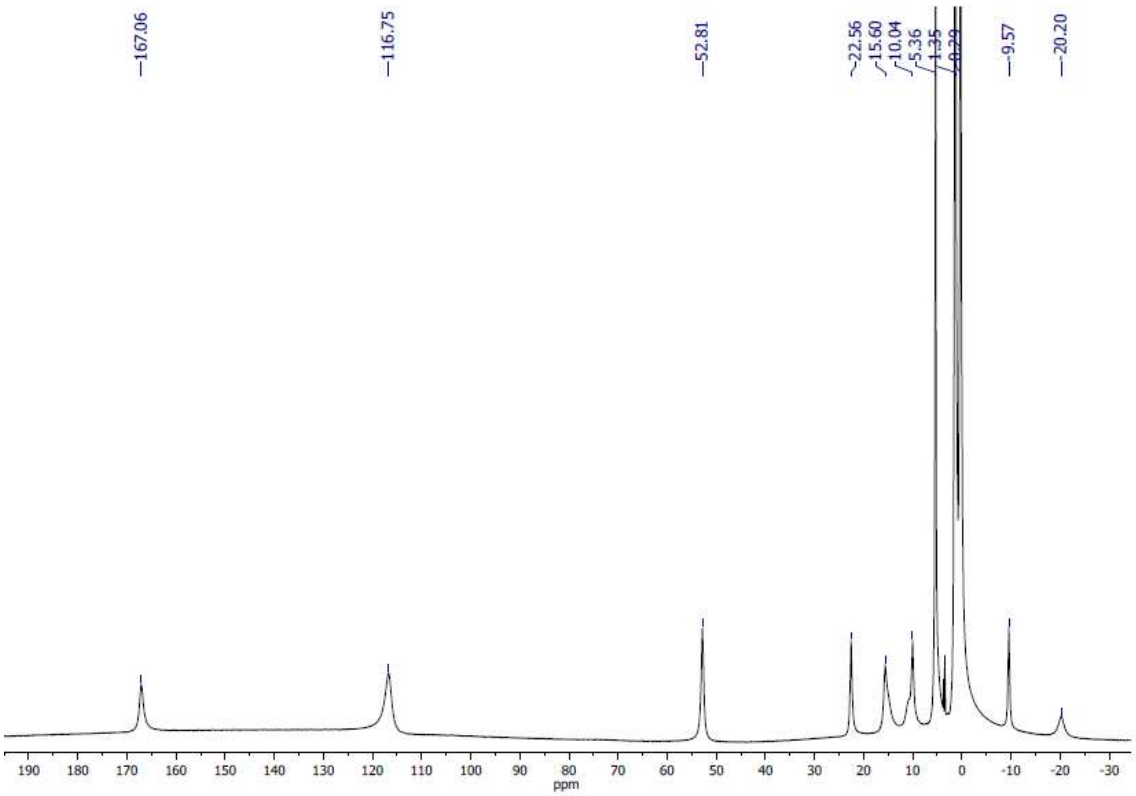

^{1}H-NMR of **CI4** in acetone-d6

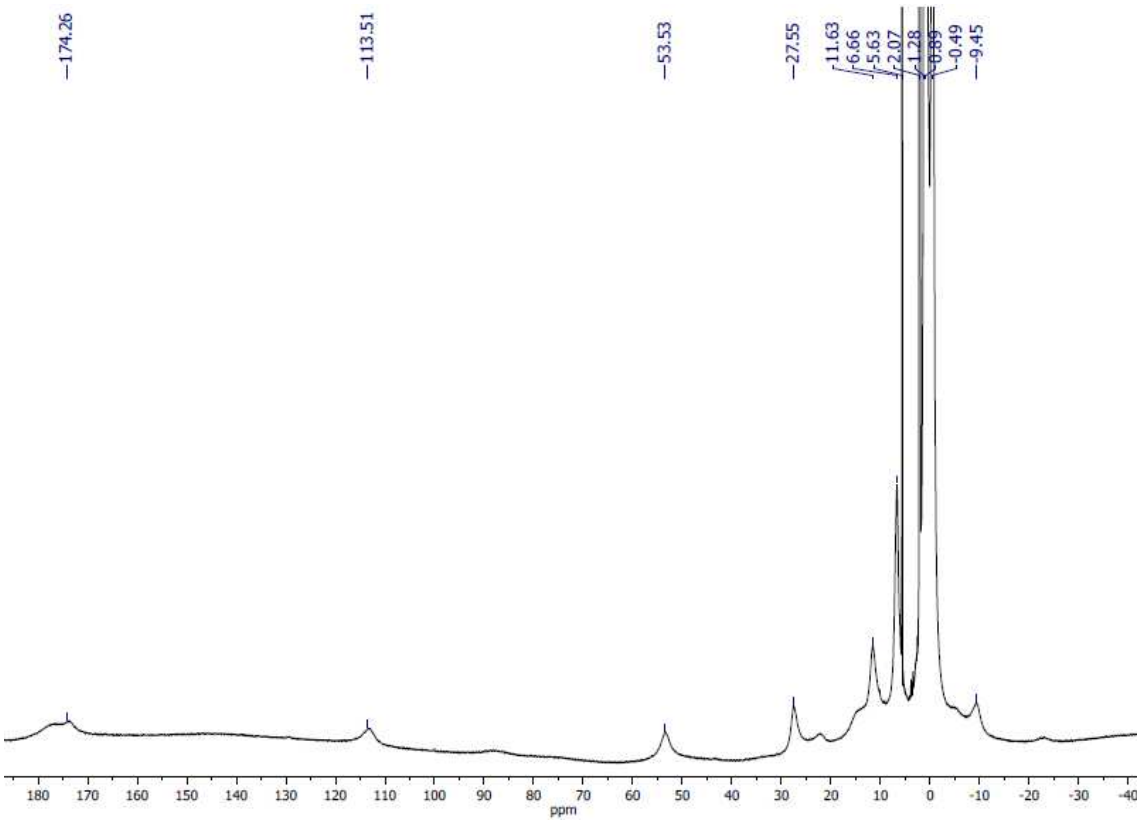

^{1}H-NMR of **C14** in CD_3CN

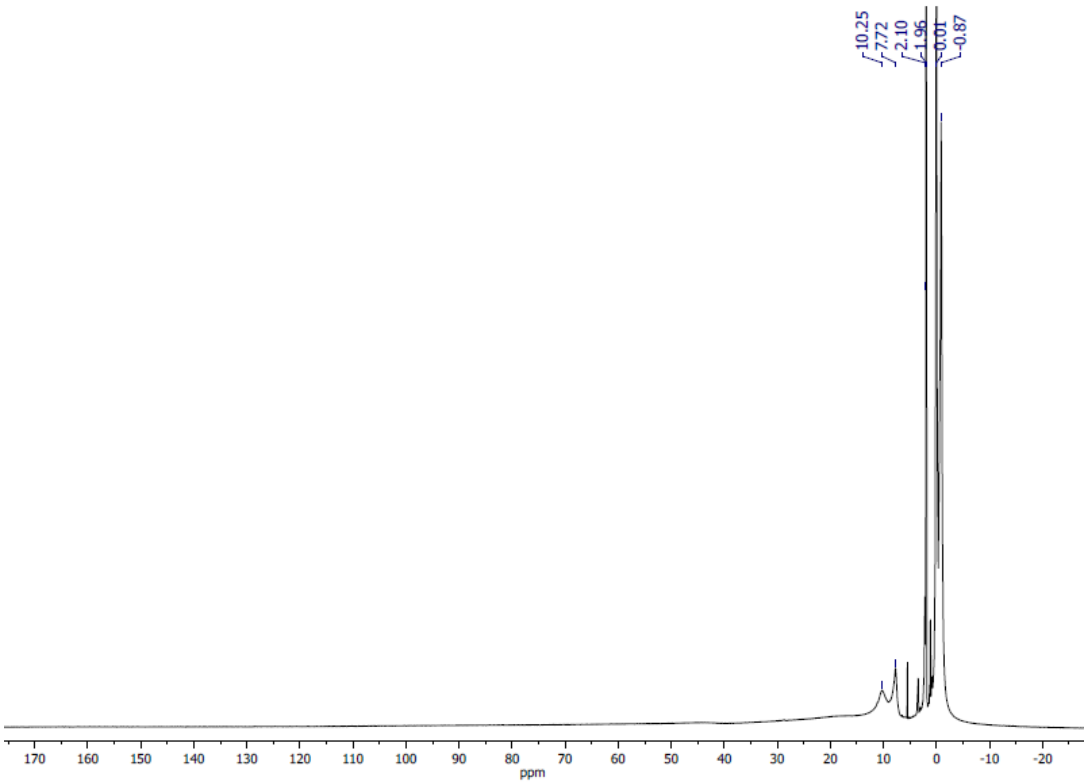

^{1}H-NMR of **C15** in CD_2Cl_2

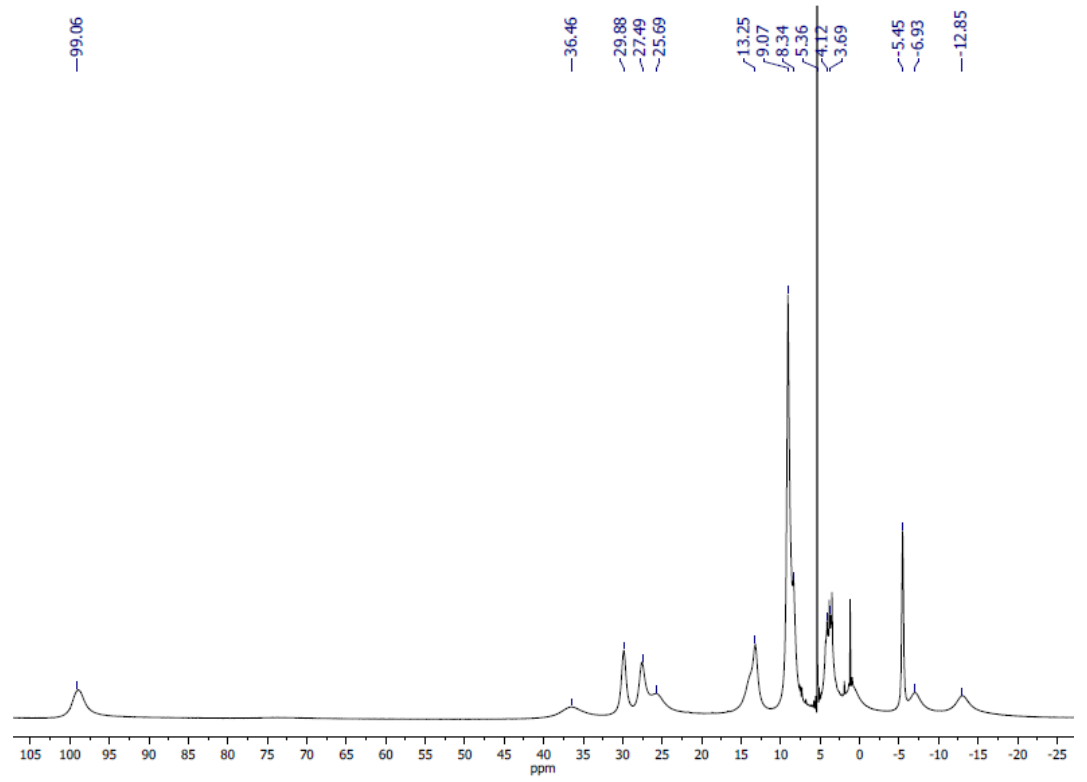

^{1}H-NMR of **C15** in acetone-d6

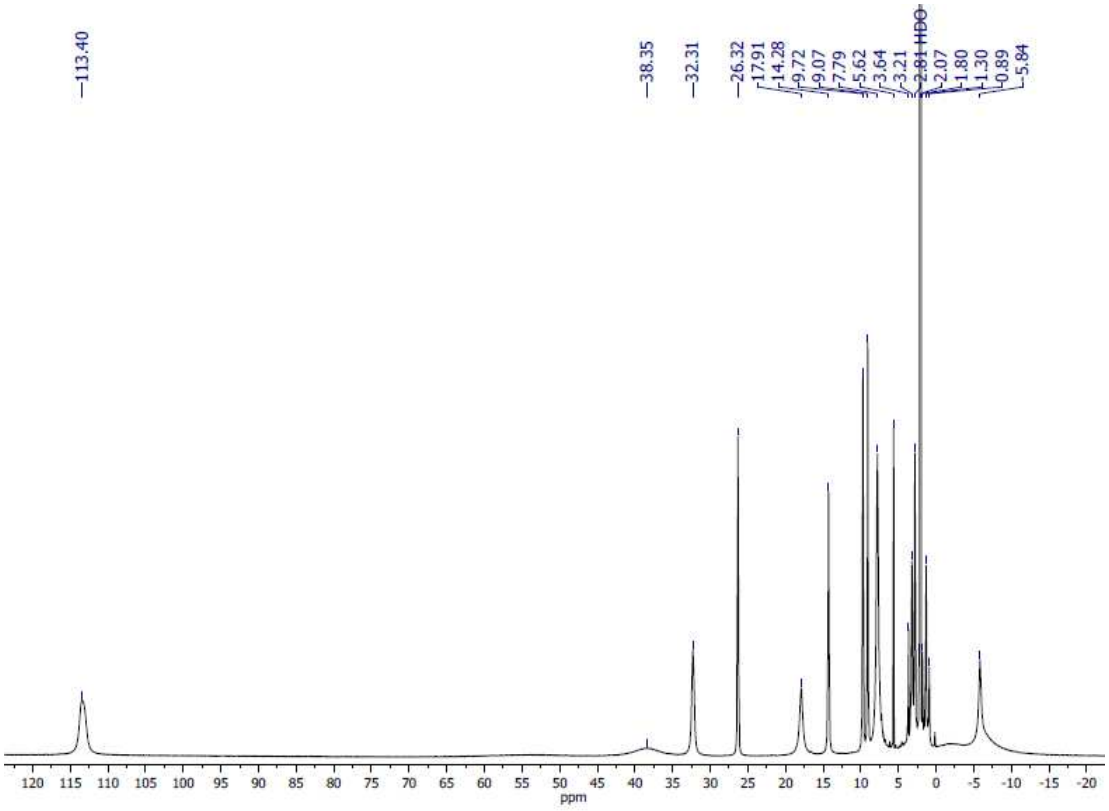

^{1}H-NMR of **C15** in CD_3CN

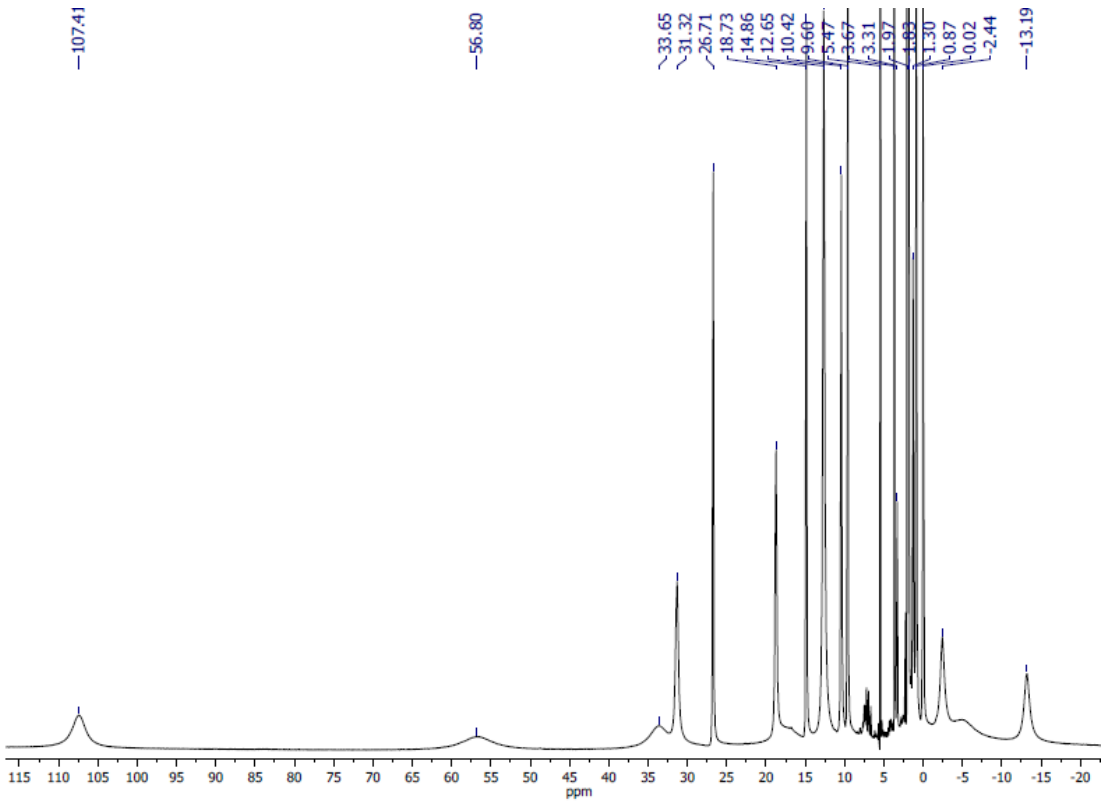

GC spectra of epoxides

P1

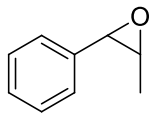

rac

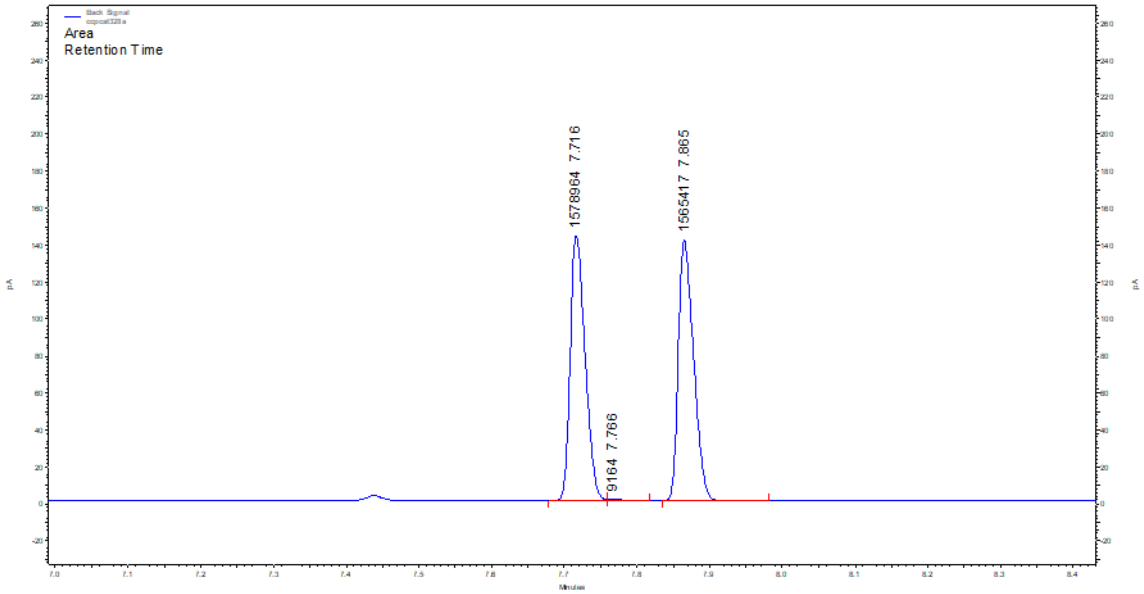

Table IV.5 entry 8

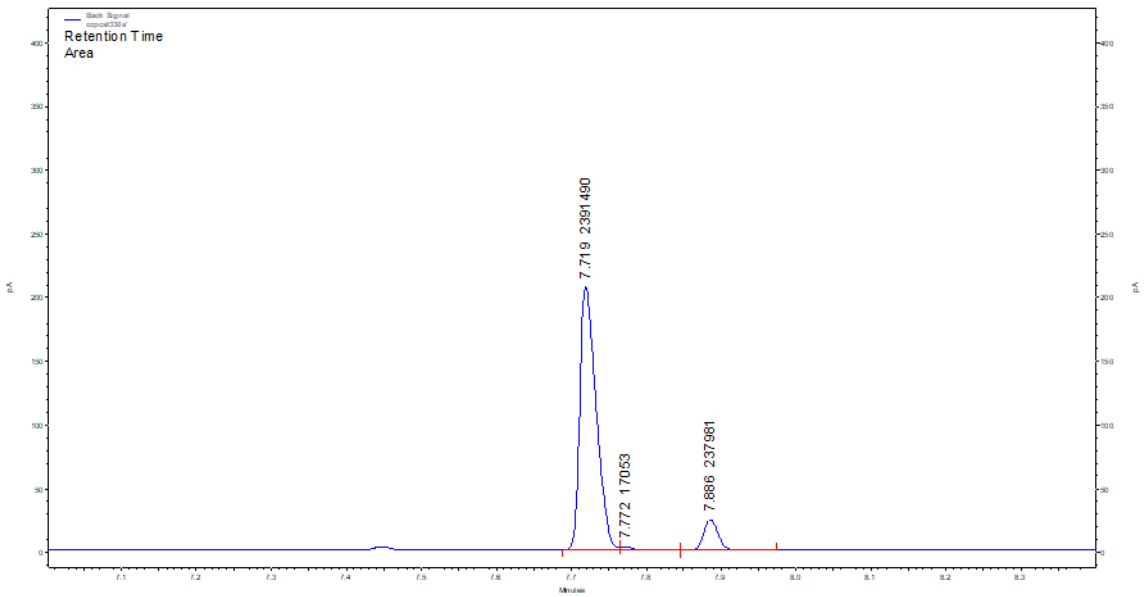

P3

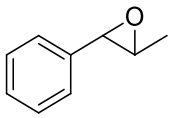

rac

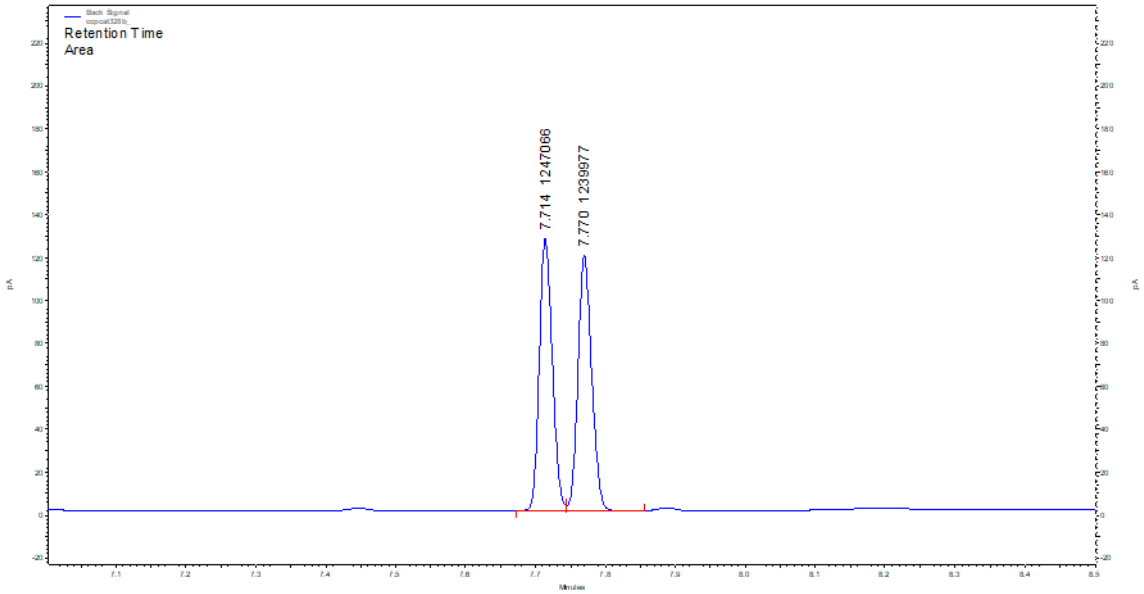

Table IV.7 entry 12

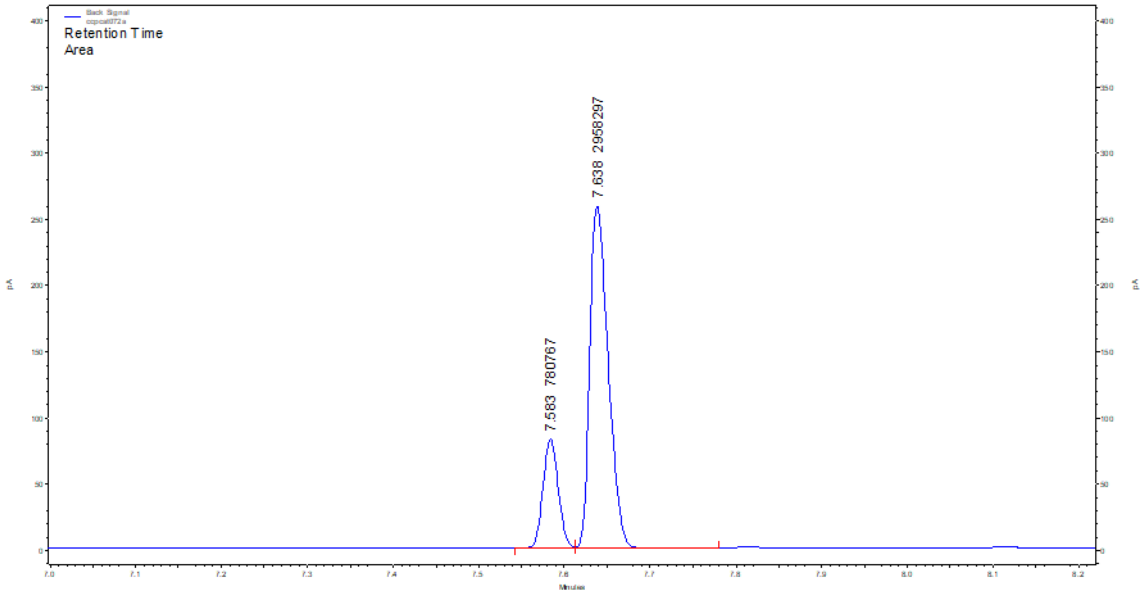

P4

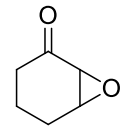

rac

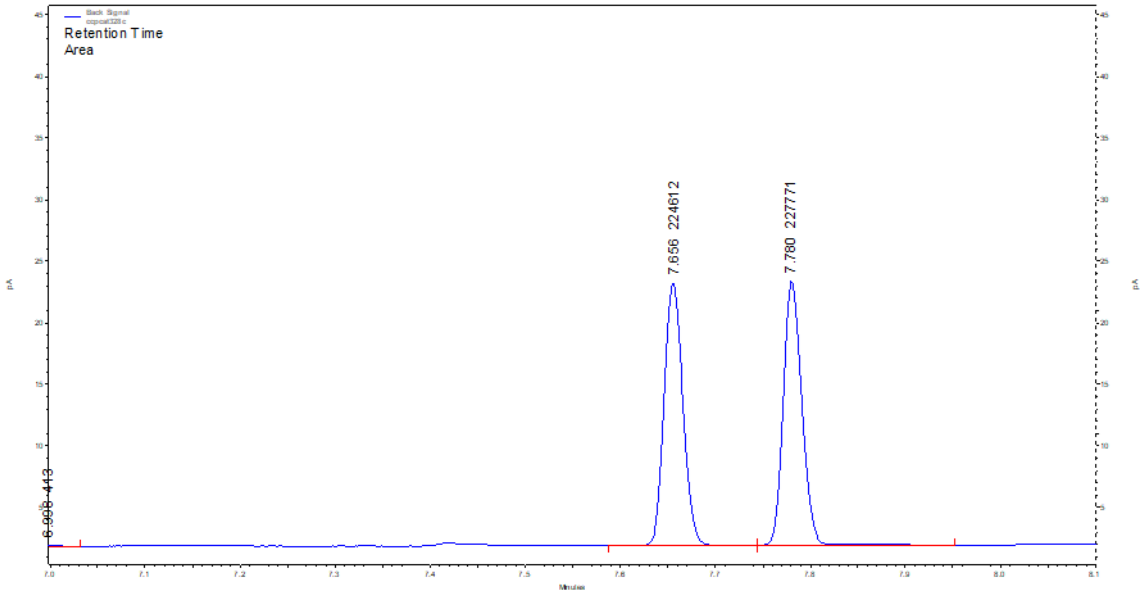

Table IV.8 entry 4

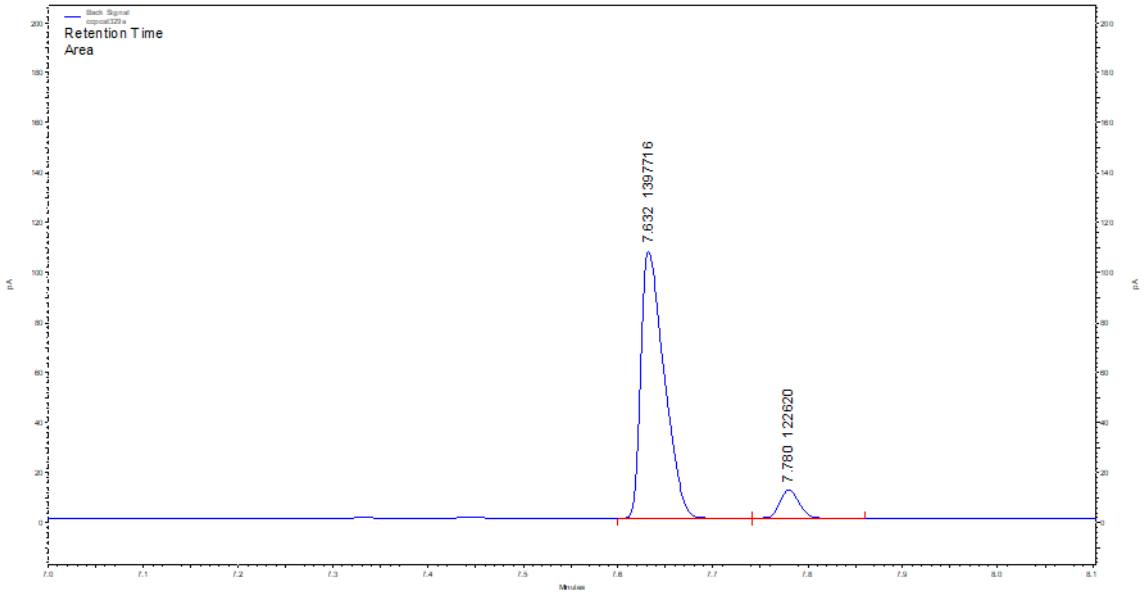

P5

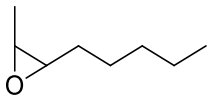

rac

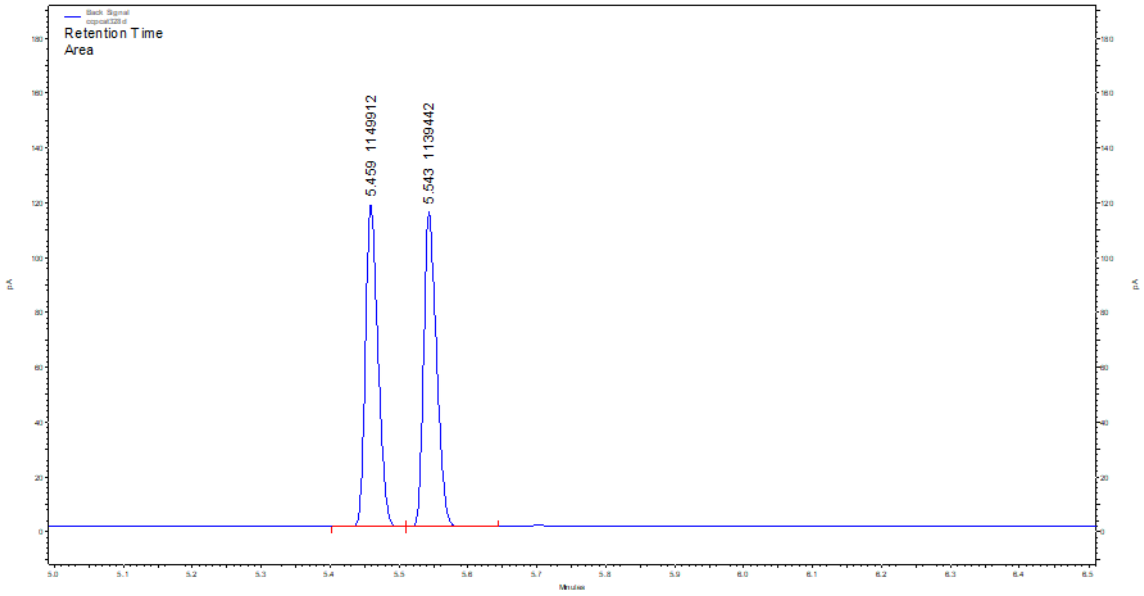

Table IV.5 entry 48

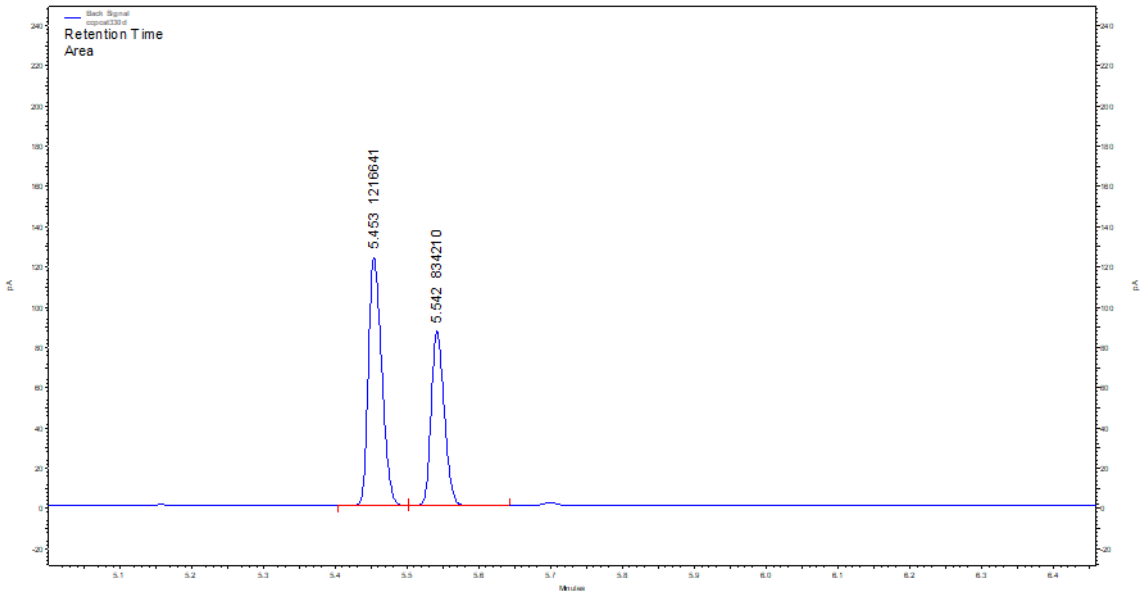

P6

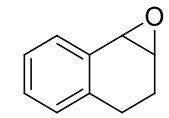

rac

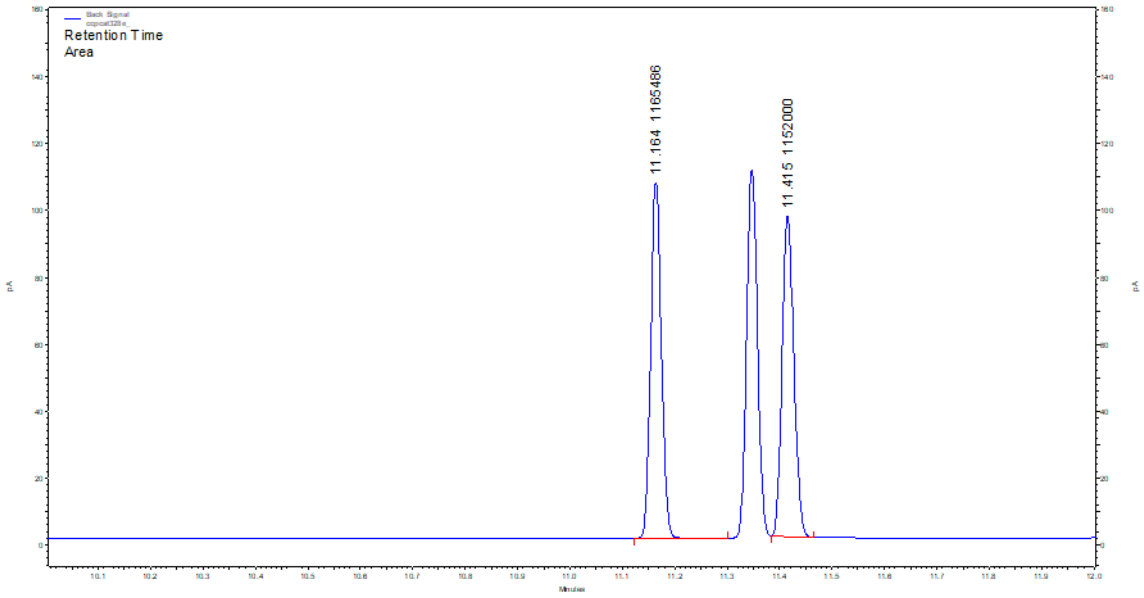

Table IV.9 entry 3

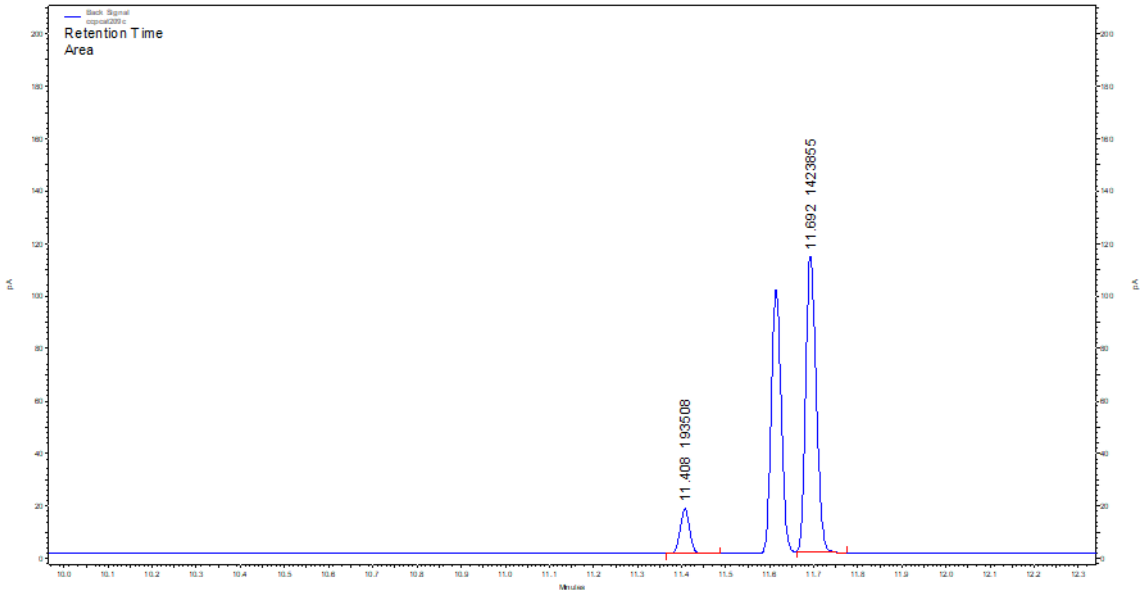

P7

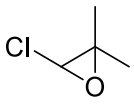

rac

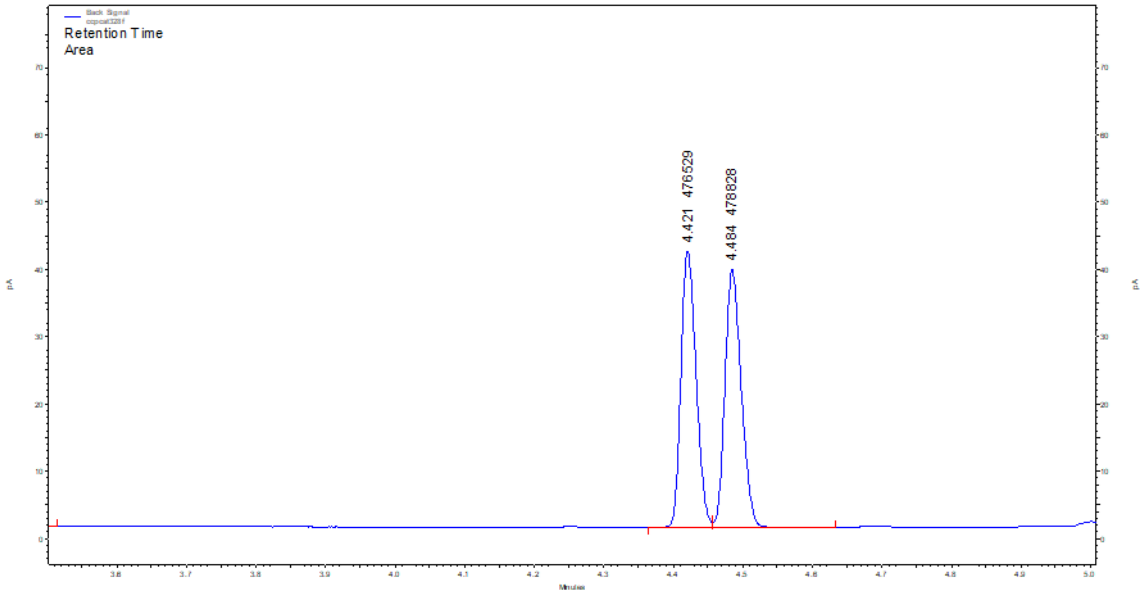

Table IV.10 entry 7

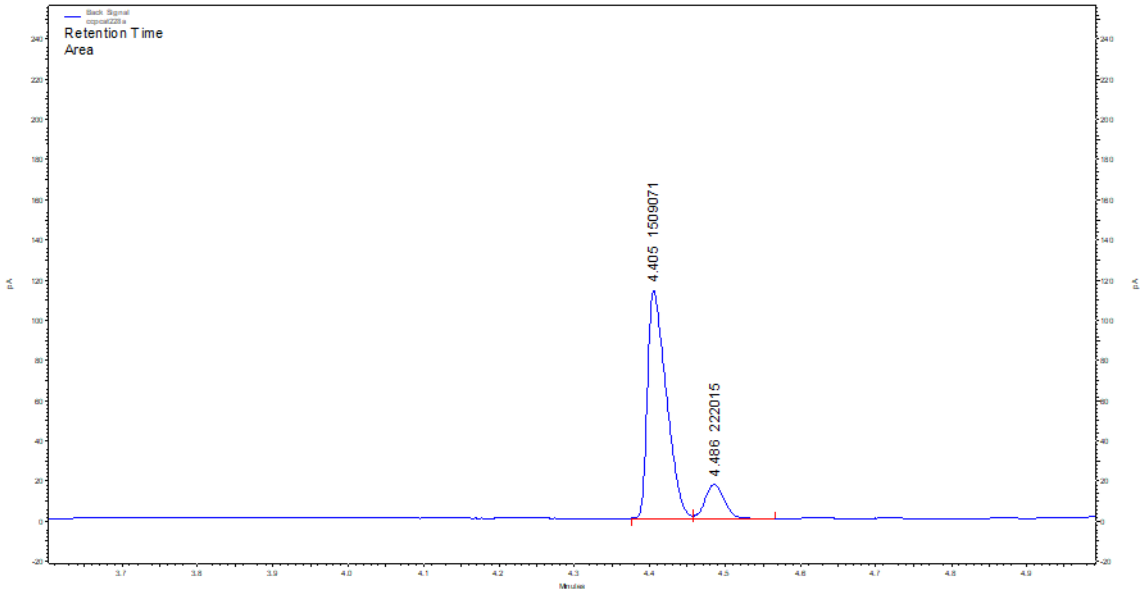

P8

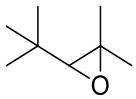

rac

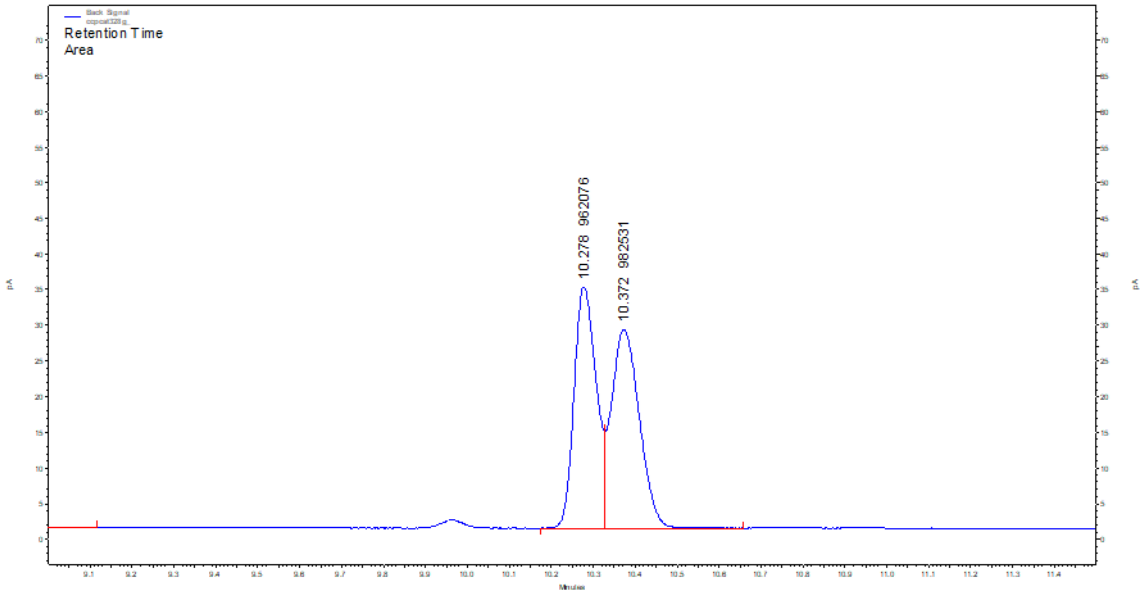

Table IV.11 entry 7

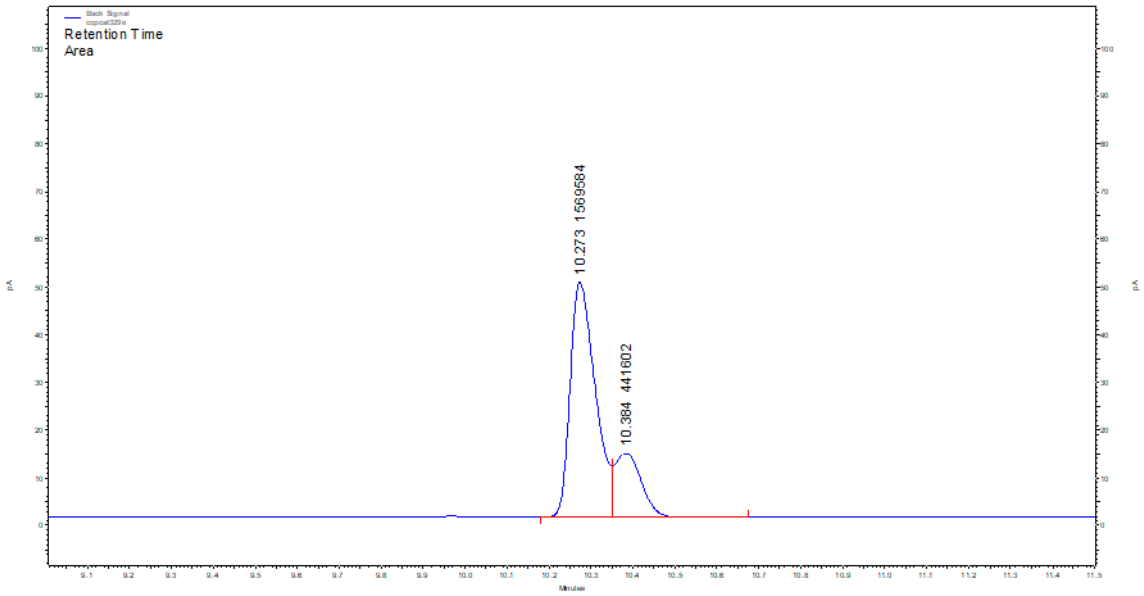

X-ray data

The X-ray structures of **C7**, **C9**, **C12**, **C13, C15**, **C16**, **C19** and **C20** complexes are depicted in figure S.1, experimental details of their crystal structure determination are collected in tables S.1 and S.2, and a list of selected bond distances and angles can be found in tables S.3 and S.4.

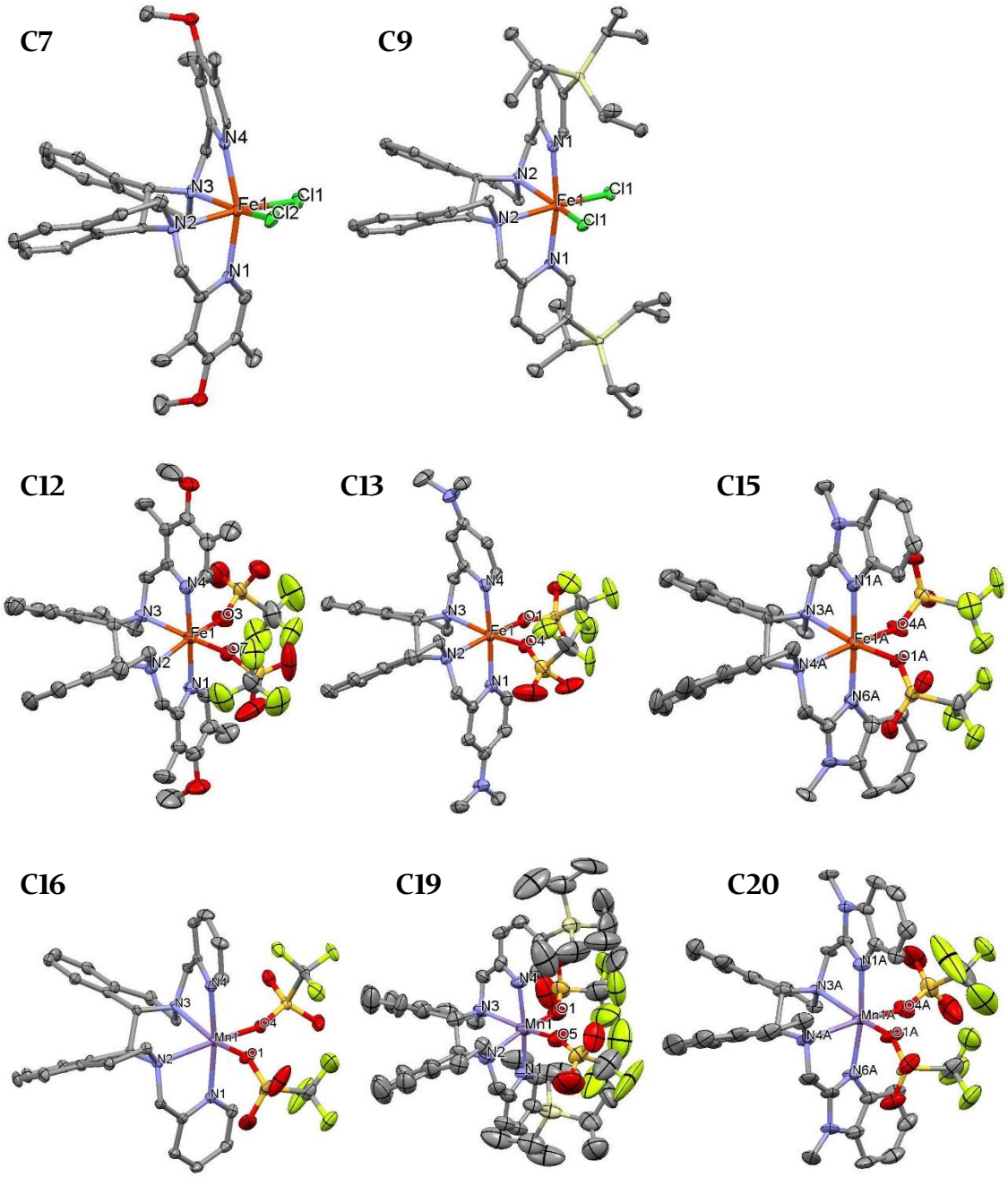

Figure S.1. Ellipsoid diagrams of **C7, C9, C12, C13, C15, C16, C19** and **C20** complexes at a 50% of probability. Hydrogen atoms were omitted for clarity.

Table S.1. Crystal data for **C7, C9, C12** and **C13** complexes.

Compound	**C7**	**C9**	**C12**	**C13**
Empirical formula	$C_{36}H_{42}Cl_2FeN_4O_2$	$C_{50}H_{74}Cl_6FeN_4Si_2$	$C_{79}H_{90}Cl_6F_{12}Fe_2N_8O_{16}S_4$	$C_{44}H_{58}Cl_4F_6FeN_6O_6S_2$
Formula weight	689.48	1055.86	2088.22	1142.73
Temperature	100 (2) K	100(2) K	100(2) K	100(2) K
Wavelength	0.71073 Å	0.71073 Å	0.71073 Å	0.71073 Å
Crystal system	Trigonal	Orthorhombic	Monoclinic	Orthorhombic
Space group	P 32	C 2 2 21	P 21	P 21 21 21
Unit cell dimensions	a = 13.8478(16) Å; α = 90°	a = 15.9696(14) Å; α = 90°	a = 14.028(5) Å; α = 90°	a = 12.639(7) Å; α = 90°
	b = 13.8478(16) Å; β = 90°	b = 17.4320(15) Å; β = 90°	b = 19.007(6) Å; β = 99.874(6)°	b = 14.208(8) Å ; β = 90°
	c = 15.415(4) Å; γ = 120°	c = 19.5727(16) Å; γ = 90°	c = 18.622(6) Å; γ = 90°	c = 26.522(15) Å; γ = 90°
Volume	2560.0(9) A^3	5448.7(8) A^3	4892(3) A^3	4763(5) A^3
Z, Density (calculated)	3, 1.342 Mg/m^3	4, 1.287 Mg/m^3	2, 1.418 Mg/m^3	4, 1.594 Mg/m^3
Absorption coefficient	0.636 mm^{-1}	0.652 mm^{-1}	0.631 mm^{-1}	0.708 mm^{-1}
F(000)	1086	2233	2148	2368
Crystal size	0.40 x 0.12 x 0.10 mm	0.20 x 0.15 x 0.12 mm	0.33 x 0.2 x 0.2 mm	0.25 x 0.10 x 0.10 mm
Θ range for data collection	1.698 to 28.286°	2.018 to 28.320°	2.220 to 24.124°	2.157 to 27.599°
Limiting indices	-12<=h<=17	-20<=h<=21	-16<=h<=16	-16<=h<=16
	-17<=k<=17	-23<=k<=23	-21<=k<=21	-18<=k<=17
	-19<=l<=20	-26<=l<=26	-21<=l<=21	-34<=l<=34
Reflections collected/unique	17643 / 7697	43402 / 6762	56709 / 15484	70864 / 11025
	[R(int) = 0.0469]	[R(int) = 0.0673]	[R(int) = 0.0584]	[R(int) = 0.0712]
Completeness to Θ	100.0% (Θ = 25.242°)	99.9% (Θ = 25.242°)	87.9% (Θ = 25.242°)	99.8% (Θ = 25.242°)
Refinement method	Full-matrix least-squares on F^2	Full-matrix least-squares on F^2	Full-matrix least-squares on F^2	Full-matrix least-squares on F^2
Data/restraints/parameters	7697 / 1 / 412	6762 / 0 / 285	15484 / 3 / 1058	11025 / 19 / 630
Goodness-of-fit on F2	1.063	1.113	1.050	1.024
Final R indices	R1 = 0.0522	R1 = 0.0438	R1 = 0.0916	R1 = 0.0626
	wR2 = 0.0971	wR2 = 0.0900	wR2 = 0.2419	wR2 = 0.1570
R indices (all data)	R1 = 0.0709	R1 = 0.0514	R1 = 0.1032	R1 = 0.0812
	wR2 = 0.1024	wR2 = 0.0937	wR2 = 0.2528	wR2 = 0.1696
Largest diff. peak and hole	0.628 and -0.415 $e.A^{-3}$	0.421 and -0.258 $e.A^{-3}$	1.370 and -1.279 $e.A^{-3}$	1.207 and -0.801 $e.A^{-3}$

Table S.2. Crystal data for **C15, C16, C19** and **C20** complexes.

Compound	**C15**	**C16**	**C19**	**C20**
Empirical formula	$C_{117}H_{114}Cl_6F_{18}Fe_3N_{18}O_{20}S_6$	$C_{34}H_{34}Cl_4F_6MnN_4O_6S_2$	$C_{102}H_{144}Cl_4F_{12}Mn_2N_8O_{12}S_4Si_4$	$C_{124}H_{132}Cl_4F_{18}Mn_3N_{18}O_{20}S_6$
Formula weight	3006.87	969.51	2394.52	3035.45
Temperature	100(2) K	100 (2) K	100 (2) K	100(2) K
Wavelength	0.71073 Å	0.71073 Å	0.71073 Å	0.71073 Å
Crystal system	Monoclinic	Monoclinic	Orthorhombic	Monoclinic
Space group	P 21	P 21	P 21 21 21	P 21
Unit cell dimensions	a = 20.69(3) Å; α = 90° b = 17.80(3) Å; β = 116.92(3)° c = 21.35(3) Å; γ = 90°	a = 10.7313(7) Å; α = 90° b = 14.7111(10) Å; β = 104.0080(10)° c = 13.7385(9) Å; γ = 90°	a = 13.5988(13) Å; α = 90° b = 24.423(2) Å; β = 90° c = 36.507(4) Å; γ = 90°	a = 21.910(4) Å; α = 90° b = 18.330(3) Å; β = 115.983(2)° c = 21.954(4) Å; γ = 90°
Volume	7011(19) A^3	2104.4(2) A^3	12125(2) A^3	7925(2) A^3
Z, Density (calculated)	2, 1.424 Mg/m^3	2, 1.530 Mg/m^3	4, 1.312 Mg/m^3	2, 1.272 Mg/m^3
Absorption coefficient	0.601 mm^{-1}	0.740 mm^{-1}	0.480 mm^{-1}	0.464 mm^{-1}
F(000)	3080	986	5016	3126
Crystal size	0.30 x 0.10 x 0.08 mm	0.20 x 0.20 x 0.20mm	0.28 x 0.20 x 0.20 mm	0.28 x 0.15 x 0.12 mm
Θ range for data collection	1.104 to 27.498°	2.062 to 28.336°	1.393 to 28.285°	2.075 to 28.407°
Limiting indices	-26<=h<=25 -22<=k<=22 -13<=l<=27	-14<=h<=14 -19<=k<=19 -18<=l<=18	-16<=h<=17 -32<=k<=31 -47<=l<=28	-29<=h<=29 -24<=k<=24 -29<=l<=29
Reflections collected/unique	49364 / 30023 [R(int) = 0.1271]	33315 / 10394 [R(int) = 0.0303]	81776 / 28026 [R(int) = 0.0727]	126391 / 38320 [R(int) = 0.0582]
Completeness to Θ	99.9% (Θ = 25.242°)	99.9% (Θ = 25.242°)	100.0% (Θ = 25.242°)	99.8% (Θ = 25.242°)
Refinement method	Full-matrix least-squares on F^2	Full-matrix least-squares on F^2	Full-matrix least-squares on F^2	Full-matrix least-squares on F^2
Data/restraints/parameters	30023 / 1129 / 1663	10394 / 1 / 460	28026 / 31 / 1179	38320 / 16 / 1713
Goodness-of-fit on F2	0.978	1.031	1.298	1.026
Final R indices	R1 = 0.0890 wR2 = 0.1902	R1 = 0.0452 wR2 = 0.1151	R1 = 0.1496 wR2 = 0.3735	R1 = 0.0808 wR2 = 0.2181
R indices (all data)	R1 = 0.2206 wR2 = 0.2602	R1 = 0.0473 wR2 = 0.1168	R1 = 0.2190 wR2 = 0.4237	R1 = 0.1005 wR2 = 0.2345
Largest diff. peak and hole	0.785 and -0.941 $e.A^{-3}$	0.581 and -0.405 $e.A^{-3}$	2.643 and -1.305 $e.A^{-3}$	2.622 and -1.604 $e.A^{-3}$

Table S.3. Selected bond lengths (Å) and angles (°) for for **C7, C9, C12** and **C13** complexes.

	C7		**C9**		**C12**		**C13**
Fe-N1	2.209(5)	Fe-N1	2.173(3)	Fe-N1	2.129(9)	Fe-N1	2.140(5)
Fe-N2	2.315(5)	Fe-N2	2.300(3)	Fe-N2	2.156(10)	Fe-N2	2.240(5)
Fe-N3	2.314(4)	Fe-N2#	2.300(3)	Fe-N3	2.227(10)	Fe-N3	2.230(5)
Fe-N4	2.197(5)	Fe-N1#	2.173(3)	Fe-N4	2.134(9)	Fe-N4	2.134(5)
Fe-Cl1	2.4093(17)	Fe-Cl1	2.4088(9)	Fe-O3	2.084(4)	Fe-O1	2.156(4)
Fe-Cl2	2.3968(17)	Fe-Cl1#	2.4088(9)	Fe-O6	2.208(5)	Fe-O4	2.140(5)
N1-Fe-N2	73.80(16)	N1-Fe-N2	96.18(10)	N1-Fe-N2	78.2(4)	N1-Fe-N2	77.04(17)
N1-Fe-N4	160.21(17)	N1-Fe-N1#	169.19(16)	N1-Fe-N4	177.8(4)	N1-Fe-N4	175.57(17)
N1-Fe-Cl2	97.92(13)	N1-Fe-Cl1#	92.81(8)	N1-Fe-O6	87.9(3)	N1-Fe-O4	91.68(18)
N1-Fe-Cl1	95.55(13)	N1-Fe-Cl1	93.70(8)	N1-Fe-O3	93.6(3)	N1-Fe-O1	90.97(18)
N2-Fe-N4	91.75(16)	N2-Fe-N1#	75.19(10)	N2-Fe-N4	101.1(4)	N2-Fe-N4	98.59(18)
N3-Fe-N4	73.55(16)	N2#-Fe-N1#	96.18(10)	N3-Fe-N4	76.3(3)	N3-Fe-N4	77.41(18)
N2-Fe-Cl2	91.09(11)	N2-Fe-Cl1#	161.14(7)	N2-Fe-O6	85.8(3)	N2-Fe-O4	95.60(16)
N4-Fe-Cl1	96.01(12)	N1#-Fe-Cl1	92.81(8)	N4-Fe-O3	87.1(3)	N4-Fe-O1	93.10(18)
N3-Fe-Cl1	93.37(11)	N2#-Fe-Cl1	161.15(7)	N3-Fe-O3	98.1(3)	N3-Fe-O1	90.06(16)
N2-Fe-N3	77.08(15)	N2-Fe-N2#	76.35(14)	N2-Fe-N3	83.1(3)	N2-Fe-N3	78.90(16)
N3-Fe-Cl2	163.57(11)	N2#-Fe-Cl1#	90.06(7)	N3-Fe-O6	160.2(3)	N3-Fe-O4	164.69(18)
Cl1-Fe-Cl2	100.26(5)	Cl1-Fe-Cl1#	105.90(5)	O1-Fe-O6	95.3(2)	O1-Fe-O4	98.56(16)

Table S.4. Selected bond lengths (Å) and angles (°) for for **C15, C16, C19** and **C20** complexes.

	C15		**C16**	**C19**	**C20**
Fe-N1	2.083(13)	Mn-N1	2.232(3)	2.179(15)	2.168(6)
Fe-N2	2.214(12)	Mn-N2	2.301(3)	2.318(14)	2.353(6)
Fe-N3	2.247(12)	Mn-N3	2.291(3)	2.325(13)	2.368(6)
Fe-N4	2.069(12)	Mn-N4	2.230(3)	2.161(15)	2.166(6)
Fe-O1	2.094(10)	Mn-O1	2.143(3)	2.130(14)	2.166(7)
Fe-O4	2.013(13)	Mn-O4	2.142(3)	2.113(14)	2.171(6)
N1-Fe-N2	76.6(5)	N1-Mn-N2	75.55(11)	75.4(5)	75.2(2)
N1-Fe-N4	172.6(5)	N1-Mn-N4	172.60(11)	171.6(5)	172.7(2)
N1-Fe-O4	90.1(5)	N1-Mn-O4	92.17(11)	96.2(5)	92.9(2)
N1-Fe-O1	94.7(4)	N1-Mn-O1	96.51(11)	89.5(5)	90.6(3)
N2-Fe-N4	100.2(5)	N2-Mn-N4	103.01(11)	97.4(5)	102.6(2)
N3-Fe-N4	75.9(4)	N3-Mn-N4	74.91(11)	74.2(5)	74.8(2)
N2-Fe-O4	166.5(5)	N2-Mn-O4	161.02(10)	99.9(5)	90.8(2)
N4-Fe-O1	91.9(4)	N4-Mn-O1	84.84(11)	96.4(5)	90.0(3)
N3-Fe-O1	160.7(5)	N3-Mn-O1	159.27(12)	90.8(5)	94.5(2)
N2-Fe-N3	78.9(4)	N2-Mn-N3	78.23(10)	76.7(5)	76.3(2)
N3-Fe-O4	100.6(5)	N3-Mn-O4	90.83(11)	162.2(5)	160.4(3)
O1-Fe-O4	94.8(4)	O1-Mn-O4	95.38(11)	97.3(5)	101.7(3)

Annex chapter V

Representative HPLC spectra of products

HPLC analysis: Chiralpack IA, n-Hex:iPrOH = 98/2, flow rate = 1 mL/min, λ = 260 nm, 25°C, t.r.el= 19.8 min, t.r.e2 = 20.6 min.

P2

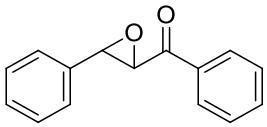

rac

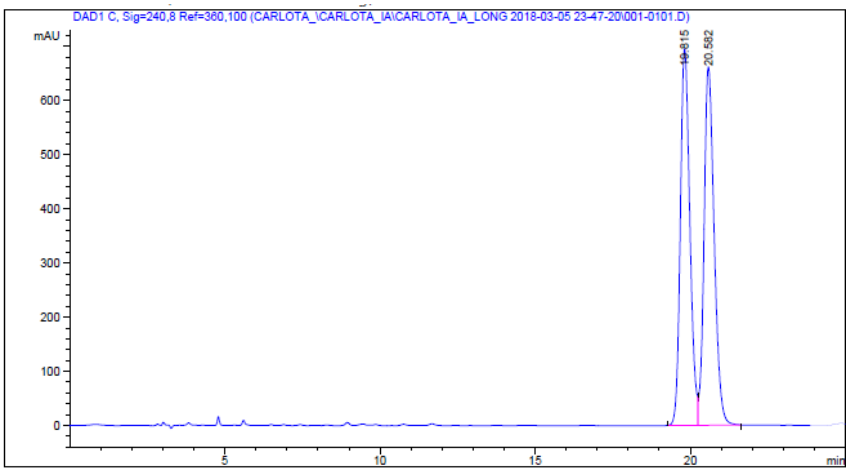

Peak #	RetTime [min]	Sig	Type	Area [mAU*s]	Height [mAU]	Area %
1	19.815	1	BV	1.48179e4	695.56134	49.5622
2	20.582	1	VB	1.50797e4	662.06061	50.4378

Table V.1 entry 4 (**C18**)

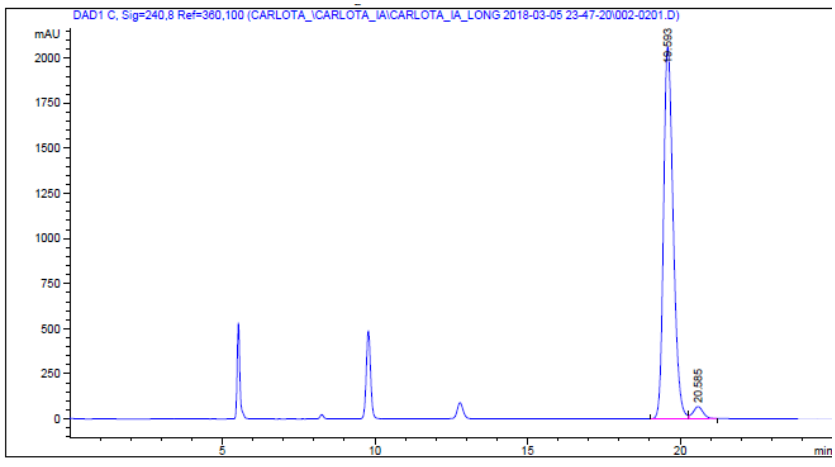

Peak #	RetTime [min]	Sig	Type	Area [mAU*s]	Height [mAU]	Area %
1	19.593	1	BV	4.53537e4	2062.85693	96.7320
2	20.585	1	VB	1532.22595	66.88808	3.2680

Table V.1 entry 5 (**C19**)

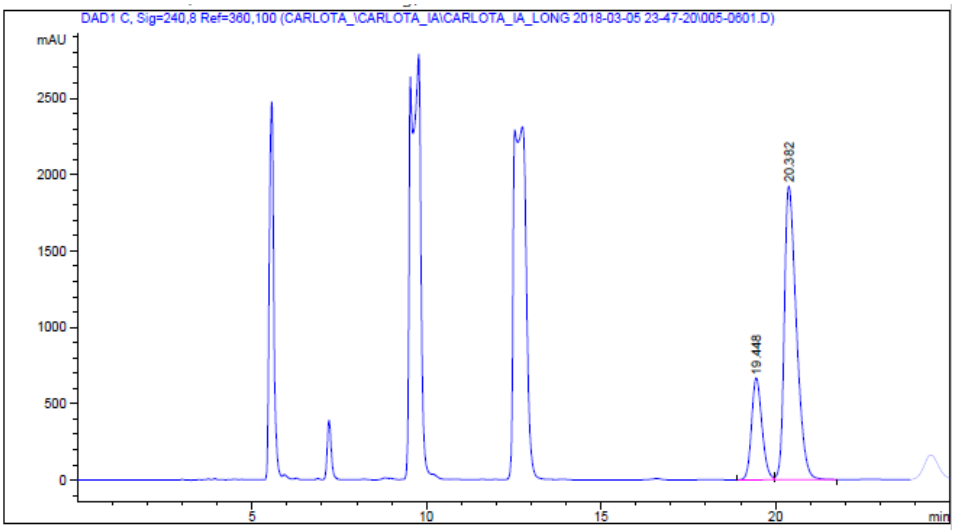

Peak #	RetTime [min]	Sig	Type	Area [mAU*s]	Height [mAU]	Area %
1	19.448	1	BV	1.38692e4	667.14166	23.0863
2	20.382	1	VB	4.62063e4	1922.49695	76.9137

HPLC analysis: Chiralpack IC, n-Hex:iPrOH = 80/20, flow rate = 1.5 mL/min, λ = 210 nm, 25°C, t.r.e1 =18.8 min, t.r.e2 = 24.6 min.

PI4

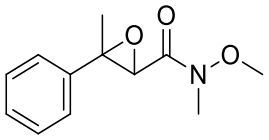

rac

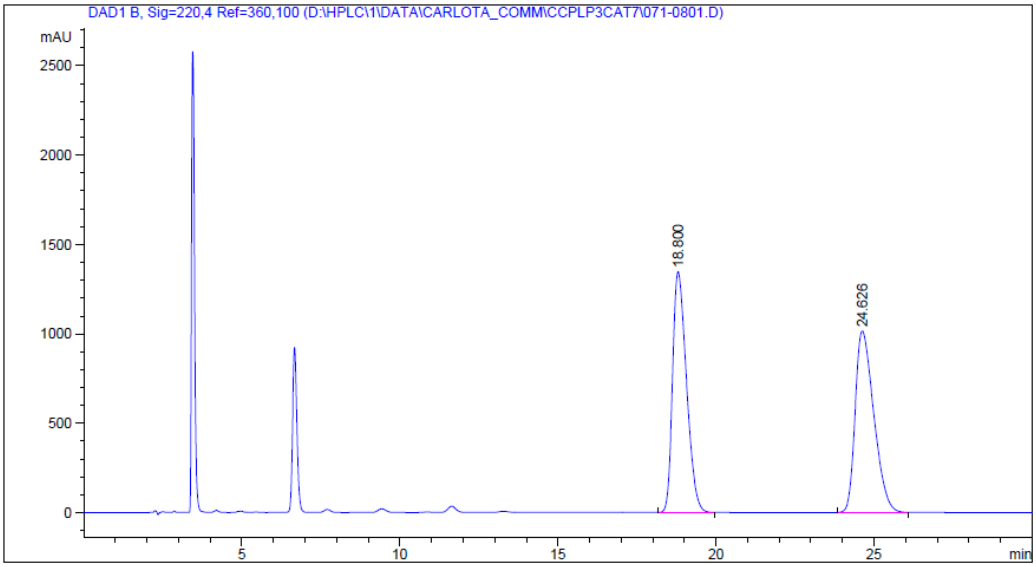

Peak #	RetTime [min]	Sig	Type	Area [mAU*s]	Height [mAU]	Area %
1	18.800	1	BB	4.11784e4	1347.11108	49.7614
2	24.626	1	BB	4.15734e4	1015.33740	50.2386

Table V.1 entry 40 (**C18**)

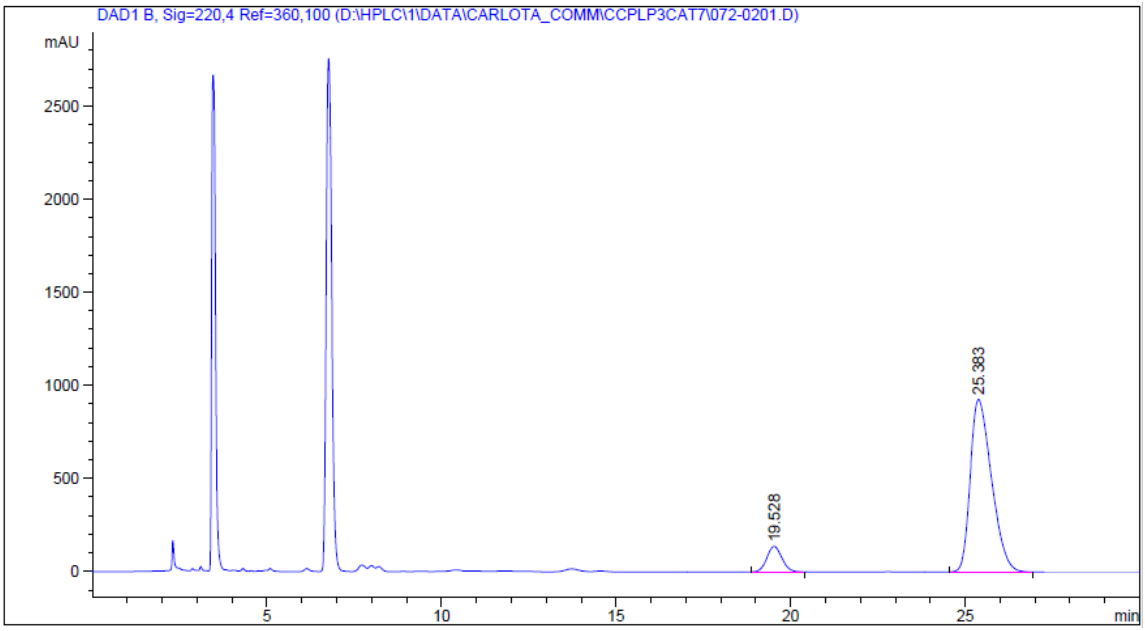

Peak #	RetTime [min]	Sig	Type	Area [mAU*s]	Height [mAU]	Area %
1	19.523	1	BB	3512.89844	117.43418	9.2651
2	25.396	1	BB	3.44026e4	824.78369	90.7349

Table V.1 entry 42 (**C19**)

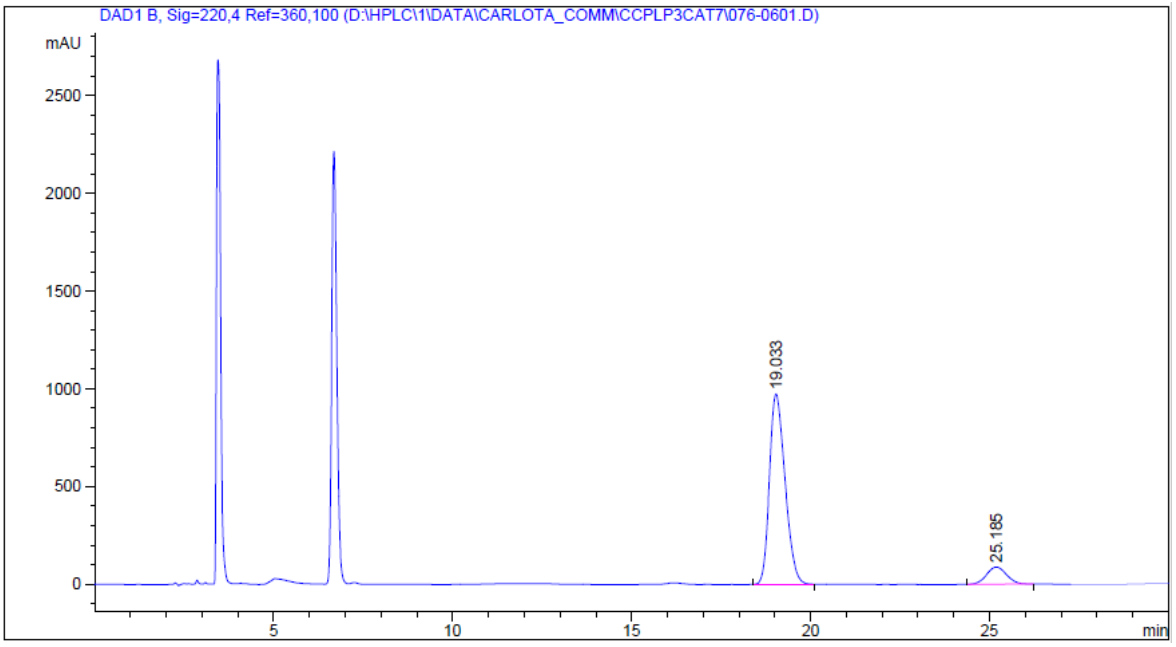

Peak #	RetTime [min]	Sig	Type	Area [mAU*s]	Height [mAU]	Area %
1	19.033	1	BB	2.94886e4	973.46149	89.5740
2	25.185	1	BB	3432.32642	88.20949	10.4260

HPLC analysis: Chiralpack IC, n-Hex:iPrOH = 80/20, flow rate = 1 mL/min, λ = 220 nm, 25°C, t.r.e1 =16.6 min, t.r.e2 = 18.9 min.

P18

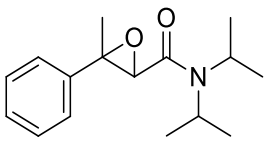

rac

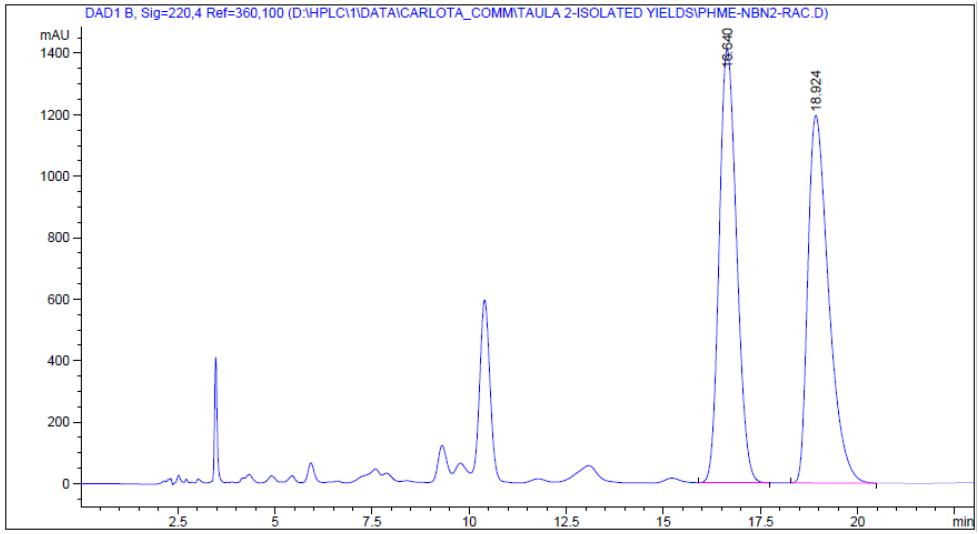

Peak #	RetTime [min]	Sig	Type	Area [mAU*s]	Height [mAU]	Area %
1	16.640	1	VB	4.40184e4	1410.32996	49.7785
2	18.924	1	BB	4.44101e4	1195.04138	50.2215

Table V.5 entry 8 (**C18**)

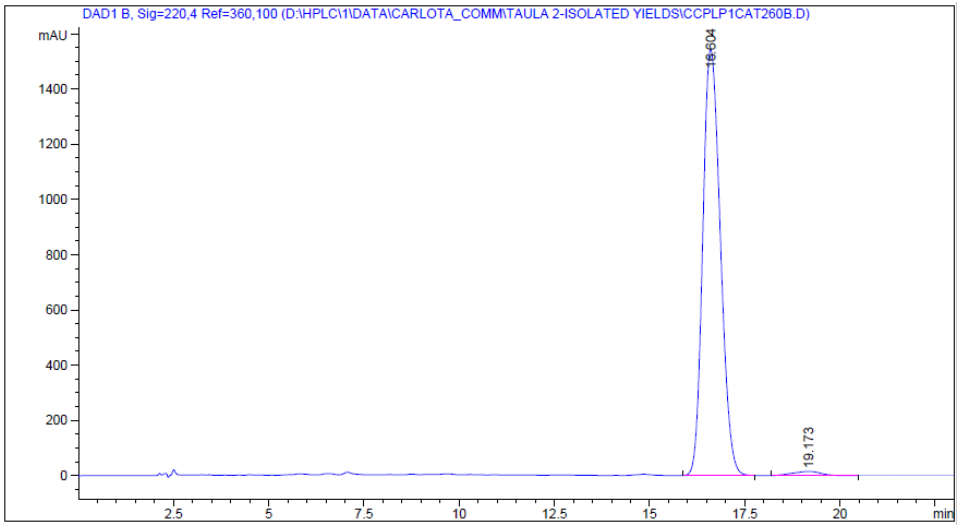

Peak #	RetTime [min]	Sig	Type	Area [mAU*s]	Height [mAU]	Area %
1	16.604	1	BB	4.94818e4	1542.41870	98.5111
2	19.173	1	BB	747.89185	14.96057	1.4889

HPLC analysis: Chiralpack IC, n-Hex:iPrOH = 80/20, flow rate = 1 mL/min, λ = 220 nm, 25°C, t.r.e1 =16.9 min, t.r.e2 = 19.6 min.

P20

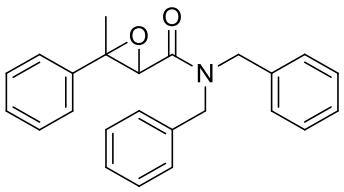

rac

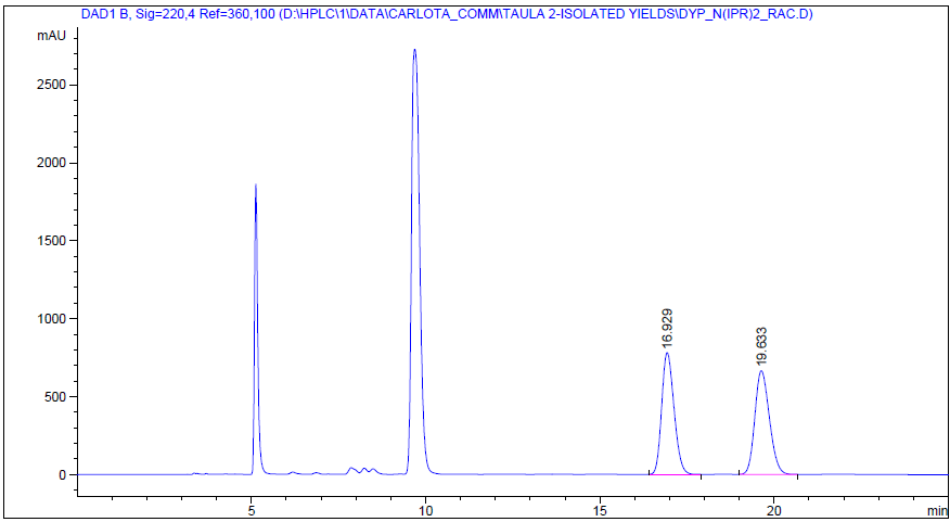

Peak #	RetTime [min]	Sig	Type	Area [mAU*s]	Height [mAU]	Area %
1	16.929	1	BB	1.92740e4	781.71869	49.9245
2	19.633	1	BB	1.93324e4	665.41058	50.0755

Table V.5 entry 13 (**C18**)

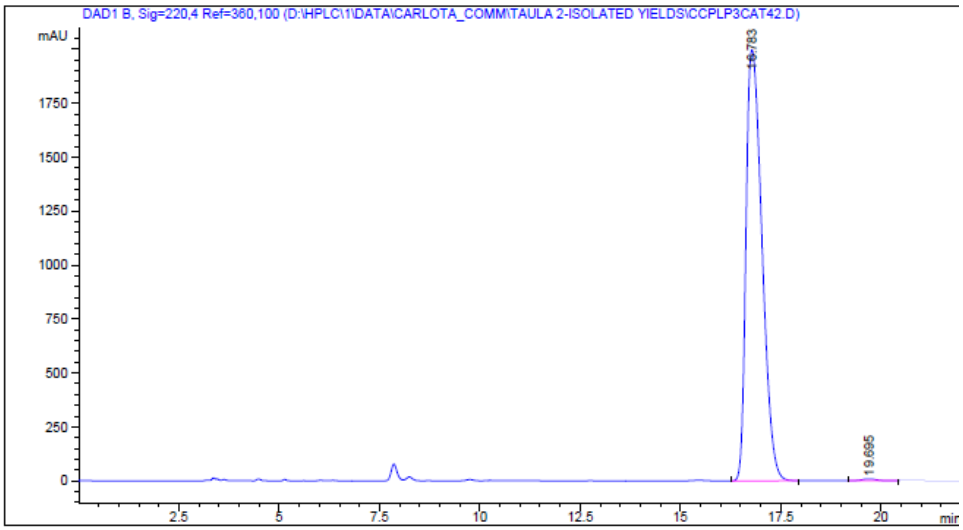

Peak #	RetTime [min]	Sig	Type	Area [mAU*s]	Height [mAU]	Area %
1	16.783	1	BB	5.51819e4	1997.44031	99.6465
2	19.695	1	BB	195.74757	7.57158	0.3535

HPLC analysis: Chiralpack IC, n-Hex:iPrOH = 80/20, flow rate = 1.5 mL/min, λ = 220 nm, 25°C, t.r.e1 =7.3 min, t.r.e2 = 14.0 min.

P24

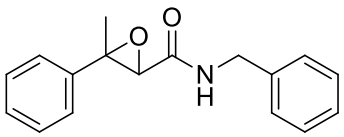

rac

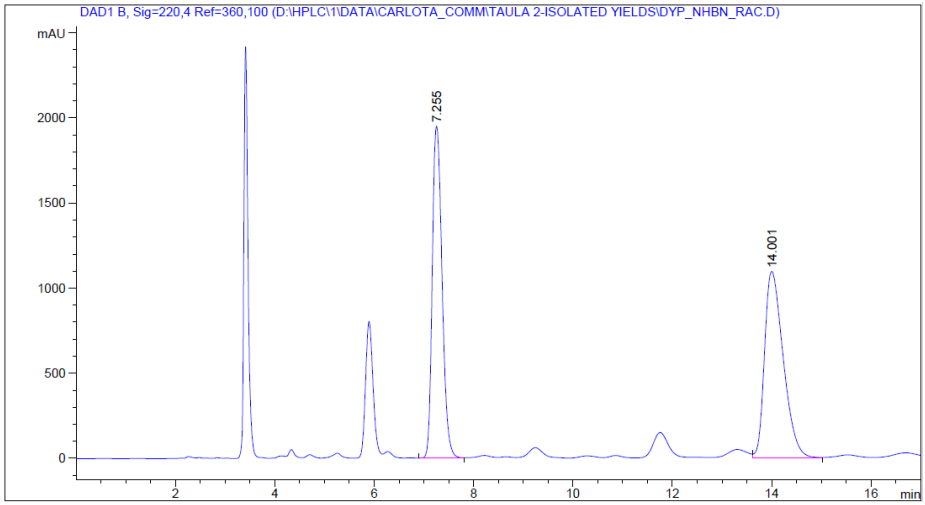

Peak #	RetTime [min]	Sig	Type	Area [mAU*s]	Height [mAU]	Area %
1	7.255	1	VV	2.66704e4	1950.68091	48.3623
2	14.001	1	VB	2.84767e4	1093.61707	51.6377

Table V.5 entry 19 (**C18**)

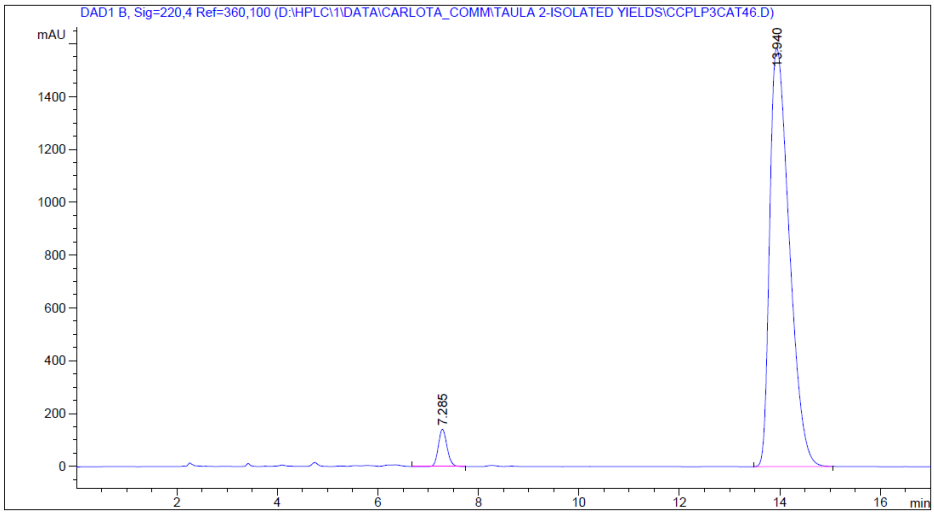

Peak #	RetTime [min]	Sig	Type	Area [mAU*s]	Height [mAU]	Area %
1	7.285	1	VB	1693.10364	141.02760	3.7981
2	13.940	1	BB	4.28841e4	1584.41846	96.2019

HPLC analysis: Chiralpack IC, n-Hex:iPrOH = 80/20, flow rate = 1.5 mL/min, λ = 220 nm, 25°C, t.r.e1 =11.7 min, t.r.e2 = 16.2 min.

P27

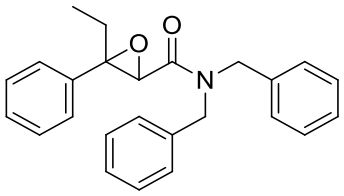

rac

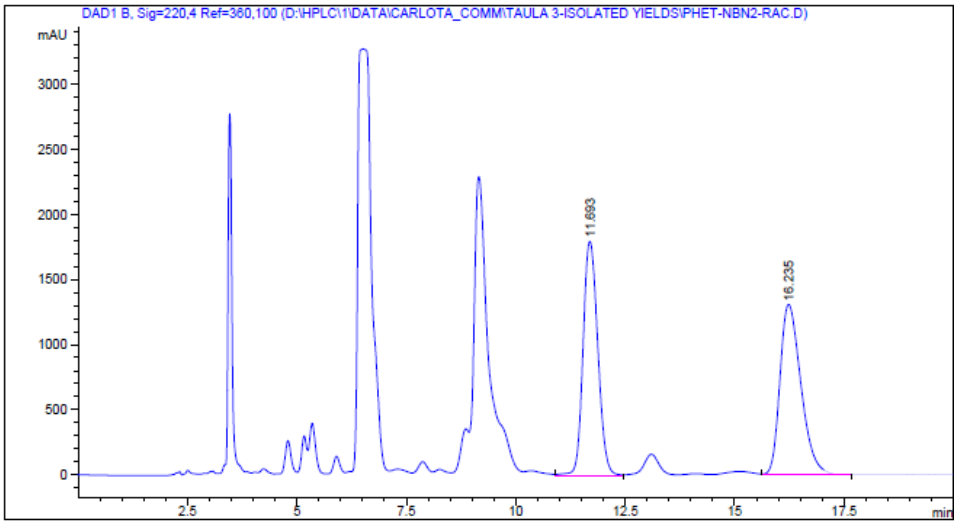

Peak #	RetTime [min]	Sig	Type	Area [mAU*s]	Height [mAU]	Area %
1	11.693	1	VV	4.19461e4	1797.18799	48.8658
2	16.235	1	VB	4.38932e4	1311.67285	51.1342

Table V.6 entry 2 (**C18**)

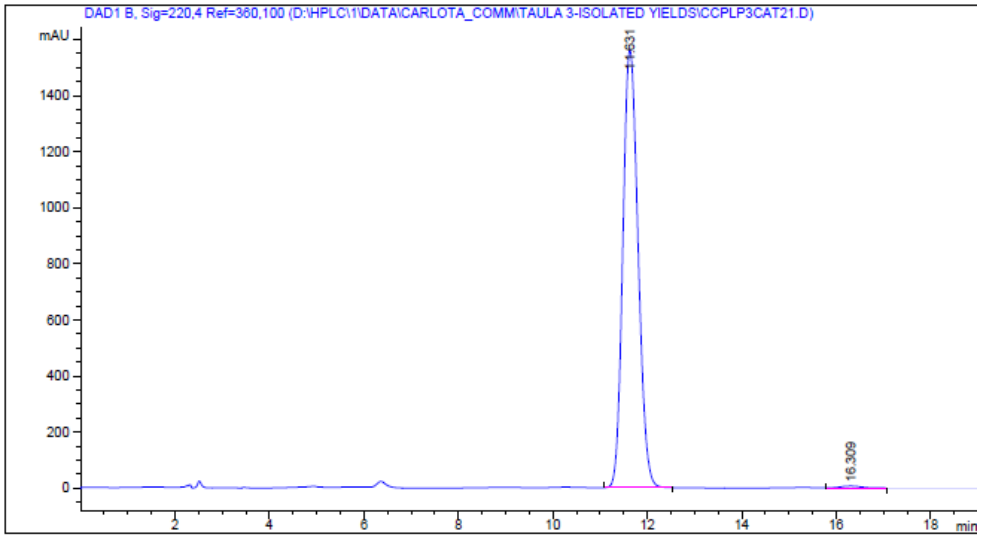

Peak #	RetTime [min]	Sig	Type	Area [mAU*s]	Height [mAU]	Area %
1	11.631	1	BB	3.49396e4	1562.86584	99.4574
2	16.309	1	BB	190.62032	6.33166	0.5426

HPLC analysis: Chiralpack IC, n-Hex:iPrOH = 80/20, flow rate = 1.5 mL/min, λ = 220 nm, 25°C, t.r.e1 =15.1 min, t.r.e2 = 18.8 min.

P31

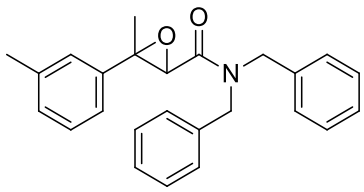

rac

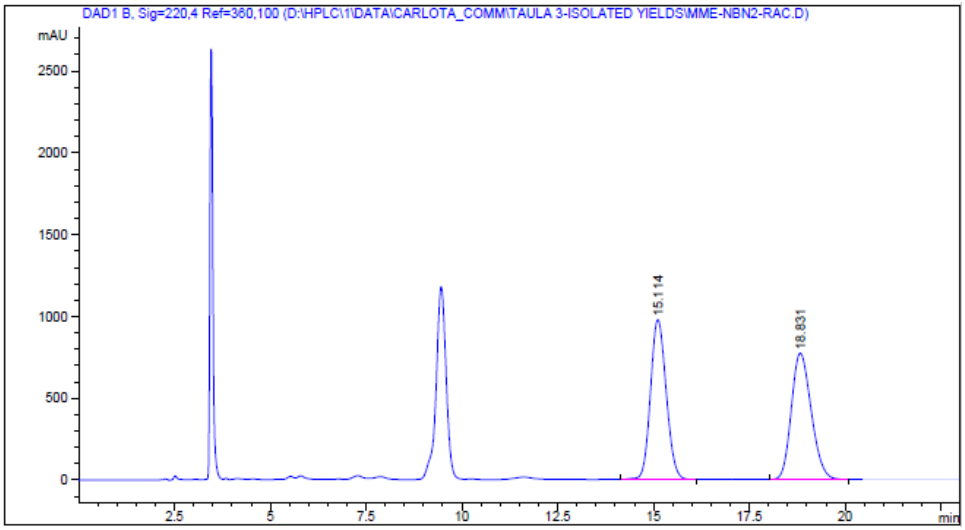

Peak #	RetTime [min]	Sig	Type	Area [mAU*s]	Height [mAU]	Area %
1	15.114	1	BB	2.78229e4	976.66205	50.0215
2	18.831	1	VB	2.77990e4	771.61194	49.9785

Table V.6 entry 8 (**C18**)

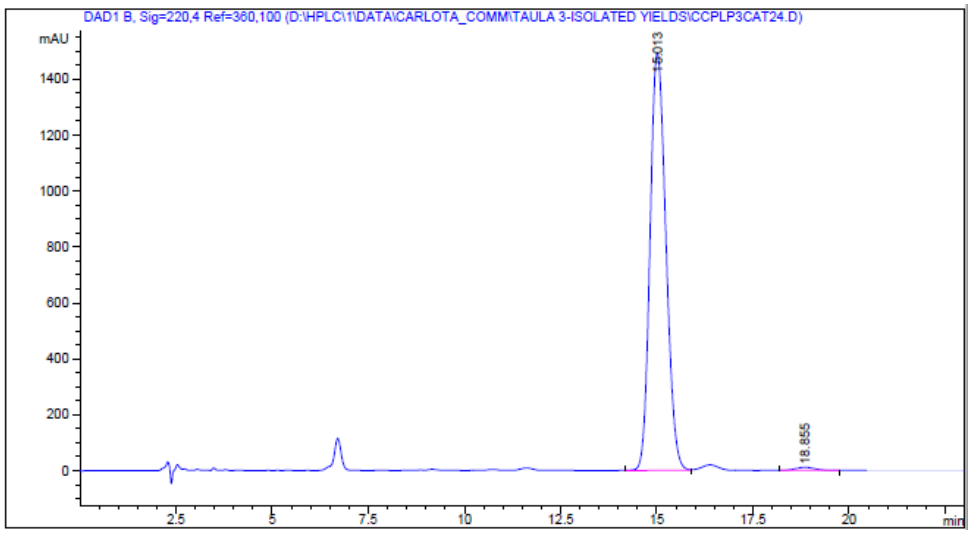

Peak #	RetTime [min]	Sig	Type	Area [mAU*s]	Height [mAU]	Area %
1	15.013	1	BV	4.28163e4	1493.05298	99.2228
2	18.855	1	BB	335.36014	10.41287	0.7772

HPLC analysis: Chiralpack IC, n-Hex:iPrOH = 90/10, flow rate = 1.5 mL/min, λ = 220 nm, 25°C, t.r.e1 =29.2 min, t.r.e2 = 31.6 min.

P36

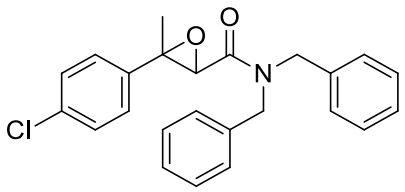

rac

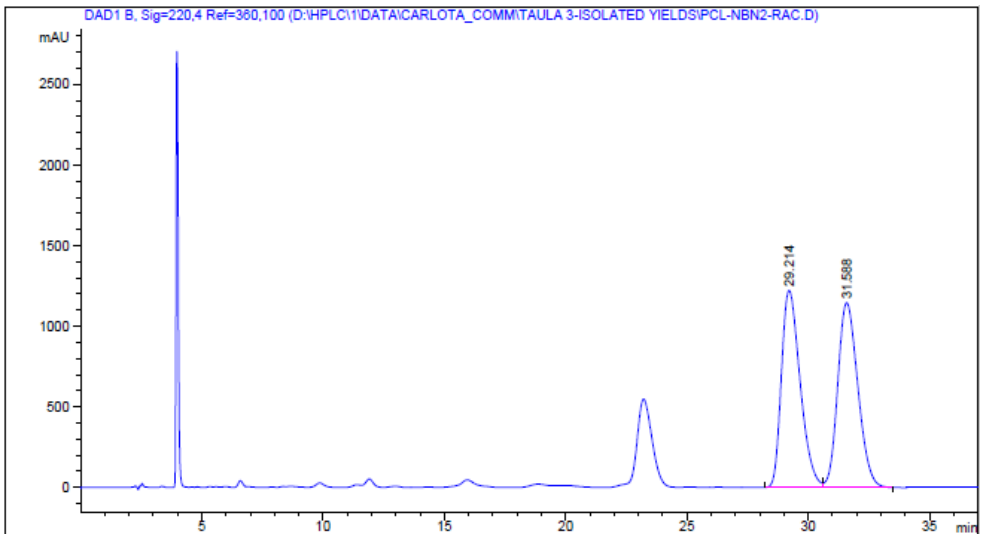

Peak #	RetTime [min]	Sig	Type	Area [mAU*s]	Height [mAU]	Area %
1	29.214	1	BV	6.57155e4	1222.97876	49.7979
2	31.588	1	VB	6.62488e4	1146.67346	50.2021

Table V.6 entry 20 (**C18**)

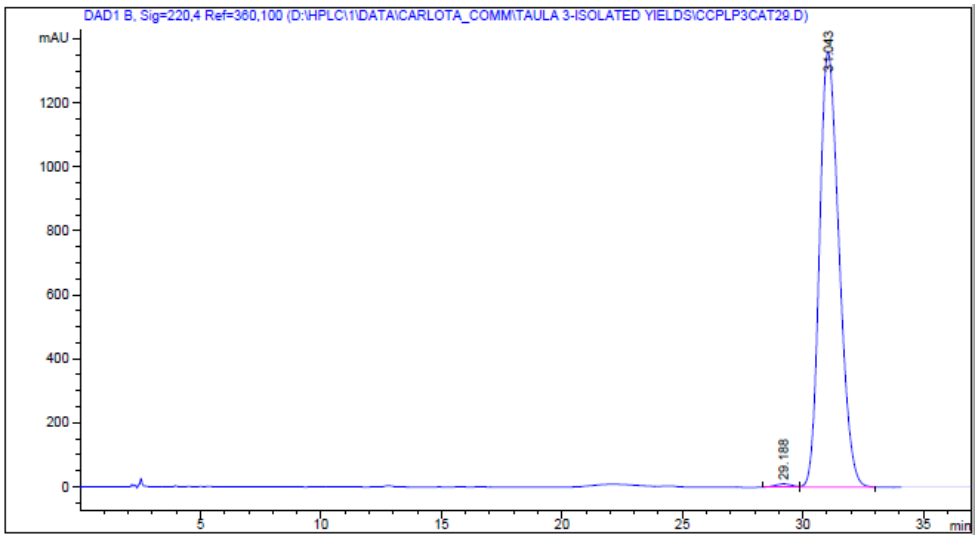

Peak #	RetTime [min]	Sig	Type	Area [mAU*s]	Height [mAU]	Area %
1	29.188	1	BV	482.96341	9.95271	0.6221
2	31.043	1	VB	7.71511e4	1361.76770	99.3779

Annex chapter VI

^{1}H and ^{13}C-NMR spectra of ligands

^{1}H-NMR of **L8** in $CDCl_3$

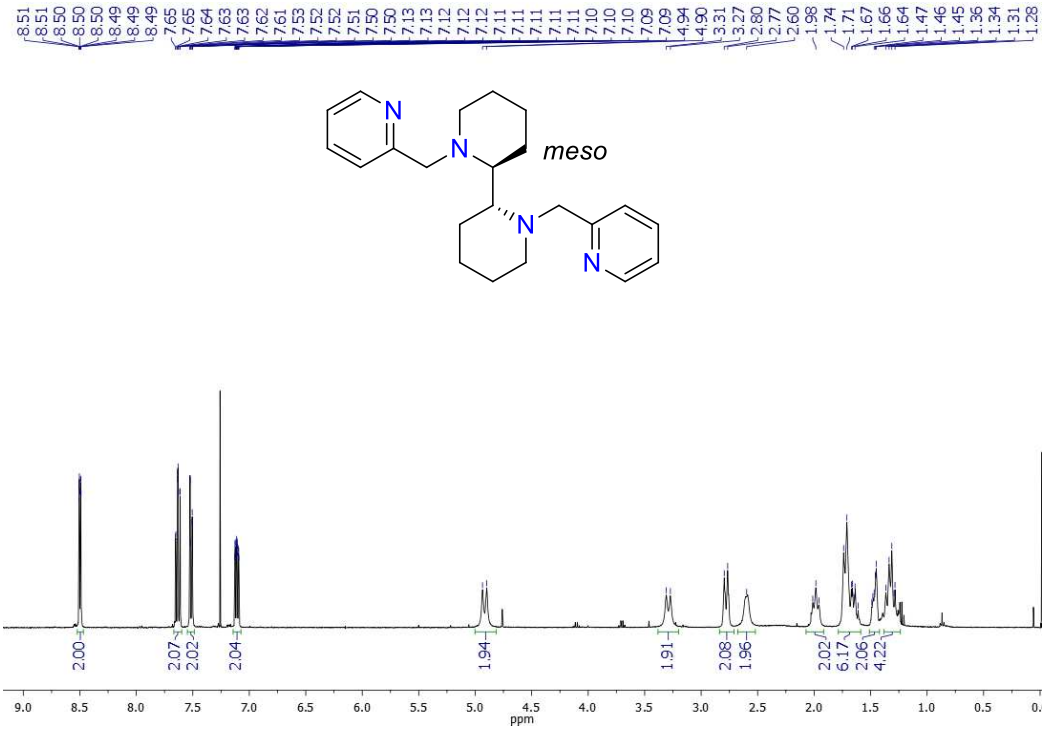

^{13}C-NMR of **L8** in $CDCl_3$

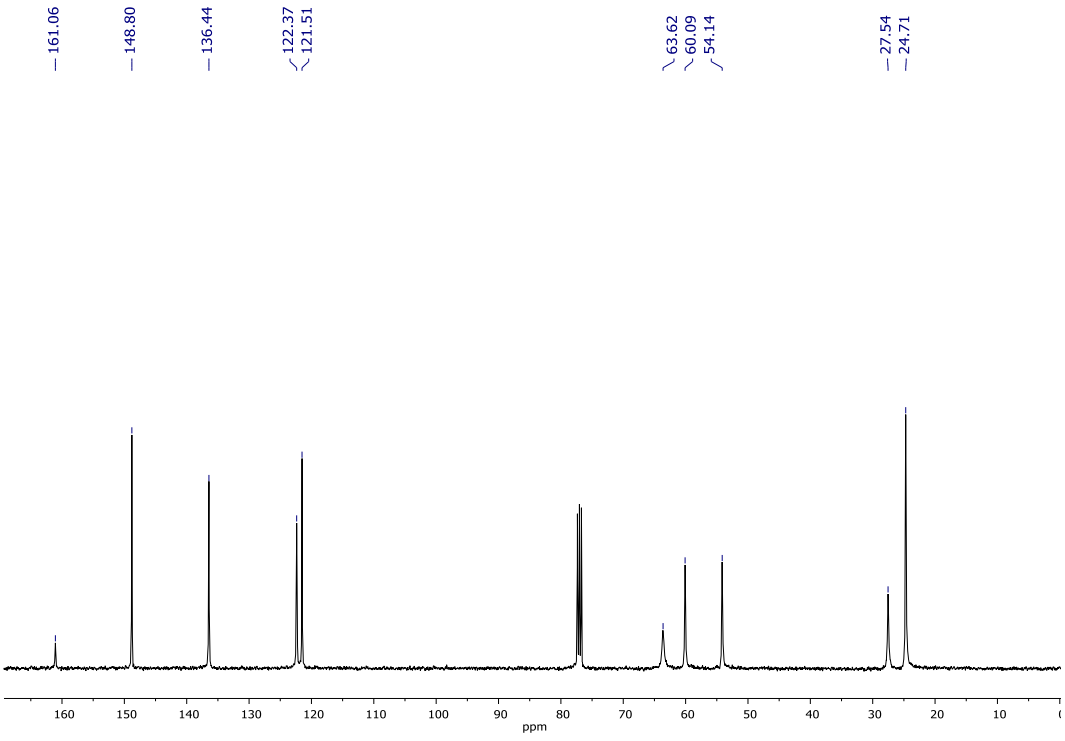

^{1}H-NMR of **L9** in $CDCl_3$

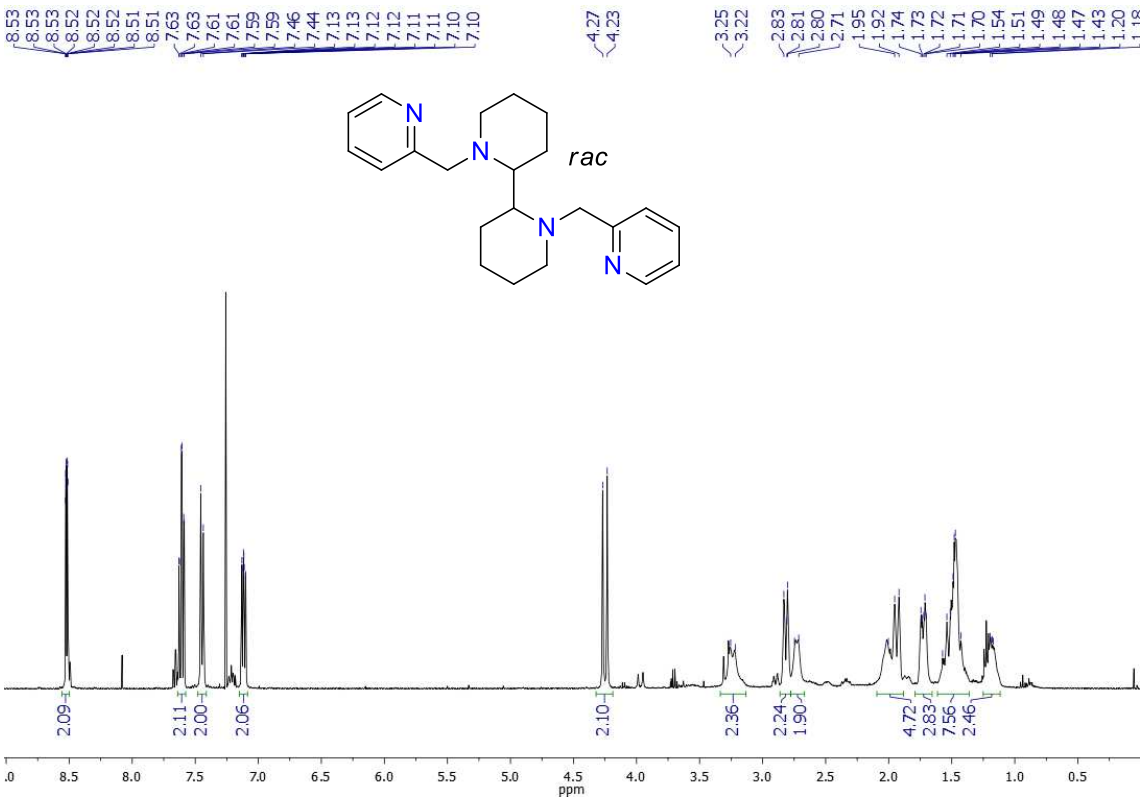

^{13}C-NMR of **L9** in $CDCl_3$

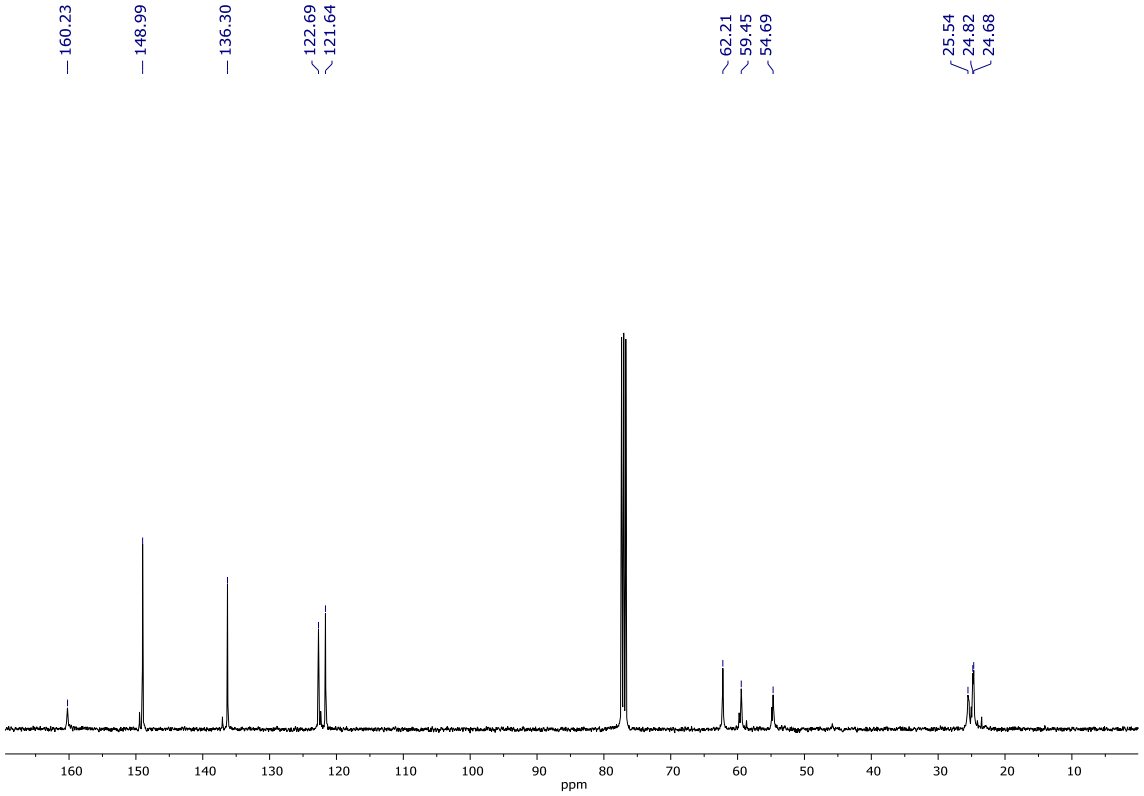

^{1}H-NMR of **L10** in $CDCl_3$

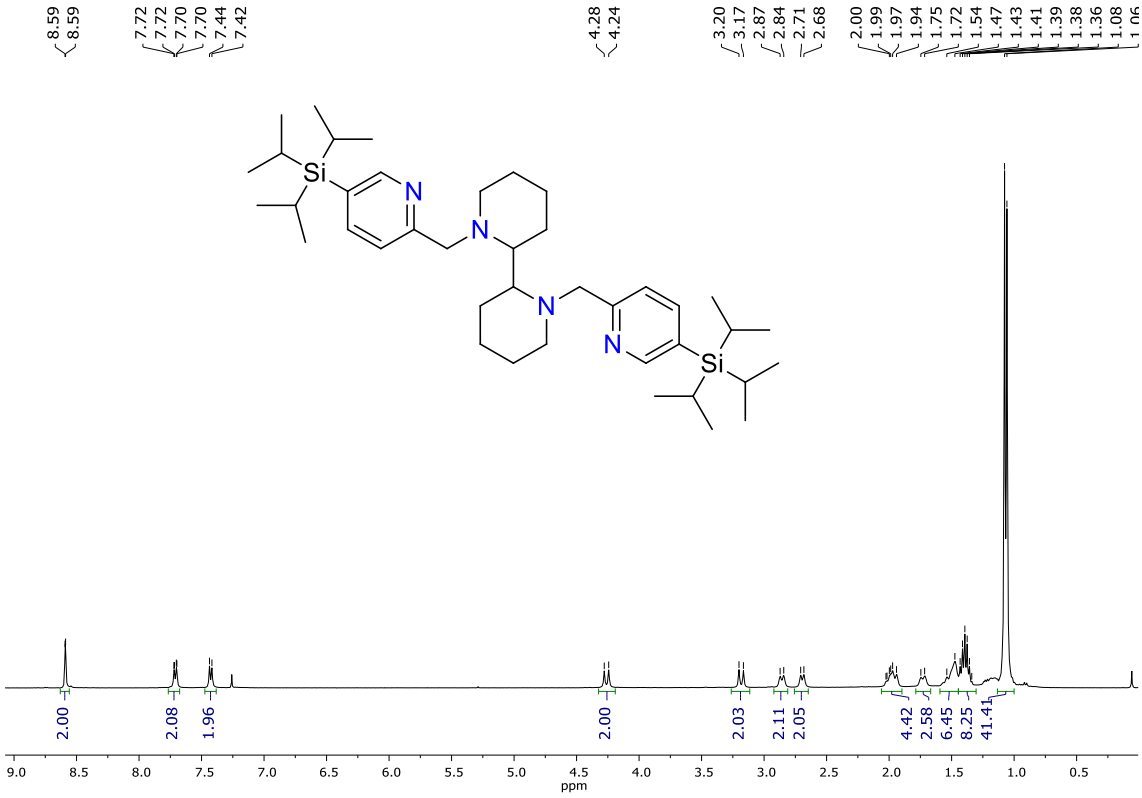

^{13}C-NMR of **L10** in $CDCl_3$

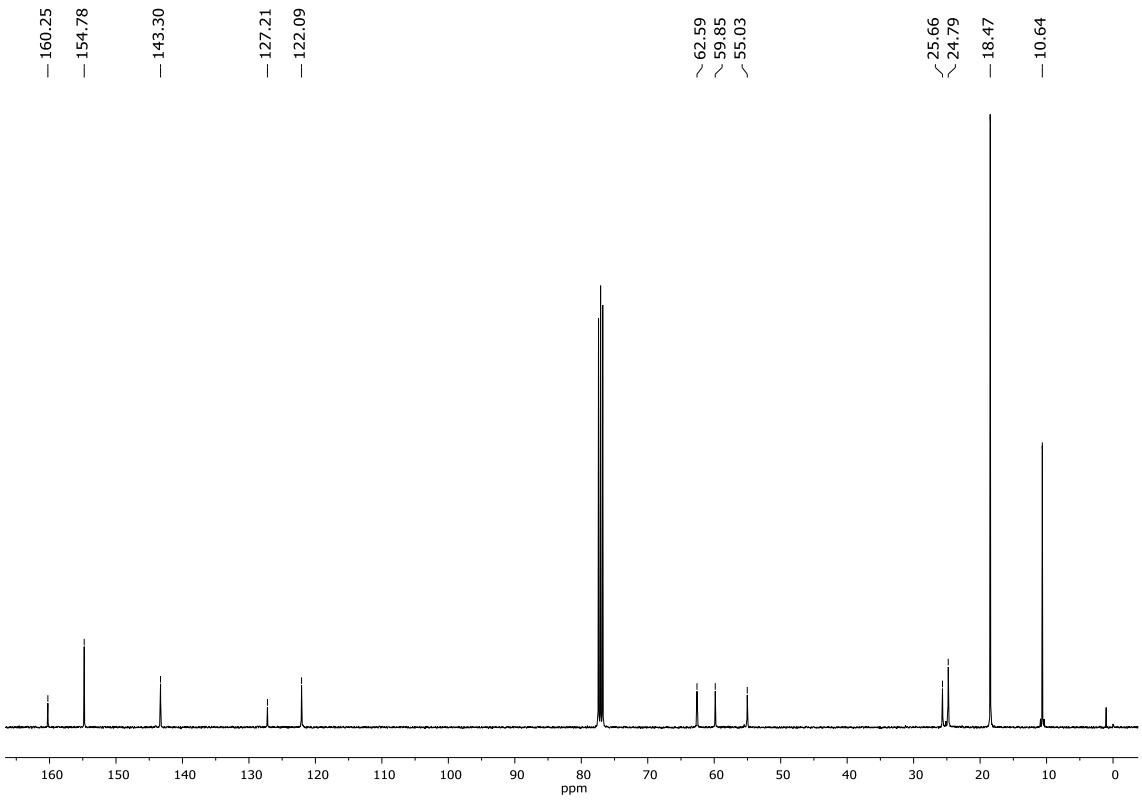

Representative GC spectra of crude reactions

Table VI.4 entry 6 (**S43**)

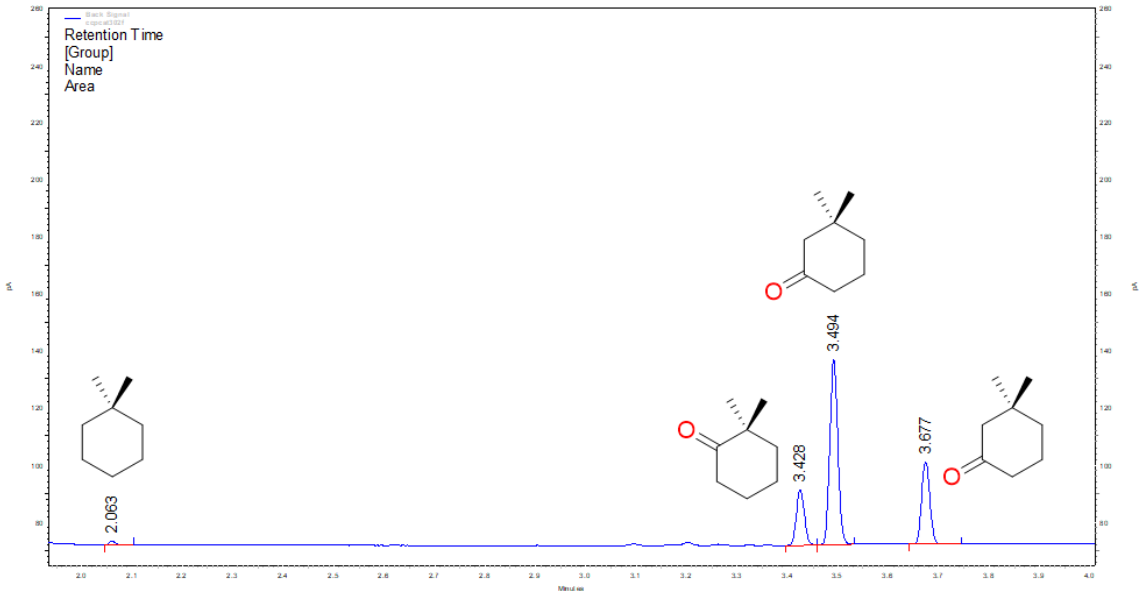

Table VI.5 entry 6 (**S44**)

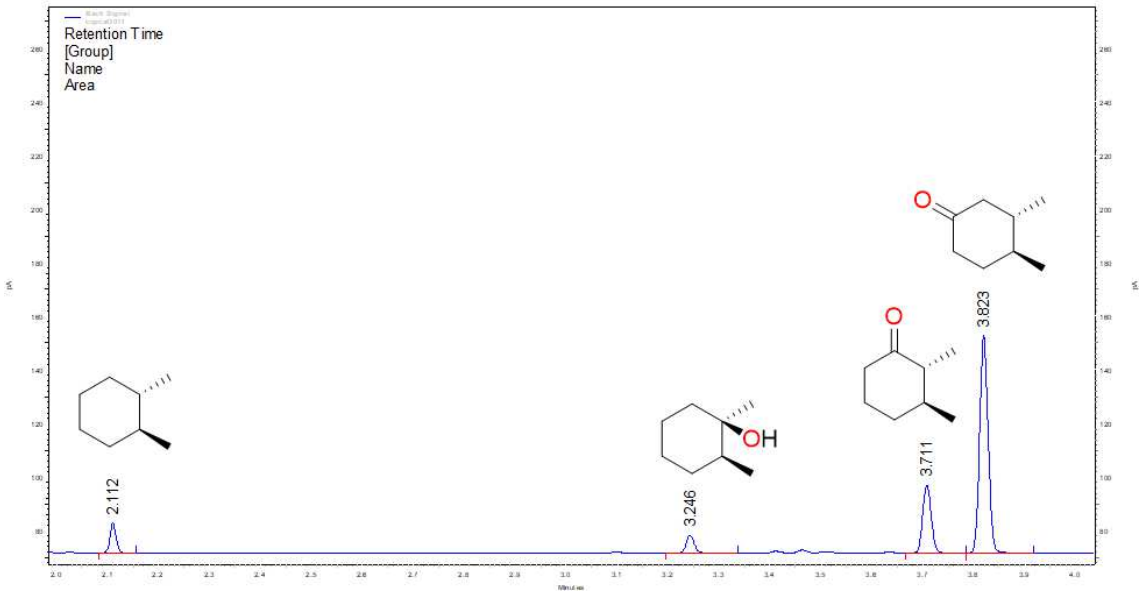

Table VI.6 entry 6 (**S45**)

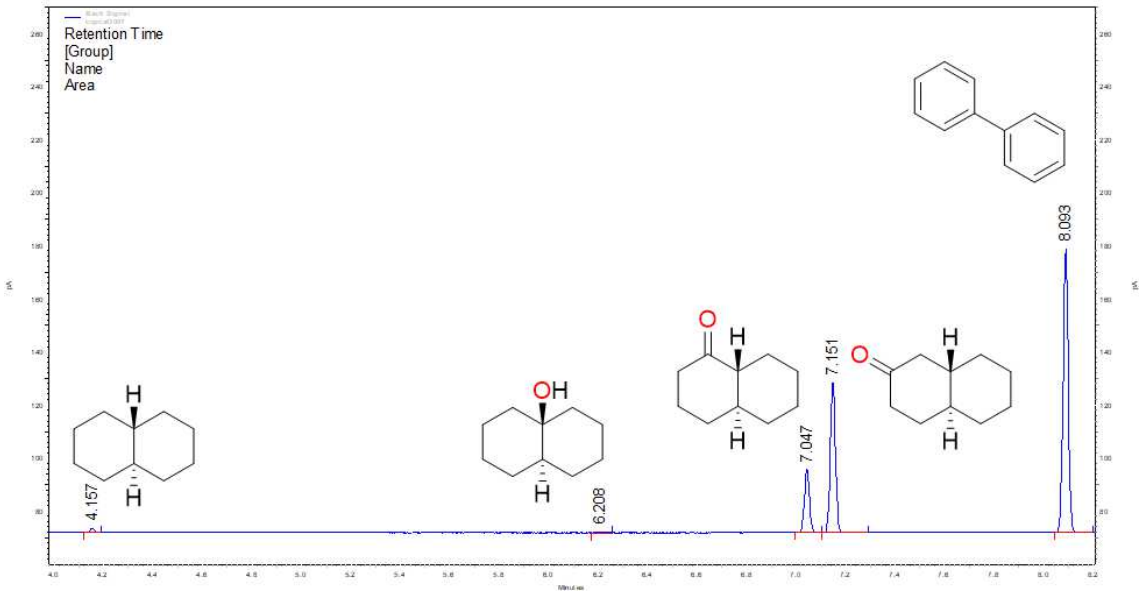

Table VI.8 entry 2 (**S46**)

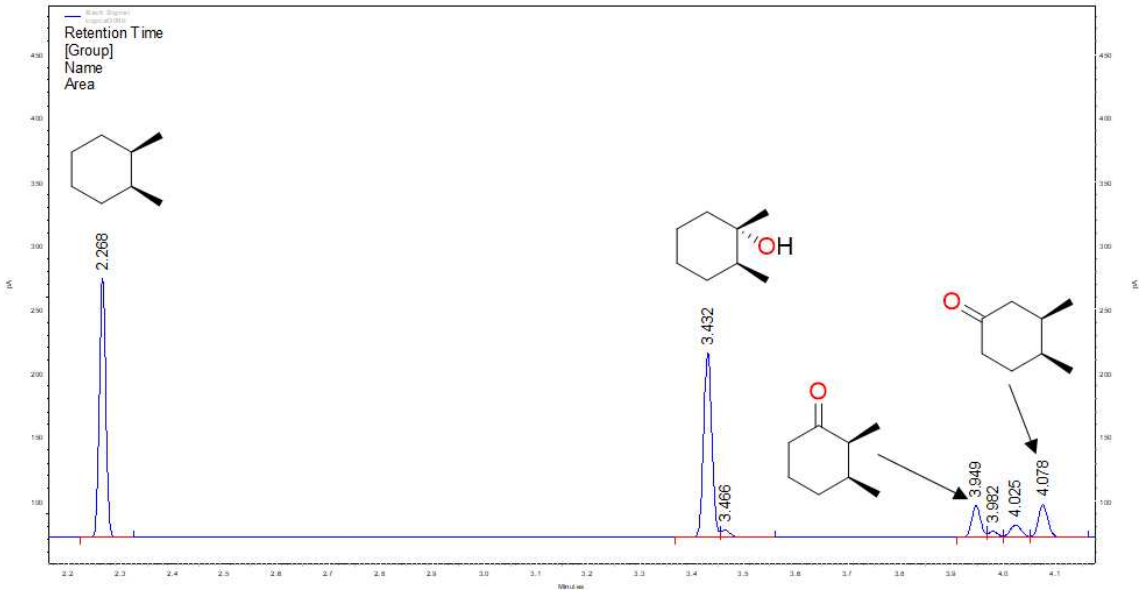

Table VI.8 entry 4 (**S47**)

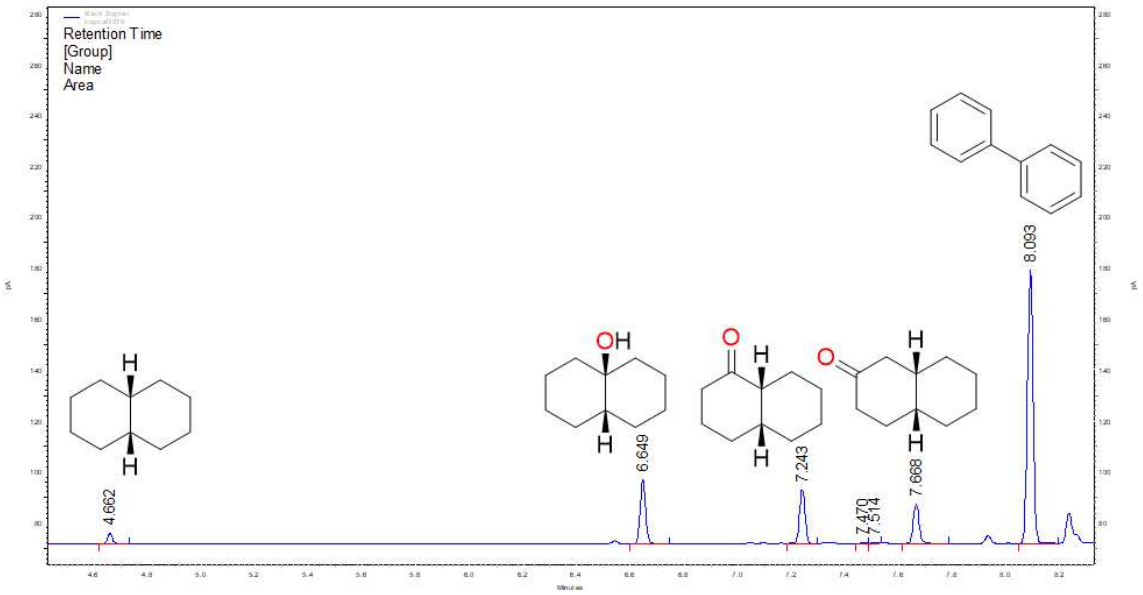

Table VI.9 entry 2 (**S48**)

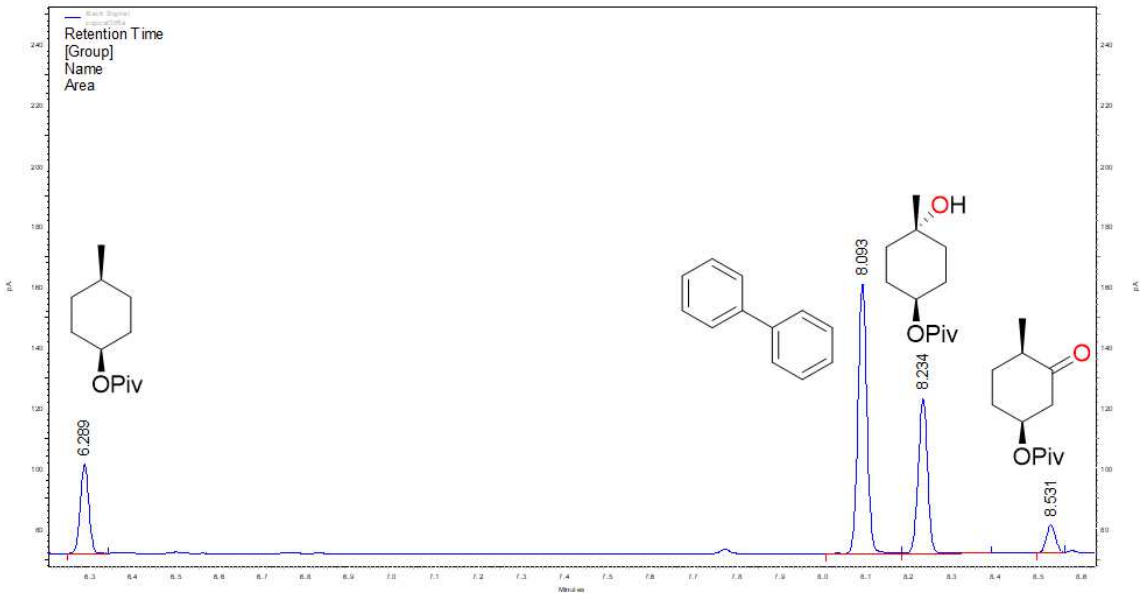

Table VI.9 entry 4 (**S49**)

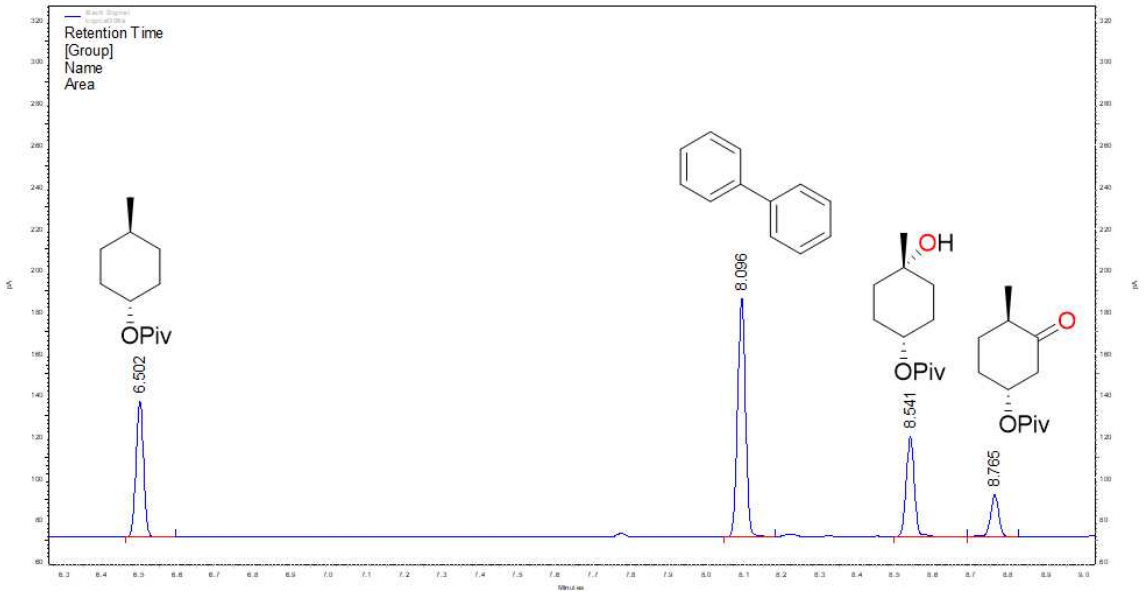

Table VI.10 entry 2 (**S50**)

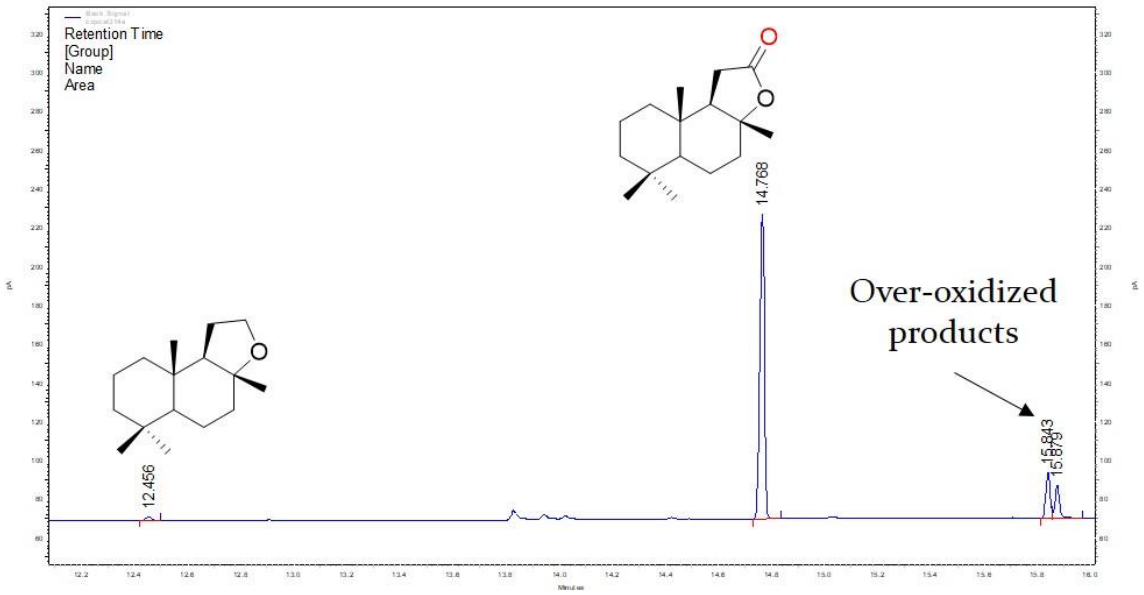

Table VI.11 entry 2 (**S51**)

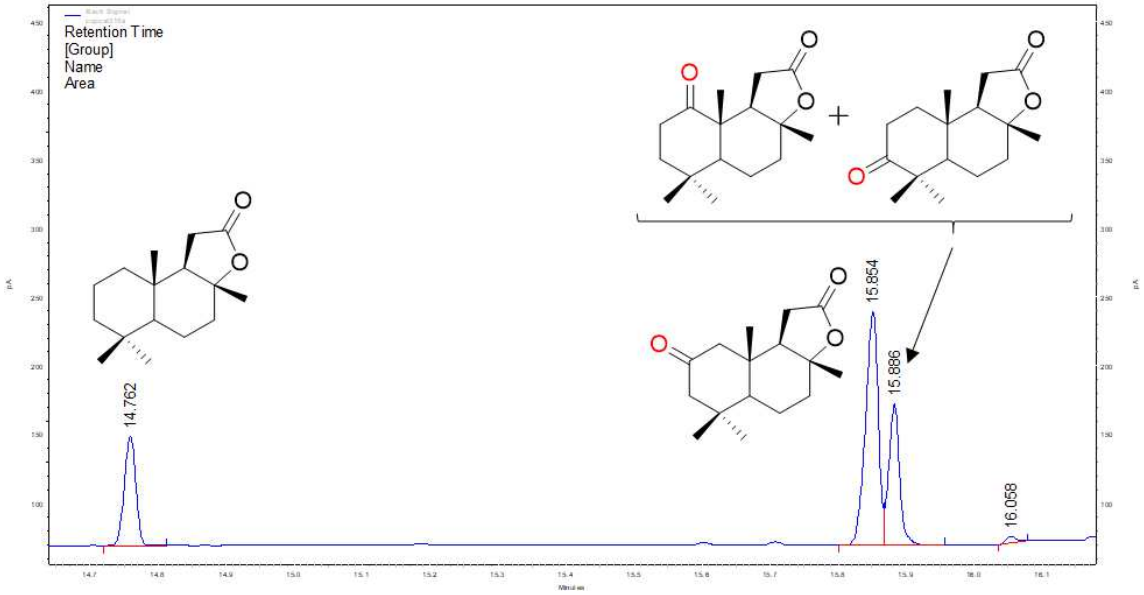

Table VI.12 entry 2 (**S52**)

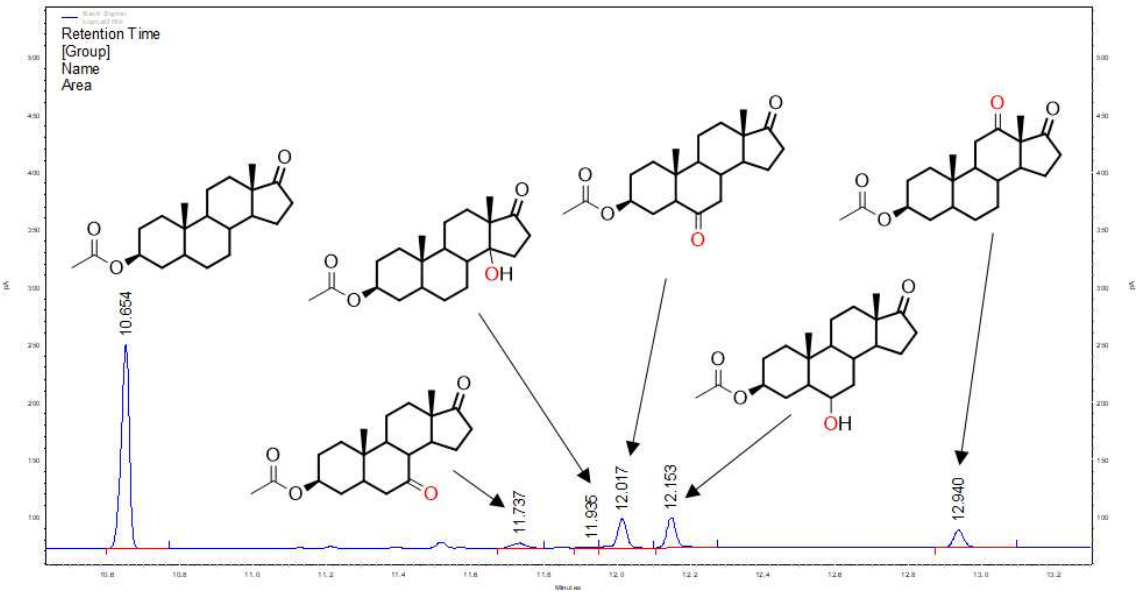

Table VI.12 entry 3 (**S52**)

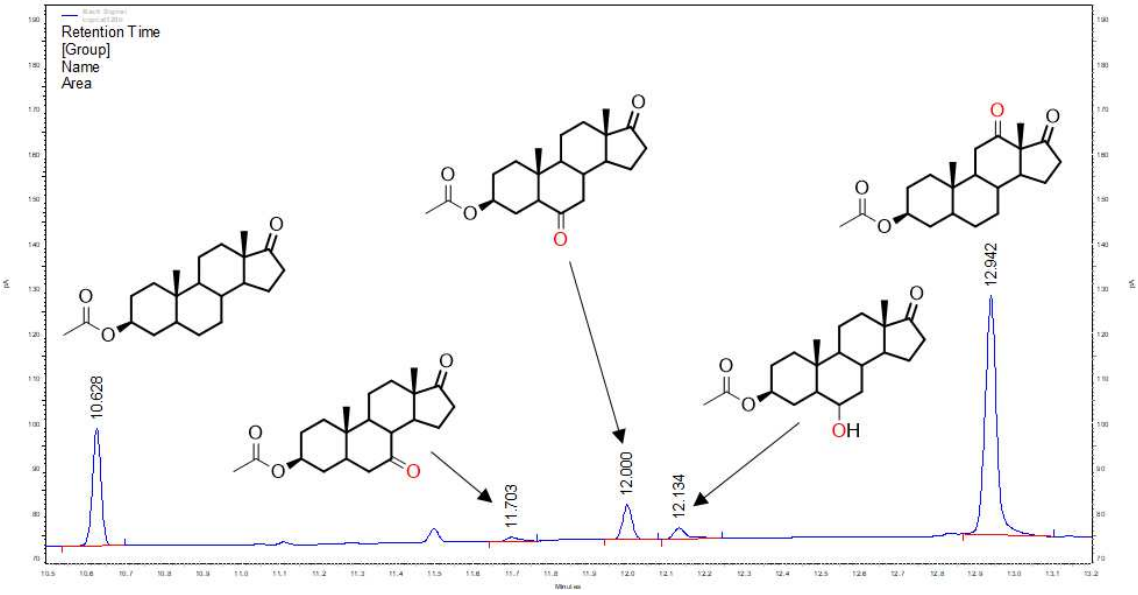

Table VI.12 entry 5 (**S53**)

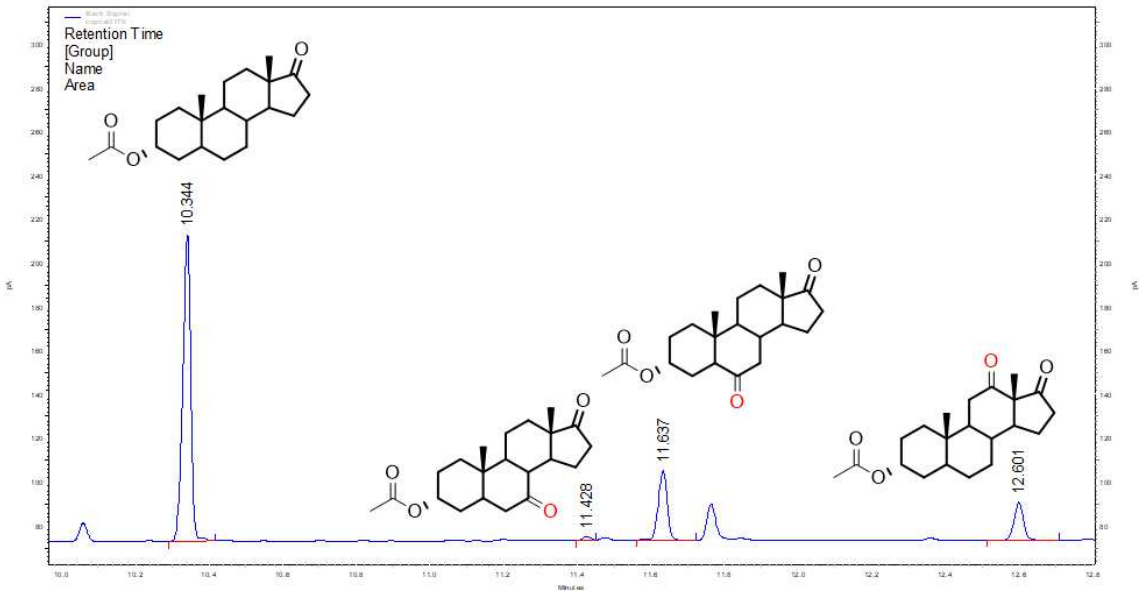

Table VI.12 entry 6 (**S53**)

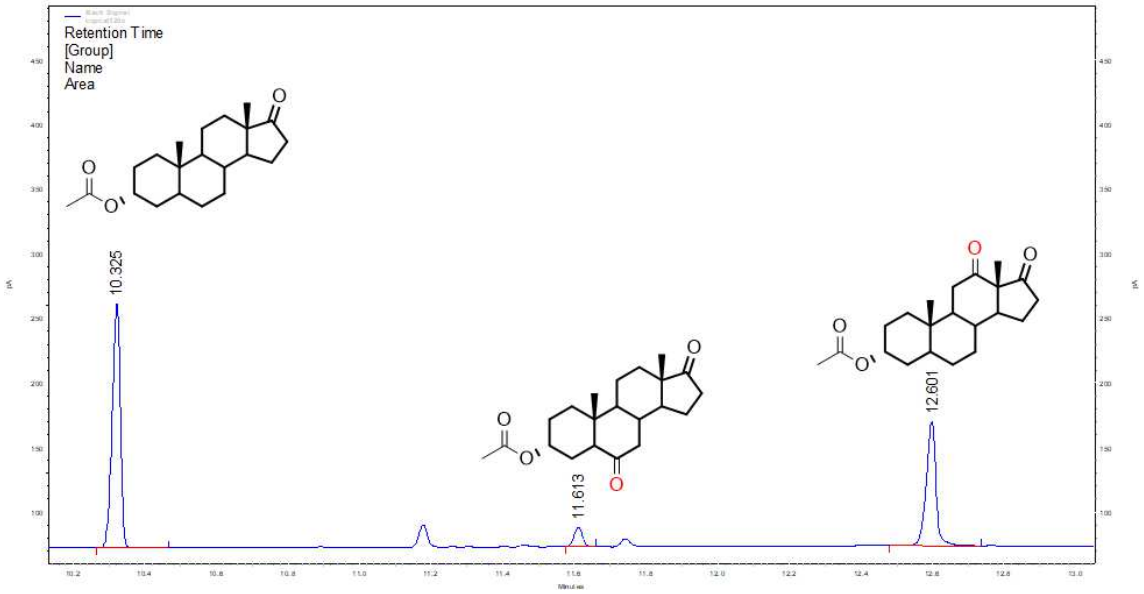

X-ray data

The X-ray structures of **C21-C26** complexes are depicted in figure S.2, experimental details of their crystal structure determination are collected in tables S.5 and S.6.

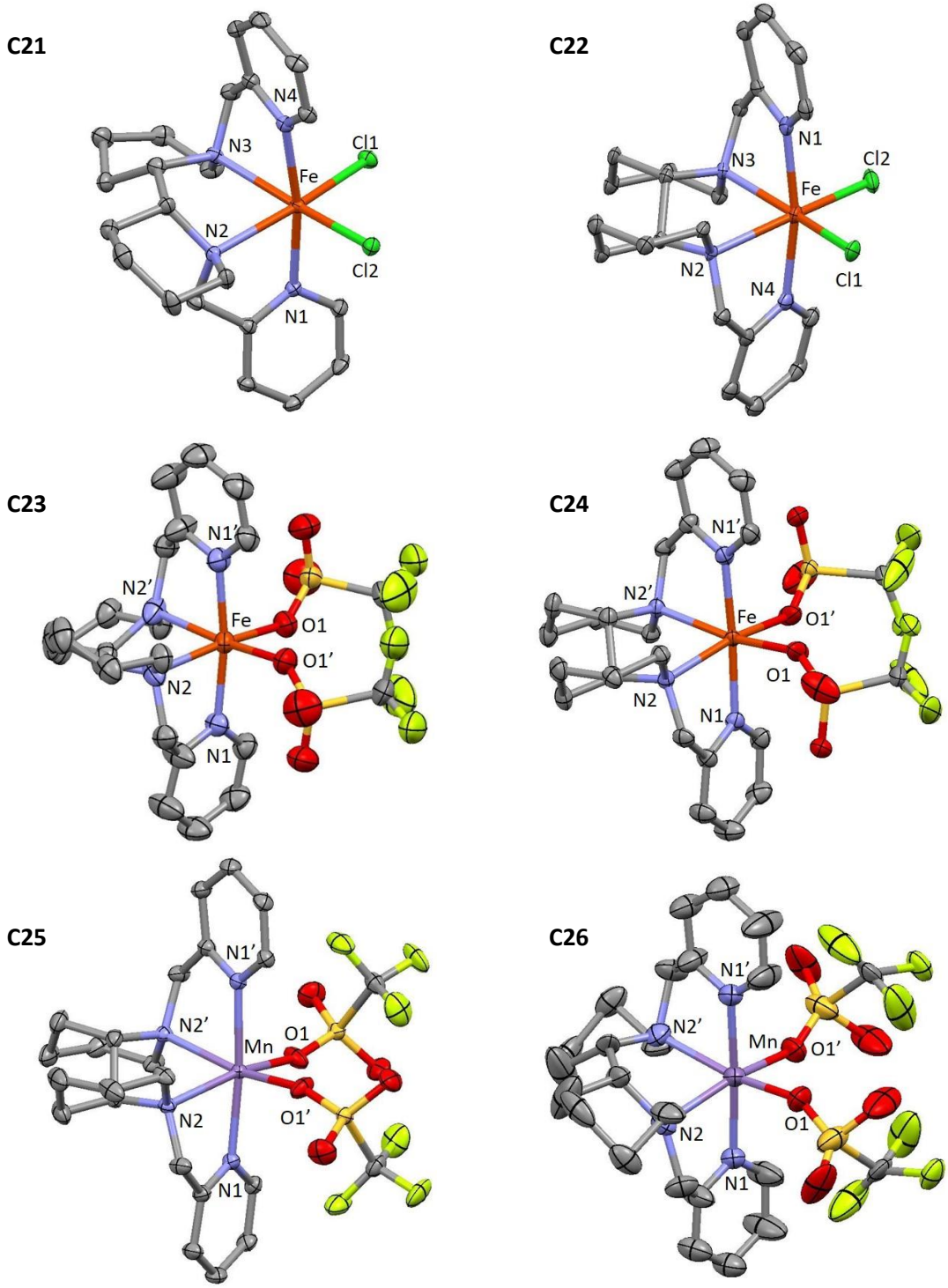

Figure S.2. Ellipsoid diagrams of **C21-C26** complexes at a 50% of probability. Hydrogen atoms were omitted for clarity.

Table S.5. Crystal data for **C21**, **C22** and **C23** complexes.

Compound	**C21**	**C22**	**C23**
Empirical formula	$C_{22}H_{30}Cl_{12}FeN_4$	$C_{24}H_{30}F_6FeN_4O_6S_2$	$C_{26}H_{34}Cl_4F_6MnN_4O_6S_2$
Formula weight	477.25	704.49	873.43
Temperature	173 (2) K	173(2) K	100(2) K
Wavelength	0.71073 Å	0.71073 Å	0.71073 Å
Crystal system	Monoclinic	Monoclinic	Monoclinic
Space group	P 21	C 2	C 2
Unit cell dimensions	a = 9.725(2) Å α = 90° b = 13.805(3) Å β = 91.968(4)° c = 16.039(4) Å γ = 90°	a = 16.665(4) Å α = 90° b = 11.523(3) Å β = 115.067(3)° c = 17.042(4) Å γ = 90°	a = 21.989(7) Å α = 90° b = 11.572(4) Å β = 127.830(6)° c = 17.578(6) Å γ = 90°
Volume	2152.0(8) A^3	2964.4(13) A^3	3533(2) A^3
Z, Density (calculated)	4, 1.473Mg/m^3	4, 1.579 Mg/m^3	4, 1.642Mg/m^3
Absorption coefficient	0.966mm^{-1}	0.733 mm^{-1}	0.872 mm^{-1}
F(000)	1000	1448	1780
Crystal size	0.25 x 0.22 x 0.10 mm	0.25 x 0.25 x 0.10 mm	0.38 x 0.35 x 0.30 mm
Θ range for data collection	2.541 to 27.749°	2.224 to 28.228°	2.115 to 28.330°
Limiting indices	-12<=h<=12 -18<=k<=17 -20<=l<=20	-22<=h<=21 -15<=k<=15 -22<=l<=22	-24<=h<=28 -10<=k<=15 -22<=l<=23
Reflections collected/unique	30506 / 5042 [R(int) = 0.0629]	22194 / 3638 [R(int) = 0.0399]	10773 / 4083 [R(int) = 0.0694]
Completeness to Θ	99.8% (Θ = 25.242°)	100.0% (Θ = 25.242°)	99.8% (Θ = 25.242°)
Refinement method	Full-matrix least-squares on F^2	Full-matrix least-squares on F^2	Full-matrix least-squares on F^2
Data/restraints/parameters	5042 / 0 / 262	3638 / 3 / 248	4083 / 0 / 323
Goodness-of-fit on F2	1.087	1.024	1.066
Final R indices	R1 = 0.0593 wR2 = 0.1255	R1 = 0.0582 wR2 = 0.1485	R1 = 0.0662 wR2 = 0.1488
R indices (all data)	R1 = 0.0795 wR2 = 0.1348	R1 = 0.0740 wR2 = 0.1605	R1 = 0.1235 wR2 = 0.1732
Largest diff. peak and hole	1.118 and -0.392 $e.A^{-3}$	1.096 and -0.932 $e.A^{-3}$	0.472 and -0.644 $e.A^{-3}$

Table S.6. Crystal data for **C24, C25** and **C26** complexes.

Compound	**C24**	**C25**	**C26**
Empirical formula	$C_{22}H_{30}Cl_{12}FeN_4$	$C_{24}H_{30}F_6FeN_4O_6S_2$	$C_{26}H_{34}Cl_4F_6MnN_4O_6S_2$
Formula weight	477.25	704.49	873.43
Temperature	100 (2) K	293(2) K	100(2) K
Wavelength	0.71073 Å	0.71073 Å	0.71073 Å
Crystal system	Monoclinic	Monoclinic	Monoclinic
Space group	P 21	C 2	C 2
Unit cell dimensions	a = 9.530(2) Å α = 90° b = 16.485(4) Å β = 92.540(5)° c = 13.956(3) Å γ = 90°	a = 16.181(11) Å α = 90° b = 11.962(8) Å β = 116.810(10)° c = 17.132(11) Å γ = 90°	a = 22.6485(13) Å α = 90° b = 11.4226(7) Å β = 128.4560(10)° c = 17.7167(11) Å γ = 90°
Volume	2190.5(9) A^3	2960(3) A^3	3589.2(4) A^3
Z, Density (calculated)	4, 1.447Mg/m^3	4, 1.581 Mg/m^3	4, 1.616Mg/m^3
Absorption coefficient	0.949mm^{-1}	0.734 mm^{-1}	0.858 mm^{-1}
F(000)	1000	1448	1780
Crystal size	0.20 x 0.15 x 0.05 mm	0.25 x 0.25 x 0.18 mm	0.25 x 0.20 x 0.20 mm
Θ range for data collection	1.913 to 28.299°	2.211 to 28.430°	2.121 to 28.335°
Limiting indices	-12<=h<=7 -21<=k<=21 -17<=l<=16	-21<=h<=21 -16<=k<=15 -22<=l<=22	-30<=h<=29 -15<=k<=15 -23<=l<=23
Reflections collected/unique	12994 / 5010 [R(int) = 0.0871]	20939 / 3660 [R(int) = 0.0344]	27771 / 4454 [R(int) = 0.0312]
Completeness to Θ	99.2% (Θ = 25.242°)	99.7% (Θ = 25.242°)	100.0% (Θ = 25.242°)
Refinement method	Full-matrix least-squares on F^2	Full-matrix least-squares on F^2	Full-matrix least-squares on F^2
Data/restraints/parameters	5010 / 0 / 262	3660 / 0 / 195	4454 / 0 / 222
Goodness-of-fit on F2	0.988	1.029	1.024
Final R indices	R1 = 0.0671 wR2 = 0.1543	R1 = 0.0495 wR2 = 0.1183	R1 = 0.0398 wR2 = 0.0973
R indices (all data)	R1 = 0.1157 wR2 = 0.1756	R1 = 0.0563 wR2 = 0.1240	R1 = 0.0463 wR2 = 0.1016
Largest diff. peak and hole	1.262 and -0.675 $e.A^{-3}$	0.965 and -0.717 $e.A^{-3}$	0.472 and -0.644 $e.A^{-3}$